UNIVERSITÀ
DEGLI STUDI
DI PADOVA

Università degli Studi di Padova

Dipartimento di Scienze Chimiche

PhD Course in Molecular Sciences

Curriculum: Chemistry Cycle XXXV

Novel Photo- and Electrochemical Approaches to the Construction of Complex Molecular Architectures

Coordinator: Prof. Leonard J. Prins

Supervisor: Prof. Luca Dell'Amico

Co-Supervisor: Prof. Andrea Sartorel

Ph.D. student: Pietro Franceschi

Thesis written with the financial contribution of Fondazione Cariparo

Abstract

Organic synthesis is aimed at enlarging the scope of possibilities in chemical transformations. Advancements in this field are expected to benefit pharmaceutical, cosmetic and pesticide industries, that rely on the production of fine chemicals. Moreover, the development of new materials also depends on progresses in organic synthesis. One of the primary challenges of the field is to reduce the environmental impact of the chemical processes. Among the promising methods that have emerged, electro- and photochemistry, besides opening new synthetic possibilities, employ electrons or photons as "traceless reagents". This allows a reduction in waste production and in the use of toxic or dangerous reagents. Flow chemistry is another enabling technology that helps improving the safety and efficiency profile of chemical reactions. Its application in electro- and photochemistry is further promoting the development of these latter. Besides the enhancements in the sustainability of the process brought by these new methods, the utilisation of renewable sources is of extraordinary importance, not only in terms of energy but also of chemicals and raw materials. Amid these potential resources, carbon dioxide has attracted the interest of chemists for its availability and non-toxicity. By harnessing the potential of the above-mentioned techniques, exploitation of these new sources has become increasingly efficient and affordable.

This thesis deals with the development of previously unexplored synthetic methods in the frame of the challenge to a more sustainable and efficient chemistry. In particular:

- Chapter I introduces the general concepts of photo-, electro- and flow chemistry, focusing on their application in organic synthesis. Both the underlying physicochemical principles and operative examples are illustrated.

- Chapter II focuses on the development of novel photochemical strategies to generate highly-functionalised indoline structures through a light-promoted Paternò–Büchi [2+2]-heterocycloaddition. Section 1 shows how the use of visible light suppressed undesired side reactivity allowing the formation of product in excellent yield (up to > 98%) and selectivity (dr > 20:1). In Section 2, implementation of a flow setup greatly improved the productivity of the process (78 μmol/h vs 6 μmol/h obtained in batch) and allowed a gram-scale of the reaction (up to 1.18 g of product).

- Chapter III discusses the use of carbon dioxide in carboxylation reactions. Section 1 focuses on the mechanism of electrochemical carboxylation of α,β-unsaturated carbonyl compounds. Potentiostatic electrolysis experiments helped to identify the active dianionic intermediates capable of fixing carbon dioxide, which remained unclear from previous reports employing galvanostatic setups. In Section 2 applications of flow electrochemistry were studied in the fixation of carbon dioxide onto α,β-unsaturated carbonyl compounds. Few examples of flow electrochemical carboxylation processes have been reported, despite the advantages of this technique. Despite with some substrates a >50-fold increase of the productivity was observed (from 0.19 mmol/h in batch to 10.1 mmol/h in flow for the carboxylation of methyl crotonate), the process displays a limited substrate scope and still shows some operative limitations. Section 3

describes a photocatalytic carboxylation procedure using an unprecedented approach based on a proton-coupled electron transfer pathway to generate benzylic radicals from dihydropyridines derivatives. By designing a redox-neutral methodology, no sacrificial redox agents were required, moreover, the transformation can be carried out at room pressure and temperature with yields up to 76%.

Chapter II - Section 1 & 2

Visible light Paternò-Büchi reaction towards the construction of oxeto-indolinic scaffolds

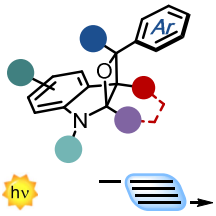

- *34 examples, up to >98% yield*
- *application in flow*

Chapter III - Section 1

Electrochemical carboxylation of α,β-unsaturated carbonyl compounds

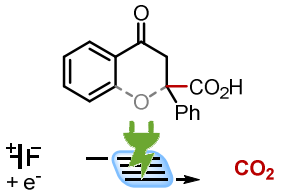

- *mechanistic investigation*
- *implementation in flow*

Chapter III - Section 2

Redox-neutral photocatalytic carboxylation using a novel PCET-SET strategy

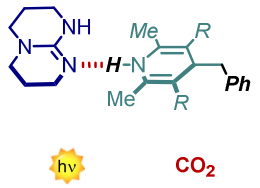

- *18 examples, up to 76% yield*
- *study on the mechanism*

List of Abbreviations

In the following pages, a list of abbreviations and acronyms used along the thesis is summarized.

3DPA2FBN: 2,4,6-Tris(diphenylamino)-3,5-difluorobenzonitrile

3DPAFIPN: 2,4,6-Tris(diphenylamino)-5-fluoroisophthalonitrile

4CzBnBN: (2,3,4,6)-3-benzyl-2,4,5,6-tetra(9*H*-carbazol-9-yl)benzonitrile

4CzIPN: 2,4,5,6-Tetrakis(9*H*-carbazol-9-yl) isophthalonitrile

A: Acceptor

Ac: Acetyl

Ar: Aryl

BET: Back electron transfer

Bn: Benzyl

Boc: *tert*-Butyloxycarbonyl

C: Graphite

Cbz: Benzoyloxycarbonyl

CCE: Controlled current electrolysis

CCI: Crossing of conical intersection

CE: Counter electrode

CO_2: Carbon dioxide

CPE: Controlled potential electrolysis

CT: Charge transfer

CV: Cyclic voltammetry

Cz: Carbazole

D: Donor

DBN: 1,5-Diazabicyclo[4.3.0]non-5-ene

DBU: 1,8-Diazabicyclo[5.4.0]undec-7-ene

DCC: *N,N'*-Dicyclohexylcarbodiimide

DCMA: *N,N*-Dicyclohexylmethylamine

DFT: Density functional theory

DHP: Dihydropyridine

DIPEA: *N,N*-diisopropylethylamine

DMAc: Dimethylacetamide

DMAP: 4-(Dimethylamino)pyridine

DMF: Dimethylformamide

DMSO: Dimethylsulfoxide

dr: diasteroisomeric ratio

E: Electrochemical potential

EDA: Electron donor acceptor

EDG: Electron donor group

EI: Electron ionisation

EnT: Energy transfer

equiv.: Equivalent

ESI: Electrospray ionisation

Et: Ethyl

EtOAc: Ethyl acetate

EWG: Electron withdrawing group

F: Fluorescence

Fc: Ferrocene

GC: Glassy carbon

HAT: Hydrogen atom transfer

HOMO: Highest occupied molecular orbital

HRMS: High resolution mass spectroscopy

HSOMO: Highest singly occupied molecular orbital

IC: Internal conversion

IR: Infra-red

ISC: Inter system crossing

LED: Light-emitting diode

LSOMO: Lowest singly occupied molecular orbital

LUMO: Lowest occupied molecular orbital

Me: Methyl

MeCN: Acetonitrile

MFP: Microfluidic photoreactor

MFR: Microfluidic reactor

Moc: Methyloxycarbonyl

MS-PCET: Multi-site proton-coupled electron transfer

MW: Microwave

NMR: Nuclear magnetic resonance

P: Phosphorescence

PB: Paternò-Büchi

PC: Photocatalyst

PCET: Proton-coupled electron transfer

PET: Photoinduced electron transfer

PG: Protecting group

Ph: Phenyl

PhMe: Toluene

Q: Quencher

RE: Reference electrode

rt: Room temperature

S: Singlet

SCE: Standard calomel electrode

SEE: Silyl enol ether

SET: Single electron transfer

SS: Stainless steel

T:	Triplet
TBD:	1,5,7-Triazabicyclo[4.4.0]dec-5-ene
TBS:	*tert*-butyldimethylsilyl
THF:	Tetrahydrofuran
TIPS:	Triisopropylsilyl
TLC:	Thin layer chromatography
TM:	Transition metal
TMG:	1,1,3,3-Tetramethylguanidine
UV:	Ultra-violet
Vis:	Visible
VR:	Vibrational relaxation
WE:	Working electrode

Table of Contents

Chapter I

Innovative Methods in Organic Synthesis

General Overview on Innovative Methods in Organic Synthesis

Chapter 1.1. - Photochemistry

- *Basics of photochemistry*
- *Direct photochemistry*
- *Energy transfer photocatalysis*
- *Photoredox catalysis*

Chapter 1.2. - Electrochemistry

- *Basics of electrochemistry*
- *Controlled potential electrolysis*
- *Controlled current electrolysis*

Chapter 1.3. - Flow Chemistry

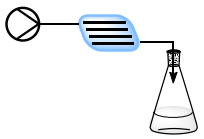

- *Basics of flow chemistry*
- *Flow vs batch*
- *Flow photochemistry*
- *Flow electrochemistry*

In this Chapter an overview of the methods employed in this thesis is provided, in the order: photochemistry, electrochemistry, flow chemistry. After a brief historical background, the physicochemical bases of each methodology are summarised and followed by examples of application in organic synthesis.

1.1. – Photochemistry and organic synthesis

Photochemistry is the "branch of chemistry concerned with the chemical effects of ultraviolet, visible, or infrared radiation".[1] Since ancient times, humans have noticed the effects of sunlight on the aspect of some materials, and have also tried to use the energy of the sun, though only in its thermal component.[2] It was only after the birth of chemistry as a science, at the end of eighteenth century, that the first photochemical experiments were carried out.[3] Among the pioneering observations reported during the 19th century,[4] particularly interesting is that of Trommsdorff on transformations of santonin,[5] as it can be considered the birth of organic photochemistry.[6] Exposing santonin to blue or violet light, he could observe a change in its colour and bursting of its crystals. Further studies on these processes were done by Santini and Cannizzaro,[7] who isolated different photoproducts of the transformation of santonin and tried to describe their structures with the basic techniques at their disposal. However, the birth of organic photochemistry as a systematic study has to be accounted to Ciamician and Silber, who had previously worked with Cannizzaro.[8] In between the 19th and 20th centuries they published a series of papers on different photochemical processes such as photoreduction and fragmentation of carbonyl compounds and photoisomerisation and dimerisation of olefins. The physico-chemical understanding of these processes, however, came only after physicians investigated the nature of light and of its interaction with molecules, during the first half of the 20th century.[9] With knowledge on quantum mechanics and orbital theory, physical chemists like Norrish could analyse and understand the nature of the transformations previously observed by Ciamician and Silber.[10] With all these theoretical basis, together with new techniques such as NMR, the field of organic photochemistry finally blossomed. The interest in the discipline has continuously grown, prompted by evolution of new strategies from direct

photochemistry to energy transfer photocatalysis and more recently to photoredox catalysis.[11]

1.1.1. – Basics of photochemistry

The basic photophysical processes that can arise from interaction of light and a molecule are here briefly summarised, with a schematic picture of these phenomena being offered by the Jablonski diagram (Figure 1.1).[12] When a molecule is shined with light, the energy of the photons is transferred to the molecule. This energy is determined by Equation 1.1, where h is Planck's costant, υ the frequency of the radiation, c the speed of light and λ the wavelength of the radiation.[13]

$$E = h\upsilon = h\,{}^{c}/_{\lambda} \qquad \text{Equation 1.1.}$$

When this energy is high enough, the molecule is promoted to an electronically excited state with a different electronic configuration compared to that of the initial ground state S_0. Different excited states (S_1, S_2 and so on) can be reached depending on the energy of the photons absorbed; these high-energy excited states can decay through many processes (Figure 1.1).[14]

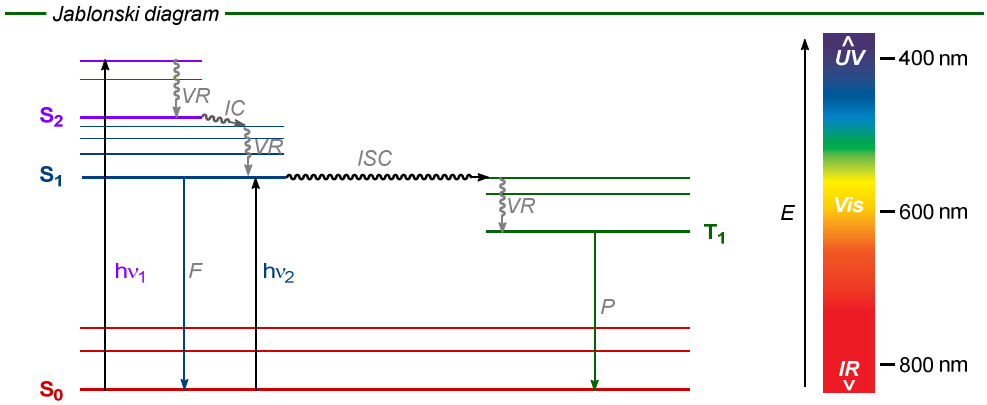

Figure 1.1. – Jablonski diagram with basic decay processes indicated. On the right the visible light spectrum is reported.

Energy can be released through a radiative decay, i.e. emission of light (photons) from singlet S_1 state (fluorescence, F) or triplet T_1 state (phosphorescence, P). Otherwise, non-radiative processes can take place. With vibrational relaxation (VR) lower vibrational levels in the same excited state are reached, releasing energy to the surroundings. Internal conversion (IC) is the transition to a lower electronic state with same spin multiplicity (for example S_2 to S_1). Finally, intersystem crossing (ISC) is the transition between electronic states of different multiplicity (for example S_1 to T_1). The T_1 state is normally longer lived compared to the S_1 state because phosphorescence is a slower process than fluorescence. These are all unimolecular processes, but if the excited molecule is long-lived enough, reactions with other molecules can take place: this is the base of synthetic photochemistry.

1.1.2. – Direct photochemistry

The first examples of photochemical reactions are based on irradiation of a solution of reagents with light of a certain wavelength. The principle behind this process is the light absorption of one of the components (hereafter indicated as chromophore), generating its excited state. This latter can be considered as a

new chemical entity because it has different chemical and physical properties with respect to the ground state, and it should actually be considered the real reagent itself (Scheme 1.1a).

The choice of the irradiation wavelength is related with the absorption properties of the chromophore and is of crucial importance for the reaction outcome. If the light used is a high-energy radiation, such in the case of ultraviolet (UV), it can trigger side reactions, such as decomposition of reagents and products. On the other side, the use of low-energy radiation, such as infrared (IR), would leave the reaction mixture unchanged.

A lot of examples on direct photochemical reactivity have been explored: cyclizations[15] and isomerisations[16] of double bonds, photo-induced electron transfers (PET)[17,18] and fragmentations of different substrates with generation of radical intermediates[19] (Scheme 1.1b).

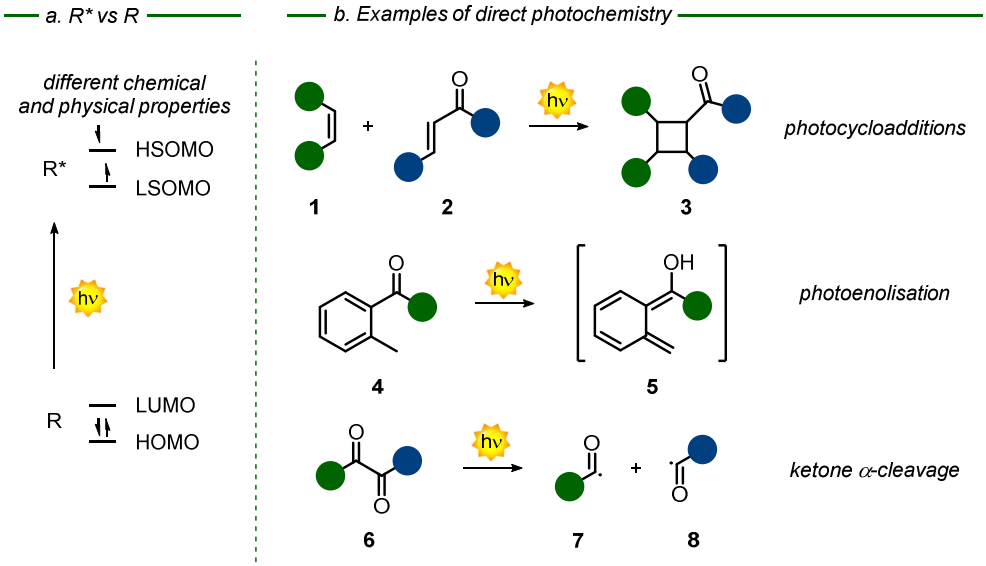

Scheme 1.1. – a. Schematic representation of chemical transformation due to light absorption. b. General examples of direct photochemical reactivity.

In these examples, often UV light is needed, that can cause the above-mentioned issues of side-reactivity. This problem has prompted researcher to develop new and milder strategies, disclosing the field of photocatalysis.

1.1.3. – Energy transfer photocatalysis

A photocatalyst (PC) is a "catalyst able to produce, upon absorption of light, chemical transformations of the reaction partners. The excited state of the photocatalyst repeatedly interacts with the reaction partners forming reaction intermediates and regenerates itself after each cycle of such interactions".[1] As an interaction between the excited photocatalyst (PC*) and the substrate is involved, the lifetime of PC* needs to be long enough (in the order of ns to μs) to approach the substrate.[20]

In energy transfer (EnT), the excited photocatalyst transfer excited-state energy to the substrate. Different types of EnT have been observed, but in organic photocatalysis the predominant is the Dexter energy transfer, also known as two-electron-exchange mechanism (Scheme 1.2a).[21] This mechanism is possible only at short distances, thus the substrate and the PC* must collide and form an encounter complex with orbital overlap before exchanging electrons. As the S_1 state of PC rapidly decays to ground state or T_1 state, usually energy transfer happens from the longer-lived triplet state. After formation of the encounter complex, the photocatalyst in its T_1 state exchanges electrons with the substrate: the high-energy electron in the highest singly-occupied molecular orbital (HSOMO) of the T_1 PC is transferred to the lowest unoccupied molecular orbital (LUMO) of the substrate (with spin multiplicity conservation), while one electron from the highest occupied molecular orbital (HOMO) of the substrate is transferred to the lowest singly-occupied molecular orbital (LSOMO) of the PC. At the end of the process the PC and the substrate are in their ground and triplet excited states, respectively.[22]

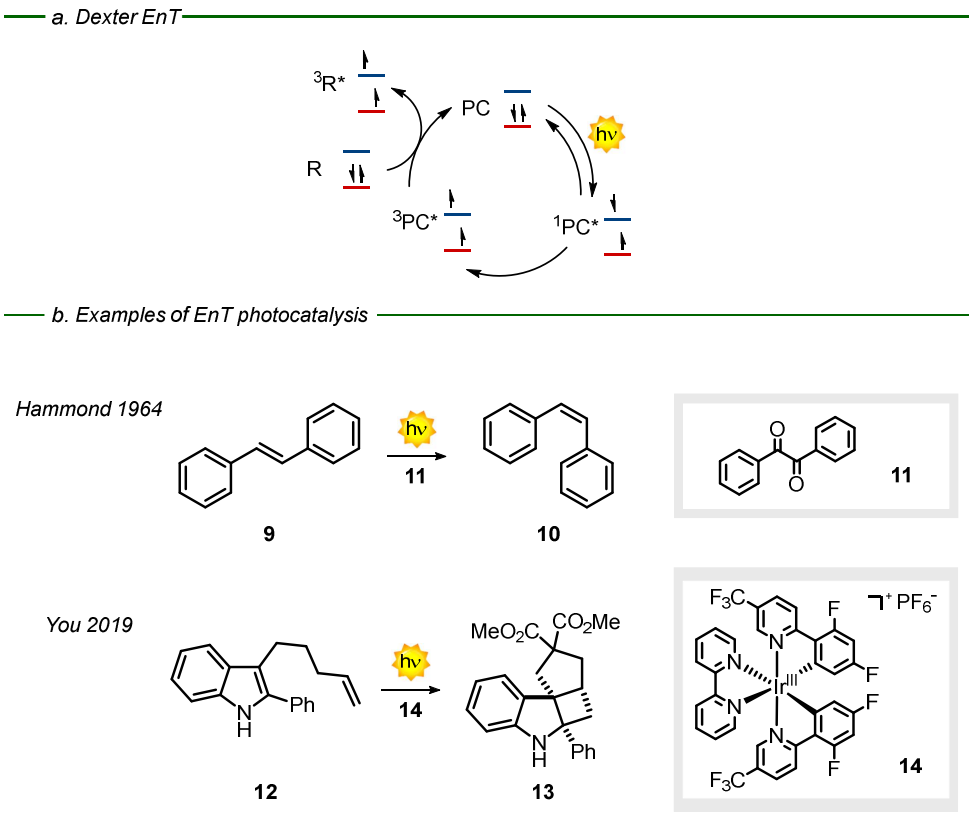

Scheme 1.2. – a. Mechanistic picture of a Dexter EnT. b. Examples of EnT photocatalysis with organic[23] (**11**)and metal-based[24] (**14**) photosensitisers.

Energy transfer can be considered as an indirect excitation, as the final effect is to generate the substrate excited state, and for this reason it is sometimes referred to as photosensitisation. EnT catalysis is advantageous when direct absorption is hampered by low absorption coefficient of the substrate or when short-wavelength irradiation is needed. Indeed, typical photocatalysts absorb in the visible region and have high extinction coefficient and long lifetime. Furthermore, PC must have a higher triplet-energy than the substrate, for the process to be thermodynamically favoured. First studies can be dated back to the 1950s, though, more recently, renewed interest in the field was prompted by the

use of highly-efficient transition-metal photocatalysts.[20] Olefins are the classical substrates in these processes because they suffer from the above-mentioned problems, and typical transformations are olefin isomerisation and cyclization[21] (Scheme 1.2b).

1.1.4. – Photoredox catalysis

Besides energy transfer, a photocatalyst can also be engaged in a single electron transfer (SET), i.e., a redox transformation. PC*, having two unpaired electrons, can act both as an oxidant, filling its LSOMO with an electron from a quencher (Q), and as a reductant, transferring to Q the high-energy electron in the HSOMO. Thus, the photocatalytic cycle can be initiated both by PC reduction (with Q_D being oxidised) or by PC oxidation (with Q_A being reduced); the processes are referred to as reductive and oxidative quenching, respectively. After the first electron transfer, the resulting radical-ion of the catalyst ($PC^{\bullet-}$ or $PC^{\bullet+}$) typically undergoes a second SET with an e^--acceptor A or donor D to regenerate the neutral PC in its ground state[25] (Scheme 1.3a). Often, only one of the two SET processes is synthetically useful, while the other requires the use of a sacrificial acceptor or donor. When a sacrificial acceptor (Q_A or A) is needed, the process is net oxidising, viceversa it is net reducing when a sacrificial donor (Q_D or D) is needed. If both SET are productive, with PC interacting with two different chemically useful reagents or intermediates, this is called a redox-neutral process. As for EnT photocatalysis, the PC should have high extinction coefficient and long lifetime. Besides, the redox potentials of the different forms of PC should match with that of substrates and intermediates, in order to transfer the electrons. Also in this case, absorption by the PC in the visible region is an added value, in particular because if absorption by reagents and products is avoided, side-reactions are typically prevented.[26]

A wide variety of applications of photoredox catalysis has been reported, as they can be applied in virtually every redox process. The use in combination with other catalysts such as organocatalyst or transition metal catalyst has also been widely explored[27] (Scheme 1.3b).

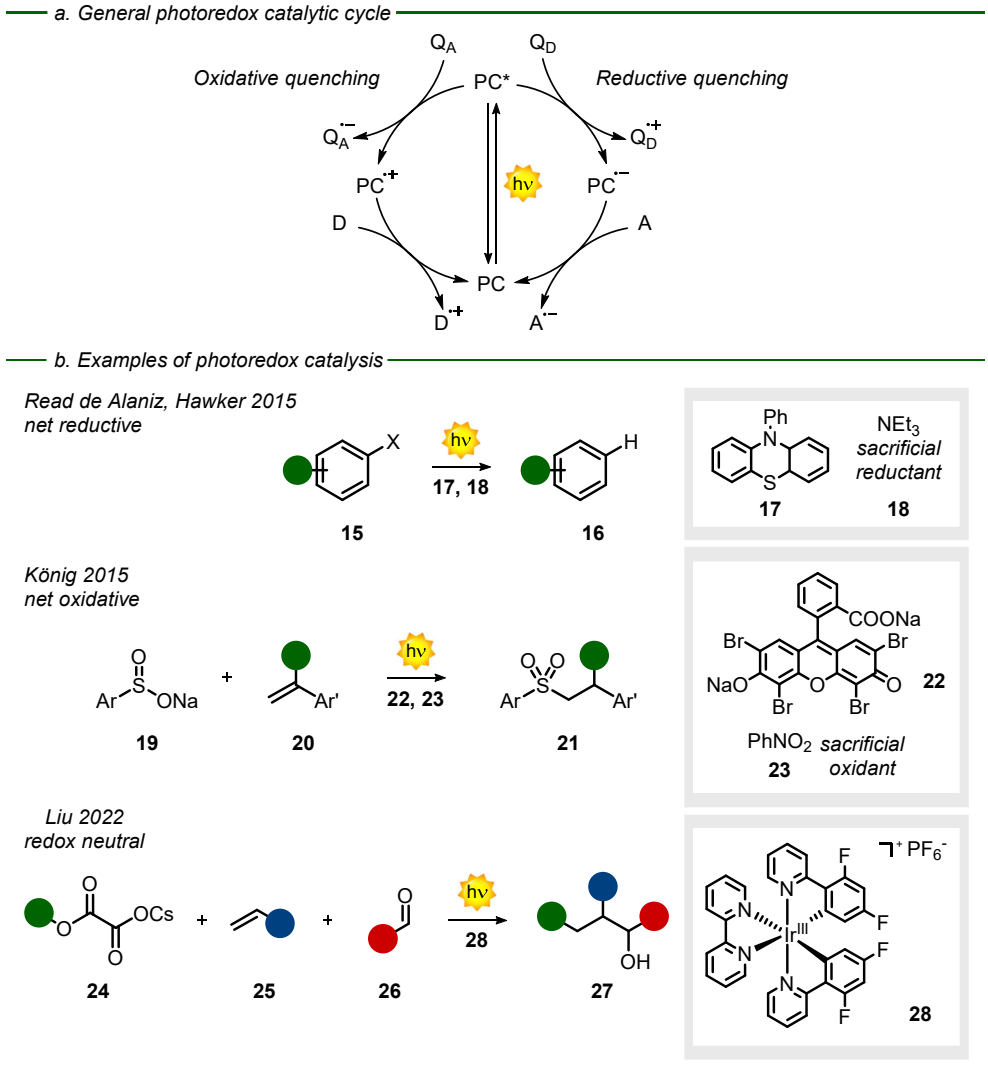

Scheme 1.3 - a. General scheme for oxidative and reductive quenching in photoredox catalysis. b. Examples of photoredox catalysis in net-reductive,[28] net-oxidative[29] and redox-neutral[30] transformations.

1.2. – Electrochemistry and organic synthesis

Electrochemistry studies the relationship between chemical reactants and electric current. The birth of this science can be dated back to 1800, when Volta invented the first electrochemical battery.[31] This allowed the first experiments with electric current in inorganic chemical processes,[32] indeed, shortly after, Carlisle and Nicholson performed the first electrolysis of water.[33] The first electrolysis on organic compounds was carried out by Faraday, using sodium acetate,[34] briefly after reporting his fundamental laws on electrolysis.[35] A period of intense research on organic electrochemistry followed, with some notable examples reported by Kolbe,[36] Tafel,[37] and Haber.[38] With the beginning of the 20th century the interest of organic community slowly decreased, while new electroanalytical methods like polarography,[39] and circular voltammetry (CV)[40] were developed. After 1960, organic electrochemistry underwent a rapid development:[41] important industrial applications were reported, like Simons fluorination[42] and the Monsanto process for adiponitrile production,[43] and indirect electrolysis with organic mediators was developed.[44] Nevertheless, it was only in more recent years that the organic synthetic community put more attention to the field of electrochemistry, thanks to the efforts of pioneering groups in making more understandable and experimentally affordable the technique.[45]

1.2.1. – Basics of electrochemistry

In an electrochemical process, chemical reactions are initiated by electron transfer between the electrodes and the species in solution. This is a heterogeneous process, where mass transfer to the surface and absorption and desorption onto it need to be considered (Figure 1.2). The electron transfer processes, from reagent $\mathbf{R'_{ads}}$ to intermediate $\mathbf{I_{ads}}$ are reversible until a chemical

reaction transforms **I** into products **P** or other intermediates; this reaction can happen also before desorption of **I**.

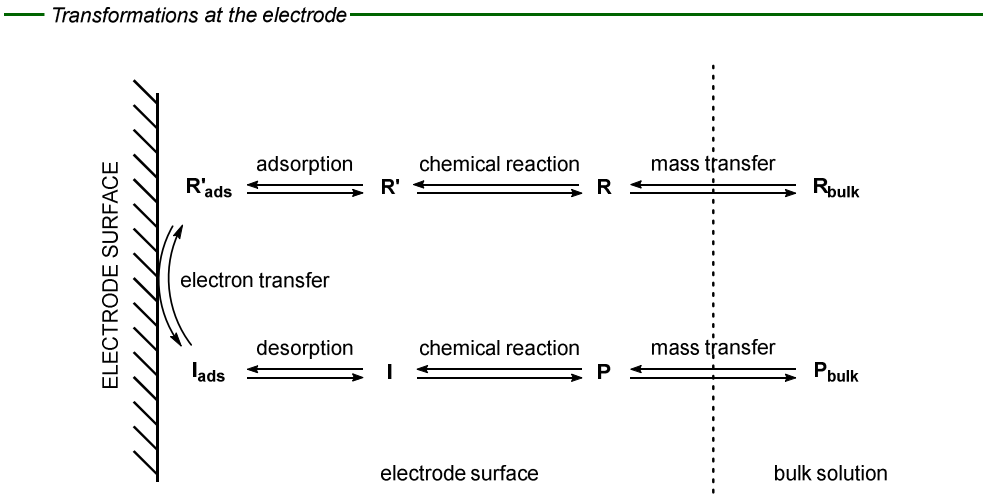

Figure 1.2. – Schematic representation of the steps of electron transfer at the electrode.

In the simplest electrolytic set up, two electrodes connected to an electric generator are dipped in the solution containing the substrate. The electric current passes through the solution to close the circuit, helped by presence of a supporting electrolyte that improves the conductivity of the solution. Usually, the desired reaction takes place at the "working electrode" (WE), the anode if the substrate is oxidised or the cathode if the substrate is reduced. The other electrode is named "auxiliary" or "counter electrode" (CE), there, a simple reaction like H^+ reduction (at the cathode) or oxidation of sacrificial reagents (at the anode) takes place. When both anodic and cathodic reaction are needed to form the product, the process is defined as paired electrolysis. A divided cell can also be employed, where the cathode is separated from the anode, for the cases in which it is desirable to avoid interference between the two processes.

The two compartments are connected through a membrane, usually a glass frit, which allows passage of current but not of the analytes in solution (Figure 1.3).

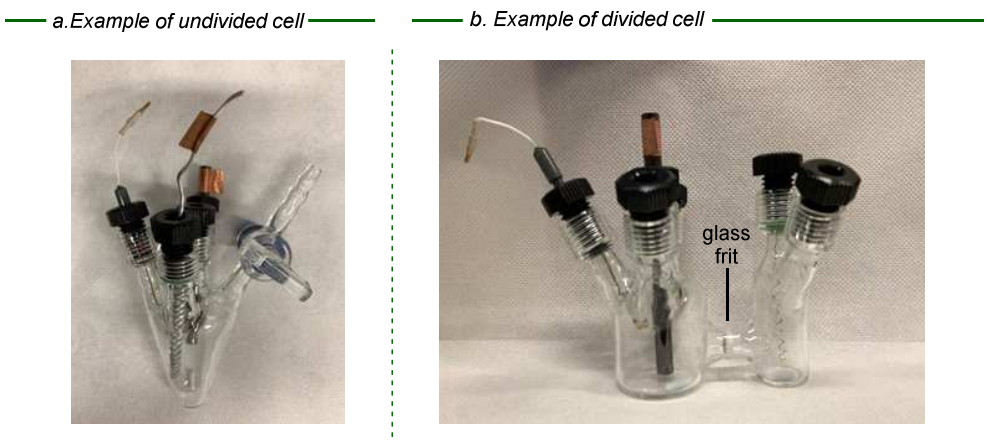

Figure 1.3. – General electrochemical a. undivided and b. divided cell.

Quantitative information on the amount of product formed can be obtained from Faraday's laws on electrolysis, described by Equation 1.2:

$$n = {}^{Q}/_{zF} \qquad \text{Equation 1.2.}$$

Where n is the amount of moles of product formed, Q the amount of charge passed, z the number of electrons transferred for every molecule of product, F the Faraday's constant ($96485\ \text{C}\cdot\text{mol}^{-1}$). As Q is related to the current intensity i by Equation 1.3, the duration of the experiment can also be predicted.

$$Q = \int_0^t i\delta t; \qquad \text{for constant } i\text{:} \quad Q = i\Delta t \qquad \text{Equation 1.3.}$$

However, unwanted electron transfer from the working electrode to other species can take place, thus causing side processes. In these cases, more charge will be needed to obtain the same amount of product respect to an ideal process.

1.2.2. – Controlled potential electrolysis

In controlled potential electrolysis (CPE), or potentiostatic electrolysis, the potential (E) is monitored and kept constant throughout all the experiment, and the current varies accordingly. This is a newer and less used technique, because it requires a more complex three-electrode setup and a potentiostat, which was first built in 1942 by Hickling.[46] The third electrode, called "reference electrode" (RE) is needed in order to monitor and control the potential at the working electrode. The counter electrode cannot be used as a reference because no electric current should pass through the reference electrode, to avoid changing its potential.

One advantage of CPE is that a high selectivity is obtained, as only transformations happening at a certain potential are taking place. This is particularly useful when the product of the first transformation can still be transformed at the electrode or when more electroactive species are present in solution. An example is that of Yoshida *et al.*[47] in which selective oxidation of the telluroglycoside **29** is afforded in the presence **30** which can be oxidised but at higher potentials (Scheme 1.4a). Besides the complex setup, the disadvantage of CPE is the time required for the electrolysis. With the advancement of the reaction lower concentration of the reagent causes a decrease of the current, thus complete conversion is often not achieved (See Scheme 1.4b, the negative current is decreasing in absolute value).

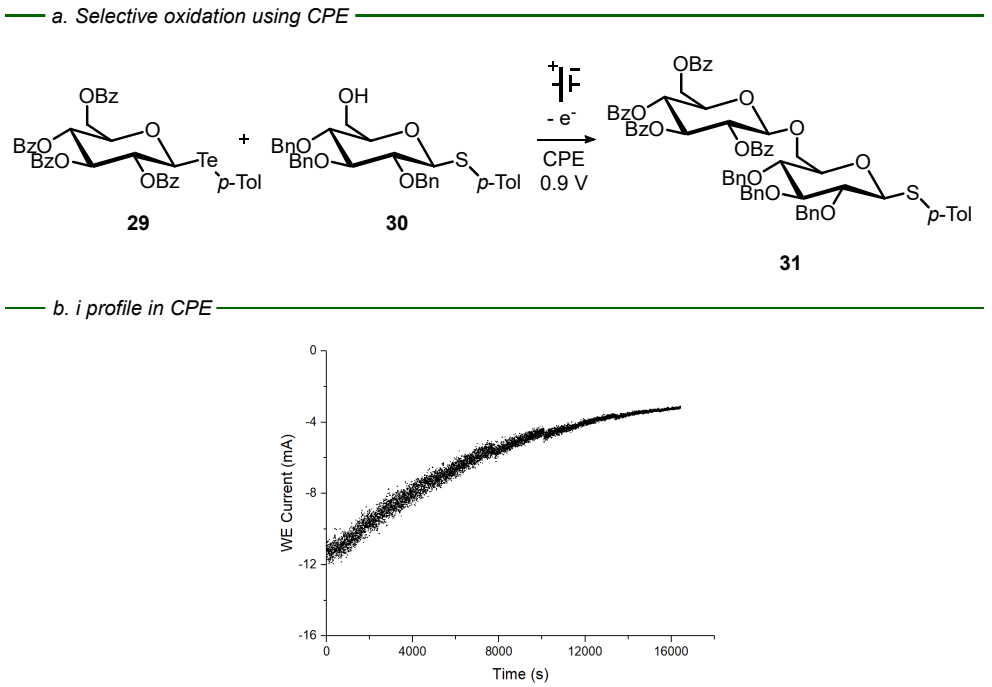

Scheme 1.4. – a. Example of CPE for selective transformations. b. Current profile versus time in a reductive CPE.

1.2.3. – Controlled current electrolysis

Controlled current electrolysis (CCE), or galvanostatic electrolysis, does not require the use of three electrodes nor of a potentiostat, thus, both set up and instrumentation are simpler. The current is kept constant during the electrolysis, and the potential between the electrodes adjusts consequently. Since the potential is related to the current density, by setting up this latter product selectivity can be regulated. However, during the process, consumption of the substrate will cause a change in the electrode potential, which will increase in the case of oxidation, or decrease in case of reduction (Scheme 1.5a). This variation may impact the selectivity, particularly in the advanced stage of the reaction. Nonetheless, this is the prevalent technique for electrolysis: reduced reaction time and ease in the setup makes CCE the perfect choice for synthetic chemists. Scheme 1.5b shows a recent example on electroreductive disylilation

of alkenes by Lin *et al.*,[48] where good yield and selectivity are obtained in a simple CCE setup.

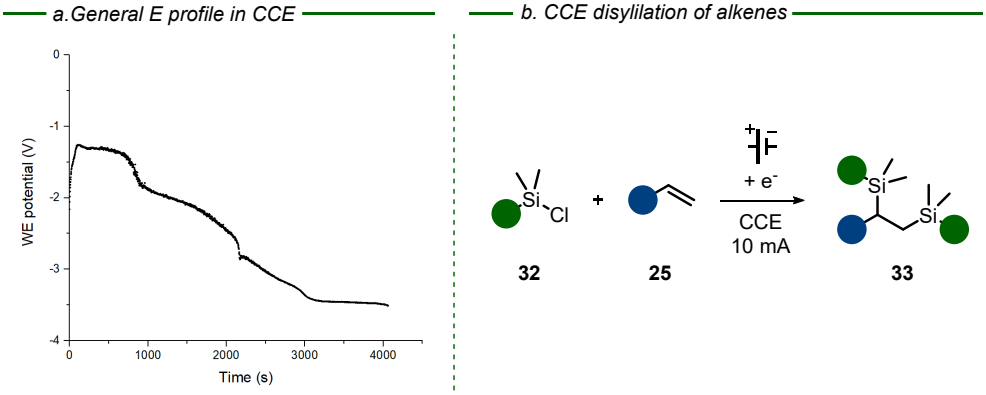

Scheme 1.5. – a. *E* profile during time in a reductive CCE. b. Example of a CCE.

1.3. – Flow chemistry

Flow chemistry studies chemical reactions taking place in continuous flow reactors. These devices are made of one or more channels where the reaction mixture flows: the reagents are continuously pumped in, while the products exit the reactor. While continuous-flow technology is well-established in industry,[49] only in the 1990s it started to be explored at an academic laboratory level.[50] On this scale, microfluidic reactors (MFR) are employed, characterised by channels with typical dimensions in the 0.25-0.75 mm range. Compared to classical batch-type reactors, they are characterised by an extremely large surface to volume ratio, thus they are optimal in heterogeneous or interface processes such as photo- and electrochemistry.[51]

1.3.1. – Basics of flow chemistry

In flow chemistry the setup of a reaction gains further importance with respect to batch setup. Several additional parameters must be considered, and the increased operational possibilities demand for a more attentive design of the process.[52]

One peculiarity of flow chemistry is that, working in a continuous mode, the reaction time assumes a different meaning. In fact, conversion of the reagents is not reached in time, but through the reactor length. When steady-state conditions are reached, the concentration of the reagents, in a fixed point of the reactor, is constant throughout the reaction time. Increasing this latter will only increase the amount of reagent used. An important parameter to consider in this case is the residence time (t_r), i.e., the time that takes a segment of flow to travel throughout the reactor, described by Equation 1.4:[51]

$$t_r = {}^{V_r}/_{f} \qquad \text{Equation 1.4.}$$

Where V_r is the reactor volume and f the flow rate, usually expressed in mL/min or μL/min.

Regulation of the residence time influences the conversion and yield and can be done through variation of V_r or f.

Regarding the setup, the most basic one employs a pump (for liquids) or a mass-flow controller (for gases) to push the reaction mixture directly through the reactor. Products collection can be done in any chemical vessel if no special care is required. A first modification to the setup is to add the solutions of the reagents separately, using a mixer or a simple junction to combine them. In this case, the different flow rates can be regulated independently influencing the reagents ratio and the kinetics of the mixing process. Already at this level, different types of pumps, reactors or mixers can be selected. This choice will affect the concentration profiles through the reactor length, and consequently the yield and the selectivity of the process. Accurate selection of the component is particularly needed for multi-phase reactions. Additionally, quenching and/or pressure-regulation modules can be installed before the collection step, if needed (Figure 1.4).

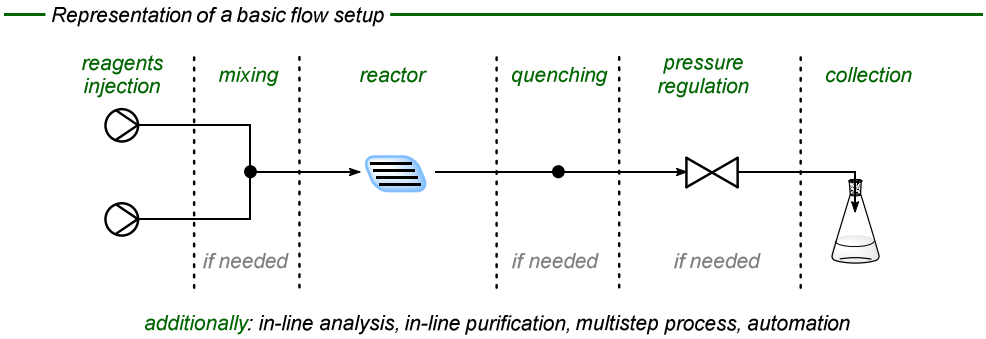

Figure 1.4. – General representation of a flow setup.

Even more sophisticated setups can be assembled for multi-step processes or in-line analysis or purification, usually in perspective of automation and industrialisation.[53]

1.3.2. – Flow vs batch

In comparing results obtained in flow and batch, as well as in different flow procedures, process chemists have designed more informative metrics than reaction yield. Productivity p (Equation 1.5a) takes in consideration also the time t to obtain a certain amount of product in moles (n_p), while space-time yield sty (Equation 1.5b), used for catalytic processes, takes also in consideration the amount of catalyst used in volume (V_c).[54]

$$p = {}^{n_p}/_{t} \qquad \text{Equation 1.5a;} \qquad sty = {}^{n_p}/_{V_c t} \qquad \text{Equation 1.5b.}$$

Compared to batch reactors, the small dimension of MFRs imparts them an amazingly high surface to volume ratio which translates into more controlled and homogeneous conditions. Hence, the flow setup generally guarantees safer and more selective reactions, as well as faster and more productive processes. Besides, their modular nature makes them versatile and prone to scaling-up and automation. However, MFR are more expensive than typical batch instrumentation, more time-demanding in the planning and optimisation of the process, and they require a certain degree of engineering knowledge. A limitation of MFRs is that use of solid reagents, or reactions with solid formation should be avoided. These, in fact, cause problems of clogging, which are not always possible to solve without making the process less efficient or by using more complex setups.[55]

Nonetheless, the advantages of MFR often outcompete their drawbacks, in particular in cases where higher surface area is needed, or where selectivity or

safety issues are present.[50b] For example, multiphase systems, especially gas-liquid mixtures, benefits from the use of MFR. The increased contact area facilitates phase transfer which is often rate limiting. Moreover, different types of flow can be achieved regulating flow ratio and flow rates, and this can further increase mixing and phase transfer. MFRs also display a fast and more homogenous mixing, due to smaller dimensions and a more ordered laminar flow. Indeed, under the batch setup, the flow is turbulent close to the stirring bar, but laminar on the outside of the container.[51] Flow is beneficial when absence of concentration gradient is required, e.g. in flash reactions, where accumulation of product can lead to parasite reactivity.[56] The larger surface area also aids heat transfer, which turns in increased temperature control. This favours MFR in highly exothermic reactions, which can be conducted safely, but also reactions where temperature controls isomer selectivity or by-product formation (Curtin-Hammett principle). Moreover, slow reactions can be carried out in high-temperature and high-pressure conditions more easily and safely in flow processes.[51] Beside these applications, two fields particularly benefit from application of flow conditions: photochemistry and electrochemistry.

1.3.3. – Flow photochemistry

Photochemistry relies on light absorption by the reaction mixture, which is described by the Lambert-Beer law (Equation 1.6).

$$A = \varepsilon c l = \log_{10}\left({}^{1}/_{T}\right) \qquad \text{Equation 1.6.}$$

Where T is the transmittance, described as "the ratio of the transmitted radiant power to that incident on the sample",[57] A the absorption, ε is the molar absorption coefficient of the chromophore, c the molar concentration of the chromophore and l the distance travelled by the radiation in the chromophore solution.

The main problem when operating in batch is that only the first layers of solution absorb photons and react, while light radiation is not transmitted to the inner part of the solution.[6] For example, considering a 2 mM solution of 2,4,5,6-Tetrakis(9H-carbazol-9-yl)isophthalonitrile (4CzIPN), a typical photocatalyst employed in organic synthesis, less than 5% of the radiant power will be transmitted after 0.11 cm in the solution (Figure 1.5, red line). Using more concentrated solutions, light penetration will be even more reduced (Figure 1.5).

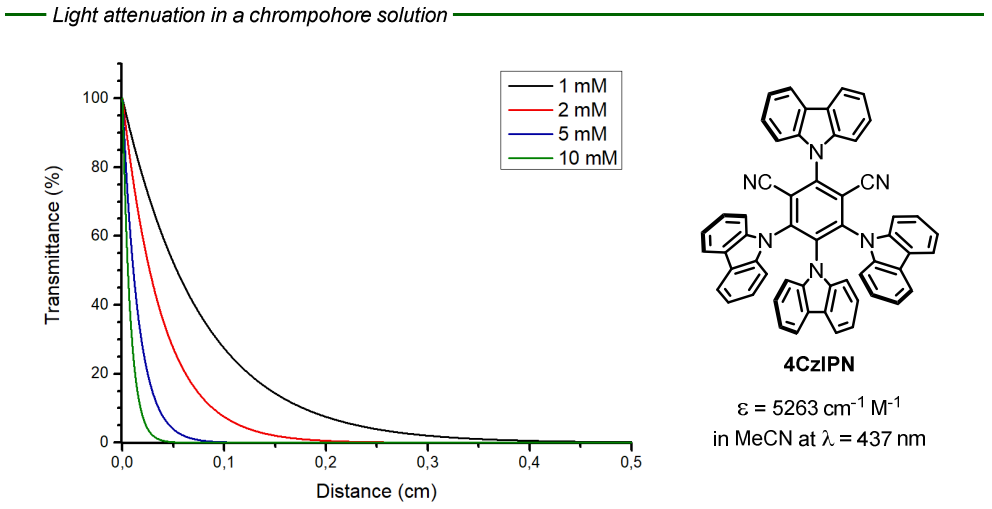

Figure 1.5. – Transmittance profiles for different concentrations of 4CzIPN in acetonitrile (MeCN). ε = 5623 L·mol^{-1}·cm^{-1} at λ = 437 nm in MeCN.

This reduced and non-homogeneous irradiation slows down the reaction, also causing problems of over-irradiation of the solution with product degradation or side-products formation.[58] Use of MFRs greatly diminish this problem. In fact, typical channels employed have an inner diameter which allows irradiation of all the solution,[51] moreover, higher surface area means higher irradiated surface, thus faster process. Light penetration also hampers scale up of batch

photoreactions, where the problems showed above are even intensified. Using flow chemistry this problem is avoided, as higher amount of product is made increasing the reaction time, without depleting the yield or the productivity. Beside these effects, the other general benefits of flow are also valid.[59]

In the past decade, the application of flow technology to photochemistry has received increasing attentions. New examples of photochemical reactions have been reported where the use of flow is necessary to perform the desired reaction. One clear example is the photocatalytic oxidation of thiols reported by Nöel *et al.*,[60] where furfuyl disulfide **35** could be obtained only in flow conditions. When carrying out the reaction in batch, overoxidation was observed before complete conversion of **34** (Scheme 1.6). Dell'Amico *et al.* reported the addition of photogenerated **38** to coumarin **37**, the reaction requires the use of flow, otherwise extensive dimerization of coumarin is observed (Scheme 1.6).[61]

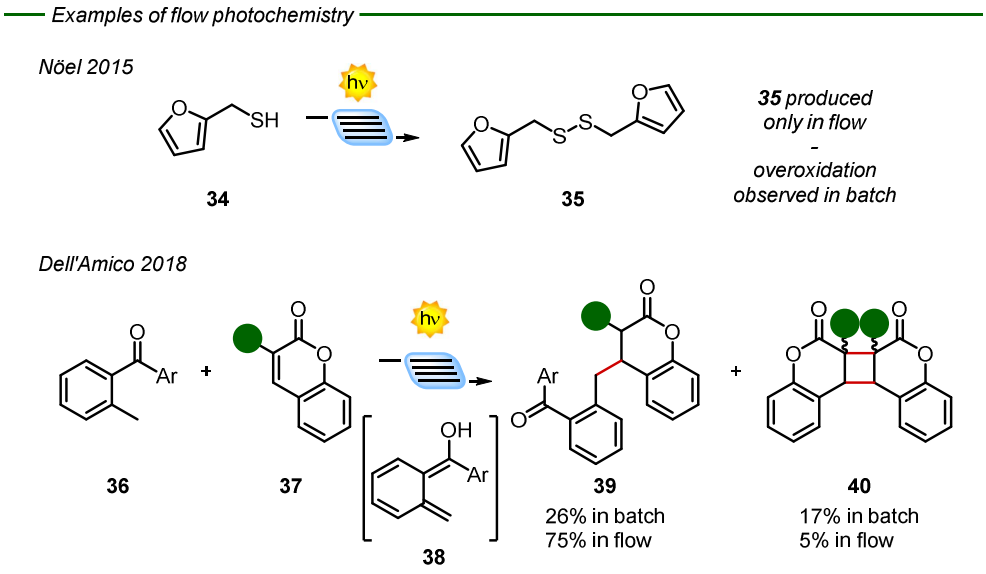

Scheme 1.6. – Examples of application of flow photochemistry for efficient and selective reactions.

1.3.4. – Flow electrochemistry

Electrochemistry is based on electron transfer processes at the electrodes and mass transfer processes in the solution toward the electrode. Both processes are positively influenced in microfluidic setups, in facts, the electrode surface is way larger than in batch, and the interelectrode gap is diminished. The electrochemical process is sped up both by larger active area (the electrode), and smaller distance that molecules have to travel to reach the active area (interelectrode gap).[62] The smaller distance also minimises the additive potential (ΔE_{ohm}), called *Ohmic drop* or *iR drop* (Equation 1.7), needed to pass current through the solution, that can also cause a non-uniform potential at the working electrode.[51] The solution in facts has an electrical resistance R_s that depends on its conductivity κ, the interelectrode gap d and the electrode active area A_e. ΔE_{ohm} is proportional to this electrical resistance and to the current intensity i.

$$\Delta E_{ohm} = iR_s = {id}/{A_e\kappa} \qquad \text{Equation 1.7.}$$

In batch, to overcome R_s, large amounts of supporting electrolyte are used to increase the conductivity of the solution. However, excess of electrolyte can interfere with the purification process. In microfluidic setups ΔE_{ohm} is already reduced by smaller d and largeer A_e, thus the electrolyte can be excluded or at least reduced in quantity. High R_s also causes heating of the solution, as it is described by the Joule's first law for currents passing through resistances (Equation 1.8), that can cause selectivity or degradation issues. With MFRs the problem is solved by the reduced R_s, as well as by their intrinsic good heat-transfer ability and by physical removal of the heated solution for the action of flow.[63]

$$P = i^2R_s \qquad \text{Equation 1.8.}$$

Where *P* is the power of heating developed. Also in this case, the general advantages of flow apply, adding to the above mentioned effects in providing improved selectivity and productivity of the processes.

Similar considerations to the ones discussed in Chapter 1.2 regarding electrochemistry are also valid in flow setups: both divided (Scheme 1.6a) and undivided cell (Scheme 1.6b) can be employed,[64] though the first is less practical and thus less used. Three-electrode arrangements require sophisticated setups, and are unpractical, therefore constant current electrolysis is the principal operational mode for flow electrochemistry. A constant cell potential electrolysis can be performed, where the cell voltage is kept constant, but the potential of the working electrode is in any case unknow.[65]

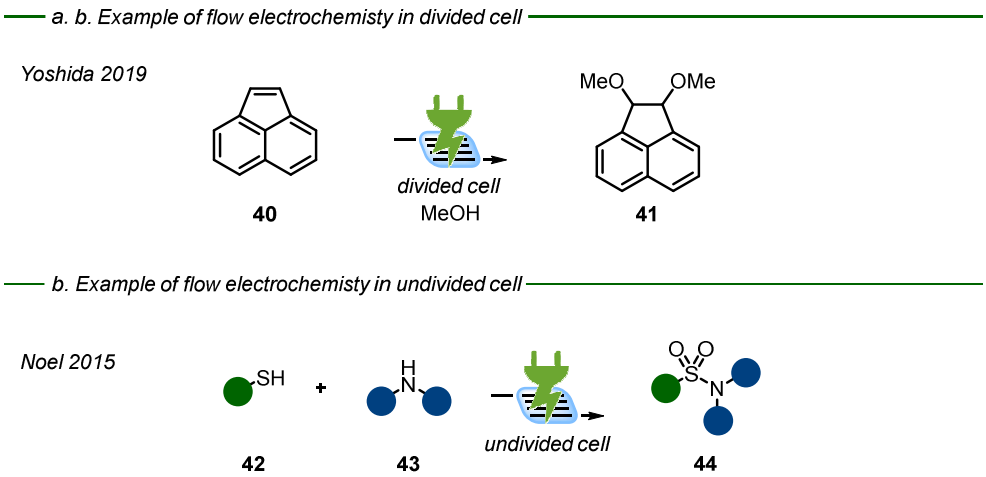

Scheme 1.6. – Examples of flow electrochemistry in a. divided[66] and b. undivided[67] in cell setup.

The quantitative considerations of Faraday's laws on electrolysis are valid also in flow, and can be rearranged, for CCE, integrating the parameters of flow chemistry (Equation 1.9).

$$n = {}^{iV_r}/_{zFf}$$ Equation 1.9.

Where n is the amount of moles of product formed, i the current intensity, V_r the reactor volume, z the number of electrons transferred for every molecule of product, F the Faraday's constant $\left(96485\ \mathrm{C{\cdot}mol^{-1}}\right)$ and f the flow rate expresses in mL/min or μL/min.

1.4. – References - Chapter I

1. Braslavsky, S. E., Glossary of terms used in photochemistry, 3rd edition (IUPAC Recommendations 2006). *Pure & Appl. Chem.* **2007,** 79, 293-465.

2. Roth, H.-D., The Beginnings of Organic Photochemistry. *Angew . Chem. Int. Ed.* **1989,** 28, 1193-1207.

3. Priestley, J., *Experiments and Observations on Different Kinds of Air*: *And Other Branches of Natural Philosophy, Connected with the Subject* ; *in Three Volumes* ; *Being the Former Six Volumes Abridged and Methodized, with Many Additions*. Thomas Pearson: Birmingham, 1790.

4. Schroll, P., Early pioneers of organic photochemistry. In *Chemical Photocatalysis*, Burkhard, K., Ed. De Gruyter: Berlin, Boston, 2013; pp 3-18.

5. Trommsdorff, H., Ueber Santonin. *Ann. Pharm.* (*Lemgo, Ger.*) **1834,** 11, 190-207.

6. Knowles, J. P.; Elliott, L. D.; Booker-Milburn, K. I., Flow photochemistry: Old light through new windows. *Beilstein J. Org. Chem.* **2012,** 8, 2025-52.

7. Cannizzaro, S.; Santini, F., Ricerche sulla santonina. *Gazz. Chim. Ital.* **1873,** 3, 241-251.

8. Heindel, N. D.; Pfau, M. A., A Profitable Partnership - Giacomo Ciamician and Paul Silber. *J. Chem. Educ.* **1965,** 42, 383-386.

9. (a) VI. General Discussion At The Fifth Solvay Conference: Unpublished Manuscript From Folder Labelled Notes From Solvay Meeting(1927). In *Niels Bohr Collected Works*, Kalckar, J., Ed. Elsevier: 1985; Vol. 6, pp 99-106. (b) de Broglie, L. Recherches sur la théorie des Quanta. Migration - université en cours d'affectation, 1924.

10. (a) Dainton, F. S.; Thrush, B. A., Ronald George Wreyford Norrish, 9 November 1897 - 7 June 1978. *Biogr. Mem. Fellows R. Soc.* **1981,** 27, 379-424. (b) Norrish, R. G. W.; Kirkbride, F. W., 204. Primary photochemical processes. Part I. The decomposition of formaldehyde. *J. Chem. Soc.* **1932**, 1518-1530.

11. Beeler, A. B., Introduction: Photochemistry in Organic Synthesis. *Chem. Rev.* **2016,** 116, 9629-9630.

12. Klessinger, M.; Michl, J., *Excited States and Photochemistry of Organic Molecules*. VCH: New York, 1995.

13. Turro, N. J.; Ramamurthy, V.; Scaiano, J., *Modern Molecular Photochemistry of Organic Molecules*. University Science Books: 2010.

14. Introduction to Fluorescence. In *Principles of Fluorescence Spectroscopy*, Lakowicz, J. R., Ed. Springer US: Boston, MA, 2006; pp 1-26.

15. Crimmins, M. T.; Reinhold, T. L., Enone Olefin [2 + 2] Photochemical Cycloadditions. In *Organic Reactions*, 2004; pp 297-588.

16. Dunning, H. N., Review of Olefin Isomerization. *Ind. Eng. Chem.* **1953,** 45, 551-564.

17. see chapter 2.1.2. for more details

18. Albrecht, E.; Averdung, J.; Bischof, E. W.; Heidbreder, A.; Kirschberg, T.; Müller, F.; Mattay, J., Photoinduced electron transfer (PET) in organic synthesis. [3 + 2]-type cycloaddition, cyclization and C□C bond cleavage reactions. *J. Photochem. Photobiol., A* **1994,** 82, 219-232.

19. (a) Grimshaw, J.; de Silva, A. P., Photochemistry and photocyclization of aryl halides. *Chem. Soc. Rev.* **1981,** 10, 181-203. (b) Ciamician, G.; Silber, P. J. B. d. d. c. G., Chemische Lichtwirkungen. *Ber. Dtsch. Chem. Ges.* **1907,** 40, 2415-2424.

20. Strieth-Kalthoff, F.; Glorius, F., Triplet Energy Transfer Photocatalysis: Unlocking the Next Level. *Chem* **2020,** 6, 1888-1903.

21. Neveselý, T.; Wienhold, M.; Molloy, J. J.; Gilmour, R., Advances in the E → Z Isomerization of Alkenes Using Small Molecule Photocatalysts. *Chem. Rev.* **2022,** 122, 2650-2694.

22. Dexter, D. L., A Theory of Sensitized Luminescence in Solids. *J. Chem. Phys.* **1953,** 21, 836-850.

23. Hammond, G. S.; Saltiel, J.; Lamola, A. A.; Turro, N. J.; Bradshaw, J. S.; Cowan, D. O.; Counsell, R. C.; Vogt, V.; Dalton, C., Mechanisms of Photochemical Reactions in Solution. XXII.1 Photochemical cis-trans Isomerization. *J. Am. Chem. Soc.* **1964,** 86, 3197-3217.

24. Zhu, M.; Zheng, C.; Zhang, X.; You, S. L., Synthesis of Cyclobutane-Fused Angular Tetracyclic Spiroindolines via Visible-Light-Promoted Intramolecular Dearomatization of Indole Derivatives. *J. Am. Chem. Soc.* **2019,** 141, 2636-2644.

25. Romero, N. A.; Nicewicz, D. A., Organic Photoredox Catalysis. *Chem. Rev.* **2016,** 116, 10075-166.

26. Shaw, M. H.; Twilton, J.; MacMillan, D. W., Photoredox Catalysis in Organic Chemistry. *J. Org. Chem.* **2016,** 81, 6898-926.

27. Skubi, K. L.; Blum, T. R.; Yoon, T. P., Dual Catalysis Strategies in Photochemical Synthesis. *Chem. Rev.* **2016,** 116, 10035-74.

28. Discekici, E. H.; Treat, N. J.; Poelma, S. O.; Mattson, K. M.; Hudson, Z. M.; Luo, Y.; Hawker, C. J.; de Alaniz, J. R., A highly reducing metal-free photoredox catalyst: design and application in radical dehalogenations. *Chem. Commun.* **2015,** 51, 11705-11708.

29. Meyer, A. U.; Jäger, S.; Prasad Hari, D.; König, B., Visible Light-Mediated Metal-Free Synthesis of Vinyl Sulfones from Aryl Sulfinates. *Adv. Synth. Catal.* **2015,** 357, 2050-2054.

30. Sun, W.-H.; Zou, J.-Y.; Xu, X.-J.; Wang, J.-L.; Liu, M.-L.; Liu, X.-Y., Photo-Catalyzed Redox-Neutral 1,2-Dialkylation of Alkenes. *Adv. Synth. Catal.* **2022,** 364, 2260-2265.

31. Volta, A., XVII. On the electricity excited by the mere contact of conducting substances of different kinds. In a letter from Mr. Alexander Volta, F. R. S. Professor of Natural Philosophy in the University of Pavia, to the Rt. Hon. Sir Joseph Banks, Bart. K.B. P. R. S. **1800,** 90, 403-431.

32. Bagotsky, V. S., Frontmatter. In *Fundamentals of Electrochemistry*, The Electrochemical Society: 2005; pp i-xxviii.

33. Nicholson, W., Accounts of the new electrical or Galvanic Apparatus of Sig. Alex. Volta, and Experimets performed with the same. *J. Nat. Philos. Chem. Arts* **1801,** 4, 179-187.

34. Faraday, M., VI. Experimental researches in electricity.-Seventh Series. *Philos. Trans. R. Soc. London* **1834,** 124, 77-122.

35. Hamann, C. H.; Hamnett, A.; Vielstich, W., *Electrochemistry*. Wiley-VCH: 2007.

36. Kolbe, H., Beobachtungen über die oxydirende Wirkung des Sauerstoffs, wenn derselbe mit Hülfe einer elektrischen Säule entwickelt wird. *J. Prakt. Chem.* **1847,** 41, 137-139.

37. Tafel, J.; Hahl, H., Vollständige Reduktion des Benzylacetessigesters. *Ber. Dtsch. Chem. Ges.* **1907,** 40, 3312-3318.

38. Haber, F., Elektrolytische Darstellung von Phenyl-β-Hydroxylamin. *Z. Elektrochem. Angew. Phys. Chem.* **1898,** 5, 77-78.

39. Heyrovsky, J., XXIX. Electrolysis with a dropping mercury cathode. Part I. Deposition of alkali and alkaline earth metals. *Philos. Mag.* **1923,** 45, 303-315.

40. Randles, J. E. B., A cathode ray polarograph. Part II.—The current-voltage curves. *Trans. Faraday Soc.* **1948,** 44, 327-338.

41. Lund, H., A Century of Organic Electrochemistry. *J. Electrochem. Soc.* **2002,** 149, S21-S33.

42. Simons, J. H., Production of Fluorocarbons. *J. Electrochem. Soc.* **1949,** 95, 47-52.

43. Baizer, M. M., Recent developments in electro-organic synthesis. *Naturwissenschaften* **1969,** 56, 405-409.

44. Steckhan, E., Indirect Electroorganic Syntheses—A Modern Chapter of Organic Electrochemistry [New Synthetic Methods (59)]. *Angew. Chem. Int. Ed.* **1986,** 25, 683-701.

45. (a) Yan, M.; Kawamata, Y.; Baran, P. S., Synthetic Organic Electrochemical Methods Since 2000: On the Verge of a Renaissance. *Chem. Rev.* **2017,** 117, 13230-13319. (b) Kingston, C.; Palkowitz, M. D.; Takahira, Y.; Vantourout, J. C.; Peters, B. K.; Kawamata, Y.; Baran, P. S., A Survival Guide for the "Electro-curious". *Acc. Chem. Res.* **2020,** 53, 72-83. (c) Pollok, D.; Waldvogel, S. R., Electro-organic synthesis - a 21(st) century technique. *Chem. Sci.* **2020,** 11, 12386-12400. (d) Nutting, J. E.; Gerken, J. B.; Stamoulis, A. G.; Bruns, D. L.; Stahl, S. S., "How Should I Think about Voltage? What Is Overpotential?": Establishing an Organic Chemistry Intuition for Electrochemistry. *J. Org. Chem.* **2021,** 86, 15875-15885. (e) Zhu, C.; Ang, N. W. J.; Meyer, T. H.; Qiu, Y.; Ackermann, L., Organic Electrochemistry: Molecular Syntheses with Potential. *ACS Cent. Sci.* **2021,** 7, 415-431. (f) Leech, M. C.; Lam, K., A practical guide to electrosynthesis. *Nat. Rev. Chem.* **2022,** 6, 275-286.

46. Hickling, A., Studies in electrode polarisation. Part IV.—The automatic control of the potential of a working electrode. *Trans. Faraday Soc.* **1942,** 38, 27-33.

47. Yamago, S.; Kokubo, K.; Hara, O.; Masuda, S.; Yoshida, J.-i., Electrochemistry of Chalcogenoglycosides. Rational Design of Iterative Glycosylation Based on Reactivity Control of Glycosyl Donors and Acceptors by Oxidation Potentials. *J. Org. Chem.* **2002,** 67, 8584-8592.

48. Lu, L.; Siu, J. C.; Lai, Y.; Lin, S., An Electroreductive Approach to Radical Silylation via the Activation of Strong Si-Cl Bond. *J. Am. Chem. Soc.* **2020,** 142, 21272-21278.

49. Kirschning, A., Chemistry in flow systems. *Beilstein J. Org. Chem.* **2009,** 5, 15.

50. (a) Elvira, K. S.; i Solvas, X. C.; Wootton, R. C. R.; deMello, A. J., The past, present and potential for microfluidic reactor technology in chemical synthesis. *Nat. Chem.* **2013,** 5, 905-915. (b) Yoshida, J.; Nagaki, A.; Iwasaki, T.; Suga, S., Enhancement of Chemical Selectivity by Microreactors. *Chem. Eng. Technol.* **2005,** 28, 259-266.

51. Plutschack, M. B.; Pieber, B.; Gilmore, K.; Seeberger, P. H., The Hitchhiker's Guide to Flow Chemistry parallel. *Chem. Rev.* **2017,** 117, 11796-11893.

52. Guidi, M.; Seeberger, P. H.; Gilmore, K., How to approach flow chemistry. *Chem. Soc. Rev.* **2020,** 49, 8910-8932.

53. Hone, C. A.; Kappe, C. O., Towards the Standardization of Flow Chemistry Protocols for Organic Reactions. *Chem.*: *Methods* **2021,** 1, 454-467.

54. Hagen, J., *Industrial Catalysis*: *A Practical Approach, Third Edition.* Wiley-VCH Verlag GmbH & Co. KGaA-: 2015; p 1-16.

55. Akwi, F. M.; Watts, P., Continuous flow chemistry: where are we now? Recent applications, challenges and limitations. *Chem. Commun.* **2018,** 54, 13894-13928.

56. Yoshida, J.-i.; Takahashi, Y.; Nagaki, A., Flash chemistry: flow chemistry that cannot be done in batch. *Chem. Commun.* **2013,** 49, 9896-9904.

57. Verhoeven, J. W., Glossary of terms used in photochemistry (IUPAC Recommendations 1996). *Pure & Appl. Chem.* **1996,** 68, 2223-2286.

58. Cambie, D.; Bottecchia, C.; Straathof, N. J.; Hessel, V.; Noel, T., Applications of Continuous-Flow Photochemistry in Organic Synthesis, Material Science, and Water Treatment. *Chem. Rev.* **2016,** 116, 10276-341.

59. Noël, T., A personal perspective on the future of flow photochemistry. *J. Flow Chem.* **2017,** 7, 87-93.

60. Talla, A.; Driessen, B.; Straathof, N. J. W.; Milroy, L.-G.; Brunsveld, L.; Hessel, V.; Noël, T., Metal-Free Photocatalytic Aerobic Oxidation of Thiols to Disulfides in Batch and Continuous-Flow. *Adv. Synth. Catal.* **2015,** 357, 2180-2186.

61. Mateos, J.; Cherubini-Celli, A.; Carofiglio, T.; Bonchio, M.; Marino, N.; Companyo, X.; Dell'Amico, L., A microfluidic photoreactor enables 2-methylbenzophenone light-driven reactions with superior performance. *Chem. Commun.* **2018,** 54, 6820-6823.

62. Zheng, S.; Yan, J.; Wang, K., Engineering Research Progress of Electrochemical Microreaction Technology—A Novel Method for Electrosynthesis of Organic Chemicals. *Engineering* **2021,** 7, 22-32.

63. Noel, T.; Cao, Y.; Laudadio, G., The Fundamentals Behind the Use of Flow Reactors in Electrochemistry. *Acc. Chem. Res.* **2019,** 52, 2858-2869.

64. Atobe, M.; Tateno, H.; Matsumura, Y., Applications of Flow Microreactors in Electrosynthetic Processes. *Chem. Rev.* **2018,** 118, 4541-4572.

65. Maljuric, S.; Jud, W.; Kappe, C. O.; Cantillo, D., Translating batch electrochemistry to single-pass continuous flow conditions: an organic chemist's guide. *J. Flow Chem.* **2020,** 10, 181-190.

66. Horcajada, R.; Okajima, M.; Suga, S.; Yoshida, J.-i., Microflow electroorganic synthesis without supporting electrolyte. *Chem. Commun.* **2005**, 1303-1305.

67. Laudadio, G.; Barmpoutsis, E.; Schotten, C.; Struik, L.; Govaerts, S.; Browne, D. L.; Noel, T., Sulfonamide Synthesis through Electrochemical Oxidative Coupling of Amines and Thiols. *J. Am. Chem. Soc.* **2019,** 141, 5664-5668.

Chapter II

Visible-light Paternò-Büchi Reaction for the Construction of Indolinic Structures

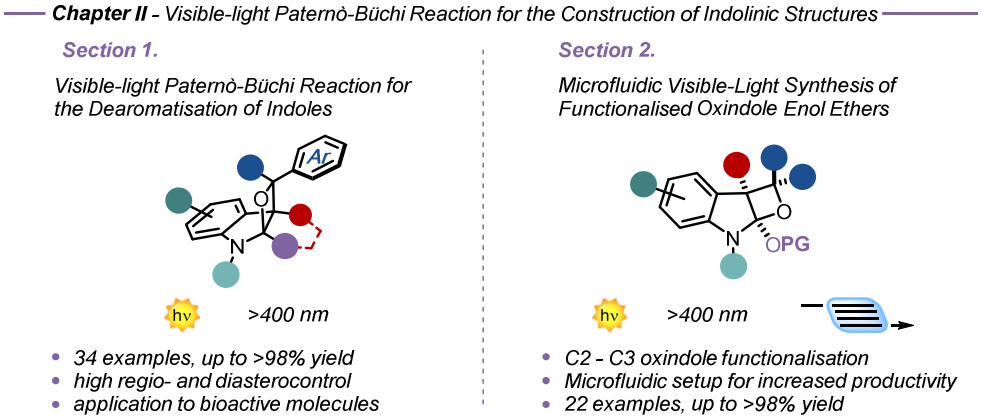

In this Chapter the Paternò-Büchi reaction, its possible mechanisms and the related selectivity are illustrated. Section 1 and 2 shows its application in indole dearomatisation and its in-flow implementation.

Pubblications:

- Mateos, J.; Vega-Penaloza, A.; Franceschi, P.; Rigodanza, F.; Andreetta, P.; Companyo, X.; Pelosi, G.; Bonchio, M.; Dell'Amico, L. A visible-light Paterno-Buchi dearomatisation process towards the construction of oxeto-indolinic polycycles. *Chem Sci*, **2020**, 11, 6532-6538.

- Franceschi, P., Mateos, J., Vega-Peñaloza, A.; Dell'Amico, L. Microfluidic Visible-Light Paternò–Büchi Reaction of Oxindole Enol Ethers. *Eur. J. Org. Chem.*, **2020**, 6718-6722.

2. – Introduction

The Paternò-Büchi (PB) reaction is a photochemical transformation in which a carbonyl compound **1** and alkene **2** are coupled (Figure 2.1a). It was first reported in 1909 by Emanuele Paternò,[1] but only in 1954 George H. Büchi identified and studied the mechanism.[2] The reaction is a hetero [2+2]-photocycloaddition, and the product is an oxetane **3**, a 4-membered O-containing cyclic compound. Besides being used in the synthesis of several linear and branched polymers,[3] the scaffold is present in many biologically active compounds and is studied for its pharmacophoric activity as bioisostere of the carbonyl group[4] (Figure 2.1b). The PB reaction is a simple one-step procedure for the synthesis of oxetanes and requires no additives and no prefunctionalised reagents. It comes with no surprise that, after first efforts by Büchi, several other chemists have investigated the mechanism of this transformation and have explored its generality.[5]

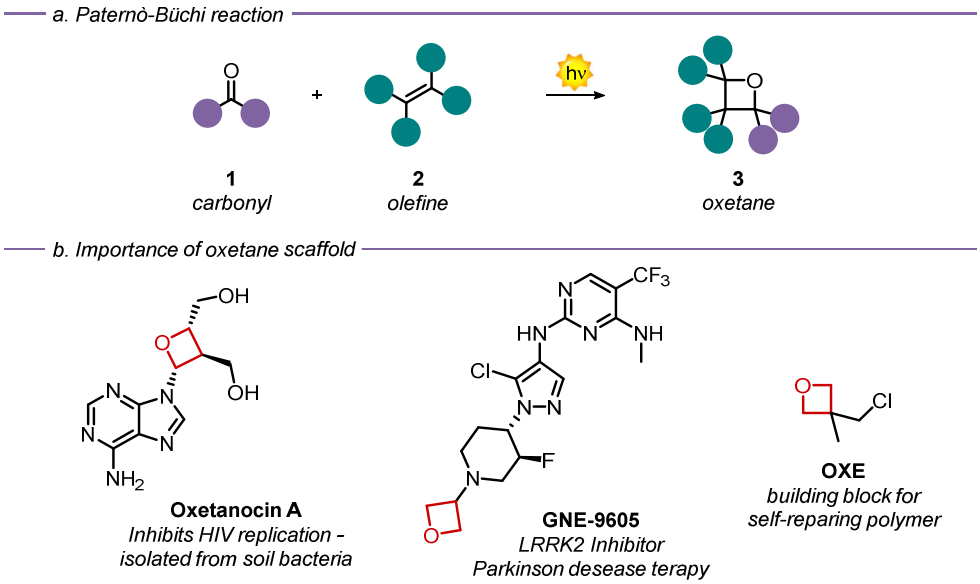

Figure 2.1. – a. General scheme of the Paternò-Büchi reaction. b. Oxetane containing compounds studied in different applications.

Mechanism of the reaction

Depending on the electronic features of the two reagents and on which species is excited, several mechanisms, with different intermediate species, have been shown for the PB reaction.[5d]

Generally, light is absorbed by the carbonyl partner **1**, triggering a $n_p \rightarrow \pi^*$ transition to the first singlet excited state **1-S$_1$** (Scheme 2.1). The half-filled n_p orbital is electrophilic, thus, it can react with olefins. Usually, fast ISC occurs, and the triplet state carbonyl compound **1-T$_1$** reacts with the olefin **2**. A triplet 1,4-diradical **4-T** is obtained, and this can close to the oxetane product **3** or go back to starting materials trough ISC processes. If the first ISC is slow enough (this usually happens with aliphatic aldehydes and napthaldehyde) the singlet excited carbonyl **1-S$_1$** can react with the alkene **2**. Also the singlet 1,4-diradical **4-S** that is formed can close to the oxetane product **3** or go back to starting material, but this happens through crossing of conical intersection (CCI) processes, as no change in multiplicity is needed. Additionally, ISC from the singlet **4-S** to the triplet diradical **4-T** can take place.[6]

Reaction mechanism

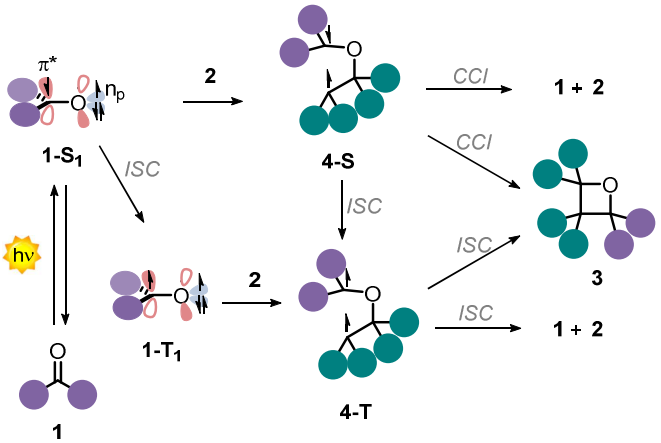

Scheme 2.1. – General reaction mechanism through carbonyl electrophilic singly-occupied n_p orbital.

With electron-poor olefins, carbonyls in their n_p-π^* state react through their $\pi\pi^*$ system, which is nucleophilic. Turro *et al.* proposed formation of exciplexes **6** from the orbital interaction of the π systems of excited carbonyls and ground-state olefins (Scheme 2.2).[7] They observed product formation only for singlet carbonyls. When triplet state carbonyls were generated, only alkene isomerisation and homocoupling was observed.[8] Product 7 is generated via a concerted or quasi-concerted mechanism, where the formation of the two new bonds happens at the same time. However, formation of a 1,4-diradical intermediate **8** has also been postulated.[9]

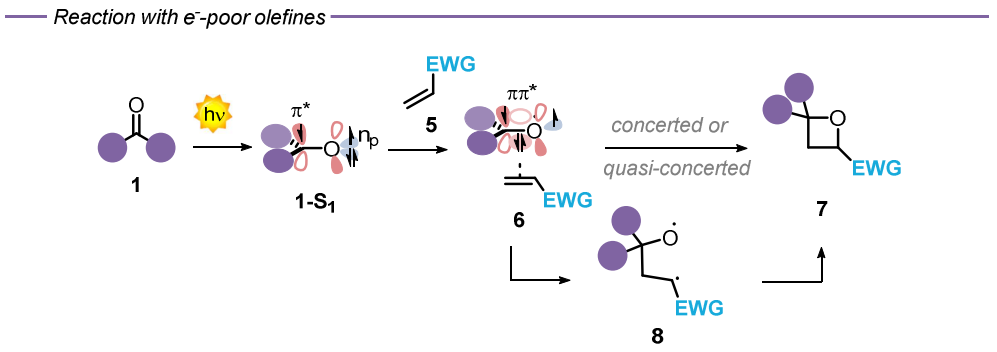

Scheme 2.2. – General reaction mechanism through carbonyl nucleophilic $\pi\pi^*$ system.

Mattay *et al.* studied the reaction of various ketones with electron-rich olefins,[10] in this case a charge transfer (CT) exciplex **10** is formed, which evolves to a 1,4-diradical **11**, that yields product **12** (Scheme 2.3). If the HOMO of the alkene is higher in energy than the reactive excited state of the carbonyl, a PET process from the olefin to the carbonyl takes place, forming radical ion pair **13**.[11] Experimentally, the feasibility of the process can be predicted using the Gibbs energy of PET equation derived by Rehm and Weller:[10a, 12]

$$\Delta G_{PET} = E^{ox}(D) - E^{red}(A) - \Delta E_{exc} + \Delta E_{coul}$$ Equation 2.1.

Where ΔG_{PET} is the Gibbs energy for a PET process, $E^{ox}(\mathrm{D})$ and $E^{red}(\mathrm{A})$ are the potential for the oxidation of the olefin (donor) and reduction of the carbonyl compound (acceptor), ΔE_{exc} is the energy gap between the carbonyl excited and ground states and ΔE_{coul} is a coulombic factor dependent on the solvent.

Radical ion pair **13** can give product **12** passing through the 1,4-diradical **11**[7, 13] or through zwitterion **14**.[14] The radical ion pair **13** is not easy to be distinguished from the exciplex **10** with high CT character.[10b] **13** and **10** can also undergo back electron transfer (BET) takes place,[5d] and radical ion pair **13** can also be separated by the solvent, to give solvent separated radical ions.

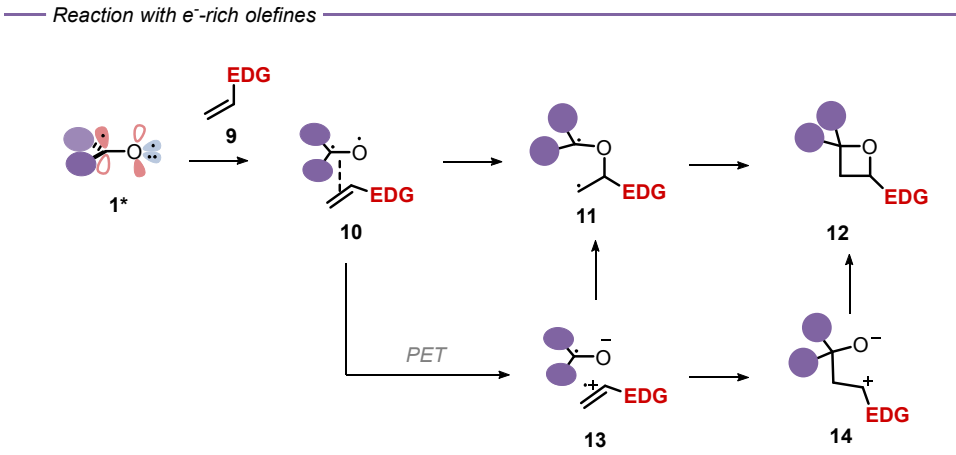

Scheme 2.3. – General reaction mechanism through CT exciplex **10**.

Additionally, the π-π* state of the carbonyl can be the reactive one in the case of conjugation with an extended π system, where the π-π* state is lower in energy than the n_p-π*. Usually, these transformations are more efficient, as fewer excited state decay is observed.[15] In this case the excited ketone has a

nucleophilic character and can also react through the conjugated olefin moiety to give cyclobutene products with the alkene partner.

When particularly electron-poor carbonyl compounds **15** are used in combination with very electron-rich olefins **9**, an association equilibrium in the ground state can be observed (Scheme 2.4).[16] The complex formed is usually referred to as electron donor acceptor complex (EDA complex), because by excitation of this new entity a PET occurs: the donor gives an electron to the acceptor, with formation of a radical ion pair **17**, which is consumed in the same ways of **13**. EDA complexes absorb light at longer wavelength respect to their non-associated components. This phenomenon can be useful if the EDA complex absorbs in the visible region, to avoid the use of UV light. Moreover, selective irradiation of non-associated carbonyl **15** or EDA complex can be achieved, as both are present in solution due to the existing equilibrium. When non-associated carbonyl **15** is irradiated, an exciplex similar to **10** is generated. In case of different geometry of radical ion pairs **17** and **13**, it is possible to achieve different stereoselectivity, because they are obtained from two different complexes **16** and **10** respectively. However, irradiation of the EDA complex usually is less effective because BET is faster for **16**, having a singlet multiplicity.[17]

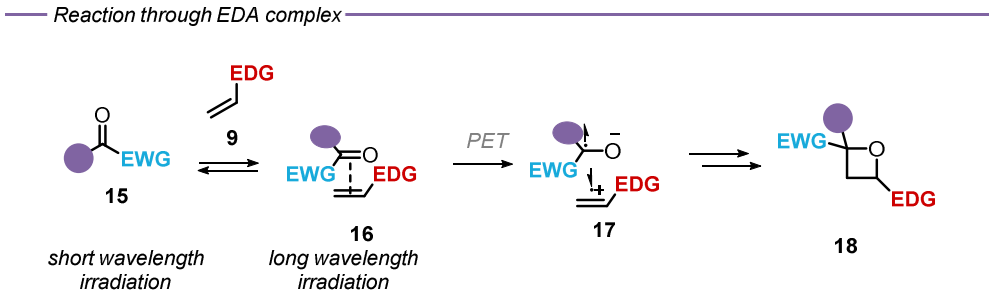

Scheme 2.4. – General reaction mechanism through EDA complex excitation.

Notably, using appropriate triplet photosensitizers, we can use longer wavelengths to generate triplet state carbonyls. Correspondingly, π-π* state of the alkene can be generated by energy transfer and can attack the carbonyl partner to yield the oxetane product.[18]

Selectivity in the Paternò-Büchi reaction

The importance of understanding the mechanism of a reaction is evident when considering the possible isomers that can be obtained. Depending on the mechanism, in fact, regio- and stereoselectivity can change.

Regioselectivity concerns the different combinations of relative orientations of the alkene and of the carbonyl. For carbonyls in their n_p-π* state reacting with electron-rich olefins **9**, the attack of the electrophilic O is directed toward the more electron-rich carbon. With electron-poor olefins **5** the exciplex formation is controlled by orbital overlap. The carbonyl C, where the electron density of the π* orbital is higher, connects with the less electron-poor carbon of the olefin.[19] In the case of radical-ion pairs, the regioselectivity will depend on charge distribution and spin densities of the atoms involved. In all cases steric factors can play a role inhibiting the expected selectivity (Figure 2.2).[5d]

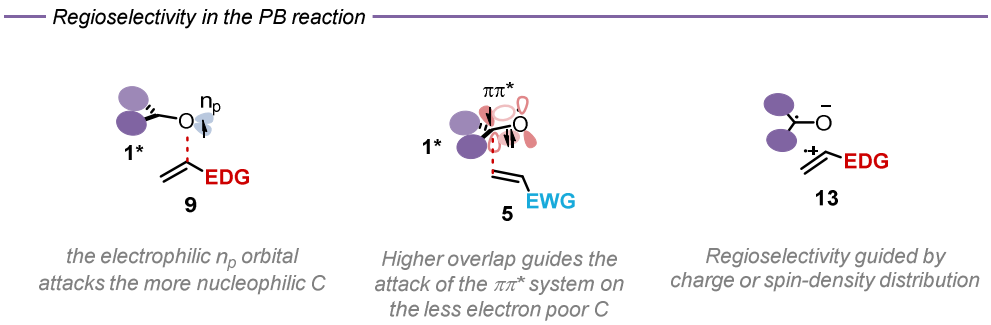

Figure 2.2. – Different factors guiding regioselectivity in PB reaction.

Stereoselectivity depends on the intermediate leading to the product and on their spin multiplicity. Reaction with electron-poor olefins are usually more

stereoselective because of orbital interactions in the exciplex.[20] Also when PET is taking place the reaction is typically highly stereoselective,[21] and the diasteroselectivity depends on the mechanism of initial formation of the covalent bond in the ion pair. For reactions going through a diradical intermediate **4**, the bond rotation must be taken into account, and for this reason stereoselectivity loss is observed with longer lived triplet diradicals.[22] In the case of triplet diradicals **4-T**, the stereoselectivity can be explained with the Griesbeck model (Figure 2.3).[23] This model takes into account the Salem and Rowland rules[24] for the bond formation in a triplet diradical. According to the model, this event occurs from a configuration in which the two half-filled orbitals are perpendicular, in order to minimise their interactions. The new bond is formed through an ISC and concerted rotation of one of these two orbitals.[25] When more than one possible geometry of the 1,4-diradical would lead to different stereoisomers, the more stable diradical influence the selectivity. In this case, attractive interactions, for examples H bonding, and repulsive interactions, such as steric hindrance, in the possible diradical intermediate must be considered.

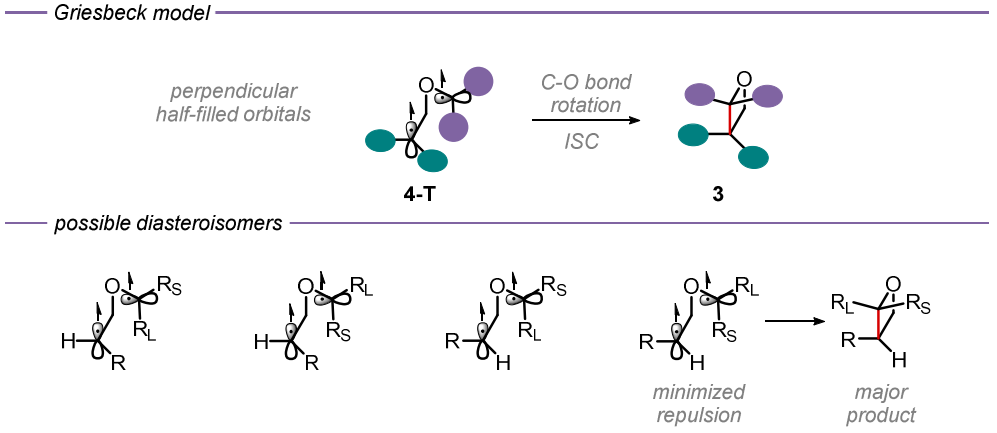

Figure 2.3. – Griesbeck model for diastereoselectivity in oxetane formation through triplet 1,4-diradical species.

Chapter II – Section 1

Visible-light Paternò-Büchi Reaction for the Dearomatisation of Indoles

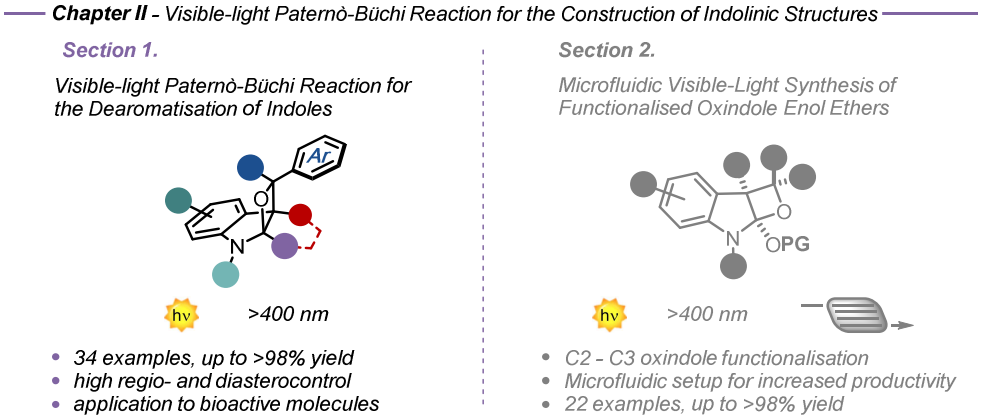

This Section shows the development of a visible-light mediated Paternò-Büchi reaction using benzophenone and related ketones. The choice of the wavelength proved fundamental for inhibiting side reactivity and allowed formation of oxetane products in high yield and selectivity. After showing gram-scale synthesis and product manipulation, the role of light and the mechanism of the reaction were studied as well.

This work has been published: Mateos, J.; Vega-Penaloza, A.; Franceschi, P.; Rigodanza, F.; Andreetta, P.; Companyo, X.; Pelosi, G.; Bonchio, M.; Dell'Amico, L. A visible-light Paterno-Buchi dearomatisation process towards the construction of oxeto-indolinic polycycles. *Chem Sci*, **2020**, 11, 6532-6538.

2.1.1. – Introduction

The generation of new chemical architectures starting from abundant, inexpensive materials is one of the main goals of the synthetic chemical community.[26] The evolution of 3-D molecular arrangements starting from planar π-systems is of particular interest due to the possibility of assembling complex polycyclic structures from readily available aromatic feedstocks. In this context, the polycycles originating from indoles are one of the most relevant class of pharmacophores, since their wide occurrence in natural alkaloids and drugs.[27] The development of effective methods towards the dearomatisation of indoles is an attractive strategy to access complex polycyclic indoline scaffolds. Light-driven dearomatisation methods are recently emerging as a complementary sustainable approach to accessing strained polycyclic systems, difficult or impossible to obtain under polar reactivity (Scheme 2.5).[28] In fact, the common strategy for the photochemical construction of this polycycles rely on the use of energy transfer (EnT) photocatalysts capable of sensitise indole moities.[29]

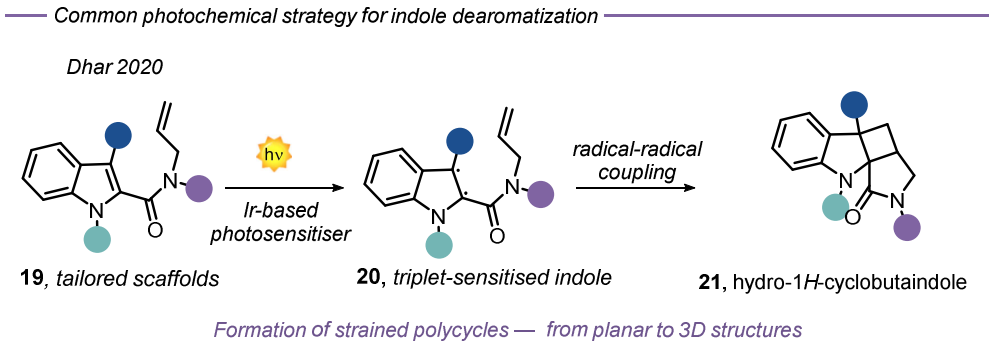

Scheme 2.5. – Common photosensitized strategy for the dearomatisation of indoles.

On the other hand, the formation of heterocyclic polycycles such as oxetanes is of wide interest.[4] Oxetanes are present in a variety of biologically active molecules, being promising structural modules in drug discovery. [30] Regrettably, the construction of oxetane-based polycyclic scaffolds is a challenging synthetic task owing to the high ring-strain of this heterocycle when compared to the all-carbon analogue. PB reaction can be the perfect tool for the assembly of these complex biorelevant structures.[5d] However, progresses towards large-scale syntheses have been largely hampered by the need of UV-light sources (Hg or Xe lamps) together with the corresponding specific reaction setups (e.g. quartz vessels). Further limitations of the reported PB methodologies are posed by the lack of generality and selectivity, leading to high substrate-dependency and poor regio- and diastereocontrol.[5b, 5d] These drawbacks have precluded the development of general and scalable PB methods for the dearomatisation of heterocycles,[31] including indoles (Scheme 2.6).[32] In facts, the realization of such a general method is complicated by additional synthetic issues, including: *i*) the polar aldol-type addition between the reagents; *ii*) the electronic nature of the indole's alkene moiety, which has to match with the amphoteric nature of the excited carbonyl species; and not less important *iii*) the presence of light-driven side reactions, such as the dimerization of the carbonyl compound.[33]

main issues: *UV light/Hg-lamp - low regio- and diasterocontrol - substrate dependent - low yields*

Julian 1973

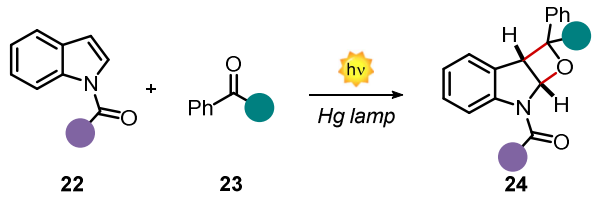

22 23 24

Machida 1983, 1988 and 1994

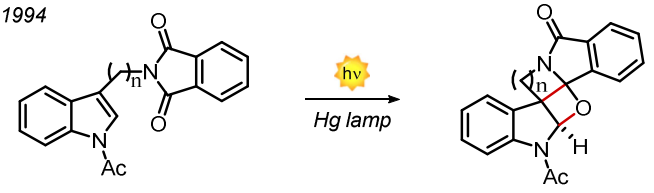

25 26

Machida 1985 and 1988

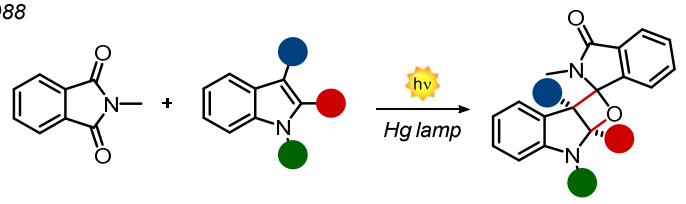

27 28 29

Scheme 2.6. –Main issues in the previous examples of dearomatisation of indoles using PB reaction.

2.1.2. – Aim of the project

Due to the high relevance of oxetanes, both in natural products and synthetic molecules, this reaction has an immense synthetic potential.[5b] The successful development of a PB reaction with indoles would open the way to the construction of biorelevant indolinic scaffolds with up to three contiguous stereocenters in one step, from readily available aromatic feedstocks. However, a general and efficient process has yet to be developed, due to the above-mentioned obstacles. From a broader perspective, a general and scalable light-driven indole dearomatisation process should also involve the use of visible-light

(>400 nm), thus avoiding side reactions, potential product decomposition as well as the need of sophisticated reaction setups.[34] We envisaged that the PB reaction, where the direct excitation of a carbonyl compound triggers a [2+2]-heterocycloaddition with an olefin, could yield strained polycycles in a single step avoiding the use of EnT photocatalysts.

2.1.3. – Results and discussion

Reaction optimisation

We started our study investigating the reaction of different indoles **30a-d** with benzophenone **31a**. 3-Benzyl indoles were selected as substrates with the aim of generating a valuable all-carbon quaternary stereocenter within product **32** (Table 2.1). Irradiation at 365 nm of an equimolar mixture of unprotected 3-benzyl indole **30a** and benzophenone **31a** in toluene resulted in the complete recovery of unreacted starting materials (Table 2.1, entry 1). Similarly, *N*-methyl indole **30b** was fully recovered, together with formation of trace amounts of **33**. We reasoned that reducing the electron density on the indole double bond would facilitate its reactivity with the triplet (T_1) biradical excited state of **31a**. Indeed, subjecting the *N*-Boc indole **30c** to the reaction conditions furnished the strained fused oxetane **32c**, albeit in modest yield (17%). In fact, extensive UV-light irradiation led to increasing amounts of the dimer **33** along with product decomposition. To further modulate the electronics of the reactive double bond, we placed a methyl group at C2-position of the indole (**30d**). In this case, prolonged reaction times (5h, Table 2.1, entry 4) resulted in improved reaction performances (55% yield). Nevertheless, marginal amounts of **33**, hindering the isolation of **32d**, were still detected. At this point, a screening of different solvents showed no beneficial effects on the yield nor on the suppression of the formation of **33** (Table 2.1, entries 5 and 6).

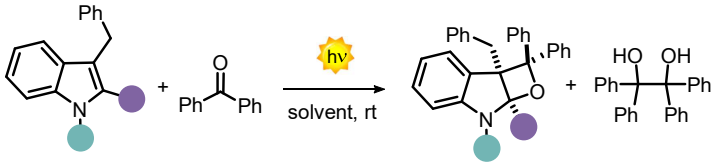

30 0.1 mmol **31a** 1 eq. **32** **33**

entry	●	●	**30**	*reaction time*	*solvent*	*light source*	*(32) yield %*	*dr*
1	H	H	**30a**	3 h	PhMe	365 nm	- **32a**	-
2	Me	H	**30b**	3 h	PhMe	365 nm	- **32b**	-
3	Boc	H	**30c**	3 h	PhMe	365 nm	17 **32c**	>20:1
4	Boc	Me	**30d**	5 h	PhMe	365 nm	55 **32d**	>20:1
5	Boc	Me	**30d**	5 h	MeCN	365 nm	35 **32d**	>20:1
6	Boc	Me	**30d**	5 h	CH_2Cl_2	365 nm	nr **32d**	-

Table 2.1. – Initial optimisation of the reaction conditions between indoles and diaryl ketones.

At this point, reasoning on the possible competitive photoreaction giving rise to formation of **33**, we assumed that an inferior amounts of T_1 ketone excited state could preferentially channel the system towards the intended PB reactivity. This is consistent with the operation of two alternative side-reaction pathways *i* and *ii* that can stem from the generation of excited benzophenone **31a*** (Scheme 2.7).[35]

i) On one hand, excited aromatic ketones in presence of electron-rich amines, such as electron-rich nitrogen heterocycles **30b**, are reported to undergo PET processess (Scheme 2.7a). In this case, one molecule of **34** reduces the T_1 state of **31a** in favour of the corresponding ketyl radical **35**. Then, **35** deprotonates the acidic α-position of **36** triggering the formation of the pinacol product **33**. This is in line with the observed experimental trend when passing from **30a** to **30d**. For this reason, the indole protecting group plays an important role in the reaction outcome.

ii) On the other hand, excited aromatic ketones are well known hydrogen atom abstractors. When using solvents with a low C-H bond dissociation energy (BDE), such as toluene, (C-H BDE = 89.6 kcal·mol^{-1})[36] the protonated ketyl radical **35-H** is directly formed after HAT. Thus, favouring the homodimerisation towards **33**.

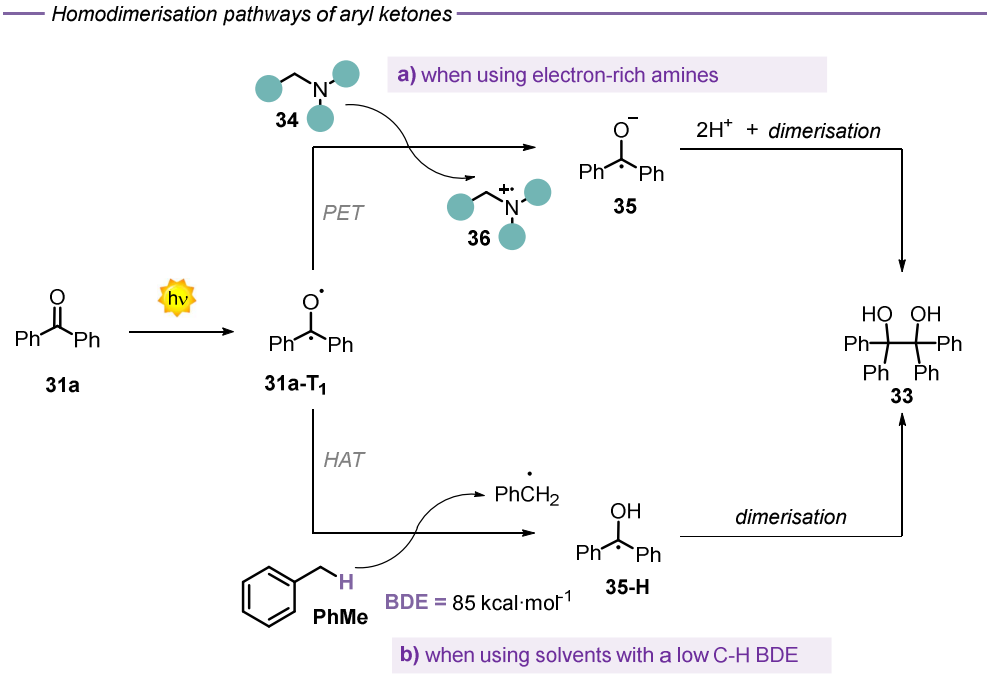

Scheme 2.7. – The two possible pathways behind the homodimerisation of diaryl ketones. a) PET pathway. b) HAT pathway.

In both cases, this side-reaction can be avoided decreasing the amount of **31a-T_1**. Hence, we decided to investigate the role of the light source to reduce the amount of T_1 excited state. Firstly, we employed a light source with a maximum emission set at 400 nm (vs 365 nm), close to the limit of absorption of benzophenone **31a**. Interestingly, despite the reaction was slower (9 hours to

reach full conversion), **33** was only detected in trace amounts along with a promising 67% isolated yield of **32d** (Table 2.2, entry 1). A slightly red-shifted light source, resulted in the optimal balance between reactivity and reaction time, delivering **32** in quantitative yield and complete diastereocontrol after 12 h (Table 2.2, entry 2). Importantly, neither homodimer **33** nor product decomposition were detected. An additional solvent screening revealed acetone to be the best solvent for the present system, with quantitative formation of **32d** (>98% yield) in reduced reaction time (7 h in entry 3 vs 12 h in entry 2). Under these conditions product **32d** was obtained by simple solvent evaporation. Interestingly, the C-H BDE of acetone is higher than that of toluene, further suppressing the formation of pinacol by-product.

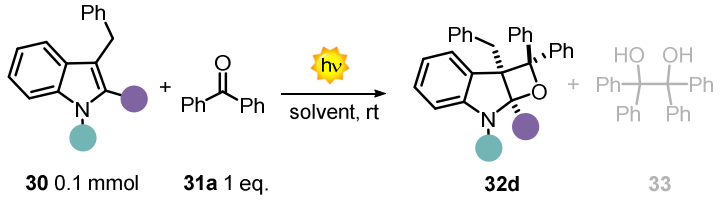

entry	●	●	**30**	*reaction time*	*solvent*	*light source*	*(19) yield %*	*dr*
1	Boc	Me	**30d**	9 h	PhMe	400 nm	67 **32d**	>20:1
2	Boc	Me	**30d**	12 h	PhMe	405 nm	>98 **32d**	>20:1
3	Boc	Me	**30d**	7 h	Acetone	405 nm	>98 **32d**	>20:1

Table 2.2. – Rational optimisation of the reaction conditions.

Generality of the reaction

Having found optimal conditions for the generation of **32d**, we next explored the generality of this visible-light PB reaction. Since toluene (PhMe) and acetone (ace) gave quantitative yields in the optimised conditions, all the reactions were performed in both solvents, providing a general evaluation of the synthetic protocol.

When looking at the substitution effects in the indole moiety (Table 2.3), 3-benzylindoles with substituents at the ortho, meta and para positions furnished the corresponding tricyclic products **37**-**41** in high yields spanning from 72% to >98% and complete diastereocontrol. 3-Methyl and 3-hydroxymethyl indoles formed products **42** and **43** as single diastereoisomers in excellent yields (up to 85%). Remarkably, the reaction of 3-allylindole produced the oxetane **44** in up to 67% yield with exquisite site-, regio- and diastereoselectivity. Indole derivatives bearing different substituents on the aromatic ring (**45**-**48**), diverse *N*-protecting groups (**49** and **50**) as well as various C2-substituents (**51** and **52**) efficiently participated in the visible-light PB reaction, furnishing diversified strained tetrahydrooxeto[2,3-*b*]indole scaffolds in yields up to 92% and >20:1 dr.

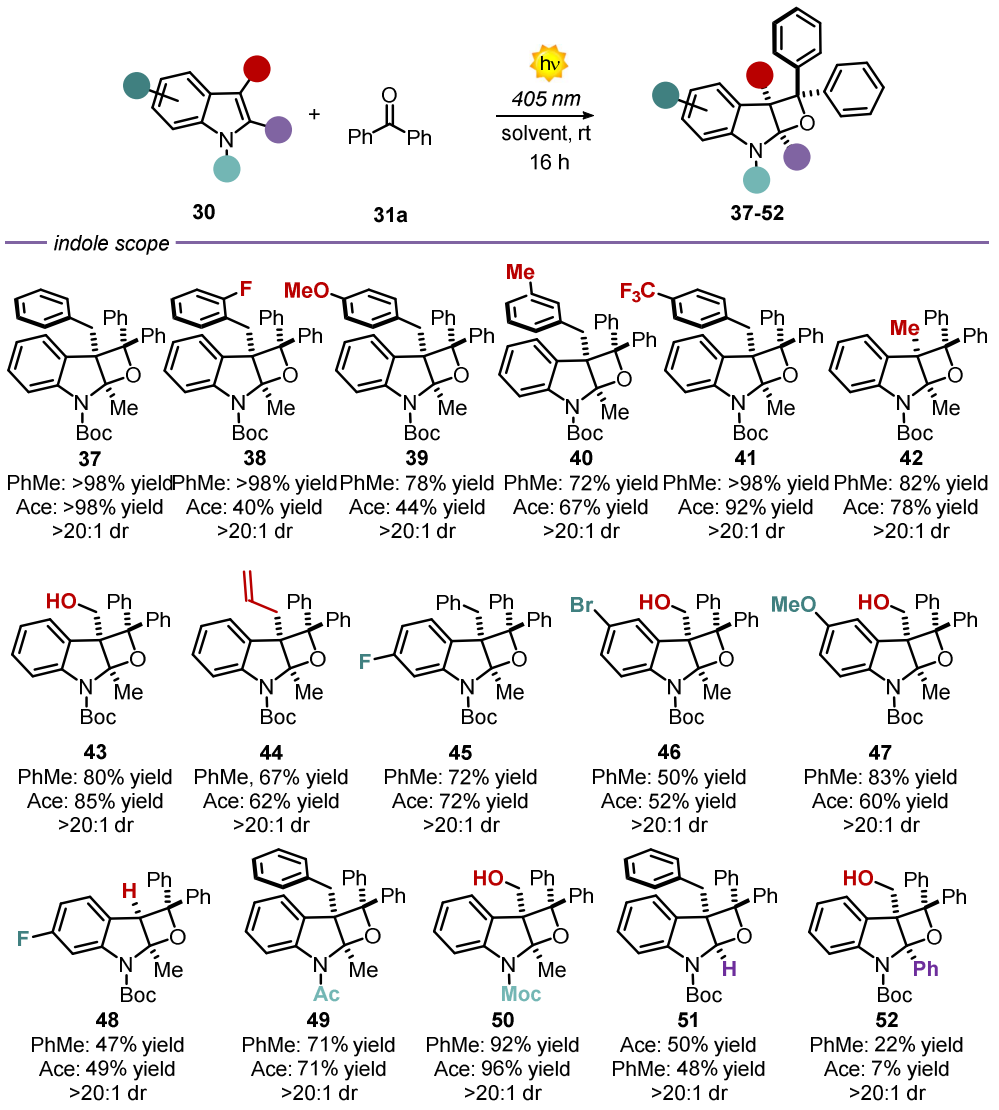

Table 2.3. – Substrate table when using different indole derivatives.

When moving to different substituted benzophenones, the reaction performed smoothly (Table 2.4) forming the corresponding product **53**-**57** in high yields (up to 86%) and excellent diastereocontrol (>20:1).

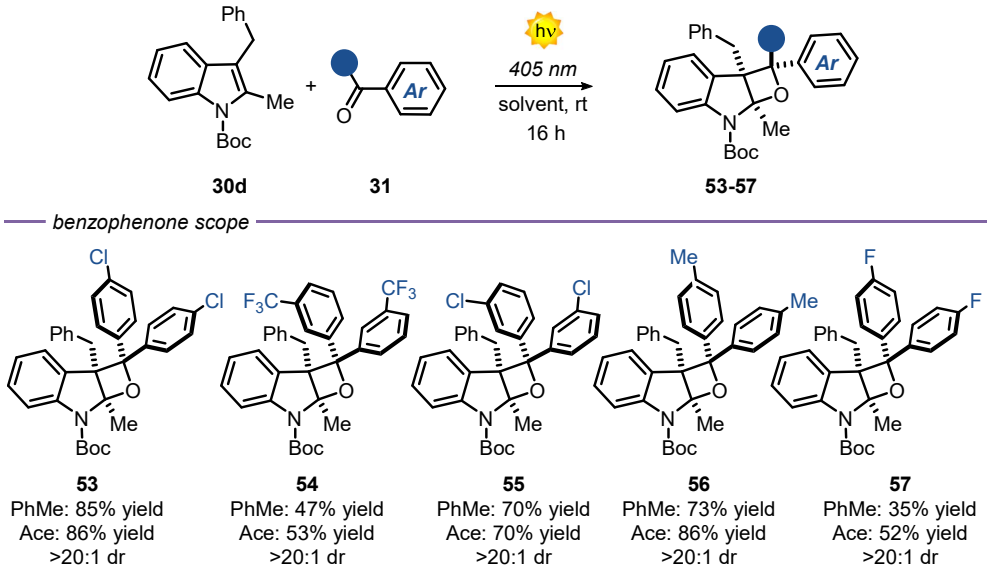

Table 2.4. – Substrate table when using different benzophenone derivatives.

Remarkably, also the prochiral benzil **31b** successfully engaged in the [2+2]-heterocycloadditon process, delivering up to 0.50 g of dearomatized product **58** in batch conditions (>98% yield) with complete diastereocontrol over the three generated stereocenters (Table 2.5). Its relative stereochemistry was inferred by X-ray analysis on single crystal. Diverse benzil derivatives yielded products **59-61** quantitatively and with complete diastereocontrol. Also, differently substituted indoles performed well, delivering the products **62** and **63** in up to 85% yield. For all the benzil derivatives, 465 nm illumination could be employed, thanks to their more red-shifted absorption, moreover no traces of side products were observed.

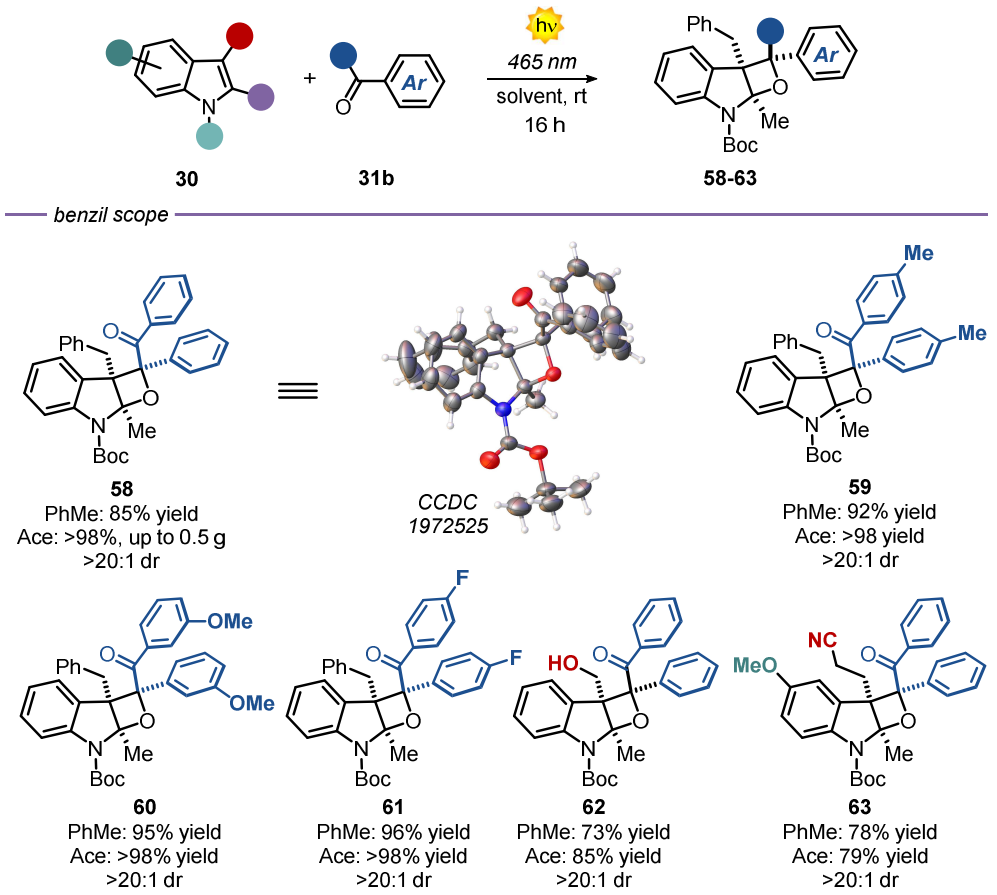

Table 2.5. – Substrate table when using different benzil derivatives.

We next sought to apply the developed dearomatisation protocol to accessing relevant bioactive pharmacophoric cores (Table 2.6). A series of oxeto-indolinic derivates **64-67**, bearing up to three contiguous stereocenters, were synthesised in high yields (48%-82%) and complete diastereocontrol. Further, marketed drugs such as Melatonin proved a useful substrate for the present method, affording the corresponding product **68** in 42% yield. Thus, demonstrating the synthetic potential of the developed method towards structural modifications of bioactive ingredients. Interestingly, enantiopure *N*-protected Tryptophan took part in the developed method both with **31a** and benzil **32b**, delivering

attractive chiral tetrahydrooxeto[2,3-*b*]indole **69** and **70** in high yields and 2.5:1 to 5:1 dr, respectively.

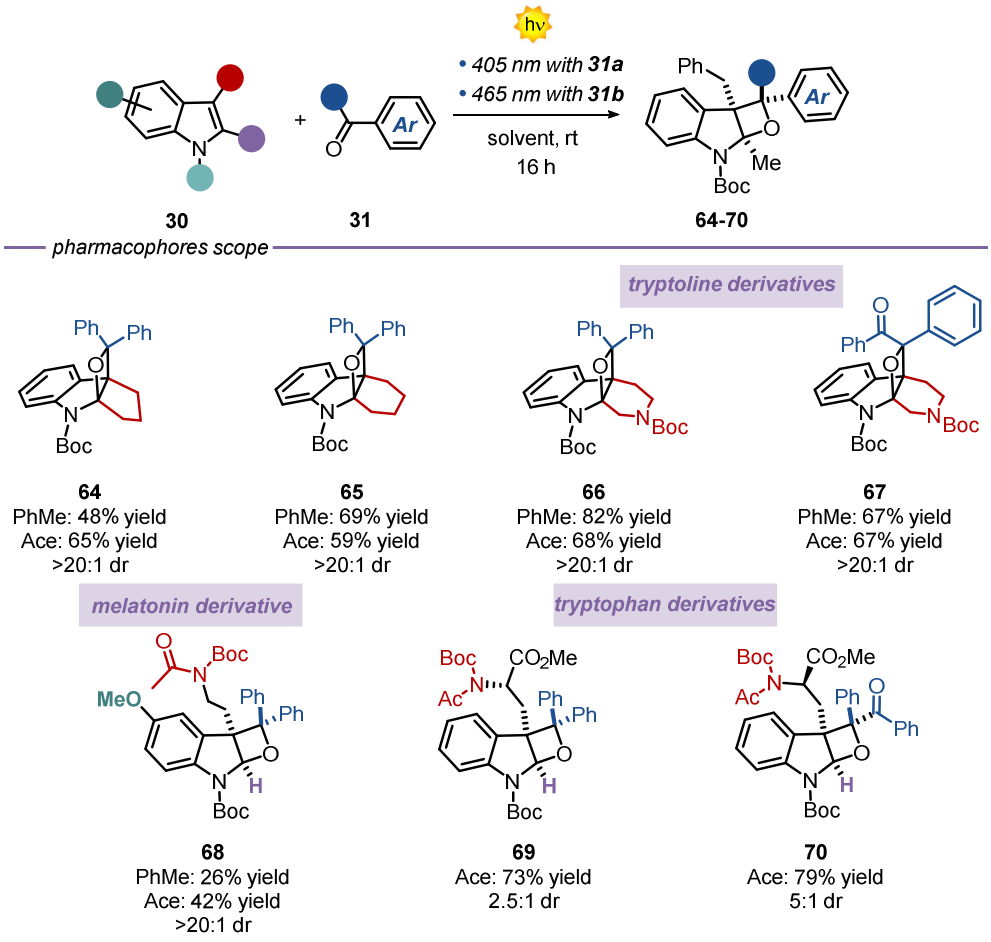

Table 2.6. – Substrate table when using different pharmacophore derivatives.

Gram-scale synthesis and product manipulation

At this point, we wanted to further demonstrate the generality and the operational simplicity of the developed method. For this reason, the benchmark reactions of indole **30d** with ketones **31a** and **31b** were performed under sunlight irradiation. Both reactions performed smoothly delivering the

corresponding products **32** and **58** in 96% and 86%, within 6 h reaction time (Scheme 2.8a).

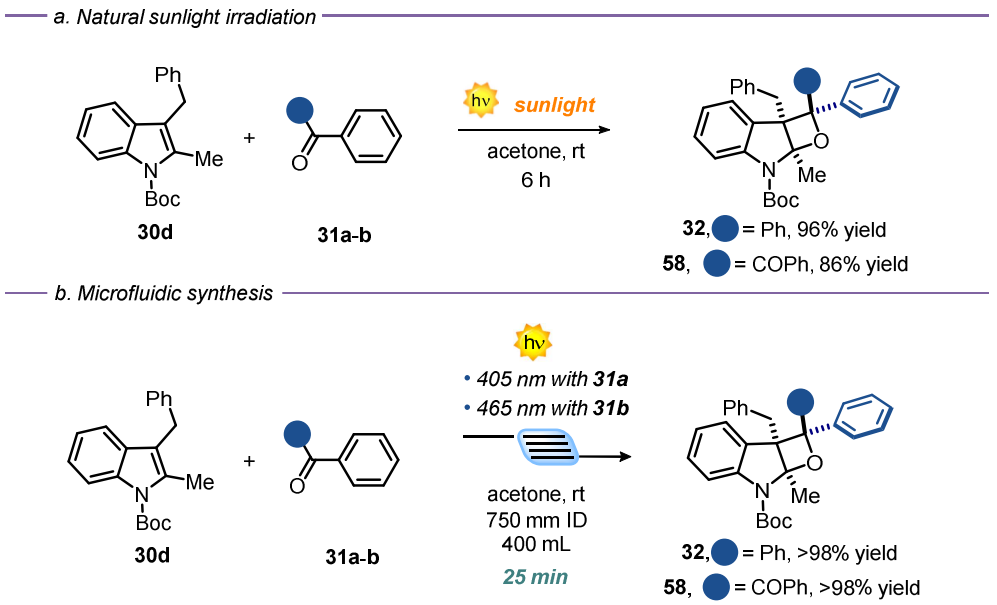

Scheme 2.8. – a. Natural sun irradiation for synthesis of **32** and **58**. b. Small scale microfluidic synthesis of **32** and **58**.

Additionally, the synthetic method was implemented under a microfluidic photoreactor (Scheme 2.8b). The oxeto-indolinic products **32** and **58** formed rapidly, within 25 min residence time, in quantitative yields. Encouraged by these results, we set up a larger-scale microfluidic synthesis of **43**, which was obtained with improved synthetic performances and productivity with respect to the batch setup (96% yield and 0.176 mmol·h^{-1} in flow vs 80% yield and 0.080 mmol·h^{-1} in batch). The microfluidic setup allowed the isolation of **43** in up to 1.20 g within 15 h (Scheme 2.9).

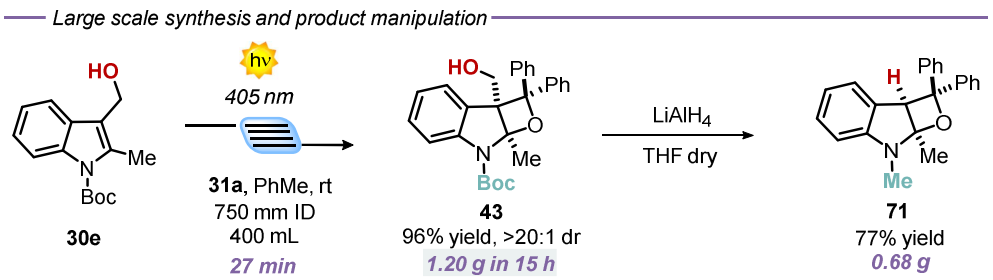

Scheme 2.9. – Microfluidic gram-scale synthesis of **43** and manipulation.

Thanks to the larger-scale synthesis of compound **43**, we were able to study its manipulation (Scheme 2.9). The use of $LiAlH_4$ delivered the *N*-methyl protected tetrahydrooxeto[2,3-b]indole **71** in 77% yield (0.68 g) with the unexpected formal removal of the hydroxymethyl group. It should be noted that *N*-methyl indoline-alkaloids possess widespread biological activities,[26] and the oxeto-scaffold **58** is an unprecedented representative of this class of molecules.

Mechanistic considerations

After having evaluated the generality and limits of the present PB process, we investigated the photochemical bases of the observed reactivity. Over imposing the absorption spectrum of benzophenone **31a** (under the optimised conditions) with the 405 nm LED emission spectrum, revealed a region (390-400 nm) of possible absorption (Figure 2.4), confirming that the direct excitation of **31a** can take place also under visible light illumination

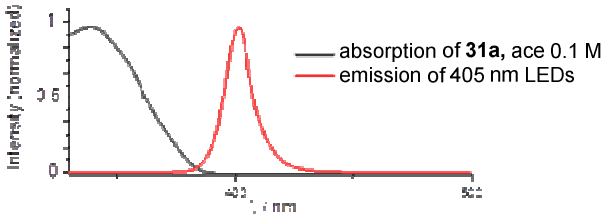

Figure 2.4. – Normalized absorption of **31a** vs normalized emission of the 405 nm LEDs used in this study.

We then evaluated any possible ground- or excited-state association of the reagents.[37] The absorption spectra of the isolated species (**30d** and **31a**) and the reaction mixture (**30d** + **31a**) did not present any significant spectral variations. Instead, Stern-Volmer analysis of **31a** excited state revealed an efficient quenching of the T_1 by **30d** (Figure 2.5), with no detection of excimer emission spectra. Analogous analysis with **31b** lead to the same results. Taken together, these observations point to a direct excitation of **31a** and **31b** under visible light towards the formation of its S_1 state, which rapidly decays to the T_1 excited state, followed by the indole trapping.

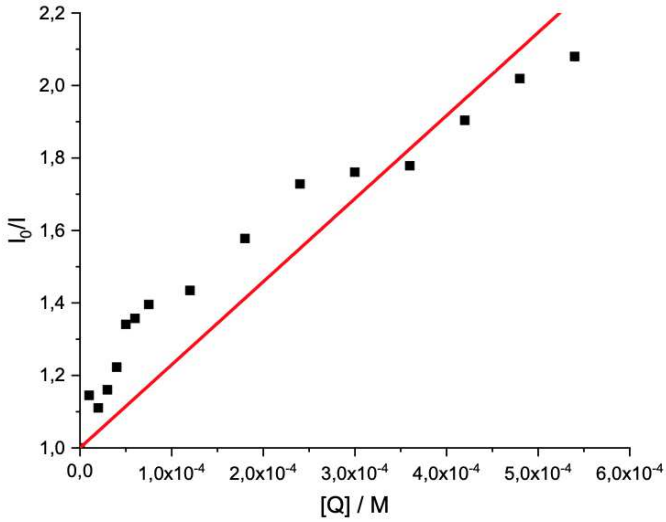

Figure 2.5. – Stern-Volmer of **31a** in the presence of **30d** in MeCN. (λ_{ex}=365 nm)

This mechanistic hypothesis was further confirmed by performing control experiments in the presence of an effective tertiary-amine T_1 quencher[38] such as DABCO[38a] (1,4-diazabicyclo[2,2,2]octane, Scheme 2.9a). When the reactions between **30d** and ketone **18a** or **18b** were performed in the presence of 1 equiv. of DABCO the reactivity dropped dramatically, demonstrating that the T_1 excited state of the carbonyl counterpart is the key reactive intermediate with both carbonyl reagents. However, diverse reaction mechanisms may originate from the T_1 excited state. The conventional PB reaction involves a radical combination between the T_1 excited state of the aromatic ketone and the indole (see Paragraph 2). An alternative mechanistic scenario deals with PET from the electron-rich indole to the ketone, to generate a radical ion pair which rapidly collapses into the final oxetane (Scheme 2.9b). To evaluate the feasibility of this process, we calculated the ΔG_{PET} from the Gibbs energy of PET equation (see

Paragraph 2). For the reaction with benzophenone **31a** we found a ΔG_{PET} = +1.35 eV, corresponding to 28.83 kcal mol^{-1}. This value indicates that the operation of a PET process is unlikely. Having already excluded ground- and excited state associations of the starting materials, the only feasible pathway is a radical trap by the indole **30d** of the T_1 state of the aromatic ketone, where the regio- and stereocontrol are governed by steric factors (see intermediate **73**). On the other hand, for benzil **31b**, we calculated a $\Delta \mathbf{G_{PET}}$ = 0.27 eV (6.23 kcal mol^{-1}), thus indicating the feasibility of the PET mechanism (path b, Scheme 2.9b). On these grounds, we proposed two alternative yet convergent reaction paths that are summarized in Scheme 2.9b. As mentioned in Paragraph 2, a PET mechanism usually leads to a higher diasteroselectivity, this matches well with the observed complete regio- and diastereoselectivity (Scheme 2.9b, path b). After the initial PET from **30** to **31b***, a reactive radical ion pair **72** is formed. The regioselectivity of the C–O bond-forming event is controlled by the relative charge distributions and further reinforced by steric factors. The stereoselectivity of the process is secured by the cyclic indole reagent, with the formation of a cis-oxetane. The high stereocontrol over the third stereocenter can be explained with respect to the same intermediate **72**, which rapidly collapses into the final oxetane product (Scheme 2.9b). Interestingly, intermediate **72** is stabilised by a favorable π–π stacking between the two aromatic rings. In fact, when the same reaction was performed with the *N*-Boc protected pyrrole the final product was obtained as a mixture of diastereoisomers (86% yield and 2.2 : 1 dr).[31c] Hence, the presence of the aromatic ring within the indole precursor **30** is essential to ensure the diastereocontrol of the process and corroborates the proposed mechanistic hypothesis.

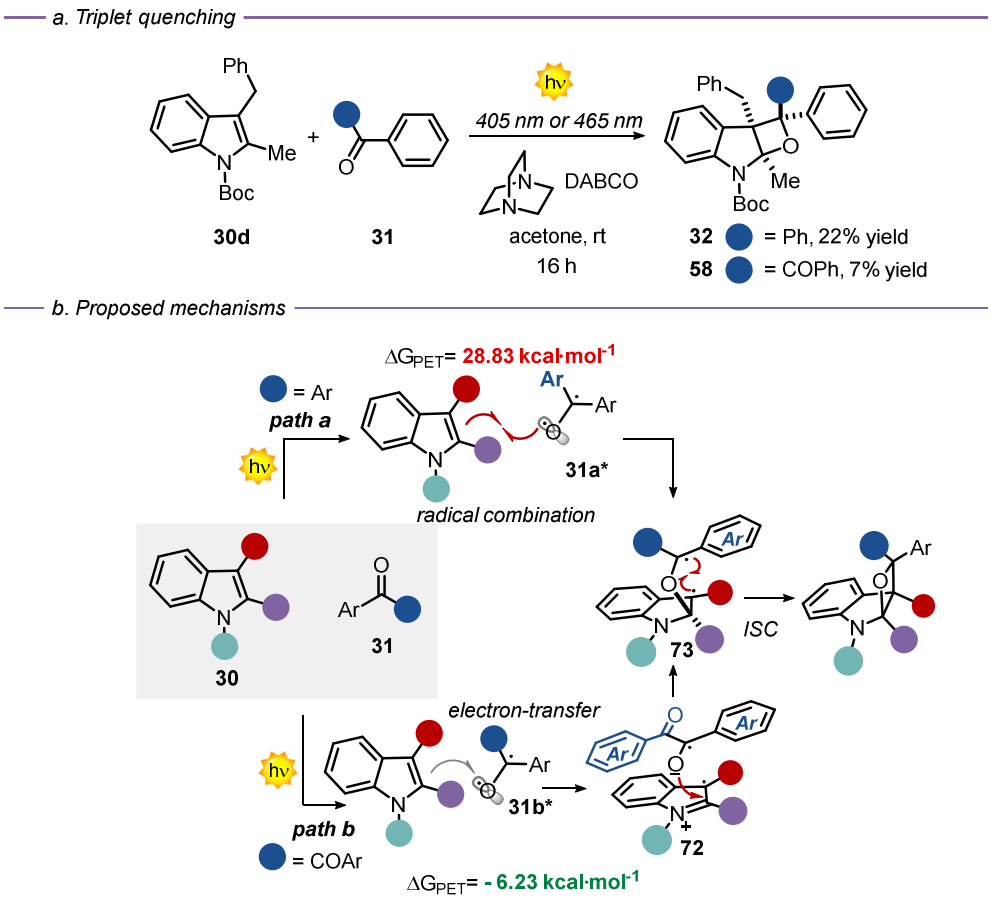

Scheme 2.9. – a. Quenching experiments with DABCO. b. Proposed mechanisms.

2.1.4. – Concluding remarks

In summary, this section reports an extremely mild visible-light PB process able to access strained oxeto[2,3-*b*]indole scaffolds starting from readily available substrates. This has been accomplished by the careful selection of the visible light source (405 or 465 nm), which enabled the complete shutting down of the ketone dimerisation side reaction. The generality of the PB process has been demonstrated for a large variety of indoles and aromatic ketones with excellent results (up to >98% yield and complete dr). Importantly, the reaction is

applicable to the assembly of diverse pharmacophoric cores and for the installation of oxetanes into diverse indole-based marketed drugs. Further, the reaction can be easily performed under sunlight as well as into a microfluidic photoreactor with definite advantages in terms of scalability (g scale), generality and productivity (up to 0.176 $mmol \cdot h^{-1}$). Finally, oxeto-indolinic products can be easily converted into biorelevant *N*-methylated counterparts (up to 0.68 g).

Despite the broad generality of the method, we found two main limitations. In the first case, a limitation is posed by the use of visible-light sources, hindering the use of benzaldehyde and acetophenone derivatives This class of molecules represent an important category of prochiral carbonyl compounds. Nevertheless, the marked UV absorption of these two families prevented the application of the developed method. In the second case, the instability of the oxeto-indolinic products presents an important limitation to the isolation of different compounds and limiting the manipulation of this scaffold. This fact can be ascribed to the instability of this polycyclic scaffolds towards a retrocyclic reaction.

2.1.5. – Experimental section

The NMR spectra were recorded on Bruker 400 Avance III HD equipped with a BBI-z grad probe head 5mm and Bruker 500 Avance III equipped with a BBI-ATM-z grad probehead 5mm. The chemical shifts (δ) for ^{1}H and ^{13}C are given in ppm relative to residual signals of the solvents ($CHCl_3$ @ 7.26 ppm ^{1}H NMR, 77.16 ppm ^{13}C NMR, Acetone @ 2.09 ppm ^{1}H NMR, 30.60 ppm ^{13}C NMR). Coupling constants are given in Hz. The following abbreviations are used to indicate the multiplicity: s, singlet; d, doublet; t, triplet; q, quartet; m, multiplet; br, broad signal.

The ^{1}H, ^{13}C and ^{19}F NMR spectra are available in literature free of charge.[39]

High-Resolution Mass Spectra (HRMS) were obtained using Waters GCT gas chromatograph coupled with a time-of-flight mass spectrometer with electron ionization (EI).

Chromatographic purification of products was accomplished using flash chromatography on silica gel (SiO_2, 0.04-0.063 mm) purchased from Machery-Nagel, with the indicated solvent system according to the standard techniques. Thin-layer chromatography (TLC) analysis was performed on pre-coated Merck TLC plates (silica gel 60 GF254, 0.25 mm). Visualization of the developed chromatography was performed by checking UV absorbance (254nm) as well as with aqueous ceric ammonium molybdate and potassium permanganate solutions. Organic solutions were concentrated under reduced pressure on a Büchi rotary evaporator.

Materials: Commercial grade reagents and solvents were purchased at the highest commercial quality from Sigma Aldrich or FluoroChem and used as received, unless otherwise stated.

The reaction set up images are available free of charge in literature.[39]

Light sources emission spectra

The following spectra were recorded using an AvaSpec ULS3648 high-resolution fiber-optic spectrometer which was placed at a fixed distance of 0.5 cm from the light source.

(*more info at*: *https://www.avantes.com/products/spectrometers/starline/item/209-avaspec-uls3648-high-resolution-spectrometer*).

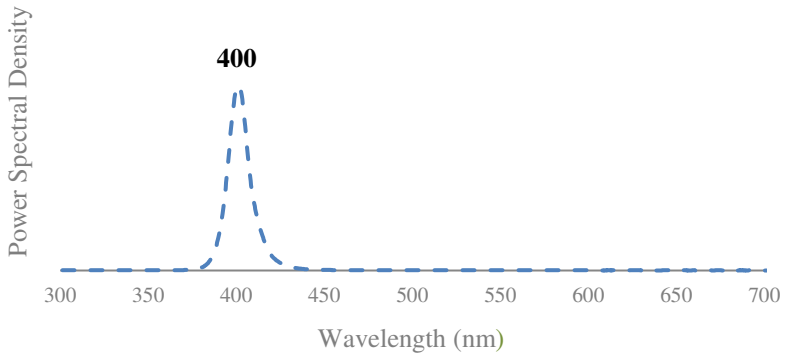

Figure Exp2.1. – Emission spectra of the 400 nm LEDs used in this section.

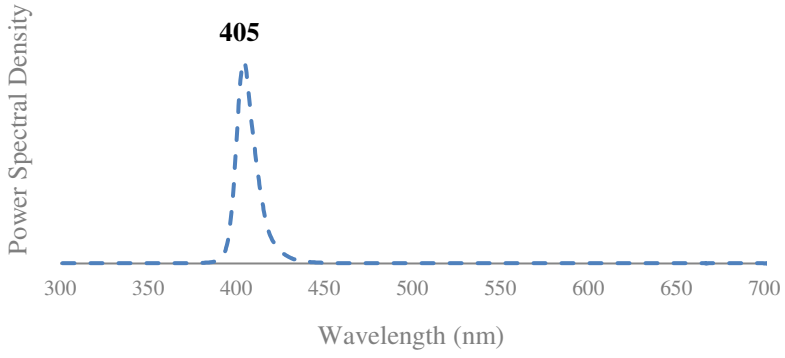

Figure Exp2.2. – Emission spectra of the 405 nm LEDs used in this section.

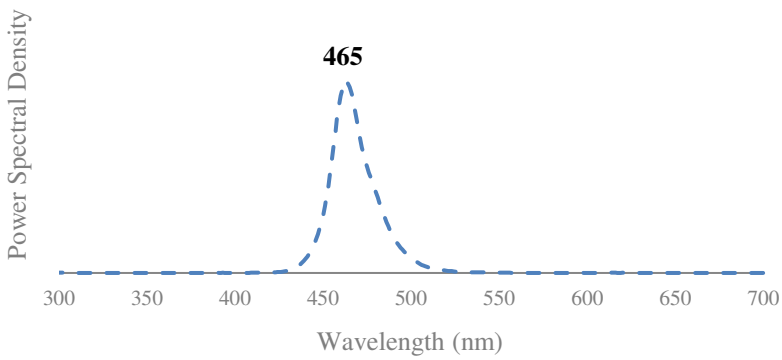

Figure Exp2.3. – Emission spectra of the blue LEDs used in this section.

Synthesis and characterization of the used indole derivatives

Preparation of 3-benzyl-sustituted indoles as synthetic precursors

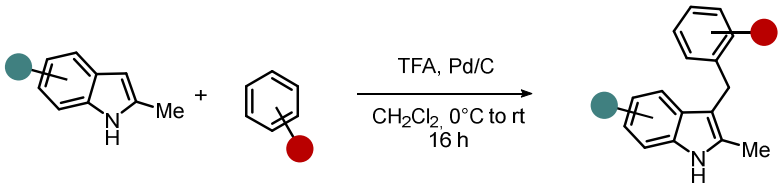

In a two-necked round bottom flask, a solution of 2-methylindole (0.66 g, 5 mmol) and benzaldehyde (765 µL ,7.5 mmol) in dichloromethane (25 mL, 0.2 M) was added to a stirring ice-cold mixture of trifluoroacetic acid (38 µL, 0.5 mmol, 10 mol%) and Pd/C (5 wt%) in CH_2Cl_2. This flask was filled with hydrogen and the mixture was stirred at 0 °C. After full consumption of the starting material, monitored by TLC (2% acetone in hexane), the palladium on carbon was filtered and the solvent was concentrated under reduced pressure. The crude product was purified by chromatography (9:1, hexane:EtOAc), giving 2-methyl-3-benzyl indole as a white solid that turned red overtime (1.04 g, 94% yield).

3-benzyl-2-methyl-1*H*-indole (30b)

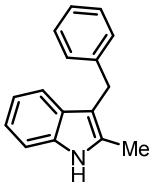

^{1}H-NMR (400 MHz, $CDCl_3$): δ: 7.73 (*br* s, 1H, NH), 7.38 (d, *J* = 8.0 Hz, 1H, Ar), 7.27 – 7.20 (m, 5H, Ar), 7.16 – 7.07 (m, 2H, Ar), 7.03 – 7.00 (m, 1H, Ar), 4.06 (s, 2H, CH_2), 2.37 (s, 3H, CH_3) ppm. **^{13}C-NMR (101 MHz, $CDCl_3$):** δ 141.6, 135.3, 131.6, 128.9, 128.2, 125.6, 121.0, 119.2, 118.4, 110.6, 110.1, 30.1, 11.8. ppm.

3-(2-fluorobenzyl)-2-methyl-1*H*-indole

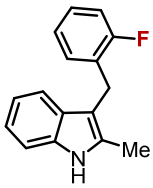

^{1}H-NMR (400 MHz, $CDCl_3$): δ 7.81 (*br* s, 1H, NH), 7.46 (d, *J* = 8.0 Hz, 1H, Ar), 7.31 (d, *J* = 8.0 Hz, 1H, Ar), 7.16 – 6.96 (m, 6H, Ar), 4.10 (s, 2H, CH_2), 2.43 (s, 3H, CH_3) ppm. **^{13}C-NMR (101 MHz, $CDCl_3$):** δ 162.2, 159.7, 150.8, 135.3, 131.9, 130.4 (d, *J* = 4.5 Hz), 128.8, 128.4 (d, *J* = 8.0 Hz), 127.4 (d, *J* = 16.4 Hz), 123.9 (d, *J* = 3.6 Hz), 121.1, 119.3, 118.3, 115.1 (d, *J* = 22.9 Hz), 110.2, 109.1, 22.8 (d, *J* = 4.1 Hz), 11.8 ppm. **^{19}F-NMR (376 MHz, $CDCl_3$):** δ -118.56 (q, *J* = 6.8 Hz, 1F, ArF) ppm. **HRMS(ESI-MS)** calculated for $C_{16}H_{15}FN^+$ $[M+H^+]$ 140.1110, found 240.1109.

3-(4-methoxybenzyl)-2-methyl-1*H*-indole

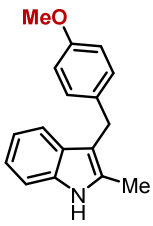

^{1}H-NMR (400 MHz, $CDCl_3$): δ 7.61 (*br* s, 1H, NH), 7.44 (d, *J* = 8.0 Hz, 1H, Ar), 7.29 – 7.24 (m, 5H, Ar), 7.17 – 7.14 (m, 1H, Ar), 7.10 – 7.07 (m, 1H, Ar), 4.11 (s, 2H, CH_2), 2.34 (s, 3H, CH_3) ppm. **^{13}C-NMR (101 MHz, $CDCl_3$):** δ 141.8, 135.4, 131.8, 129.0, 128.4 (x2), 128.4 (x2), 125.8, 121.1, 119.3, 118.5, 110.7, 110.4, 30.2, 11.8 ppm.

3-(3-methylbenzyl)-2-methyl-1*H*-indole

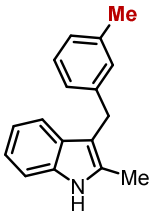

^{1}H-NMR (400 MHz, $CDCl_3$): δ 7.77 (*br* s, 1H, NH), 7.31 (d, *J* = 8.0 Hz, 1H, Ar), 7.20 – 7.01 (m, 6H, Ar), 7.17 – 7.14 (m, 1H, Ar), 7.10 – 7.07 (m, 1H, Ar), 4.09 (s, 2H, CH_2), 2.43 (s, 3H, CH_3), 2.33 (s, 3H, CH_3) ppm. **^{13}C-NMR (101 MHz, $CDCl_3$):** δ 141.6, 137.8, 135.3, 131.6, 129.1, 129.0, 128.2, 126.5, 125.4, 121.0, 119.3, 118.5, 110.7, 110.2, 30.1, 21.5, 11.9 ppm. **HRMS(ESI-MS)** calculated for $C_{17}H_{18}N^+$ [M+H$^+$] 236.1361, found 236.1370.

3-(4-trifluoromethylbenzyl)-2-methyl-1*H*-indole

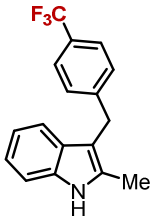

^{1}H-NMR (400 MHz, $CDCl_3$): δ 7.87 (*br* s, 1H, NH), 7.48 (d, *J* = 8.0 Hz, 2H, Ar), 7.38 – 7.31 (m, 4H, Ar), 7.38 – 7.31 (m, 4H, Ar), 7.12 (t, *J* = 6.4 Hz), 7.06 (t, *J* = 6.4 Hz, Ar), 4.14 (s, 2H, CH_2), 2.42 (s, 3H, CH_3) ppm. **^{13}C-NMR (101 MHz, $CDCl_3$):** δ 145.8, 135.3, 131.9, 128.6, 128.5 (x2), 125.2 (q, *J*= 3.8 Hz), 121.3, 119.5, 118.1, 110.3, 109.6, 30.0, 11.8 ppm. **^{19}F-NMR (376 MHz, $CDCl_3$):** δ -62.66 (s, 3F, $ArCF_3$) ppm. **HRMS(ESI-MS)** calculated for $C_{17}H_{15}F_3N^+$ [M+H$^+$] 290.1078, found 290.1081.

6-fluoro-2-methyl-1*H*-indole

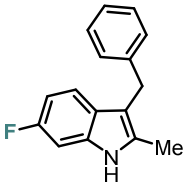

^{1}H-NMR (400 MHz, $CDCl_3$): δ 7.75 (*br* s, 1H, NH), 7.30 – 7.24 (m, 6H, Ar), 6.98 (dd, *J* = 9.6, 2.3 Hz, 1H, Ar), 6.81 (ddd, *J* = 9.8, 8.6, 2.3 Hz, 1H, Ar), 4.07 (s, 2H, CH_2), 2.40 (s, 3H, CH_3) ppm. **^{13}C-NMR (101 MHz, $CDCl_3$):** δ 159.5 (d, *J* = 236.1 Hz), 141.4, 135.1 (d, *J* = 12.4 Hz), 131.8 (d, *J* = 3.7 Hz), 128.4 (x2), 128.2 (x2), 125.8, 125.4, 118.9 (d, *J* = 24.0 Hz), 110.6, 107.8 (d, *J* = 26.0

Hz), 96.7 (d, J = 26.0 Hz), 30.1, 11.8 ppm. **^{19}F-NMR (376 MHz, $CDCl_3$):** δ -123.08 – -123.15 (m, 1F, ArF) ppm. **HRMS(ESI-MS)** calculated for $C_{16}H_{15}FN^+$ [M+H$^+$] 240.1110, found 240.1093.

N-Boc Protection of Indole Derivatives

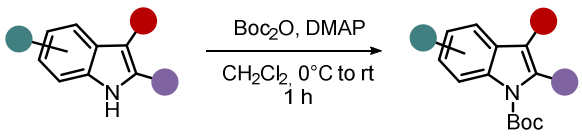

3-benzyl-2-methylindole (221.3 mg, 1 mmol, 1.0 equiv.) and DMAP (12.2 mg, 0.1 mmol, 0.1 equiv.) were dissolved in dichloromethane (5 mL, 0.2 M). Subsequently, di-*tert*-butyl dicarbonate (334 µL, 1.5 mmol, 1.5 equiv.) were added dropwise at 0 °C. After full consumption of the starting material, monitored by TLC (5% EtOAc in hexane), the reaction was quenched with 10 mL of HCl 4 M. The organic layer was washed with 10 mL of HCl 4 M, 10 mL of a saturated $NaHCO_3$ solution and 10 mL of brine solution. The organic layer was dried over $MgSO_4$, filtered and concentrated under reduced pressure. The crude product was purified by chromatography (95:5, hexane:EtOAc), giving *N*-Boc-3-benzyl-2-methylindole as a white solid (306 mg, 95% yield).

***tert*-butyl 3-benzyl-2-methyl-1*H*-indole-1-carboxylate (30d)**

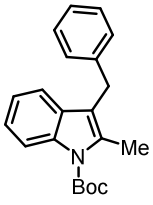

^{1}H-NMR (400 MHz, $CDCl_3$): δ 8.14 (d, J = 8.5 Hz, 1H, Ar), 7.37 (d, J = 8.0 Hz, 1H, Ar), 7.27 – 7.14 (m, 7H, Ar), 4.05 (s, 2H, CH_2), 2.60 (s, 3H, CH_3), 1.70 (s, 9H, ^{t}Bu-Boc) ppm. **^{13}C-NMR (101 MHz, $CDCl_3$):** δ 150.8, 140.3, 135.8, 134.0, 130.1, 128.4 (× 2), 128.1 (× 2), 125.9, 123.3, 122.4, 118.2, 116.8, 115.3, 83.5, 29.8, 28.3 (× 3), 14.1 ppm.

***tert*-butyl 3-(2-fluorobenzyl)-2-methyl-1*H*-indole-1-carboxylate (30f)**

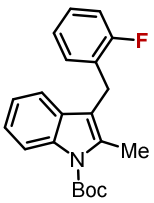

^{1}H-NMR (400 MHz, $CDCl_3$): δ 8.14 (d, *J* = 8.5 Hz, 1H, Ar), 7.39 (d, *J* = 8.1 Hz, 1H, Ar), 7.26 – 7.16 (m, 3H, Ar), 7.08 – 6.97 (m, 3H, Ar), 4.07 (s, 2H, CH_2), 2.61 (s, 3H, CH_3), 1.72 (s, 9H, ^{t}Bu-Boc) ppm. **^{13}C-NMR (101 MHz, $CDCl_3$):** δ 162.1, 159.7, 150.8, 135.8, 134.5, 130.0 (d, *J* = 4.5 Hz), 130.0, 127.6 (d, *J* = 8.0 Hz), 127.0 (d, *J* = 16.4 Hz), 124.0 (d, *J* = 3.6 Hz), 123.4, 122.5, 118.1, 115.5, 115.4, 115.2, 115.0, 83.6, 28.3 (× 3), 27.4, 22.5 (d, *J* = 4.1 Hz), 14.1 ppm. **^{19}F-NMR (376 MHz, $CDCl_3$):** δ -118.21 (q, *J* = 7.1 Hz, 1F, ArF) ppm. **HRMS(ESI-MS)** calculated for $C_{21}H_{23}FNO_2^+$ [M+H$^+$] 340.1635, found 340.1632.

***tert*-butyl 3-(4-methoxybenzyl)-2-methyl-1*H*-indole-1-carboxylate (30g)**

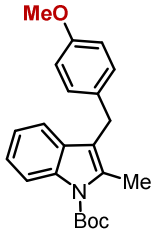

^{1}H-NMR (400 MHz, $CDCl_3$): δ 8.10 (d, *J* = 8.5 Hz, 1H, Ar), 7.33 (d, *J* = 8.1 Hz, 1H, Ar), 7.20 – 7.09 (m, 4H, Ar), 6.78 (d, *J* = 8.2 Hz, 2H, Ar), 3.98 (s, 2H, CH_2), 3.75 (s, 3H, OCH_3), 2.58 (s, 3H, CH_3), 1.69 (s, 9H, ^{t}Bu-Boc) ppm. **^{13}C-NMR (101 MHz, $CDCl_3$):** δ 157.9, 150.9, 135.8, 133.9, 132.4, 130.1, 129.0 (× 2), 123.3, 122.4, 118.3, 117.3, 115.4, 113.8 (x2), 83.5, 29.0, 28.3 (× 3), 14.1 ppm. **HRMS(ESI-MS)** calculated for $C_{22}H_{26}NO_3^+$ [M+H$^+$] 351.1934, found 351.1930.

***tert*-butyl 3-(3-methylbenzyl)-2-methyl-1*H*-indole-1-carboxylate (30h)**

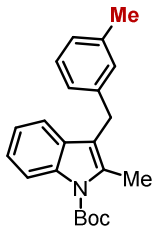

^{1}H-NMR (400 MHz, $CDCl_3$): δ 8.15 (d, *J* = 8.5 Hz, 1H, Ar), 7.39 (d, *J* = 8.1 Hz, 1H, Ar), 7.27 – 7.23 (m, 1H, Ar), 7.20 – 7.15 (m, 2H, Ar), 7.04 – 7.00 (m, 3H, Ar), 4.04 (s, 2H, CH_2), 2.62 (s, 3H, CH_3), 2.32 (s, 3H, CH_3), 1.73 (s, 9H, ^{t}Bu-Boc) ppm. **^{13}C-NMR (101 MHz, $CDCl_3$):** δ 150.9, 140.3, 138.0, 135.8, 134.1, 130.2, 128.9, 128.3, 126.8, 125.2, 123.3, 122.5, 118.3, 117.0, 115.4, 83.5, 29.8, 28.4 (×3), 21.5, 14.2 ppm. **HRMS(ESI-MS)** calculated for $C_{22}H_{26}NO_2^+$ $[M+H^+]$ 336.1885, found 336.1880.

***tert*-butyl 3-(4-trifluoromethylbenzyl)-2-methyl-1*H*-indole-1-carboxylate (30i)**

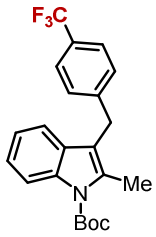

^{1}H-NMR (400 MHz, $CDCl_3$): δ 8.14 (d, *J* = 8.5 Hz, 1H, Ar), 7.51 (d, *J* = 8.1 Hz, 2H, Ar), 7.34 – 7.15 (m, 5H, Ar), 7.20 – 7.15 (m, 2H, Ar), 7.04 – 7.00 (m, 3H, Ar), 4.12 (s, 2H, CH_2), 2.60 (s, 3H, CH_3), 1.72 (s, 9H, ^{t}Bu-Boc) ppm. **^{13}C-NMR (101 MHz, $CDCl_3$):** δ 150.8, 144.5, 135.8, 134.4, 129.8, 128.4 (x2), 125.3 (q, *J*= 3.8 Hz), 123.6, 122.6, 118.0, 115.9, 115.5, 83.8, 29.8, 28.3 (× 3), 14.2 ppm. **^{19}F-NMR (376 MHz, $CDCl_3$):** δ -62.75 (s, 3F, $ArCF_3$) ppm. **HRMS(ESI-MS)** calculated for $C_{22}H_{23}F_3NO_2^+$ $[M+H^+]$ 390.1603, found 390.1605.

***tert*-butyl 2,3-dimethyl-1*H*-indole-1-carboxylate (30j)**

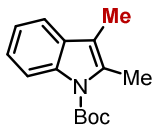

^{1}H-NMR (400 MHz, $CDCl_3$): δ 8.11 – 8.03 (m, 1H, Ar), 7.43 – 7.34 (m, 1H, Ar), 7.23 – 7.15 (m, 2H, Ar), 2.51 (s, 3H, CH_3), 2.17 (s, 3H, CH_3), 1.66 (s, 9H, ^{t}Bu-Boc) ppm. **^{13}C-NMR (101**

MHz, $CDCl_3$): δ 150.8, 135.6, 132.8, 130.8, 123.2, 122.3, 117.7, 115.3, 113.7, 83.2, 28.3, 13.9, 8.7 ppm.

***tert*-butyl 3-allyl-2-methyl-1*H*-indole-1-carboxylate (30k)**

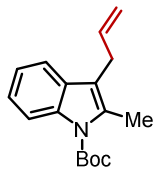

^{1}H-NMR (400 MHz, $CDCl_3$): δ 8.12 (d, *J* = 8.0 Hz, 1H, Ar), 7.46 (d, *J* = 8.2 Hz, 1H, Ar), 7.28 — 7.21 (m, 2H, Ar), 5.96 (ddt, *J* = 17.0, 10.0, 5.9 Hz, 1H, Csp^2-H), 5.09 — 5.03 (m, 2H, Csp^2-H_2), 3.45 (d, *J* = 6.0 Hz, 2H, CH_2), 2.56 (s, 3H, CH_3), 1.71 (s, 9H, ^{t}Bu-Boc) ppm. **^{13}C-NMR (101 MHz, $CDCl_3$):** δ 150.8, 136.0, 135.8, 133.7, 130.0, 123.3, 122.3, 118.0, 115.7, 115.4, 115.1, 83.4, 28.3 (x3), 28.3, 13.9 ppm. **HRMS(ESI-MS)** calculated for $C_{17}H_{22}NO_2^+$ $[M+H^+]$ 272.1572, found 272.1569.

***tert*-butyl 3-benzyl-6-fluoro-2-methyl-1*H*-indole-1-carboxylate (30l)**

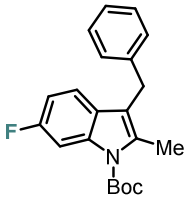

^{1}H-NMR (400 MHz, $CDCl_3$): δ 7.96 (d, *J* = 8.0 Hz, 1H, Ar), 7.34 – 7.24 (m, 6H, Ar), 5.96 (dt, *J* = 8.8, 2.3 Hz, 1H, Ar), 4.08 (s, 2H, CH_2), 2.66 (s, 3H, CH_3), 1.77 (s, 9H, ^{t}Bu-Boc) ppm. **^{13}C-NMR (101 MHz, $CDCl_3$):** δ 160.5 (d, *J* = 236.1 Hz), 150.6, 140.2, 136.1 (d, *J* = 12.4 Hz), 134.2 (d, *J* = 3.7 Hz), 128.5 (x2), 128.2 (x2), 126.4, 126.2, 118.7 (d, *J* = 24.0 Hz), 116.7, 110.5 (d, *J* = 26.0 Hz), 103.1 (d, *J* = 26.0 Hz), 84.0, 29.9, 28.3 (x3), 14.3 ppm. **^{19}F-NMR (376 MHz, $CDCl_3$):** δ -119.51 – -119.58 (m, 1F, ArF) ppm. **HRMS(ESI-MS)** calculated for $C_{21}H_{22}FNO_2^+$ $[M+H^+]$ 340.1635, found 340.1633.

***tert*-butyl 6-fluoro-2-methyl-1*H*-indole-1-carboxylate (30m)**

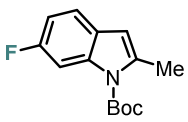

^{1}H-NMR (400 MHz, $CDCl_3$): δ 7.84 (dd, *J* = 8.0, 2.3 Hz, 1H, Ar), 7.36 – 7.26 (m, 1H, Ar), 6.93 (dt, *J* = 8.2, 2.3 Hz, 1H, Ar), 6.27 (s, 1H, CH), 2.57 (s, 3H, CH_3), 1.68 (s, 9H, ^{t}Bu-Boc) ppm. **^{13}C-NMR (101 MHz, $CDCl_3$):** δ 162.2, 157.4, 146.3, 137.7 (d, *J* = 3.9 Hz), 125.1 (d, *J* = 1.6 Hz), 150.6, 140.2, 136.1 (d, *J* = 12.4 Hz), 134.2 (d, *J* = 3.7 Hz), 119.3 (d, *J* = 9.8 Hz), 110.2 (d, *J* = 24.0 Hz), 107.1 (d, *J* = 1.1 Hz), 102.6 (d, *J* = 29.0 Hz), 84.8, 27.0 (x3), 16.7 ppm. **^{19}F-NMR (376 MHz, $CDCl_3$):** δ -119.65 – -119.72 (m, 1F, ArF) ppm. **HRMS (ESI-MS)** calculated for $C_{14}H_{17}FNO_2^+$ $[M+H^+]$ 250.1238, found 250.1244.

***tert*-butyl 2,3-dihydrocyclopenta[*b*]indole-4-carboxylate (30n)**

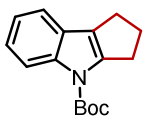

^{1}H-NMR (400 MHz, $CDCl_3$): δ 8.15 (s, 1H, Ar), 7.34 (d, *J* = 7.2 Hz, 1H, Ar), 7.22 – 7.17 (m, 2H, Ar), 3.06 (t, *J* = 7.6 Hz, 2H, CH_2), 2.76 – 2.73 (m, 2H, CH_2), 2.49 – 2.49 (m, 2H, CH_2), 1.63 (s, 9H, ^{t}Bu-Boc) ppm. **^{13}C-NMR (101 MHz, $CDCl_3$):** δ 149.9, 143.9, 140.1, 126.7, 124.4, 122.8, 122.5, 118.4, 115.7, 82.9, 29.1, 28.2, 27.3 (x3), 24.0 ppm.

***tert*-butyl 1,2,3,4-tetrahydro-9*H*-carbazole-9-carboxylate (30o)**

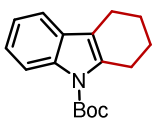

^{1}H-NMR (400 MHz, $CDCl_3$): δ 8.15 – 8.09 (m, 1H, Ar), 7.37 (m, 1H, Ar), 7.23 – 7.19 (m, 2H, Ar), 3.01 – 2.96 (m, 2H, CH_3), 2.65 – 2.61 (m, 2H, CH_2), 1.88 – 1.83 (m, 4H, 2 x CH_2), 1.65 (s, 9H, ^{t}Bu-Boc) ppm. **^{13}C-NMR (101 MHz, $CDCl_3$):** δ 150.7, 135.8, 135.6, 129.9, 123.3, 122.3, 117.4, 116.7, 115.4, 83.1, 28.3 (x3), 25.6 (x2), 22.3, 21.1 ppm.

Preparation of 3-hydroxymethyl-substituted indoles

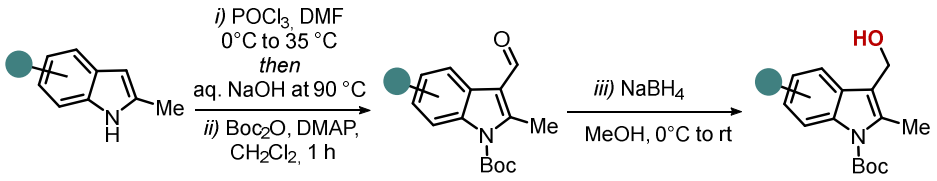

$POCl_3$ (1.73 mL, 18.6 mmol) was added dropwise to DMF (5 mL) at 0 °C. The reaction mixture was stirred at this temperature for 30 min. Then, a solution of 2-methylindole (2.03 g, 15.5 mmol) in 5 mL of DMF (3.1 M) was added slowly. The resulting reaction mixture was allowed to warm up to 35 °C and kept at this temperature for 40 min. The reaction was allowed to cool down to room temperature and 10 g of ice were added followed by 30 mL of a 5 M NaOH solution. The reaction mixture was heated at 90 °C for 30 min and allowed to cool down to room temperature again. An additional 10 g of ice were added and stirred for 30 min. The precipitate was filtered and washed with water the crude products was used without further purification steps.

ii) *The crude product was protected following the procedure previously described and used without further purification steps.*

iii) *Intermediate II* (1.16 g, 4.5 mmol) was dissolved in 20 mL of MeOH (0.23 M). Then, 1.5 equivalents of $NaBH_4$ (253 mg, 6.75 mmol) were added portionwise at 0 °C. After full consumption of the starting material, monitored by TLC, the reaction was quenched with 20 mL of water. The reaction mixture was extracted with 3 x 15 mL of EtOAc. The combined organic layers were dried over $MgSO_4$, filtered and concentrated under reduced pressure. The crude product was purified by chromatography (8:2, hexane:EtOAc), furnishing **30e** as a yellowish solid in 91% overall yield (1.05 g, 4.1 mmol) after three consecutive steps.

***tert*-butyl 3-(3-hydroxymethyl)-2-methyl-1*H*-indole-1-carboxylate (30e)**

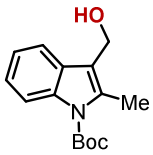

^{1}H-NMR (400 MHz, $CDCl_3$): δ 8.13 – 8.12 (m, 1H, Ar), 7.65 – 7.62 (m, 1H, Ar), 7.29 – 7.24 (m, 2H, Ar), 4.83 (s, 2H, CH_2), 2.65 (s, 3H, CH_3), 1.71 (s, 9H, ^{t}Bu-Boc) ppm. **^{13}C-NMR (101 MHz, $CDCl_3$):** δ 150.7, 135.8, 135.7, 128.9, 123.7, 122.8, 118.0, 117.6, 115.5, 83.9, 55.5, 28.3 (×3), 14.0 ppm. **HRMS(ESI-MS)** calculated for $C_{15}H_{19}NO_3^+$ $[M+H^+]$ 262.1365, found 262.1367.

***tert*-butyl 3-(3-hydroxymethyl)-5-bromo-2-methyl-1*H*-indole-1-carboxylate (30p)**

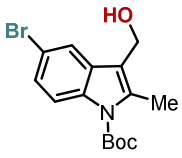

^{1}H-NMR (400 MHz, Acetone-d_6): δ 8.04 (d, *J* = 8.2 Hz, 1H, Ar), 7.79 (s, 1H, Ar), 7.36 (dd, *J* = 8.9, 2.5 Hz, 1H, Ar), 4.71 (d, *J* = 6.2 Hz, 2H, CH_2), 3.93 (t, *J* = 4.9 Hz, 1H, OH), 2.59 (s, 3H, CH_3), 1.69 (s, 9H, ^{t}Bu-Boc) ppm. **^{13}C-NMR (101 MHz, Acetone-d_6):** δ 150.2, 136.1, 134.6, 131.6, 125.7, 121.3, 118.0, 116.8, 115.2, 84.1, 54.0, 27.4 (x3), 13.2 ppm. **HRMS(ESI-MS)** calculated for $C_{15}H_{19}BrNO_3^+$ $[M+H^+]$ 340.0470, found 340.0472.

***tert*-butyl 3-(3-hydroxymethyl)-5-methoxy-2-methyl-1*H*-indole-1-carboxylate (30q)**

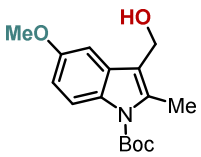

^{1}H-NMR (400 MHz, $CDCl_3$): δ 7.97 (d, *J* = 8.2 Hz, 1H, Ar), 7.06 (d, *J* = 2.6 Hz, 1H, Ar), 6.85 (dd, *J* = 8.9, 2.5 Hz, 1H, Ar), 4.76 (s, 2H, CH_2), 3.85 (s, 3H, OCH_3), 2.58 (s, 3H, CH_3), 1.67 (s, 9H, ^{t}Bu-Boc) ppm. **^{13}C-NMR (101 MHz,**

$CDCl_3$): δ 156.0, 150.6, 136.3, 130.4, 117.5, 116.3, 112.2, 100.9, 83.8, 55.7, 55.5, 28.3 (x3), 14.0 ppm. **HRMS(ESI-MS)** calculated for $C_{16}H_{22}NO_4^+$ $[M+H^+]$ 292.1471, found 292.1472.

***tert*-butyl 3-(3-hydroxymethyl)-2-phenyl-1*H*-indole-1-carboxylate (30r)**

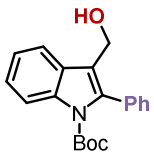

^{1}H-NMR (400 MHz, $CDCl_3$): δ 8.29 (d, *J* = 8.2 Hz, 1H, Ar), 7.77 (d, *J* = 8.1 Hz, 1H, Ar), 7.46 – 7.33 (m, 7H, Ar), 7.20 – 7.15 (m, 2H, Ar), 7.04 – 7.00 (m, 3H, Ar), 4.65 (s, 2H, CH_2), 1.27 (s, 9H, ^{t}Bu-Boc) ppm. **^{13}C-NMR (101 MHz, $CDCl_3$):** δ 150.1, 137.7, 136.7, 133.4, 129.8 (x2), 128.7, 128.0, 128.0 (x2), 124.9, 123.1, 119.6, 119.1, 115.3, 83.4, 55.9, 27.5 (x3) ppm. **HRMS(ESI-MS)** calculated for $C_{20}H_{22}NO_3^+$ $[M+H^+]$ 324.1521, found 324.1521.

N-Ac Protection of Indole Derivatives

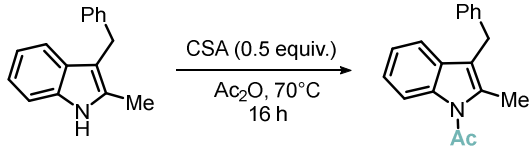

3-benzyl-2-methylindole (0.68 mmol, 150 mg) and 10-camphorsulfonic acid (0.34 mmol, 8.0 mg) were dissolved in acetic anhydride (1.5 mL, 0.45 M) at 0 °C. The reaction was heated at 70 °C and stirred vigorously for 16 h. After full consumption of the starting material, monitored by TLC, the reaction was quenched with 5 mL of brine. 10 mL of EtOAc were added and the organic layer was washed with 3 x 10 mL of a saturated $NaHCO_3$ solution. The organic layer was dried over $MgSO_4$, filtered and concentrated under reduced pressure. The crude product was purified by chromatography (95:5, hexane:EtOAc),

giving *N*-Ac-3-benzyl-2-methylindole as a yellowish solid in 30% yield (90 mg, 0.2 mmol).

1-(3-benzyl-2-methyl-1*H*-indol-1-yl)ethan-1-one (30s)

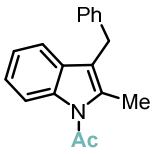

^{1}H-NMR (400 MHz, $CDCl_3$): δ 7.98 (d, *J* = 8.5 Hz, 1H, Ar), 7.40 (d, *J* = 8.0 Hz, 1H, Ar), 7.27 – 7.19 (m, 7H, Ar), 4.08 (s, 2H, CH_2), 2.79 (s, 3H, $COCH_3$), 2.64 (s, 3H, CH_3) ppm. **^{13}C-NMR (101 MHz, $CDCl_3$):** δ 170.3, 139.9, 135.8, 133.9, 130.6, 128.5 (x2), 128.2 (x2), 126.1, 123.8, 123.0, 118.7, 118.4, 115.0, 29.9, 27.7, 14.6 ppm. **HRMS (ESI-MS)** calculated for $C_{18}H_{18}NO^+$ $[M+H^+]$ 264.1310, found 264.1318.

N-Moc Protection of Indole Derivatives

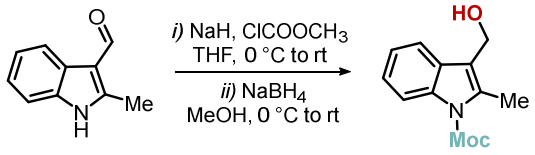

i) 2-methylindole-3-carboxaldehyde (715 mg, 4.5 mmol) were dissolved in 10 mL of anhydrous THF. Subsequently, 2.5 equivalents of NaH 60% in mineral oil (410 mg, 10.3 mmol) were added portionwise at 0 °C. After 10 min, methyl chloroformate (420 µL, 1.2 equivalents) were added at 0 °C dropwise. After full consumption of the starting material, monitored by TLC, the reaction was quenched with 20 mL of brine and extracted with 3 x 15 mL of EtOAc. The combined organic layers were dried over $MgSO_4$, filtered and concentrated under reduced pressure. The crude product was used without further purification steps.

ii) The crude product was dissolved in 20 mL of MeOH (0.23 M). Then, 1.5 equivalents of $NaBH_4$ (253 mg, 6.75 mmol) were added portionwise at 0 °C. After full consumption of the starting material, monitored by TLC, the reaction was quenched with 20 mL of water. The reaction mixture was extracted with 3 x 15 mL of EtOAc. The combined organic layers were dried over $MgSO_4$, filtered and concentrated under reduced pressure. The crude product was purified by chromatography (7:3, hexane:EtOAc), furnishing **30t** as a yellowish solid in 45% overall yield (438 mg, 2.0 mmol) after two steps.

methyl 3-(hydroxymethyl)-2-methyl-1*H*-indole-1-carboxylate (30t)

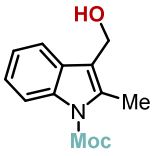

^{1}H-NMR (500 MHz, $CDCl_3$): δ 8.09 – 8.07 (m, 1H, Ar), 7.63 – 7.61 (m, 1H, Ar), 7.31 – 7.25 (m, 2H, Ar), 4.80 (s, 2H, CH_2), 4.05 (s, 3H, $COCH_3$), 2.61 (s, 3H, CH_3) ppm. **^{13}C-NMR (125 MHz, $CDCl_3$):** δ 152.9, 135.7, 135.7, 129.3, 124.1, 123.3, 118.3, 118.3, 115.6, 55.5, 53.7, 13.7 ppm. **HRMS (ESI-MS)** calculated for $C_{12}H_{14}NO_3^+$ [M+H$^+$] 220.0968, found 220.0972.

Preparation of C2 unsubstituted indoles

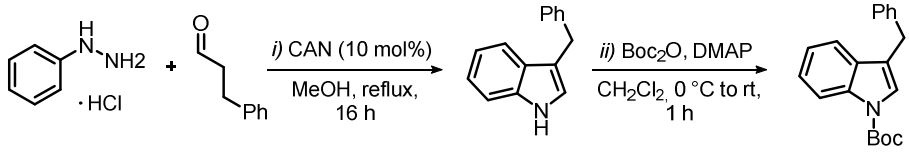

Phenyl hydrazine hydrochloride (1.44 g, 10 mmol, 1.0 equivalent) and cerium ammonium nitrate (1.1 g, 2 mmol, 0.2 equivalents) were dissolved in 20 mL of MeOH (0.5 M). Subsequently, hydrocinnamaldehyde (1.3 mL, 10 mmol, 1.0 equivalents) were added dropwise and the mixture was heated to reflux and stirred for 16 h. The reaction was cooled to room temperature and quenched

with 20 mL of water. Then, extracted with 3 x 20 mL of EtOAc. The combined organic layers were washed 3 x 15 mL of brine and the organic layer was dried over $MgSO_4$, filtered and concentrated under reduced pressure. The crude product was purified by chromatography (9:1, hexane:EtOAc), furnishing **30a** as a yellow solid in 60% overall yield (1.2 g, 6.0 mmol).

ii) The crude product was N-Boc protected following the previously described procedure and purified by column chromatography (95:5, hexane:EtOAc) furnishing 30***c*** *in* 92% *yield.*

tert-butyl 3-benzyl-1*H*-indole-1-carboxylate (30c)

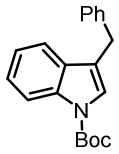

^{1}H-NMR (500 MHz, $CDCl_3$): δ 8.18 (br, 1H, Ar), 7.48 (d, *J* = 7.4 Hz, 1H, Ar), 7.41 (br, 1H, Ar), 7.36 – 7.32 (m, 5H, Ar), 7.26 – 7.21 (m, 2H, Ar), 4.08 (s, 2H, CH_2), 1.70 (s, 9H, ^{t}Bu-Boc) ppm. **^{13}C-NMR (125 MHz, $CDCl_3$):** δ 149.8, 139.6, 135.6, 130.5, 128.6 (x2), 128.4 (x2), 126.2, 124.3, 123.5, 123.3, 120.0, 119.3, 115.2, 83.4, 31.3, 28.1 (x3) ppm

Preparation of C3-cyanoethyl substituted indoles

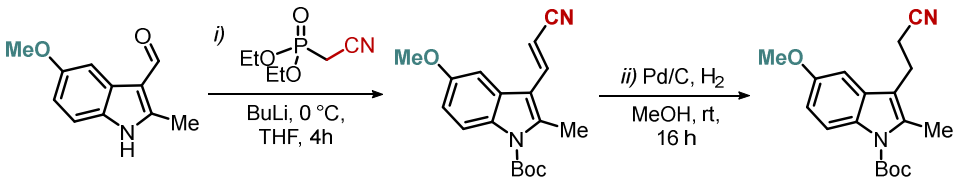

i) To a solution of diethylcyanomethyl phosphonate (842 µL, 5.2 mmol, 1.3 equiv.) in anhydrous THF (10 mL) at 0 °C, BuLi (192 µL, 4.8 mmol, 2.5 M in hexanes, 1.2 equiv.) was added dropwise and the mixture was stirred for 1h at the same temperature. A solution of 5-methoxyindole-3-carboxaldeyde (1.15 g,

4.0 mmol, 1 equiv.) in anhydrous THF (7 mL) was prepared, the solution of the Wittig reagent was added dropwise via cannula. After the addition, the reaction mixture was stirred at 0 °C for 4 h. The reaction was then concentrated, and the product was used without further purification.

ii) The crude was dissolved in 20 mL of MeOH (0.2 M). Then, the round-bottom flask was back-filled three times with H_2. After 16 h, the reaction was filtered through a pad of celite and concentrated under reduced pressure. The crude product was purified by chromatography (9:1, hexane:EtOAc), furnishing **30u** as a yellow solid in 45% overall yield (254.3 g, 1.8 mmol) after two steps.

***tert*-butyl 3-(2-cyanoethyl)-5-methoxy-2-methyl-1*H*-indole-1-carboxylate (30u)**

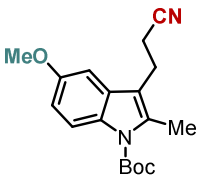

^{1}H-NMR (400 MHz, Acetone-d$_6$): δ 8.03 (d, *J* = 8.2 Hz, 1H, Ar), 7.13 (d, *J* = 2.6 Hz, 1H, Ar), 6.88 (dd, *J* = 8.9, 2.5 Hz, 1H, Ar), 3.85 (s, 3H, OCH_3), 3.08 (t, *J* = 7.2 Hz, 2H, CH_2), 2.74 (t, *J* = 7.2 Hz, 2H, CH_2), 2.60 (s, 3H, CH_3), 1.70 (s, 9H, ^{t}Bu-Boc) ppm. **^{13}C-NMR (101 MHz, Acetone-d$_6$):** δ 156.1, 150.3, 135.0, 130.3, 130.0, 119.5, 116.1, 115.2, 111.8, 100.7, 83.4, 55.0, 27.5 (x3), 19.9, 17.2, 13.5 ppm. **HRMS (ESI-MS)** calculated for $C_{18}H_{23}N_2O_3^+$ [M+H$^+$] 315.1630, found 315.1632.

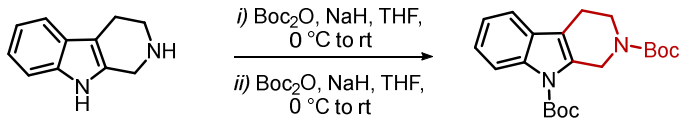

Two identical steps were performed in order to obtain 30***v***.

Tetrahydro-β-carboline (861 mg, 5.0 mmol, 1.0 equiv.) was dissolved in THF. Then, NaH (240 mg, 60 wt % mineral oil suspension, 6 mmol, 1.2 equiv.), was added portionwise at 0 °C. The mixture was warmed to room temperature, and di-*tert*-butyl dicarbonate (1.7 mL, 7.5 mmol, 1.5 equiv.) was added and stirred overnight at room temperature. After full consumption of the starting material, monitored by TLC, water was added, and the mixture was extracted with Et_2O. The combined organic layers were washed with brine, dried over $MgSO_4$ and concentrated under reduced pressure. The crude product was used without further purification and subjected to the same procedure.

The crude product was purified by chromatography (9:1, hexane:EtOAc), furnishing **30v** as a yellow solid in 73% overall yield (1.35 g, 3.7 mmol) after two consecutive steps.

di-*tert*-butyl 2,3,4,9-tetrahydrol-1*H*-β-carboline-2,9-dicarboxylate (30v)

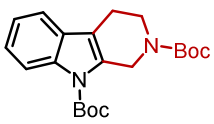

^{1}H-NMR (400 MHz, $CDCl_3$): δ 8.21 (d, *J* = 8.1 Hz, 1H, Ar), 7.43 (d, *J* = 8.0 Hz, 1H, Ar), 7.35 – 7.22 (m, 2H, Ar), 4.84 (br, 2H, CH_2), 3.76 (br, 2H, CH_2), 2.76 (br, 2H, CH_2), 1.70 (s, 9H, ^{t}Bu-Boc), 1.53 (s, 9H, ^{t}Bu-Boc) ppm. **^{13}C-NMR (101 MHz, $CDCl_3$):** δ 155.0, 150.0, 135.9, 128.9, 124.0, 122.7, 117.7, 115.4, 83.9, 80.0, 44.4, 40.2, 28.5 (x3), 28.3 (x3), 21.2 ppm.

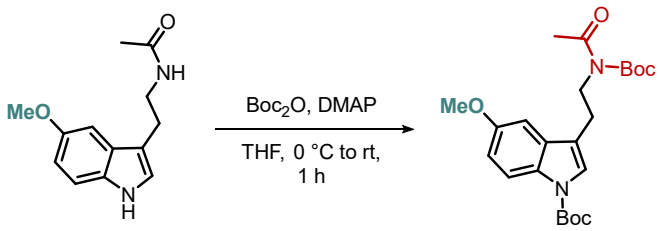

Melatonin (500 mg, 2.1 mmol, 1.0 equiv.) was dissolved in anhydrous THF (21.5 mL, 0.1 M) and DMAP (14.0 mg, 0.1 mmol, 0.05 equiv.) was added. Subsequently, di-*tert*-butyl dicarbonate (1.12 mL, 5.0 mmol, 2.4 equiv.) were added dropwise at 0 °C. After full consumption of the starting material, monitored by TLC (5% EtOAc in hexane), the reaction was quenched with 15 mL of HCl 4 M. The organic layer was washed with 10 mL of HCl 4 M, 10 mL of a saturated $NaHCO_3$ solution and 10 mL of brine solution. The organic layer was dried over $MgSO_4$, filtered and concentrated under reduced pressure. The crude product was purified by chromatography (95:5, hexane:EtOAc), giving **30w** as a transparent oil (729.3 mg, 83% yield).

tert-butyl-3-(2-(_N_-(_tert_-butoxycarbonyl)acetamido)ethyl)-5-methoxy-1_H_-indole-1-carboxylate (30w)

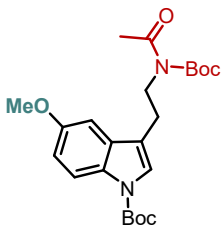

^{1}H-NMR (400 MHz, $CDCl_3$): δ 8.01 (br, 1H, Ar), 7.38 (s, 1H, Ar), 7.15 (s, 1H, Ar), 6.94 (dd, *J* = 8.9, 2.5 Hz, 1H, Ar), 3.98 (t, *J* = 8.6 Hz, 1H, CH_2), 3.90 (s, 3H, OCH_3), 2.90 (t, *J* = 8.6 Hz, 1H, CH_2), 2.53 (s, 3H, $COCH_3$), 1.67 (s, 9H, ^{t}Bu-Boc), 1.47 (s, 9H, ^{t}Bu-Boc) ppm. **^{13}C-NMR (101 MHz, $CDCl_3$):** δ 173.0, 155.9, 153.1, 123.8, 116.0, 113.1, 101.9, 83.2, 83.1, 55.8, 44.3, 28.2 (x3), 27.9 (x3), 27.1, 24.3 ppm. **HRMS (ESI-MS)** calculated for $C_{23}H_{33}N_2O_6^+$ $[M+H^+]$ 433.2260, found 433.2254.

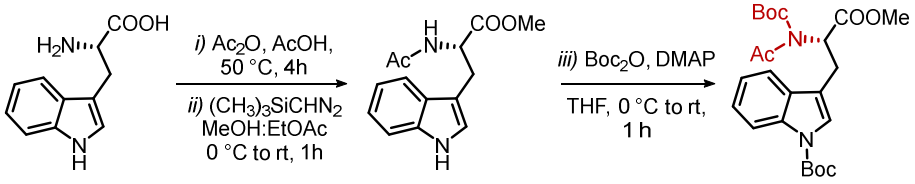

i) (*L*)-Tryptophan (1.02 g, 5.0 mmol, 1.0 equiv.) was added portion wise to acetic acid (2 mL, 2 M). Subsequently, acetic anhydride (4.5 mL, 47.5 mmol, 9.5 equiv.) was added. The mixture was stirred for 4 h at 50 °C. The reaction mixture was poured into 10 g of ice. Then, extracted with 2 x 20 mL of EtOAc, the combined organic layers were washed with 10 mL of a 2 M NaOH solution and 10 mL of brine. The organic layer was dried over $MgSO_4$, filtered and concentrated under reduced pressure. The crude product was used without further purification steps.

ii) The crude was dissolved in MeOH:EtOAc, (3:7, 45 mL, 0.1 M). Subsequently, trimethylsilyldiazomethane (6.5 mL, 13 mmol, 2.0 M in Et_2O, 2.6 equiv.) was added dropwise at 0 °C. The mixture was stirred for 1 h at room temperature. Then, acetic acid (1.14 mL, 20 mmol, 4.0 equiv.) was added dropwise and stirred for additional 5 min. The reaction was extracted with 3 x 10 mL of EtOAc. The combined organic layers were dried over $MgSO_4$, filtered, and concentrated under reduced pressure. The reaction crude product was used without further purification steps.

iii) The crude was dissolved in anhydrous THF (10 mL, 0.5 M) and DMAP (610.8 mg, 5.0 mmol, 1.0 equiv.) was added. Subsequently, di-*tert*-butyl dicarbonate (5.6 mL, 25.0 mmol, 5.0 equiv.) were added dropwise at 0 °C. After full consumption of the starting material, monitored by TLC (5% EtOAc in hexane), the reaction was quenched with 15 mL of HCl 4 M. The organic layer was washed with 10 mL of HCl 4 M, 10 mL of a saturated $NaHCO_3$

solution and 10 mL of brine solution. The organic layer was dried over $MgSO_4$, filtered and concentrated under reduced pressure. The crude product was purified by chromatography (95:5, hexane:EtOAc), giving **30x** as a yellowish oil (874.9 mg, 38% yield) after three consecutive steps.

***tert*-butyl (*R*)-3-(2-(*N*-(*tert*-butoxycarbonyl)acetamido)-3-methoxy-3-oxopropyl)-1*H*-indole-1-carboxylate (30x)**

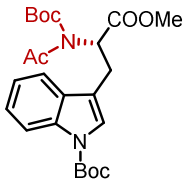

^{1}H-NMR (400 MHz, $CDCl_3$): δ 8.12 (d, *J* = 8.2 Hz, 1H, Ar), 7.52 (d, *J* = 7.7 Hz, 1H, Ar), 7.38 (s, 1H, Ar), 7.31 – 7.24 (m, 2H, Ar), 5.47 (dd, *J* = 9.7, 5.1 Hz, 1H, CH), 3.76 (s, 3H, $COOCH_3$), 3.55 (dd, *J* = 14.8, 4.9 Hz, 1H, CH_2a), 3.31 (dd, *J* = 14.8, 9.6 Hz, 1H, CH_2ß), 2.38 (s, 3H, $COCH_3$), 1.67 (s, 9H, ^{t}Bu-Boc), 1.33 (s, 9H, ^{t}Bu-Boc) ppm. **^{13}C-NMR (101 MHz, $CDCl_3$):** δ 172.8, 170.6, 152.0, 149.6, 130.4, 124.4, 124.1, 122.5, 118.8, 116.6, 115.3, 84.0, 83.5, 55.4, 52.3, 28.2 (x3), 27.6 (x3), 26.6, 25.0 ppm. **HRMS (ESI-MS)** calculated for $C_{24}H_{33}N_2O_7^+$ [M+H$^+$] 461.2210, found 461.2218.

Protection of tryptamine

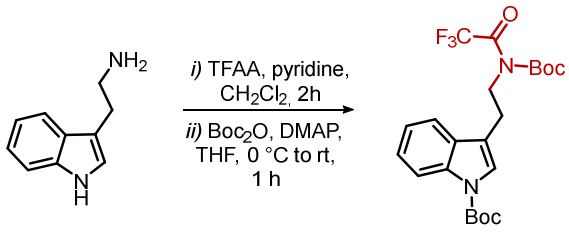

i) Tryptamine (3.2 g, 20 mmol, 1.0 equiv.) was dissolved in anhydrous CH_2Cl_2 (150 mL). Subsequently, pyridine (18 mL) was added. The solution was cooled at 0 °C and trifluoroacetic anhydride (3.1 mL, 22 mmol, 1.1 equiv.) was added

dropwise, the mixture was stirred at this temperature for 5 min. The ice bath was removed, and the mixture was stirred for another 2h at room temperature. After addition of 150 mL saturated $NaHCO_3$, the phases were separated, and the organic layer washed with 50 mL of a saturated NH_4Cl solution and 50 mL of water. The organic phase was dried over $MgSO_4$ and concentrated under reduced pressure. The crude product was used without further purification.

ii) As previously described., the crude product was purified by chromatography (95:5, hexane:EtOAc), giving **30y** as a transparent oil (6.9 g, 76% yield).

tert-butyl-3-(2-(_N_-(_tert_-butoxycarbonyl)-2,2,2-trifluoroacetamido)ethyl)-1_H_-indole-1-carboxylate (30y)

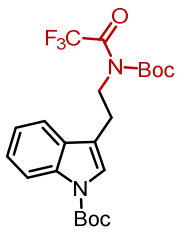

^{1}H-NMR (400 MHz, $CDCl_3$): δ 8.15 (br, 1H, Ar), 7.65 (d, *J* = 8.5 Hz, 1H, Ar), 7.45 (s, 1H, Ar), 7.38 – 7.28 (m, 2H, Ar), 4.03 (t, *J* = 8.6 Hz, 1H, CH_2), 3.05 (t, *J* = 8.6 Hz, 1H, CH_2), 1.69 (s, 9H, ^{t}Bu-Boc), 1.47 (s, 9H, ^{t}Bu-Boc) ppm. **^{13}C-NMR (101 MHz, $CDCl_3$):** δ 159.7 (q, *J* = 40.5 Hz), 150.8, 149.6, 135.6, 130.2, 124.6, 123.7, 122.7, 118.9, 116.3 (q, *J* = 110.9 Hz), 115.5, 85.9, 83.6, 46.7, 28.3 (x3), 27.4 (x3), 23.8 ppm. **^{19}F-NMR (376 MHz, $CDCl_3$):** δ -69.63 (s, 3F, $COCF_3$) ppm. **HRMS (ESI-MS)** calculated for $C_{22}H_{28}F_3N_2O_5^+$ $[M+H^+]$ 457.1872, found 457.1865.

Synthesis and characterization of the PB products

Preparation of oxeto-indolinic polycycles

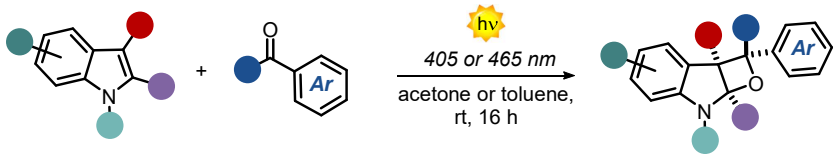

In a 4 mL vial, indole (0.1 mmol, 1.0 equiv.) and the benzophenone derivative (0.1 mmol, 1.0 equiv.) were added. The two reagents were dissolved in acetone or toluene (1 mL, 0.1 M) and the reaction mixture was bubbled with N_2 for one minute. Then, the vial was placed in front of the selected light source and irradiated for 16 h. The crude product was purified by chromatography (95:5, hexane:EtOAc) if needed or directly evaporated, giving the oxetane products in the stated yields and diastereomeric ratios.

***tert*-butyl-2a-benzyl-2,2-diphenyl-2a,7a-dihydrooxeto[2,3-*b*]indole-7(2*H*)-carboxylate (32c)**

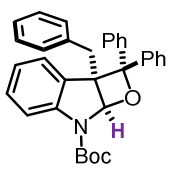

^{1}H-NMR (200 MHz, Acetone-d_6): δ 7.96 (dd, *J* = 8.4, 2.2 Hz, 2H, Ar), 7.58 – 7.54 (m, 3H, Ar), 7.53 – 7.50 (m, 3H, Ar), 7.38 – 7.34 (m, 1H, Ar), 7.15 (t, *J* = 7.8 Hz, 2H, Ar), 7.04 – 6.95 (m, 5H, Ar), 6.86 – 6.82 (m, 3H, Ar), 6.67 (br, 1H, CH), 3.53 (d, *J* = 16.7 Hz, 1H, CH_2a), 3.15 (d, *J* = 16.7 Hz, 1H, CH_2b), 1.54 (s, 9H, ^{t}Bu-Boc) ppm. **^{13}C-NMR (50 MHz, Acetone-d_6):** δ 143.5, 143.4, 136.5, 129.4 (x2), 128.3 (x2), 127.9, 127.8 (x2), 127.3, 127.2 (x2), 126.4, 126.2 (x2), 126.2, 125.5 (x2), 121.9, 114.9, 94.6, 91.9, 39.0, 27.5 (x3). ppm. **HRMS (ESI-MS)** calculated for $C_{33}H_{32}NO_3^+$ [M+H$^+$] 490.6225, found 490.6230.

***tert*-butyl-2a-benzyl-7a-methyl-2,2-diphenyl-2a,7a-dihydrooxeto[2,3-*b*]indole-7(2*H*)-carboxylate (32d)**

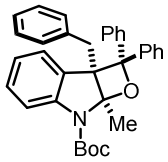

^{1}H-NMR (400 MHz, Acetone-d$_6$): δ 7.91 (d, *J* = 8.3 Hz, 2H, Ar), 7.57 (d, *J* = 8.2 Hz, 1H, Ar), 7.52 (d, *J* = 8.5 Hz, 2H, Ar), 7.45 (q, *J* = 6.9 Hz, 3H, Ar), 7.32 – 7.13 (m, 1H, Ar), 7.05 – 6.90 (m, 7H, Ar), 6.81 – 6.78 (m, 3H, Ar), 3.87 (d, *J* = 15.7 Hz, 1H, CH_2a), 3.21 (d, *J* = 15.7 Hz, 1H, CH_2b), 1.88 (s, 3H, CH_3), 1.62 (s, 9H, ^{t}Bu-Boc) ppm. **^{13}C-NMR (101 MHz, Acetone-d$_6$):** δ 151.5, 145.2, 144.0, 143.3, 137.2, 130.5, 129.7 (x3), 128.1, 128.0 (x3), 127.8 (x3), 127.1 (x3), 126.9, 126.1 (x3), 126.0, 125.7, 121.8, 115.2, 81.0, 62.8, 36.9, 27.7 (x3), 23.4 ppm. **HRMS(ESI-MS)** calculated for $C_{34}H_{34}NO_3^+$ [M+H$^+$] 504.2460, found 504.2453.

***tert*-butyl-2a-(2-fluorobenzyl)-7a-methyl-2,2-diphenyl-2a,7a-dihydrooxeto[2,3-*b*]indole-7(2*H*)-carboxylate (38)**

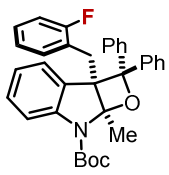

^{1}H-NMR (400 MHz, Acetone-d$_6$): δ 7.91 (d, *J* = 7.9 Hz, 2H, Ar), 7.59 (d, *J* = 8.2 Hz, 1H, Ar), 7.53 (d, *J* = 7.9 Hz, 2H, Ar), 7.45 (q, *J* = 7.3 Hz, 3H, Ar), 7.32 (t, *J* = 7.3 Hz, 1H, Ar), 7.11 – 6.92 (m, 6H, Ar), 6.81 (t, *J* = 7.5 Hz, 1H, Ar), 6.72 (t, *J* = 7.6 Hz, 1H, Ar), 6.46 (t, *J* = 7.8 Hz, 1H, Ar)., 3.70 (d, *J* = 17.0 Hz, 1H, CH_2a), 3.34 (d, *J* = 17.0 Hz, 1H, CH_2b), 1.87 (s, 3H, CH_3), 1.63 (s, 9H, ^{t}Bu-Boc) ppm. **^{13}C-NMR (101 MHz, Acetone-d$_6$):** δ 162.01 (d, *J* = 243.3 Hz), 152.4, 146.2, 144.7, 144.0, 131.2, 130.7 (d, *J* = 3.5 Hz), 129.2, 129.0 (x2), 128.7 (d, *J* = 8.7 Hz), 128.0, 127.9 (x2), 127.2 (d, *J* = 22.1 Hz), 126.9 (x2), 126.6 (x2), 125.3 (d, *J* = 13.8 Hz), 124.5, 124.4, 122.9, 116.1, 115.7 (d, *J* = 23.3 Hz), 101.7, 93.0, 82.0, 63.1, 30.6, 28.6 (x3), 23.3 ppm. **^{19}F-NMR (376 MHz, Acetone-**

d_6): δ -117.10 (q, *J* = 7.4 Hz, 1F, ArF) ppm. **HRMS(ESI-MS)** calculated for $C_{34}H_{33}FNO_3^+$ [M+H$^+$] 522.2439, found 522.2440.

***tert*-butyl-2a-(4-methoxybenzyl)-7a-methyl-2,2-diphenyl-2a,7a-dihydrooxeto[2,3-*b*]indole-7(2*H*)-carboxylate (39)**

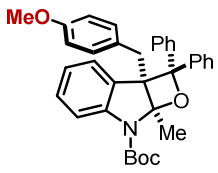

^{1}H-NMR (400 MHz, Acetone-d_6): δ 7.90 (d, *J* = 8.3 Hz, 2H, Ar), 7.58 (d, *J* = 8.3 Hz, 1H, Ar), 7.52 (d, *J* = 8.4 Hz, 2H, Ar), 7.45 (t *J* = 7.9 Hz, 3H, Ar), 7.31 (t, *J* = 7.3 Hz, 1H, Ar), 7.06 – 6.91 (m, 4H, Ar), 6.81 (t, *J* = 8.1 Hz, 1H, Ar), 6.69 (d, *J* = 8.2 Hz, 2H, Ar), 6.56 (d, *J* = 8.1 Hz, 2H, Ar) 3.78 (d, *J* = 15.7 Hz, 1H, CH_2a), 3.63 (s, 3H, OCH_3), 3.14 (d, *J* = 15.7 Hz, 1H, CH_2b), 1.88 (s, 3H, CH_3), 1.62 (s, 9H, ^{t}Bu-Boc) ppm. **^{13}C-NMR (101 MHz, Acetone-d_6):** δ 158.9, 152.4, 146.1, 144.9, 144.3, 131.6 (x2), 131.5, 129.6, 129.0, 128.9 (x2), 127.9 (x2), 127.8, 127.0 (x2), 126.9, 126.6 (x2), 122.6, 116.0, 114.0, 101.9, 93.0, 81.9, 63.8, 55.2, 36.9, 30.6, 28.6 (x3), 24.1ppm. **HRMS(ESI-MS)** calculated for $C_{35}H_{36}NO_4^+$ [M+H$^+$] 534.2566, found 534.2571.

***tert*-butyl-2a-(3-methylbenzyl)-7a-methyl-2,2-diphenyl-2a,7a-dihydrooxeto[2,3-*b*]indole-7(2*H*)-carboxylate (40)**

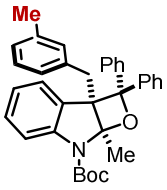

^{1}H-NMR (400 MHz, Acetone-d_6): δ 7.91 (d, *J* = 8.3 Hz, 2H, Ar), 7.60 – 7.41 (m, 6H, Ar), 7.32 (t, *J* = 7.8 Hz, 1H, Ar), 7.07 – 6.92 (m, 4H, Ar), 6.88 – 6.78 (m, 3H, Ar), 6.65 (s, 1H, Ar), 6.51 (d, *J* = 7.9 Hz, 1H, Ar), 3.84 (d, *J* = 15.7 Hz, 1H, CH_2a), 3.18 (d, *J* = 15.7 Hz, 1H, CH_2b), 2.07 (s, 3H, CH_3), 1.88 (s, 3H, CH_3), 1.62 (s, 9H, ^{t}Bu-Boc) ppm. **^{13}C-NMR (101 MHz, Acetone-d_6):** δ 152.4, 146.1, 144.8, 144.2, 137.9, 137.9, 133.3, 131.6, 131.5, 130.6, 129.3, 128.9 (x2), 128.5,

127.9 (x2), 127.8, 127.4, 127.3, 127.0 (x2), 126.6 (x2), 122.6, 116.0, 101.9, 93.0, 81.9, 63.7, 37.7, 28.6 (x3), 24.1, 21.3ppm. **HRMS(ESI-MS)** calculated for $C_{35}H_{36}NO_3^+$ [M+H$^+$] 518.2617, found 518.2622.

***tert*-butyl 2a-(4-trifluoromethylbenzyl)-7a-methyl-2,2-diphenyl-2a,7a-dihydrooxeto[2,3-*b*]indole-7(2*H*)-carboxylate (41)**

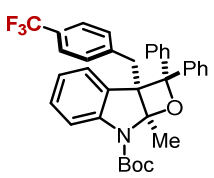

^{1}H-NMR (400 MHz, Acetone-d$_6$): δ 7.93 (d, *J* = 8.3 Hz, 2H, Ar), 7.59 (d, *J* = 8.3 Hz, 1H, Ar), 7.53 (d, *J* = 8.4 Hz, 2H, Ar), 7.48 – 7.44 (m, 3H, Ar), 7.38 – 7.31 (m, 3H, Ar), 7.07 – 6.93 (m, 6H, Ar), 6.80 (t, *J* = 8.1 Hz, 1H, Ar), 3.98 (d, *J* = 15.7 Hz, 1H, CH$_2$*a*), 3.34 (d, *J* = 15.7 Hz, 1H, CH$_2$*b*), 1.93 (s, 3H, CH$_3$), 1.63 (s, 9H, ^{t}Bu-Boc) ppm. **^{13}C-NMR (101 MHz, Acetone-d$_6$):** δ 152.4, 146.1, 144.6, 144.0, 143.0, 131.2 (x2), 130.8, 129.2, 129.3 (q, *J*= 137.0 Hz, CF$_3$), 129.0 (x2), 128.0, 128.0 (x2), 127.6, 127.1, 127.0 (x2), 126.6 (x2), 125.4 (q, *J* = 3.7 Hz), 122.8, 116.2, 101.8, 92.9, 82.1, 63.5, 37.5, 28.6 (x3), 24.2 ppm. **^{19}F-NMR (376 MHz, Acetone-d$_6$):** δ -63.37 (s, 3F, ArCF$_3$) ppm. **HRMS(ESI-MS)** calculated for $C_{35}H_{33}F_3NO_3^+$ [M+H$^+$] 572.2334, found 572.2340.

***tert*-butyl-2a,7a-dimethyl-2,2-diphenyl-2a,7a-dihydrooxeto[2,3-*b*]indole-7(2*H*)-carboxylate (42)**

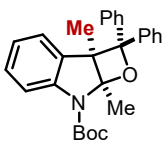

^{1}H-NMR (400 MHz, Acetone-d$_6$): δ 7.73 (d, *J* = 8.3 Hz, 2H, Ar), 7.47 – 7.37 (m, 6H, Ar), 7.25 (t, *J* = 7.8 Hz, 1H, Ar), 7.02 – 6.96 (m, 3H, Ar), 6.92 – 6.84 (m, 2H, Ar), 1.88 (s, 3H, CH$_3$), 1.64 (s, 9H, ^{t}Bu-Boc), 1.45 (s, 3H, CH$_3$) ppm. **^{13}C-NMR (101 MHz, Acetone-d$_6$):** δ 152.2, 145.0, 144.7, 133.2, 128.9, 128.8 (x2), 127.8 (x2),

127.6 (x2), 126.9, 126.4 (x2), 126.4 (x2), 126.0, 122.9, 115.6, 102.7, 92.6, 81.6, 59.3, 28.6 (x3), 21.2, 18.0 ppm. **HRMS (ESI-MS)** calculated for $C_{28}H_{30}NO_3^+$ [M+H$^+$] 428.2197, found 428.2197.

***tert*-butyl-2a-(hydroxymethyl)-7a-methyl-2,2-diphenyl-2a,7a-dihydrooxeto[2,3-*b*]indole-7(2*H*)-carboxylate (43)**

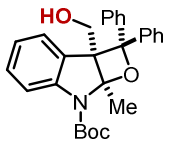

^{1}H-NMR (400 MHz, Acetone-d$_6$): δ 7.81 (d, *J* = 7.6 Hz, 2H, Ar), 7.55 (d, *J* = 8.1 Hz, 1H, Ar), 7.51 (d, *J* = 7.6 Hz, 1H, Ar), 7.45 (d, *J* = 7.6 Hz, 2H, Ar), 7.38 (t, *J* = 7.6 Hz, 2H, Ar), 7.26 (t, *J* = 7.3 Hz, 1H, Ar), 7.05 – 6.97 (m, 3H, Ar), 6.93 (t, *J* = 7.3 Hz, 1H, Ar), 6.84 (t, *J* = 7.3 Hz, 1H, Ar), 4.38 (dd, *J* = 11.4, 4.0 Hz, 1H, CH_2*a*), 3.84 (dd, *J* = 11.4, 5.6 Hz, 1H, CH_2*b*), 3.78 (dd, *J* = 5.6, 4.0 Hz, 1H, OH), 2.04 (s, 3H, CH_3), 1.65 (s, 9H, ^{t}Bu-Boc) ppm. **^{13}C-NMR (101 MHz, Acetone-d$_6$):** δ 152.3, 146.4, 144.6, 144.1, 130.2, 128.8 (x3), 127.8 (x2), 127.8, 127.3, 126.9, 126.4 (x2), 126.3 (x2), 122.6, 115.6, 101.6, 91.3, 81.6, 63.5, 61.4, 28.6 (x3), 21.9 ppm. **HRMS (ESI-MS)** calculated for $C_{28}H_{30}NO_4^+$ [M+H$^+$] 444.2169, found 444.2169.

***tert*-butyl-2a-allyl-7a-methyl-2,2-diphenyl-2a,7a-dihydrooxeto[2,3-*b*]indole-7(2*H*)-carboxylate (44)**

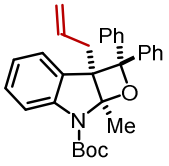

^{1}H-NMR (500 MHz, Acetone-d$_6$): δ 7.80 (d, *J* = 8.3 Hz, 2H, Ar), 7.55 – 7.53 (m, 1H, Ar), 7.45 (d, *J* = 7.8 Hz, 2H, Ar), 7.42 – 7.37 (m, 3H, Ar), 7.30 – 7.26 (m, 1H, Ar), 7.04 – 6.98 (m, 3H, Ar), 6.92 (t, *J* = 8.1 Hz, 1H, Ar), 6.85 (t, *J* = 7.9 Hz, 1H, Ar), 5.37 – 5.29 (m, 1H, Csp^{2}H), 5.01 (d, *J* = 16.0 Hz, 1H, (*E*)-Csp^{2}H$_2$), 4.86 (d, *J* = 11.2 Hz, 1H, (*Z*)-Csp^{2}H$_2$), 3.11 (dd, *J* = 15.0, 6.4 Hz, 1H, CH_2*a*),

2.55 (dd, *J* = 16.4, 8.6 Hz, 1H, CH_2*b*), 1.98 (s, 3H, CH_3), 1.64 (s, 9H, ^{t}Bu-Boc) ppm. **^{13}C-NMR (125 MHz, Acetone-d$_6$):** δ 151.4, 145.0, 143.9, 143.2, 133.9, 129.7, 128.0, 127.9 (x2), 127.0 (x2), 126.4, 126.1, 125.8 (x2), 125.6 (x2), 122.4, 121.8, 117.8, 115.0, 101.4, 91.4, 80.9, 61.7, 36.3, 27.7 (x3), 21.9 ppm. **HRMS(ESI-MS)** calculated for $C_{30}H_{32}NO_3^+$ [M+H$^+$] 454.5820, found 454.5828.

***tert*-butyl-2a-benzyl-5-fluoro-7a-methyl-2,2-diphenyl-2a,7a-dihydrooxeto[2,3-*b*]indole-7(2*H*)-carboxylate (45)**

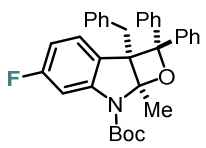

^{1}H-NMR (400 MHz, Acetone-d$_6$): δ 7.91 (d, *J* = 7.6 Hz, 2H, Ar), 7.53 (d, *J* = 7.6 Hz, 2H, Ar), 7.48 – 7.40 (m, 3H, Ar), 7.08 (t, *J* = 7.6 Hz, 2H, Ar), 7.04 – 7.03 (m, 3H, Ar), 6.97 (t, *J* = 7.3 Hz, 1H, Ar), 6.84 – 6.81 (m, 2H, Ar), 6.55 (td, *J* = 8.7, 2.4 Hz, 1H, Ar), 3.86 (d, *J* = 16.2 Hz, 1H, CH_2*a*), 3.22 (d, *J* = 16.2 Hz, 1H, CH_2*b*), 1.92 (s, 3H, CH_3), 1.63 (s, 9H, ^{t}Bu-Boc) ppm. **^{13}C-NMR (101 MHz, Acetone-d$_6$):** δ 163.5 (d, *J* = 241.0 Hz), 152.2, 147.4 (d, *J* = 12.7 Hz), 144.7, 143.9, 137.8, 130.6 (x2), 129.0 (x2), 128.7 (x2), 128.7 (d, *J* = 9.9 Hz), 128.0 (x3), 127.3 (d, *J* = 2.5 Hz), 127.0 (d, *J* = 23.7 Hz), 127.0 (x2), 126.5 (x2), 109.0 (d, *J* = 23.0 Hz), 103.8, 103.5, 102.7, 93.1, 82.6, 63.4, 37.5, 28.5 (x3), 24.2 ppm. **^{19}F-NMR (376 MHz, Acetone-d$_6$):** δ -114.69 (q, *J* = 10.1 Hz, 1F, ArF) ppm. **HRMS(ESI-MS)** calculated for $C_{34}H_{33}FNO_3^+$ [M+H$^+$] 522.2439, found 522.2445.

***tert*-butyl-5-bromo-2a-(hydroxymethyl)-7a-methyl-2,2-diphenyl-2a,7a-dihydrooxeto[2,3-*b*]indole-7(2*H*)-carboxylate (46)**

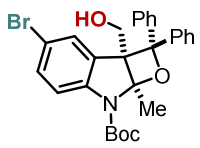

^{1}H-NMR (500 MHz, Acetone-d$_6$): δ 7.82 (d, *J* = 8.0 Hz, 2H, Ar), 7.67 (d, *J* = 2.2 Hz, 1H, Ar), 7.48 – 7.44 (m, 3H, Ar), 7.38 (t, *J* = 8.0 Hz, 2H, Ar), 7.27 (t, *J* = 7.3 Hz, 2H, Ar), 7.12 (dd, *J* = 8.7, 2.2 Hz, 1H, Ar), 7.08 (t, *J* = 8.0 Hz, 2H, Ar), 6.97 (t, *J* = 7.3 Hz, 1H, Ar), 4.42 (dd, *J* = 11.7, 4.3 Hz, 1H, CH_2a), 4.04 (dd, *J* = 5.3, 4.3 Hz, 1H, OH), 3.84 (dd, *J* = 11.7, 5.3 Hz, 1H, CH_2b), 2.02 (s, 3H, CH_3), 1.64 (s, 9H, ^{t}Bu-Boc) ppm. **^{13}C-NMR (125 MHz, Acetone-d$_6$):** δ 152.0, 145.7, 144.4, 143.7, 133.1, 131.5, 130.3, 128.9 (x2), 128.0 (x2), 128.0, 127.2, 126.4 (x2), 126.3 (x2), 117.1, 114.6, 101.9, 91.3, 82.1, 63.6, 61.1. 28.6 (x3), 21.9 ppm. **HRMS(ESI-MS)** calculated for $C_{28}H_{29}BrNO_4^+$ [M+H$^+$] 522.1274, found 522.1271.

***tert*-butyl-2a-(hydroxymethyl)-4-methoxy-7a-methyl-2,2-diphenyl-2a,7a-dihydrooxeto[2,3-*b*]indole-7(2*H*)-carboxylate (47)**

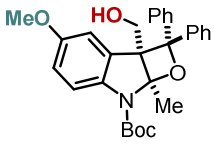

^{1}H-NMR (400 MHz, Acetone-d$_6$): δ 7.81 (d, *J* = 7.7 Hz, 2H, Ar), 7.48 (d, *J* = 7.7 Hz, 2H, Ar), 7.44 (d, *J* = 8.6 Hz, 1H, Ar), 7.38 (t, *J* = 7.7 Hz, 2H, Ar), 7.25 (t, *J* = 7.3 Hz, 1H, Ar), 7.13 (d, *J* = 2.6 Hz, 1H, Ar), 7.05 (t, *J* = 7.7 Hz, 2H, Ar), 6.94 (t, *J* = 7.3 Hz, 1H, Ar), 6.55 (dd, *J* = 8.6, 2.6 Hz, 1H, Ar), 4.40 (q, *J* = 6.6 Hz, 1H, CH_2a), 3.85 – 3.79 (m, 2H, CH_2b and OH overlapped), 3.70 (s, 3H, OCH_3), 2.01 (s, 3H, CH_3), 1.63 (s, 9H, ^{t}Bu-Boc) ppm. **^{13}C-NMR (101 MHz, Acetone-d$_6$):** δ 156.1, 152.3, 144.7, 144.2, 140.1, 131.5, 128.8 (x2), 127.9 (x2), 127.8, 127.0, 126.4 (x2), 126.3 (x2), 116.2, 114.2, 113.3, 101.7, 91.2, 81.4, 63.7, 61.5,55.9, 28.7 (x3), 22.0 ppm. **HRMS(ESI-MS)** calculated for $C_{29}H_{32}NO_5^+$ [M+H$^+$] 474.2275, found 474.2273.

***tert*-butyl-5-fluoro-7a-methyl-2,2-diphenyl-2a,7a-dihydrooxeto[2,3-*b*]indole-7(2*H*)-carboxylate (48)**

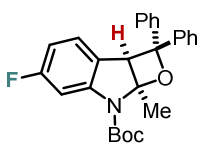

^{1}H-NMR (400 MHz, Acetone-d$_6$): δ 7.65 (d, *J* = 7.7 Hz, 2H, Ar), 7.45 (t, *J* = 7.7 Hz, 2H, Ar), 7.37 – 7.31 (m, 2H, Ar), 7.24 (d, *J* = 7.7 Hz, 2H, Ar), 7.12 (dd, *J* = 7.7, 6.1 Hz, 1H, Ar), 7.07 (t, *J* = 7.7 Hz, 2H, Ar), 6.98 (t, *J* = 7.3 Hz, 1H, Ar), 6.49 (td, *J* = 8.8, 2.4 Hz, 1H, Ar), 4.75 (s, 1H, CH), 1.92 (s, 3H, CH_3), 1.65 (s, 9H, ^{t}Bu-Boc) ppm. **^{13}C-NMR (101 MHz, Acetone-d$_6$):** δ 163.5 (d, *J* = 240.7 Hz), 152.2, 147.0, 143.3, 129.1 (x2), 128.4 (x2), 128.3, 128.2, 128.0, 127.5, 126.6 (x2), 126.3 (x2), 124.3 (d, *J* = 2.4 Hz), 109.2 (d, *J* = 22.9 Hz), 103.6 (d, *J* = 29.5 Hz), 100.2, 89.8, 82.5, 58.0, 30.6, 28.5 (x3), 25.7 ppm. **^{19}F-NMR (376 MHz, Acetone-d$_6$):** δ -115.07 (q, *J* = 9.7 Hz, 1F, ArF) ppm. **HRMS(ESI-MS)** calculated for $C_{27}H_{27}FNO_3^+$ [M+H$^+$] 432.1969, found 432.1972.

1-(2a-benzyl-7a-methyl-2,2-diphenyl-2a,7a-dihydrooxeto[2,3-*b*]indol-7(2*H*)-yl)ethan-1-one (49)

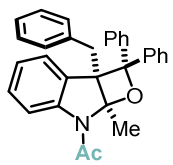

^{1}H-NMR (500 MHz, CDCl$_3$): δ 7.85 (br s, 1H, Ar), 7.73 (d, *J* = 7.6 Hz, 2H, Ar), 7.43 (t, *J* = 7.6 Hz, 2H, Ar), 7.33 – 7.29 (m, 3H, Ar), 7.13 (d, *J* = 7.6 Hz, 1H, Ar), 7.08 – 6.95 (m, 7H, Ar), 6.91 (t, *J* = 7.6 Hz, 1H, Ar), 6.68 (d, *J* = 7.6 Hz, 2H, Ar), 3.58 (d, *J* = 16.7 Hz, 1H, CH_2a), 3.18 (d, *J* = 16.7 Hz, 1H, CH_2b), 2.53 (s, 3H, $COCH_3$), 1.80 (s, 3H, CH_3) ppm. **^{13}C-NMR (125 MHz, CDCl$_3$):** δ 170.1, 146.8, 142.6, 142.4, 136.7, 129.7 (x2), 128.9, 128.5(x2), 128.2 (x2), 127.6, 127.4 (x2), 126.7, 126.3, 126.0 (x2), 125.8 (x2), 123.4, 117.1, 93.6, 63.1, 41.0, 36.9 , 24.0 ppm. **HRMS(ESI-MS)** calculated for $C_{31}H_{28}NO_2^+$ [M+H$^+$] 446.2115, found 446.2114.

methyl-2a-(hydroxymethyl)-7a-methyl-2,2-diphenyl-2a,7a-dihydrooxeto[2,3-*b*]indole-7(2*H*)-carboxylate (50)

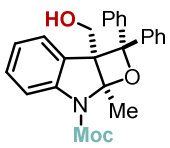

^{1}H-NMR (200 MHz, Acetone-d$_6$): δ 7.89 – 7.74 (m, 2H, Ar), 7.64 – 7.47 (m, 2H, Ar), 7.45-7.32 (m, 4H, Ar), 7.31 – 7.18 (m, 1H, Ar), 7.13 – 6.78 (m, 5H, Ar), 3.89 (s, 3H, $COOCH_3$), 3.82 (dd, *J* = 6.7, 4.5 Hz, 2H, CH_2), 2.02 (s, 3H, CH_3) ppm. **^{13}C-NMR (50 MHz, Acetone-d$_6$):** δ 143.3, 142.7, 129.1, 127.6 (x2), 127.5 (x4), 126.6 (x2), 126.6, 126.3, 125.7, 125.0 (x4), 121.7, 114.2, 60.2, 60.0, 51.4, 23.1, 20.2, 16.5 ppm. **HRMS(ESI-MS)** calculated for $C_{25}H_{24}NO_4^+$ [M+H$^+$] 402.1700, found 402.1703.

***tert*-butyl-2a-(hydroxymethyl)-2,2,7a-triphenyl-2a,7a-dihydrooxeto[2,3-*b*]indole-7(2*H*)-carboxylate (52)**

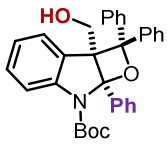

^{1}H-NMR (400 MHz, Acetone-d$_6$): δ 8.01 (d, *J* = 7.8 Hz, 2H, Ar), 7.69 (d, *J* = 7.8 Hz, 1H, Ar), 7.65 (d, *J* = 7.3 Hz, 1H, Ar)), 7.51 – 7.46 (m, 3H, Ar), 7.41 (t, *J* = 7.8 Hz, 3H, Ar)), 7.35–7.24 (m, 4H, Ar), 7.04 (q, *J* = 7.3 Hz, 3H, Ar), 6.92 (t, *J* = 7.3 Hz, 1H, Ar), 6.85 (t, *J* = 7.3 Hz, 1H, Ar), 3.97 (dd, *J* = 11.2, 4.2 Hz 1H, CH_2a), 3.62 (t, *J* = 4.2 Hz, 1H, OH), 3.39 (dd, *J* = 11.3, 4.2 Hz, 1H, CH_2b),1.22 (s, 9H, ^{t}Bu-Boc) ppm. **^{13}C-NMR (101 MHz, Acetone-d$_6$):** δ 151.8, 146.8, 145.0, 144.3, 140.0, 130.8, 130.1, 129.0, 128.8 (x2), 128.8, 128.7, 128.5, 128.3, 128.0 (x2), 127.8, 127.0, 126.5 (x2), 126.3 (x2),122.8, 114.6, 102.9, 93.3, 81.1, 65.0, 62.4, 28.2 (x3) ppm. **HRMS(ESI-MS)** calculated for $C_{33}H_{32}NO_4^+$ [M+H$^+$] 506.2326, found 506.2324.

***tert*-butyl-2a-benzyl-2,2-bis(4-chlorophenyl)-7a-methyl-2a,7a-dihydrooxeto[2,3-*b*]indole-7(2*H*)-carboxylate (53)**

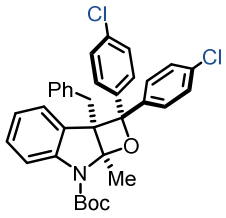

^{1}H-NMR (400 MHz, Acetone-d$_6$): δ 7.91 (d, *J* = 8.6 Hz, 2H, Ar), 7.60 (d, *J* = 8.6 Hz, 1H, Ar), 7.51 (dd, *J* = 10.7, 8.6 Hz, 4H, Ar), 7.45 (d, *J* = 7.3 Hz, 1H, Ar), 7.09 (d, *J* = 8.6 Hz, 2H, Ar), 7.05 – 7.00 (m, 4H, Ar), 6.85 – 6.80 (m, 3H, Ar), 3.88 (d, *J* = 16.0 Hz, 1H, CH_2a), 3.23 (d, *J* = 16.0 Hz, 1H, CH_2b), 1.90 (s, 3H, CH_3), 1.62 (s, 9H, ^{t}Bu-Boc). ppm. **^{13}C-NMR (101 MHz, Acetone-d$_6$):** δ 152.3, 146.0, 143.4, 142.6, 137.7,133.7, 132.7, 130.9, 130.6(x2), 129.3, 129.2 (x2), 128.7 (x2), 128.7 (x2),128.3 (x2),128.1 (x2), 127.6, 126.9, 122.9, 116.1, 102.2, 92.4, 82.2, 63.8, 37.4, 28.5 (x3), 24.1 ppm. **HRMS(ESI-MS)** calculated for $C_{34}H_{32}Cl_2NO_3^+$ [M+H$^+$] 572.1754, found 572.1758.

***tert*-butyl-2a-benzyl-7a-methyl-2,2-bis(3-(trifluoromethyl)phenyl)-2a,7a-dihydrooxeto[2,3-*b*]indole-7(2*H*)-carboxylate (54)**

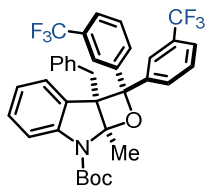

^{1}H-NMR (400 MHz, Acetone-d$_6$): δ 8.30 (d, *J* = 7.2 Hz, 1H, Ar), 8.26 (s, 1H, Ar), 7.90 – 7.72 (m, 5H, Ar), 7.58 – 7.55 (m, 2H, Ar), 7.34 – 7.32 (m, 2H, Ar), 7.25 – 7.18 (m, 2H, Ar), 7.04 – 7.00 (m, 4H, Ar), 6.84 – 6.80 (m, 3H, Ar), 4.06 (d, *J* = 16.0 Hz,1H, CH_2a), 3.23 (d, *J* = 16.0 Hz, 1H, CH_2b), 1.95 (s, 3H, CH_3), 1.63 (s, 9H, ^{t}Bu-Boc) ppm. **^{13}C-NMR (101 MHz, Acetone-d$_6$):** δ 152.2, 146.0, 145.5, 144.8, 137.5, 131.0, 130.6 (x2), 130.5, 130.4 130.3, 129.5, 129.1, 128.7 (x2), 127.7, 127.0, 125.3 (q), 124.2 (q), 123.4 (q), 123.0, 116.1, 102.5, 92.4, 82.4, 64.1, 37.2, 28.5 (x3), 24.1 ppm. **^{19}F-NMR (376 MHz, Acetone d$_6$):** δ -63.32 (s, 3F, $ArCF_3$), -63.47 (s, 3F, $ArCF_3$) ppm

HRMS(ESI-MS) calculated for $C_{36}H_{32}F_6NO_3^+$ $[M+H^+]$ 640.2281, found 640.2280.

***tert*-butyl-2a-benzyl-2,2-bis(3-chlorophenyl)-7a-methyl-2a,7a-dihydrooxeto[2,3-*b*]indole-7(2*H*)-carboxylate (55)**

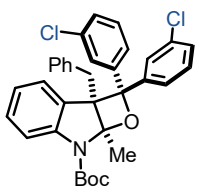

^{1}H-NMR (500 MHz, Acetone-d_6): δ 7.95 – 7.88 (m, 2H, Ar), 7.61 (d, *J* = 8.5 Hz, 1H, Ar), 7.59 – 7.57 (m, 2H, Ar), 7.55 – 7.48 (m, 2H, Ar), 7.42 – 7.38 (m, 1H, Ar), 7.13 – 7.08 (m, 1H, Ar), 7.06 – 7.00 (m, 5H, Ar), 6.91 – 6.81 (m, 3H, Ar), 4.01 (d, *J* = 16.1 Hz, 1H, CH_2a), 3.26 (d, *J* = 16.1 Hz, 1H, CH_2b), 1.93 (s, 3H, CH_3), 1.65 (s, 9H, ^{t}Bu-Boc) ppm. **^{13}C-NMR (125 MHz, Acetone-d_6):** δ 151.4, 145.8, 145.1, 145.0, 136.8, 134.0, 133.0, 130.0, 129.8, 129.7 (x2), 128.9, 128.6, 127.8 (x2), 127.5, 126.8, 126.5, 126.1, 125.8, 125.7, 124.7, 124.4, 122.0, 115.3, 101.5, 91.3, 81.4, 63.0, 36.3, 27.7, 23.2 ppm. **HRMS(ESI-MS)** calculated for $C_{34}H_{32}Cl_2NO_3^+$ $[M+H^+]$ 572.1754, found 572.1755.

***tert*-butyl-2a-benzyl-7a-methyl-2,2-di-p-tolyl-2a,7a-dihydrooxeto[2,3-*b*]indole-7(2*H*)-carboxylate (56)**

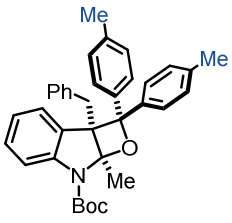

^{1}H-NMR (400 MHz, Acetone-d_6): δ 7.75 (d, *J* = 8.0 Hz, 2H, Ar), 7.59 (d, *J* = 8.0 Hz, 1H, Ar), 7.41 (d, *J* = 7.5 Hz, 1H, Ar), 7.37 (d, *J* = 8.0 Hz, 1H, Ar), 7.25 (d, *J* = 8.0 Hz, 2H, Ar), 7.01 – 6.97 (m, 4H, Ar), 6.85 (d, *J* = 8.0 Hz, 2H, Ar), 6.81 – 6.76 (m, 3H, Ar), 3.82 (d, *J* = 16.1 Hz, 1H, CH_2a), 3.21 (d, *J* = 16.1 Hz, 1H, CH_2b), 2.33 (s, 3H, $ArCH_3$), 2.09 (s, 3H, $ArCH_3$), 1.88 (s, 3H, CH_3) 1.61 (s, 9H, ^{t}Bu-Boc) ppm. **^{13}C-NMR (101 MHz,**

Acetone-d_6): δ 152.5, 146.1, 143.7, 142.2, 141.6, 138.2, 137.3, 136.1, 131.6, 130.7, 130.5 (x2), 129.8, 129.5, 128.9, 128.6 (x2), 128.5 (x2), 127.7, 126.9, 126.8, 126.5, 122.6, 116.1, 101.8, 93.1, 81.8, 63.5, 37.8, 28.6 (x3), 27.4, 21.0, 20.8 ppm. **HRMS(ESI-MS)** calculated for $C_{36}H_{38}NO_3^+$ [M+H$^+$] 532.2846, found 532.2840.

***tert*-butyl-2a-benzyl-2,2-bis(4-fluorophenyl)-7a-methyl-2a,7a-dihydrooxeto[2,3-*b*]indole-7(2*H*)-carboxylate (57)**

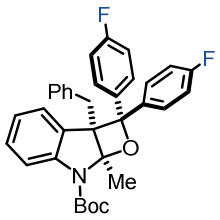

^{1}H-NMR (400 MHz, Acetone-d_6): δ 7.93 (dd, *J* = 8.9, 5.4 Hz, 2H, Ar), 7.59 (d, *J* = 8.2 Hz, 1H, Ar), 7.53 (dd, *J* = 8.9, 5.4 Hz, 2H, Ar), 7.41 (d, *J* = 7.5 Hz, 1H, Ar), 7.23 (t, *J* = 8.9 Hz, 2H, Ar), 7.04 – 7.00 (m, 4H, Ar), 6.84 – 6.79 (m, 5H, Ar), 3.86 (d, *J* = 16.0 Hz, 1H, CH_2*a*), 3.22 (d, *J* = 16.0 Hz, 1H, CH_2*b*), 1.89 (s, 3H, CH_3), 1.62 (s, 9H, ^{t}Bu-Boc) ppm. **^{13}C-NMR (101 MHz, Acetone-d_6):** δ 163.0 (d, *J* = 244.4 Hz), 160.9 (d, *J* = 244.4 Hz), 152.3, 146.1, 140.8 (d, *J* = 3.0 Hz), 140.0 (d, *J* = 3.0 Hz), 137.8, 133.5, 133.4, 131.2, 130.6 (x2),129.2, 129.1 (d, *J* = 8.0 Hz), 128.6 (d, *J* = 8.0 Hz), 128.5 (x2), 127.6, 126.9, 122.8, 116.3 (d, *J* = 22.1 Hz), 116.1, 115.8 (d, *J* = 21.5 Hz), 114.7 (d, *J* = 21.5 Hz), 102.1, 93.0, 82.1, 63.7, 37.5, 30.6, 28.6 (x3), 24.1 ppm. **^{19}F-NMR (376 MHz, Acetone-d_6):** δ -117.51 – -117.58 (m, 1F, ArF), -118.43 – -118.50 (m, 1F, ArF) ppm. **HRMS(ESI-MS)** calculated for $C_{34}H_{32}F_2NO_3^+$ [M+H$^+$] 540.2345, found 540.2340.

***tert*-butyl-2-benzoyl-2a-benzyl-7a-methyl-2-phenyl-2a,7a-dihydrooxeto[2,3-*b*]indole-7(2*H*)-carboxylate (58)**

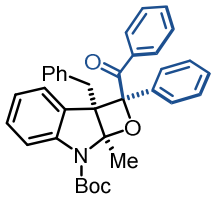

^{1}H-NMR (400 MHz, Acetone-d$_6$): δ 8.04 (d, *J* = 8.3 Hz, 2H, Ar), 7.65 (d, *J* = 7.9 Hz, 1H, Ar), 7.58 – 7.55 (m, 5H, Ar), 7.49 – 7.40 (m, 2H, Ar), 7.27 (t, *J* = 8.0 Hz, 2H, Ar), 7.21 (t, *J* = 8.1 Hz, 1H, Ar), 7.09 (t, *J* = 8.1 Hz, 1H, Ar), 7.02 – 7.00 (m, 3H, Ar), 6.79-6.76 (m, 2H, Ar), 3.54 (d, *J* = 15.7 Hz, 1H, CH_2a), 2.93 (d, *J* = 15.7 Hz, 1H, CH_2b), 1.99 (s, 3H, CH_3), 1.49 (s, 9H, ^{t}Bu-Boc) ppm. **^{13}C-NMR (101 MHz, Acetone-d$_6$):** δ 200.8, 152.2, 145.3, 138.2, 137.1, 136.9, 133.2, 130.5 (x2), 129.8 (x2), 129.6, 129.5, 129.4 (x2), 129.3, 128.7 (x2), 128.5 (x2), 127.3 (x2), 127.0, 123.3, 116.2, 102.2, 97.1, 82.3, 64.4, 37.7, 28.4 (x3), 24.0 ppm. **HRMS(ESI-MS)** calculated for $C_{35}H_{34}NO_4^+$ [M+H$^+$] 532.6520, found 532.6514.

***tert*-butyl-2a-benzyl-7a-methyl-2-(4-methylbenzoyl)-2-(*p*-tolyl)-2a,7a-dihydrooxeto[2,3-*b*]indole-7(2*H*)-carboxylate (59)**

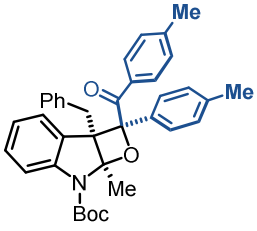

^{1}H NMR (400 MHz, Acetone-d$_6$): δ 7.88 (d, *J* = 8.0 Hz, 2H, Ar), 7.64 (d, *J* = 8.2 Hz, 1H, Ar), 7.54 (d, *J* = 8.0 Hz, 2H, Ar), 7.37 (d, *J* = 8.1 Hz, 2H, Ar), 7.21 – 7.11 (m, 3H, Ar), 7.10 – 7.05 (m, 2H, Ar), 7.04 – 6.97 (m, 3H, Ar), 6.80 – 6.76 (m, 2H, Ar) 3.53 (d, *J* = 16.0 Hz, 1H, CH_2a), 2.96 (d, *J* = 16.0 Hz, 1H, CH_2b), 2.40 (s, 3H, CH_3), 2.27 (s, 3H, CH_3), 1.99 (s, 3H, CH_3), 1.52 (s, 9H, ^{t}Bu-Boc) ppm.**^{13}C NMR (101 MHz, Acetone-d$_6$):** δ 199.0, 151.3, 144.4, 143.0, 138.0, 136.4, 134.4, 133.3, 129.6 (x2), 129.2 (x2), 129.1 (x2), 128.9, 128.5, 128.3 (x2), 127.8 (x2), 126.4 (x2), 126.0, 125.2, 122.3, 115.3, 101.1, 96.3, 81.3, 63.4, 36.9, 27.5 (x3), 23.1,

20.6, 20.2 ppm. **HRMS(ESI-MS)** calculated for $C_{37}H_{38}NO_4^+$ $[M+H^+]$ 560.2795, found 560.2796.

***tert*-butyl-2a-benzyl-2-(3-methoxybenzoyl)-2-(3-methoxyphenyl)-7a-methyl-2a,7a-dihydrooxeto[2,3-*b*]indole-7(2*H*)-carboxylate (60)**

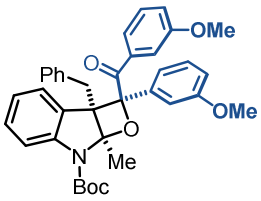

^{1}H NMR (400 MHz, Acetone-d$_6$): δ 7.66 (d, *J* = 8.2 Hz, 1H, Ar), 7.58 (t, *J* = 6.8 Hz, 3H, Ar), 7.55 – 7.45 (m, 2H, Ar), 7.29 – 7.16 (m, 3H, Ar), 7.13 – 7.04 (m, 3H, Ar), 7.05 – 6.97 (m, 3H, Ar), 6.82 – 6.76 (m, 2H, Ar), 3.91 (s, 3H, OCH_3), 3.73 (s, 3H, OCH_3), 3.58 (d, *J* = 16.0 Hz, 1H, CH_2a), 2.99 (d, *J* = 16.0 Hz, 1H, CH_2b), 2.01 (s, 3H, CH_3), 1.50 (s, 9H, ^{t}Bu-Boc) ppm. **^{13}C NMR (101 MHz, Acetone-d$_6$):** δ 199.5, 160.0, 159.0, 151.2, 144.3, 138.8, 137.2, 136.2, 130.4, 129.6 (x3), 128.8, 128.7, 128.6, 127.7 (x2), 126.0, 122.4, 121.2, 118.6, 118.2, 115.3, 113.8, 113.4, 112.3, 101.2, 96.1, 81.3, 63.6, 54.7, 54.6, 36.7, 27.5 (x3), 23.0 ppm. **HRMS(ESI-MS)** calculated for $C_{37}H_{38}NO_6^+$ $[M+H^+]$ 592.2694, found 592.2695.

***tert*-butyl-2a-benzyl-2-(4-fluorobenzoyl)-2-(4-fluorophenyl)-7a-methyl-2a,7a-dihydrooxeto[2,3-*b*]indole-7(2*H*)-carboxylate (61)**

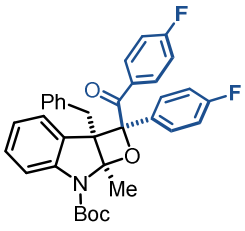

^{1}H NMR (400 MHz, Acetone-d$_6$): δ 8.07 (dd, *J* = 7.9, 6.0 Hz, 2H, Ar), 7.67 (dd, *J* = 7.5, 5.9 Hz, 2H, Ar), 7.62 (d, *J* = 8.2 Hz, 1H, Ar), 7.52 (d, *J* = 7.6 Hz, 1H, Ar), 7.35 (t, *J* = 8.7 Hz, 2H, Ar), 7.19 (t, *J* = 7.8 Hz, 1H, Ar), 7.12 – 6.98 (m, 6H, Ar), 6.79 (d, *J* = 4.7 Hz, 2H, Ar), 3.55 (d, *J* = 16.0 Hz, 1H, CH_2a), 2.97 (d, *J* = 16.0 Hz, 1H, CH_2b), 2.00 (s, 3H, CH_3), 1.52 (s, 9H, ^{t}Bu-Boc) ppm.**^{13}C NMR (101 MHz, Acetone-d$_6$):** δ 198.6, 165.1

(d, *J* = 220.Hz), 162.7 (d, *J* = 220.Hz), 151.1, 144.3, 136.0, 133.1 (d, *J* = 2.9 Hz), 132.4 (d, *J* = 3.0 Hz), 131.9 (d, *J* = 9.4 Hz, x2), 129.6 (x2), 129.2, 128.6 (d, *J* = 8.3 Hz, x2), 128.5 (d, *J* = 21.9 Hz, x2), 127.8 (x2), 126.1, 122.5, 115.3 (d, *J* = 21.0 Hz, x2), 115.2, 114.6 (d, *J* = 21.9 Hz, x2), 101.5, 95.8, 81.5, 63.5, 36.5, 27.5 (x3), 23.0 ppm. **^{19}F-NMR (376 MHz, Acetone-d$_6$):** δ -107.85 – -107.91 (m, 1F, ArF), -115.89 – -115.95 (m, 1F, C-F Ar) ppm. **HRMS(ESI-MS)** calculated for $C_{35}H_{32}NO_4^+$ [M+H$^+$] 568.2294, found 568.2297.

***tert*-butyl-2-benzoyl-2a-(hydroxymethyl)-7a-methyl-2-phenyl-2a,7a-dihydrooxeto[2,3-*b*]indole-7(2*H*)-carboxylate (62)**

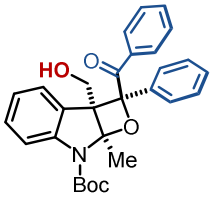

^{1}H-NMR (400 MHz, Acetone-d$_6$): δ 7.88 (d, *J* = 7.9 Hz, 2H, Ar), 7.63 (d, *J* = 7.9 Hz, 1H, Ar), 7.59 (d, *J* = 7.9 Hz, 2H, Ar), 7.52 – 7.47 (m, 3H, Ar), 7.40 (q, *J* = 7.2 Hz, 2H, Ar), 7.26 (t, *J* = 7.9 Hz, 2H, Ar), 7.18 (t, *J* = 7.9 Hz, 1H, Ar), 7.07 (t, *J* = 7.9 Hz, 1H, Ar), 4.08 (dd, *J* = 11.3, 3.6 Hz, 1H, CH_2*a*), 3.70 – 3.59 (m, 2H, CH_2*b* and OH overlapped), 2.10 (s, 3H, CH_3), 1.48 (s, 9H, ^{t}Bu-Boc) ppm. **^{13}C-NMR (101 MHz, Acetone-d$_6$):** δ 199.8, 152.0, 145.6, 137.8, 136.7, 133.2, 129.9 (x2), 129.3 (x2), 129.2, 129.1, 128.5 (x2), 128.5, 126.5 (x2), 123.2, 115.7, 102.1, 95.1, 81.9, 64.1, 61.1, 41.8, 28.4 (x3), 21.9 ppm. **HRMS(ESI-MS)** calculated for $C_{29}H_{30}NO_5^+$ [M+H$^+$] 472.2118, found 472.2119.

***tert*-butyl-2a-(2-cyanoethyl)-4-methoxy-7a-methyl-2,2-diphenyl-2a,7a-dihydrooxeto[2,3-*b*]indole-7(2*H*)-carboxylate (63)**

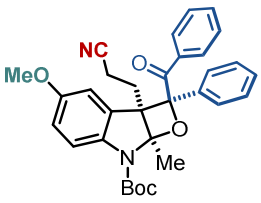

^{1}H-NMR (500 MHz, Acetone-d$_6$): δ 7.91 (d, *J* = 7.5 Hz, 2H, Ar), 7.60 – 7.57 (m, 3H, Ar), 7.53 (t, *J* = 7.5 Hz, 2H, Ar), 7.44 – 7.41 (m, 2H, Ar), 7.27 (t, *J* = 7.5 Hz, 2H, Ar), 7.19 (d, *J* = 2.7 Hz, 1H, Ar), 6.81 (dd, *J* = 9.1, 2.7 Hz, 1H, Ar), 3.87 (s, 3H, OCH_3), 2.47 (ddd, *J* = 16.8, 11.2, 5.8 Hz, 1H, CH_2), 2.11 (s, 3H, CH_3), 2.13 – 2.07 (m, 2H, CH_2) 1.88 (ddd, *J* = 15.7, 10.1, 5.8 Hz, 1H, CH_2), 1.48 (s, 9H, ^{t}Bu-Boc) ppm. **^{13}C-NMR (125 MHz, Acetone-d$_6$):** δ 200.0, 156.9, 152.0, 138.7, 137.6, 136.6, 133.4, 129.9 (x2), 129.5 (x2), 129.4, 129.2, 128.6 (x2), 126.9 (x2), 120.0, 117.0, 115.8, 113.9, 102.0, 95.9, 82.0, 63.7, 56.1, 28.4, 27.8 (x3), 22.2, 13.2 ppm. **HRMS(ESI-MS)** calculated for $C_{32}H_{33}N_2O_5^+$ [M+H$^+$] 525.2384, found 525.2389.

***tert*-butyl-9,9-diphenyl-2,3-dihydro-1*H*,4*H*-3a,8b-(epoxymethano)cyclopenta[*b*]indole-4-carboxylate (64)**

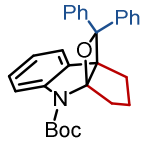

^{1}H-NMR (400 MHz, Acetone-d$_6$): δ 7.72 (d, *J* = 7.9 Hz, 2H, Ar), 7.48 (d, *J* = 7.9 Hz, 2H, Ar), 7.42 – 7.38 (m, 3H, Ar), 7.26 (t, *J* = 7.5 Hz, 1H, Ar), 7.02 – 6.92 (m, 4H, Ar), 6.89 – 6.81 (m, 2H, Ar), 2.70 – 2.61 (m, 2H, CH_2), 1.90 – 1.74 (m, 3H, CH_2), 1.64 (s, 9H, ^{t}Bu-Boc), 1.58 – 1.46 (m, 1H, CH_2) ppm. **^{13}C-NMR (101 MHz, Acetone-d$_6$):** δ 152.0, 145.2, 144.4, 132.8, 129.2, 128.7 (x3), 128.6, 128.0 (x2), 127.5, 127.3, 126.9, 126.7, 126.2 (x2), 125.9 (x2), 123.2, 115.1, 91.4, 55.0, 34.1, 28.6 (x3), 28.3, 28.2 ppm. **HRMS(ESI-MS)** calculated for $C_{29}H_{30}NO_3^+$ [M+H$^+$] 440.2220, found 440.2222.

tert-butyl-11,11-diphenyl-5,6,7,8-tetrahydro-9*H*-8a,4b-(epoxymethano)carbazole-9-carboxylate (65)

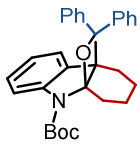

^{1}H-NMR (400 MHz, Acetone-d$_6$): δ 7.64 (d, *J* = 7.9 Hz, 2H, Ar), 7.44 – 7.37 (m, 6H, Ar), 7.23 (t, *J* = 7.3 Hz, 1H, Ar), 6.97 (q, *J* = 7.3 Hz, 3H, Ar), 6.89 (q, *J* = 7.3 Hz, 2H, Ar), 2.57 – 2.51 (m, 1H, CH_2), 2.25 – 2.21 (m, 1H, CH_2), 2.18 – 2.00 (m, 2H, CH_2), 1.64 (s, 9H, ^{t}Bu-Boc), 1.52 – 1.44 (m, 4H) ppm. **^{13}C-NMR (101 MHz, Acetone-d$_6$):** δ 152.0, 145.3, 145.1, 131.8, 129.1, 129.0 (x2), 127.7 (x2), 127.5, 126.7, 126.3 (x2), 126.0 (x2), 125.6, 122.8, 115.0, 101.3, 94.4, 81.4, 58.9, 28.7 (x3), 28.0, 19.9, 19.7 ppm. **HRMS (ESI-MS)** calculated for $C_{30}H_{32}NO_3^+$ [M+H$^+$] 454.2377, found 454.2375.

di-_tert_-butyl-11,11-diphenyl-3,4-dihydro-9*H*-9a,4a-(epoxymethano)pyrido[3,4-*b*]indole-2,9(1*H*)-dicarboxylate (66)

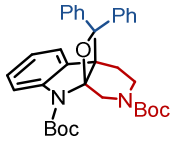

^{1}H-NMR (400 MHz, Acetone-d$_6$): δ 7.69 (t, *J* = 7.1 Hz, 2H, Ar), 7.49 – 7.37 (m, 6H, Ar), 7.27 (q, *J* = 7.1 Hz, 1H, Ar), 7.03 – 6.98 (m, 3H, Ar), 6.93 – 6.86 (m, 2H, Ar), 4.44 (d, *J* = 14.1 Hz, 1H, CH_2), 3.95 (d, *J* = 14.1 Hz, 1H CH_2), 3.34 – 3.24 (m, 1H, CH_2), 2.78 – 2.70 (m, 1H, CH_2), 2.46 – 2.30 (m, 2H, CH_2), 1.68 (s, 9H, ^{t}Bu-Boc), 1.43 (s, 4H, $C(CH_3)_3$), 1.28 (s, 5H, $C(CH_3)_3$) ppm. **^{13}C-NMR (101 MHz, Acetone-d$_6$):** δ 155.7, 155.0, 151.7, 151.7, 144.6, 144.4, 129.4, 129.3, 129.1 (x2), 128.0, 127.9, 127.8, 127.8, 127.1 (x2), 126.2 (x2), 125.8 (x2), 123.2, 123.1, 115.2, 94.9, 82.0, 79.7, 79.6, 41.8, 40.7, 40.2, 28.7 (x3), 28.6 (x3), 28.6 (x3), 28.5 (x3), 27.3, 26.8, 24.4, 21.3, 17.8 ppm. **HRMS (ESI-MS)** calculated for $C_{34}H_{39}N_2O_5^+$ [M+H$^+$] 555.2853, found 555.2859.

di-*tert*-butyl-11-benzoyl-11-phenyl-3,4-dihydro-9H-9a,4a-(epoxymethano)pyrido[3,4-*b*]indole-2,9(1*H*)-dicarboxylate (67)

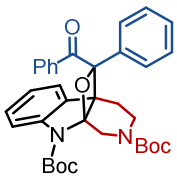

^{1}H NMR (400 MHz, Acetone-d$_6$): δ 7.84 (d, *J* = 7.7 Hz, 2H, Ar), 7.60 (t, *J* = 8.7 Hz, 2H, Ar), 7.52 (t, *J* = 7.2 Hz, 2H, Ar), 7.49 – 7.41 (m, 4H, Ar), 7.31 (t, *J* = 7.5 Hz, 2H, Ar), 7.24 (t, *J* = 7.8 Hz, 1H, Ar), 7.13 (t, *J* = 7.4 Hz, 1H, Ar), 4.25 (dd, *J* = 37.5, 14.3 Hz, 2H, CH_2), 3.20 (*br*, 1H, CH_2), 2.76 – 2.69 (m, 1H, CH_2), 2.19 – 2.10 (m, 2H, CH_2), 1.50 (s, 5H, ^{t}Bu-Boc), 1.47 (s, 9H, ^{t}Bu-Boc), 1.33 (s, 4H, ^{t}Bu-Boc) ppm.**^{13}C NMR (101 MHz, Acetone-d$_6$):** δ 199.2, 137.2, 136.0, 132.3, 129.6, 128.9 (x2), 128.8 (x2), 128.7, 128.2, 128.1, 127.7 (x2), 126.7, 125.5 (x2), 123.0, 114.5, 97.6, 45.5, 39.5, 38.9, 27.7 (x3), 27.5 (x3), 26.1, 25.7, 23.5, 16.9, ppm. **HRMS(ESI-MS)** calculated for $C_{35}H_{39}N_2O_6^+$ [M+H$^+$] 583.2803, found 583.2800.

***tert*-butyl-2a-(2-(*N*-(*tert*-butoxycarbonyl)acetamido)ethyl)-4-methoxy-2,2-diphenyl-2a,7a-dihydrooxeto[2,3-*b*]indole-7(2*H*)-carboxylate (68)**

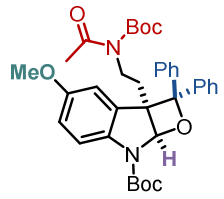

^{1}H NMR (400 MHz, Acetone-d$_6$): δ 7.85 (d, *J* = 7.8 Hz, 2H, Ar), 7.56 (d, *J* = 7.7 Hz, 3H, Ar), 7.44 (t, *J* = 7.7 Hz, 2H, Ar), 7.30 (t, *J* = 7.3 Hz, 1H, Ar), 7.16 (t, *J* = 10.0 Hz, 2H, Ar), 7.07 (d, *J* = 2.5 Hz, 1H, Ar), 7.03 (t, *J* = 7.3 Hz, 1H, Ar), 6.66 (dd, *J* = 8.8, 2.5 Hz, 1H, Ar), 6.54 (*br*, 1H, CH), 3.73 (s, 3H, OCH_3), 3.32 (ddd, *J* = 13.3, 10.7, 5.9 Hz, 1H, CH_2), 3.19 – 3.12 (m, 1H, CH_2), 2.50 – 2.38 (m, 1H, CH_2), 2.27 (s, 3H, $COCH_3$), 1.96 – 1.90 (m, 1H, CH_2), 1.63 (s, 9H, $C(CH_3)_3$), 1.46 (s, 9H, ^{t}Bu-Boc) ppm. **^{13}C NMR (101 MHz, Acetone-d$_6$):** δ 171.6, 155.7, 152.6, 143.3, 128.2 (x4), 127.2 (x4), 127.2, 126.4, 125.9 (x2), 125.5 (x2), 114.1, 112.5, 94.1, 92.5, 82.5, 55.1,

40.9, 39.9, 31.7, 27.6 (x3), 27.2 (x3), 25.9, 23.5, 20.5 ppm. **HRMS (ESI-MS)** calculated for $C_{36}H_{43}N_2O_7^+$ $[M+H^+]$ 615.3065, found 615.3066.

tert-butyl-2a-(2-(_N_-(_tert_-butoxycarbonyl)acetamido)-3-methoxy-3-oxopropyl)-2,2-diphenyl-2a,7a-dihydrooxeto[2,3-_b_]indole-7(2_H_)-carboxylate (69)

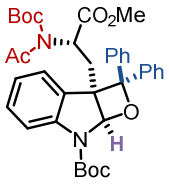

Mixture of diastereoisomers.

^{1}H NMR (400 MHz, Acetone-d$_6$): δ 7.84 (d, *J* = 7.8 Hz, 2H, Ar), 7.49 – 7.44 (m, 5H, Ar), 7.37 – 7.25 (m, 2H, Ar), 7.14 – 6.95 (m, 4H, Ar), 6.81 (t, *J* = 7.5 Hz, 1H, Ar), 6.73 (*br*, 1H, CH), 5.28 (t, *J* = 6.4 Hz, 1H, CH), 3.56 (s, 3H, $COOCH_3$), 2.86 – 2.72 (m, 2H, CH_2), 1.92 (s, 3H, $COCH_3$), 1.65 (s, 9H, ^{t}Bu-Boc), 1.40 (s, 9H, ^{t}Bu-Boc) ppm. **^{13}C NMR (101 MHz, Acetone-d$_6$):** δ 171.3, 170.4, 151.4, 143.3, 143.2, 128.1 (x4), 128.1, 127.2, 127.1, 127.0 (x4), 126.2, 126.1 (x2), 125.6 (x2), 124.2, 122.0, 95.0, 92.3, 83.5, 52.0, 51.5, 32.6, 27.6, 27.0, 25.5 ppm. **HRMS (ESI-MS)** calculated for $C_{32}H_{33}N_2O_5^+$ $[M+H^+]$ 643.3014, found 643.3016. $[a]_D^{20}$ = -0.043 (c=0.62, MeOH).

tert-butyl-2-benzoyl-2a-(-2-(_N_-(_tert_-butoxycarbonyl)acetamido)-3-methoxy-3-oxopropyl)-2-phenyl-2a,7a-dihydrooxeto[2,3-_b_]indole-7(2_H_)-carboxylate (70)

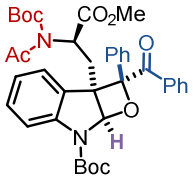

Mixture of diastereoisomers.

^{1}H NMR (400 MHz, Acetone-d$_6$): δ 7.94 (t, *J* = 7.0 Hz, 2H, Ar), 7.66 – 7.53 (m, 5H, Ar), 7.52 – 7.37 (m, 2H, Ar), 7.33 – 7.22 (m, 3H, Ar), 7.20 – 7.08 (m, 1H, Ar), 6.84 (s, 1H, CH), 5.16 (t, *J* = 6.8 Hz, 1H, CH), 3.53 (s, 3H, $COOCH_3$), 2.44 (qd, *J* = 15.1,

6.9 Hz, 2H, CH_2), 2.03 (s, 3H, $COCH_3$), 1.61 (s, 9H, ^{t}Bu-Boc), 1.39 (s, 9H, ^{t}Bu-Boc) ppm. **^{13}C NMR (101 MHz, Acetone-d$_6$):** δ 198.5, 171.2, 151.4, 137.5, 135.2, 133.0, 132.8, 129.3, 129.2, 129.1 (x2), 129.0, 128.8, 128.6, 128.0, 127.9 (x2), 125.9 (x2), 125.7, 122.8, 98.1, 92.5, 83.7, 83.5, 51.8, 51.6, 51.5, 33.0, 27.6 (x3), 27.1 (x3), 30.0, 25.5, 16.9 ppm. **HRMS(ESI-MS)** calculated for $C_{38}H_{43}N_2O_9$ [M+H$^+$] 671.2963, found 671.2970. $[a]_D^{20}$ = -0.017 (c=0.38, MeOH).

Synthesis and characterization of the PB products manipulations

LiAlH$_4$ reduction

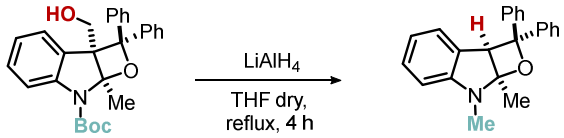

43 (100 mg, 0.225 mmol, 1 equiv.) was dissolved in 10 mL of anhydrous THF (0.025 M). Subsequently, a 1 M solution of $LiAlH_4$ in THF (1.13 mL, 1.125 mmol, 5 equiv.) was added dropwise, the mixture was stirred at reflux for 4 h. Then, the reaction was quenched with 10 mL of EtOAc at 0 °C, 10 mL of a saturated Rochelle salt solution was added, and the mixture was stirred for 30 min. The organic layer was washed with 2 x 10 mL of Rochelle salt saturated solution and 10 mL of a saturated NH_4Cl solution. The organic layer was dried over $MgSO_4$, filtered and concentrated under reduced pressure, giving **71** as a white solid in 77% yield (56.7 mg, 0.174 mmol).

7,7a-dimethyl-2,2-diphenyl-2,2a,7,7a-tetrahydrooxeto[2,3-*b*]indole (71)

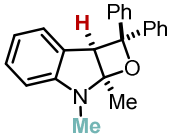

^{1}H-NMR (300 MHz, CDCl$_3$): δ 7.56 (br, 1H, Ar), 7.39 – 7.36 (m, 1H, Ar), 7.29 – 7.26 (m, 2H, Ar), 7.23 – 7.11 (m, 8H, Ar), 7.04 – 6.90 (m, 2H, Ar), 5.71 (s, 1H, CH), 2.23 (s,

3H, NCH_3), 2.12 (s, 3H, CH_3) ppm. **^{13}C-NMR (125 MHz, Acetone-d$_6$):** δ 145.6 (x2), 135.8, 131.0, 129.6, 128.1 (x4), 126.8 (x2), 126.5 (x4), 120.2, 118.2, 117.4, 110.1, 105.7, 75.3, 10.5, 7.7 ppm. **HRMS (ESI-MS)** calculated for $C_{23}H_{22}NO^+$ [M+H$^+$] 328.1696, found 328.1672.

X-ray crystallographic analysis of 58

X-ray structure of 58

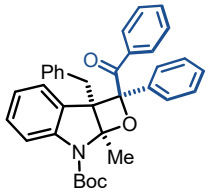

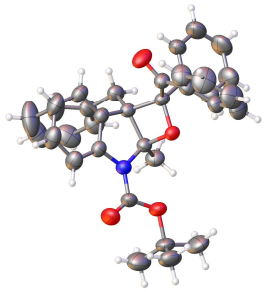

Yellow crystals of **58** were grown by slow evaporation of a diethylether solution at ambient temperature. **Mp**: 120-124 °C.

Crystal data: $C_{35}H_{33}NO_4$

Orthorhombic, *F*2dd, a=8.4764(13)Å, b=33.008(5)Å, c=40.934(6) Å, V=11453(3)Å3; Z=16; dcalc=1.233 mg/cm^3 , F(000)= 4512, mu=0.080, Tot. refl.= 34654 hkl range= -10<h<10, -41<k<41, -50<l<50; Theta max 26.5°, ref.tot.= 5881, number of parameters = 365, GooF= 1.013, R=0.0417, wR2=0.0911.

CCDC 1972525 contains the supplementary crystallographic data for this compound. These data can be obtained free of charge from The Cambridge Crystallographic Data Centre via www.ccdc.cam.ac.uk/data_request/cif

ΔG_{PET} Calculations

Using the Gibbs energy of PET equation (see Paragraph 2.) ΔG of PET processes between *N*-Boc protected indole **30d** and benzophenone **31a** or benzil **31b** has been calculated. $E^{ox}(D)$ is the oxidation potential of the donor **30d**, and has been calculated through cyclic voltammetries reported in Figure Exp2.4. $E^{ox}(\mathbf{30d})$ = 1.40 eV. $E^{red}(A)$ is the reduction potential of the acceptors **31a** and **18b** and has been calculated through cyclic voltammetry reported in Figures Exp2.5 and Exp2.6. $E^{red}(\mathbf{31a})$ = -2.20 eV, $E^{red}(\mathbf{31b})$ = -1.10 eV. ΔE_{exc} is the excitation energy of the acceptor, reported in literature as 2.20 eV.[11] or calculated by onset emission of **31b** as 2.82 eV. ΔE_{coul} is a term that takes into account the ability of the solvent to separate the radical-ion pair, its value is reported as 0.05 eV for MeCN.[12]

ΔG_{ET} (**31a**) = 1.35 eV ΔG_{ET} (**31b**) = -0.27 eV

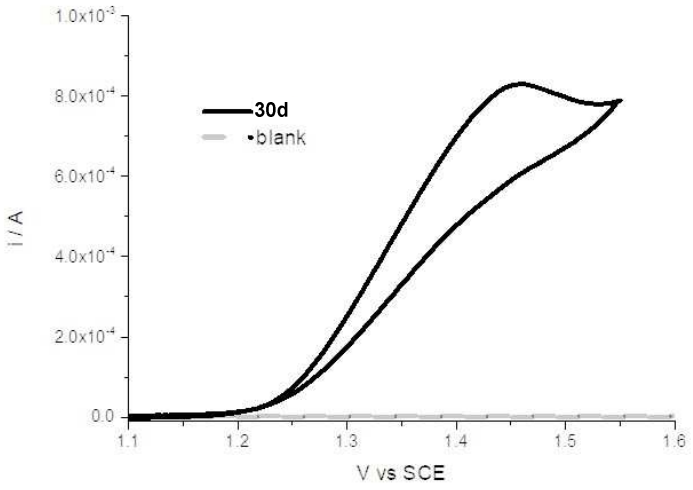

Figure Exp2.4. – Anodic CV of *N*-Boc protected indole **30d** in 0.1 M NEt_4PF_6 MeCN solution. GC electrode. Scan rate: 100 mV/s, potential referred to SCE at room temperature using a platinum wire as counter electrode.

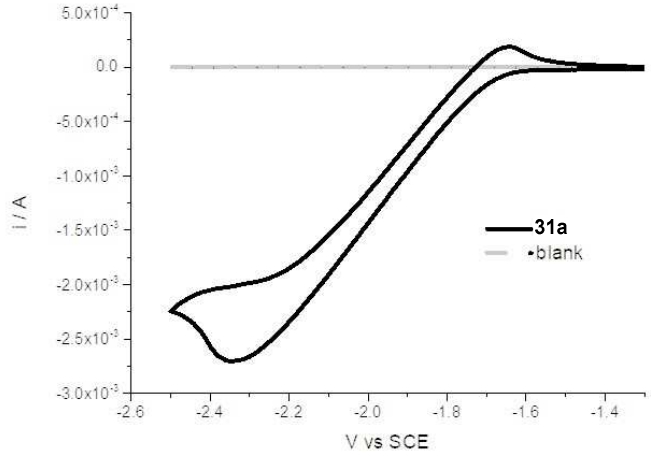

Figure Exp2.5. – Cathodic CV of benzophenone (**31a**) in 0.1 M NEt_4PF_6 MeCN solution. GC electrode. Scan rate: 100 mV/s, potential referred to SCE at room temperature using a platinum wire as counter electrode.

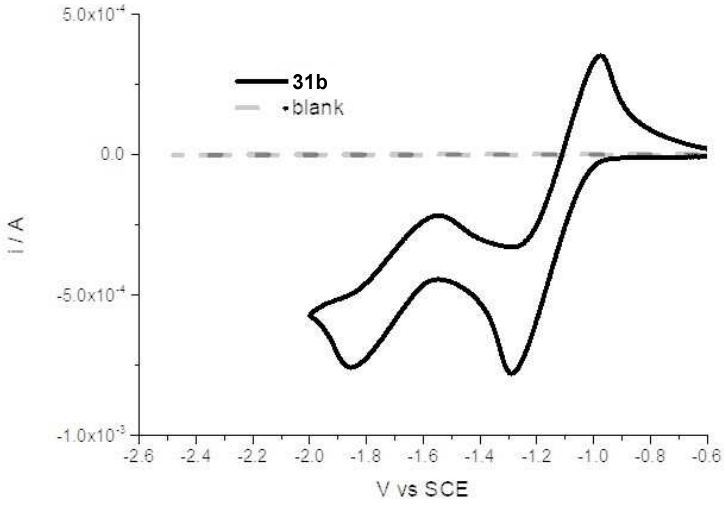

Figure Exp2.6. – Cathodic CV of benzil (**31b**) in 0.1 M NEt_4PF_6 MeCN solution. GC electrode. Scan rate: 100 mV/s, potential referred to SCE at room temperature using a platinum wire as counter electrode.

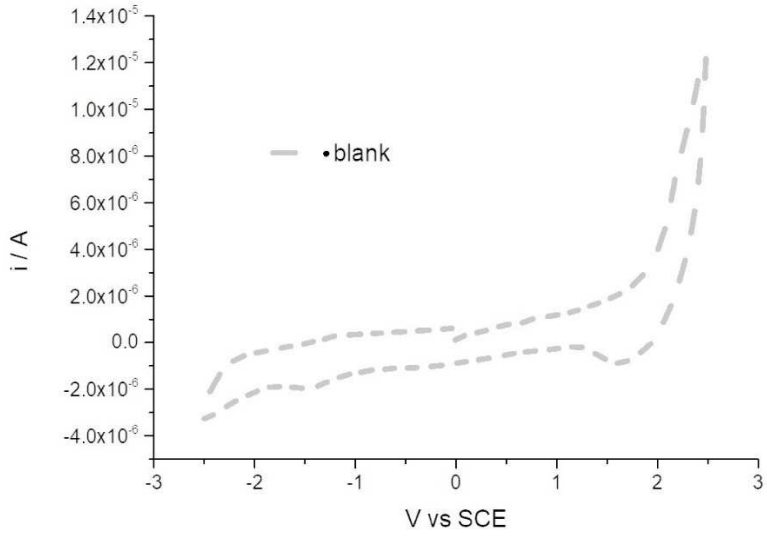

Figure Exp2.7. – Blank Cathodic CV 0.1 M NEt_4PF_6 MeCN solution. GC electrode. Scan rate: 100 mV/s, potential referred to SCE at room temperature using a platinum wire as counter electrode.

Photophisical studies

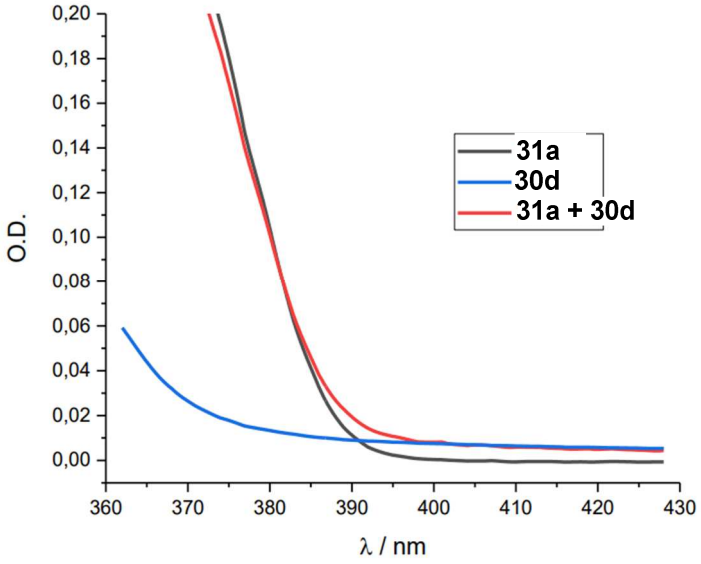

Figure Exp2.8. – Absorption spectra of **31a** (black line), **30d** (blue line) and **31a** + **30d** (red line) 0.01 M in MeCN, 298 K.

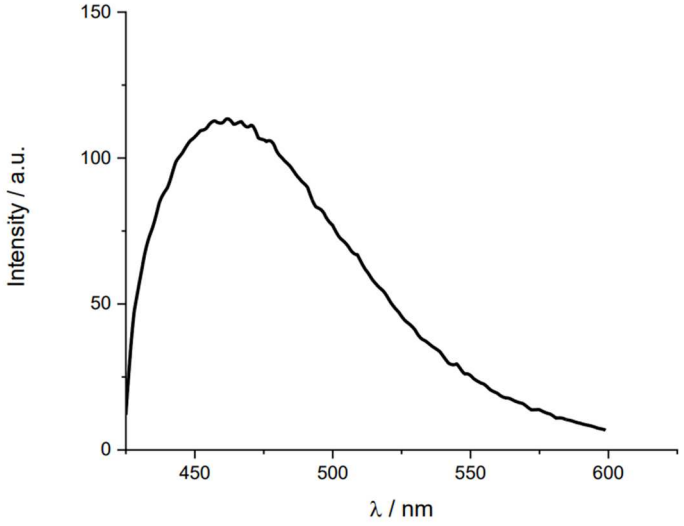

Figure Exp2.9. – Emission spectra of **31a** + **30d** 0.01 M in MeCN, 298 K (λ_{exc} = 405 nm).

Chapter II – Section 2

Microfluidic Visible-Light Synthesis of Functionalised Oxindole Enol Ethers

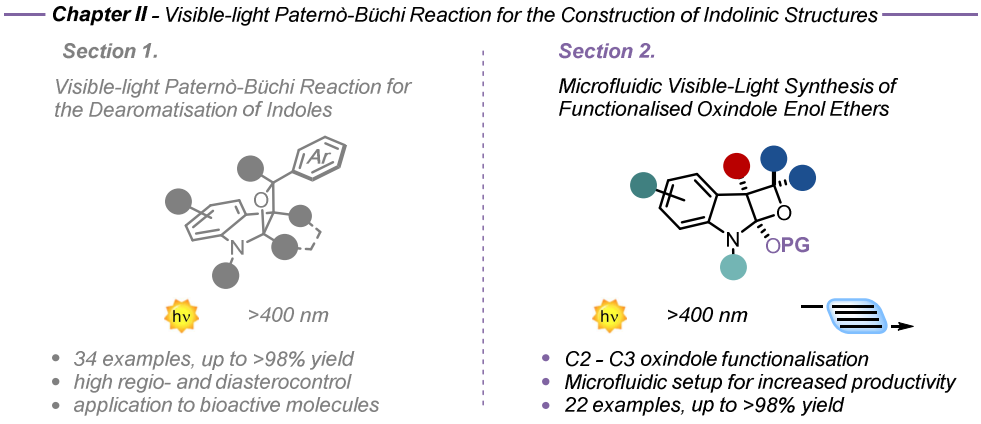

This Section shows the use of a microfluidic visible-light Paternò-Büchi process to obtain doubly functionalised oxindole enol ethers. The reaction was explored employing different oxindole derived silyl-enol-ethers, obtaining the oxeto-indolinic products in high yield and selectivity. The use of a flow reactor greatly improved the productivity of the process and allowed a gram-scale continuous two-step synthesis of two model compounds.

This work has been published: Franceschi, P., Mateos, J., Vega-Peñaloza, A.; Dell'Amico, L. Microfluidic Visible-Light Paternò–Büchi Reaction of Oxindole Enol Ethers. *Eur. J. Org. Chem.*, **2020**, 6718-6722.

2.2.1. – Introduction

The derivatisation of biorelevant heterocyclic scaffolds is a valuable target in organic synthesis.[40] Analogously to the structurally similar indole, the oxindole core is also present in numerous naturally occurring compounds and pharmaceutically active ingredients.[41] Its structural modification allows the discovery of new drug candidates and the implementation of structure-activity-relationship studies.[42]

Recently, the development of new synthetic strategies towards oxindole functionalisation has focused on the installation of the C3 quaternary centre, present in a variety of natural alkaloids.[40, 43] In general, these methodologies rely on the pronucleophilic nature of oxindole. By means of organo- or metal-catalysis a broad array of electrophilic partners can be efficiently activated.[44] While several other methods have exploited the reactivity of the corresponding oxindole enolate or enol ether.[40-42, 44] These methodologies include acylation, alkylation, and condensation reactions with carbonyl compounds (Figure 2.6a).[40] Additionally, the introduction of aryl groups at C3 can be accomplished via transition-metal catalysis with aryl electrophiles and arylboronic acids,[45] while modern approaches focused on metal-free strategies for the installation of a sp^3-sp^2 bond encompassing the activity of photoexcited EDA complexes (Figure 2.6b).[46]

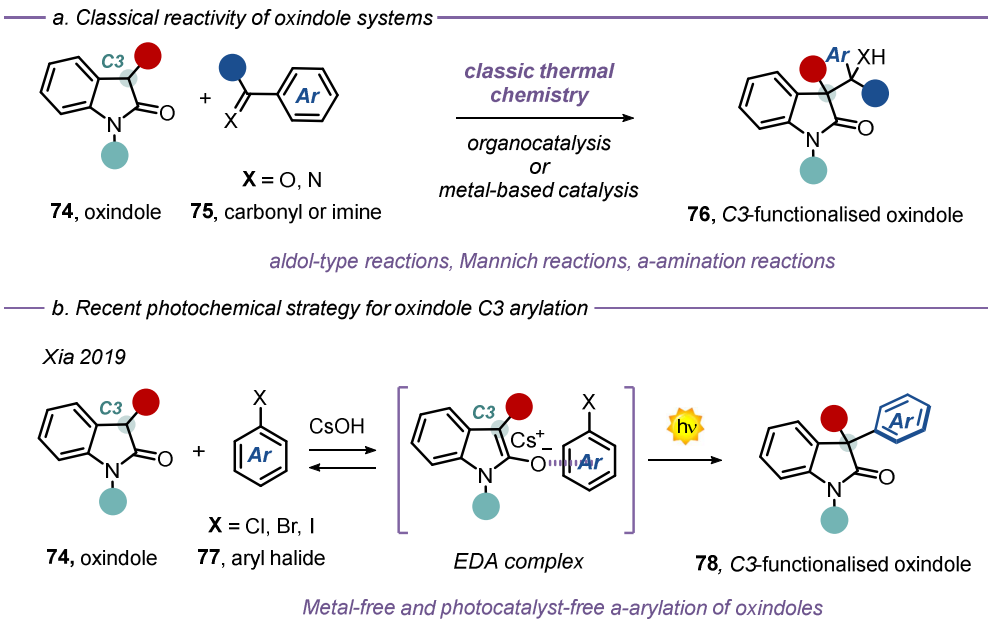

Figure 2.6. – a Classical thermal reactivity of oxindole systems. b. Recent photochemical strategy for the α-arylation of oxindoles.

Despite these recent advancements on the photochemical oxindole functionalization field, the quaternarisation at C3 with the concomitant modification at C2 are still rare. Structural modification at both positions will provide complex indolinic polycyclic scaffolds, with wide occurrence in bioactive molecules.[40] On the other hand, the installation of an oxetane moiety within the oxindole scaffold is particularly appealing thanks to the biological relevance of this four-membered pharmacophore.[4, 30] However, this represents a challenging synthetic target due to the high ring strain and to the low reactivity at C2. A sustainable strategy to fill this gap can be provided using light-generated radical intermediates.[47]

2.2.2. – Aim of the project

As showed in the previous section, light irradiation allows the photocycloaddition of various heterocyclic systems with carbonyl compounds. We thus wondered if oxindole-derived enol ethers could participate in unprecedented PB processes, delivering a C2-C3 difunctionalised indolinic products. Strained indolinic polycycles could be accessed, and the quaternarisation of C3 together with the concomitant C2 functionalisation would be accomplished within a single synthetic operation

The effective realisation of such a general method is complicated by several synthetic issues, including: *i*) the presence of light-driven side reactions, such as the dimerisation of the carbonyl compound enhanced with the use of electron-rich heterocycles, *ii*) the site-, regio- and stereoselectivity of the reaction, *iii*) and the possible desilylation pathways. Additionally, the large-scale synthesis of photochemical reactions is commonly hampered by the need of UV-light sources (Hg or Xe lamps) in batch setups. In this scenario, the use of visible light guarantees a clean and efficient process and the combination with microfluidic photoreactors (MFPs) offer decisive advantages to implement safer and general versions of the PB reaction. Indeed, the MFP setup overcomes some fundamental issues related to photochemical batch protocols, such as: scale up, homogeneous irradiation, reproducibility and generality.[48]

2.2.3. – Results and discussion

Reaction optimisation

We began our studies by testing the silyl enol ether (SEE) **79a** (3 equiv.), derived from the corresponding 3-benzyloxindole, in the presence of benzophenone **31a** in a MFP equipped with a 365 nm light source. 3-Benzyl SEE **79a** was selected aiming to generate a valuable all-carbon quaternary

stereocenter within product **80a**. As expected, when using UV-light sources, we obtained only 12% yield of the product **80a**, along with the undesired benzophenone homodimer **33** (Table 2.7, entry 1). In this case the indole **79** is electron-richer than indoles **30** used in Section 1 of this chapter, thus we slightly modified our optimisation strategy. First, we investigated how the reagent ratio affected the reaction outcome. When **31a** was used in excess, formation of **80a** increased up to a modest 42% yield as single diastereoisomer (entry 2). Regrettably, its purification was complicated by the presence of **33**. As previously stated, a possible solution to circumvent the undesired consumption of benzophenone when using electron-rich heterocycles is the use of visible-light emission sources. In fact, the inferior amount of **31a** T_1 excited state, attenuates the ketone homodimerisation and channels the reactivity towards the intended PB product **80a**. Irradiation of the same reaction mixture at 405 nm resulted in 96% yield of **80a** (entry 3) and no ketone homodimer was detected. Gratefully, we were able to reduce the residence time up to 12 min (entry 4) mantaining excellent yield (98%) and diastereoselectivity (>20:1), while boosting the productivity of the process. Interestingly, when the reaction was performed using an equimolar mixture of reagents, the system maintained decent levels of reactivity (entry 5). Importantly, equimolar mixtures under MFP setups using different solvents such as acetone yielded **80a** in good yields (entry 6, 56% yield).

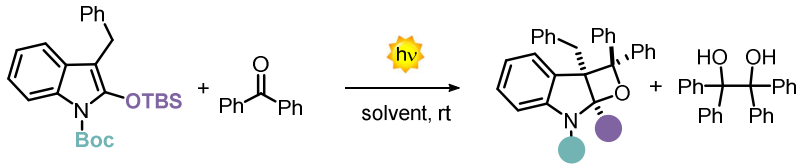

79a 0.1 mmol **31a** 1 eq. **80a** **33**

entry	*light source*	ratio 79a:31a	*residence time*	*solvent*	*(80a) yield %*	*dr*
1	365 nm	3:1	25 min	PhMe	12	>20:1
2	365 nm	1:3	25 min	PhMe	42	>20:1
3	405 nm	1:3	25 min	PhMe	96	>20:1
4	405 nm	1:3	12 min	PhMe	98	>20:1
5	405 nm	1:1	12 min	PhMe	69	>20:1
6	405 nm	1:1	12 min	Acetone	56	>20:1

Table 2.7. – Optimisation of the visible-light dearomatisation reaction between oxindole-derived silyl enol ethers and benzophenone.

Generality of the reaction

With the optimised reaction conditions in hand, we next evaluated the generality of the visible-light PB process. As shown in Table 2.8, variations of the structural and electronic properties of the oxindole enol ether were well tolerated. Both electron-withdrawing (EWG) and electron-donating groups (EDGs) at the ortho, meta and para positions of the benzyl ring furnished the corresponding tricyclic products **80**-**86** in high yields, spanning from 64% to 98% with complete regio- and diastereocontrol. The relative stereochemistry of the products was inferred by X-ray on the single crystal of compound **80**. Also SEE of 3-methyl oxindole resulted in the formation of **87** as single regio- and diastereisomer in 98% yield.

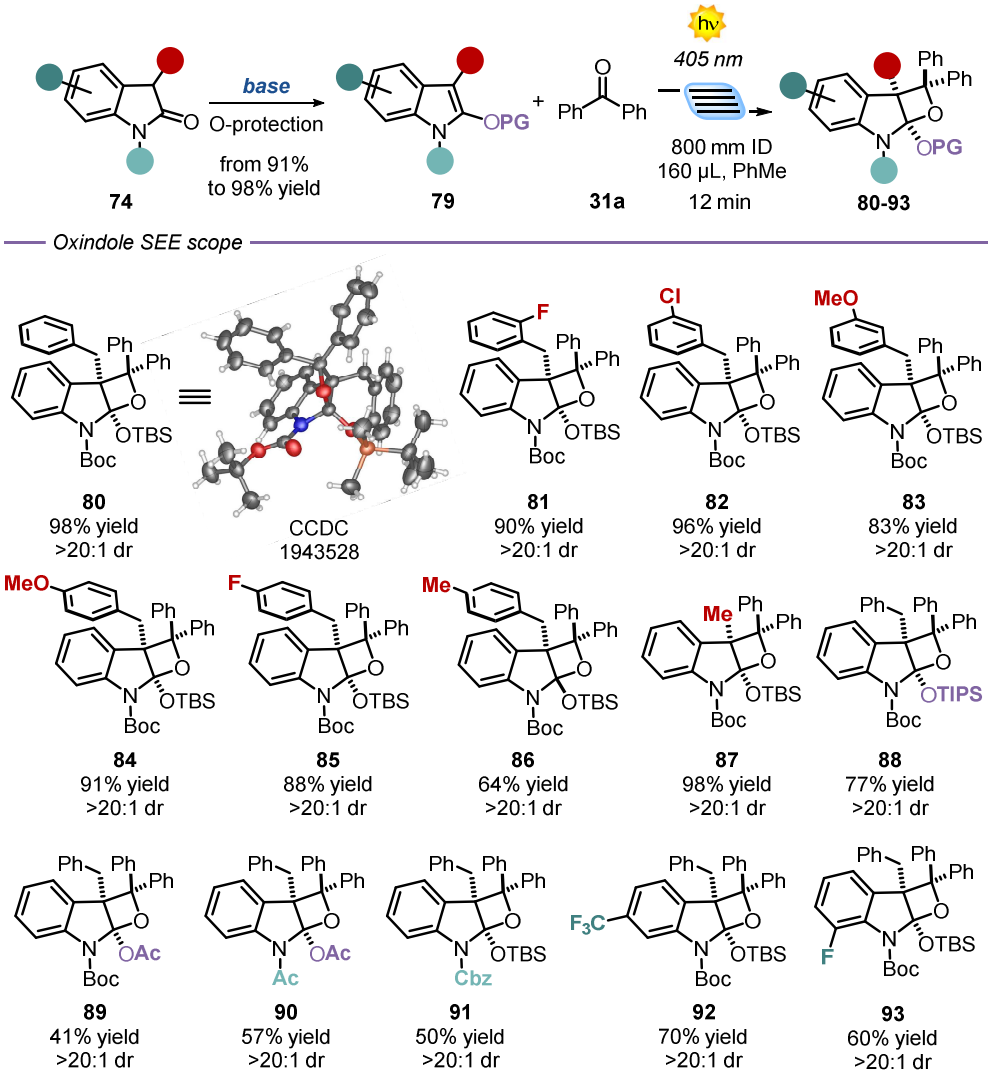

Table 2.8. – Substrate table when using different oxindole-derived silyl enol ether derivatives.

Other types of enol ethers were found competent substrates under these conditions, delivering products **88**, **89** and **90** in 77%, 41% and 57% yield, respectively. Similarly, different *N*-protected oxindoles can participate in the reported microfluidic PB process, delivering product **90** and **7691** in 57% and 50% yield and with high fidelity (>20:1 dr). Oxindole SEEs bearing both EWGs

and EDGs at different position of the oxindole core formed the desired PB products **92** and **93** in good chemical yield (70% and 60%).

We next examined the versatility of the reaction with respect to the ketone partner (Table 2.9). Remarkably, differently substituted benzophenones with both EDGs and EWGs delivered the corresponding products **94-99** in yields spanning from 41% to >98% and excellent regio- and diastereocontrol (>20:1).

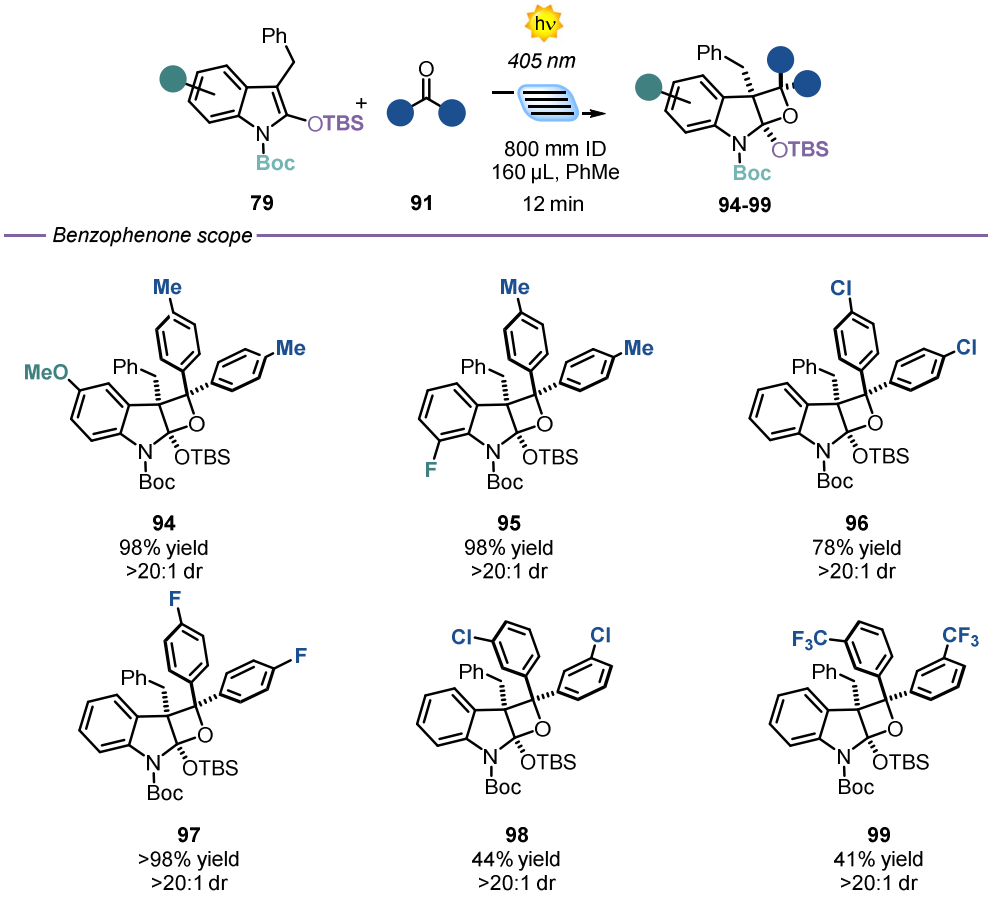

Table 2.9. – Substrate table when using different benzophenone derivatives.

We next assessed substrates with additional reactive double bonds (Figure 2.7). Compound **100**, bearing an allyl functionality, was formed with full site-selectivity (78% yield). Similarly, furan-containing product **101** was formed in 74% yield as a single site-, regio- and diastereoisomer. To understand the reason of the observed site-selectivity we performed a competition experiment in the presence of furan **102** (Figure 2.7b). In this case we used 2 equiv. of bezophenone **31a** and 1 equiv. of **79a** and **102**. After 12 min, product **80** formed in 63% yield along with traces of **103**, thus indicating the superior reactivity for the oxindole-SEE double bond, despite its sterically hindered nature.

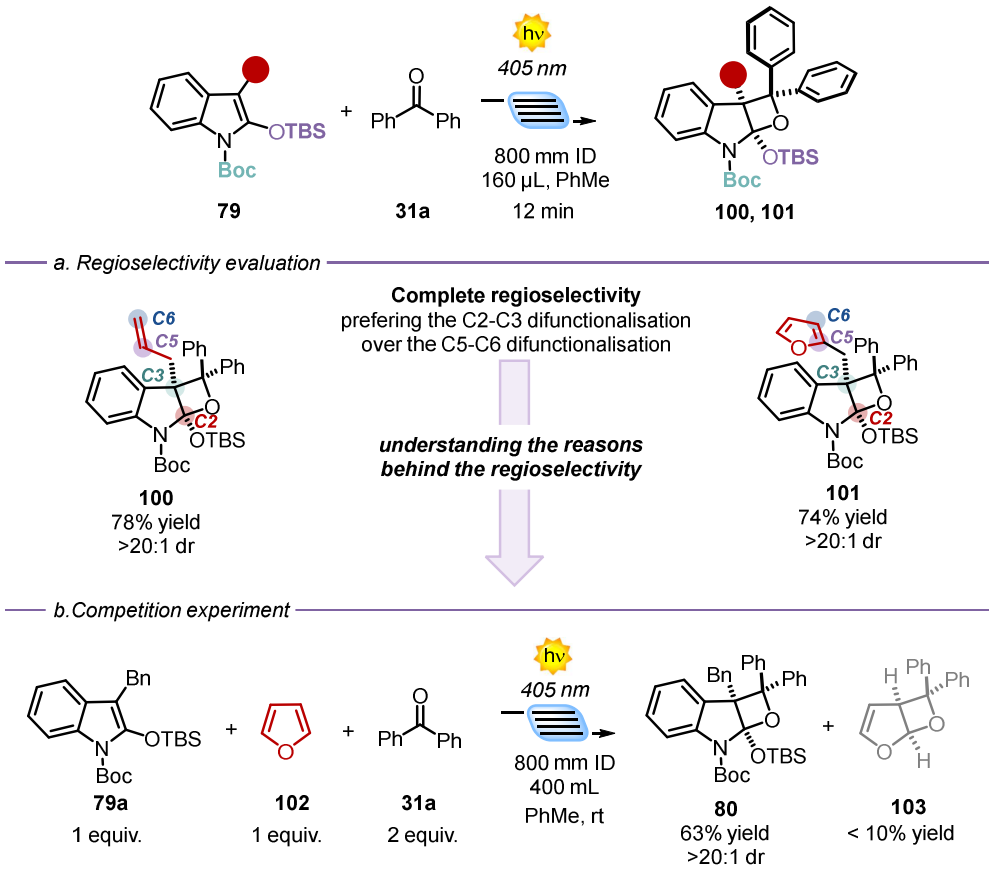

Figure 2.7. – Substrate table with oxindole-derived silyl enol ether containing additional double bonds. a. Regioselectivity evaluation. b. Competition experiment with furan.

Gram-scale synthesis

The synthetic potential of the presented microfluidic method was further demonstrated in the gram-scale functionalization of oxindoles. We implemented an in-flow process, starting from the simple 3-benzyloxindole precursor **74a** (Scheme 2.10). In this case the crude solution of 3-benzyloxidole **79a** (1.00 g, 3.1 mmol), silylating agent (TBSOTf) and base (NEt_3) in presence of the selected ketones **31a** and **31b** was pumped into two parallel MFPs with a retention time of 12 min over 19.4 h. To our delight, the final oxetane products

80 and **94** were collected in 53% and 59% yield, corresponding respectively to 1.02 g and 1.18 g. Importantly, these experiments proved the robustness of the developed method which can be performed also on crude reaction mixtures, containing organic bases and silylating agents, thus avoiding intermediate purifications.

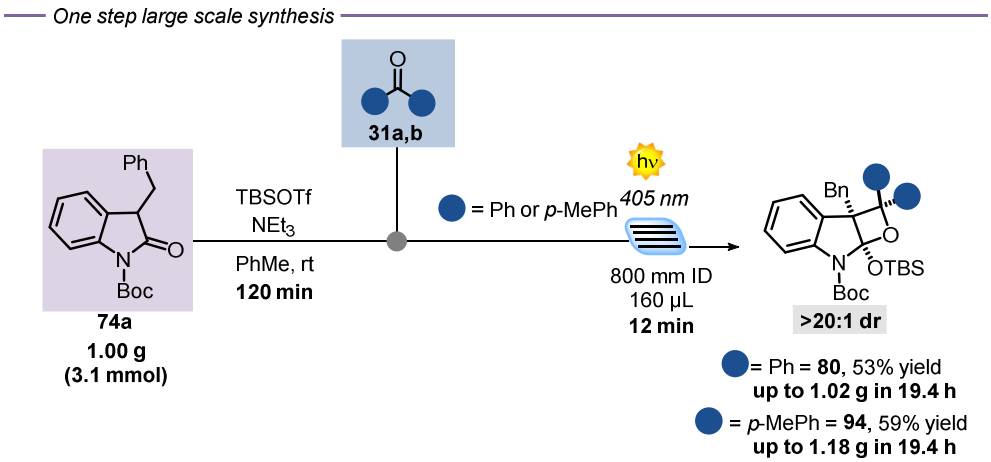

Scheme 2.10. – Gram-scale synthesis of **80** and **94**. Direct functionalization of oxindole.

Mechanistic considerations

Finally, we carried out some analyses to investigate the mechanism of the reaction. Ground or excited-state aggregations of the reagents were not detected, while the only species absorbing at 405 nm is the benzophenone, with an absorption spectrum tailing to the visible region, up to 400 nm. In addition, a photo-induced electron transfer (PET), from the SEE **79a** to the benzophenone **31a** was considered. The electron-rich SEE should be more prone to donate an electron, respect to the indoles **30**, used in the previous section. However, ΔG_{PET}, although lower than with **30a**, is still too high to anticipate a PET process (0.93 eV, corresponding to 21.45 kcal mol^{-1}). The developed PB

reaction is proposed to proceed through a classical radical combination between the light-generated benzophenone T_1 excited state and the C2-C3 double bond of the oxindole SEE. After this initial step, a 1,4-biradical intermediate is formed, which collapses into the final oxetane product with the formation of the C-C bond at C2 of the oxindole.

2.2.4. – Concluding remarks

In this section, the generation of C2-C3 functionalised indoline compounds, derived from oxindole, was disclosed. Using visible-light sources in combination with a MFP setup, the conventional limitations of PB processes were overcome. In facts, the method is general and was easily applied to a variety of different substituted oxindole-derivatives and aromatic ketones with yields up to >98%. and virtually complete site- regio- and diastereocontrol. The occurrence of side-reactions was avoided, and the process was easily scaled-up converting 1 g of 3-benzyloxindole 7**4a** into up to 1.18 g of oxetane product **94**. Despite solving the classical limitations of PB reactions, the process still holds some limitations. As shown in the previous section, employing visible light precludes the use of some important carbonyl compounds, while the strain occurring in the product structure can limit the isolation and manipulation of this latter. Moreover, in this case diminished stereoselectivity was observed when employing benzil **31b**, indicating a possible change in the mechanism of the reaction.

2.2.5. – Experimental section

The continuous flow reactions were carried out using capillary reactors made with PTFE® tubing (0.8 mm I.D., 1.58 mm O.D.) and fitting connections purchased from Sigma-Aldrich®. Reagents were pumped using a Syrris Atlas pump.

The NMR spectra were recorded on Bruker 400 Avance III HD equipped with a BBI-z grad probe head 5mm and Bruker 500 Avance III equipped with a BBI-ATM-z grad probehead 5mm. The chemical shifts (δ) for ^{1}H and ^{13}C are given in ppm relative to residual signals of the solvents ($CHCl_3$ @ 7.26 ppm ^{1}H NMR, 77.16 ppm ^{13}C NMR, Acetone @ 2.09 ppm ^{1}H NMR, 30.60 ppm ^{13}C NMR). Coupling constants are given in Hz. The following abbreviations are used to indicate the multiplicity: s, singlet; d, doublet; t, triplet; q, quartet; m, multiplet; br, broad signal.

The ^{1}H, ^{13}C and ^{19}F NMR spectra are available in literature free of charge.[49]

High-Resolution Mass Spectra (HRMS) were obtained using Waters GCT gas chromatograph coupled with a time-of-flight mass spectrometer with electron ionization (EI).

Chromatographic purification of products was accomplished using flash chromatography on silica gel (SiO_2, 0.04-0.063 mm) purchased from Machery-Nagel, with the indicated solvent system according to the standard techniques. Thin-layer chromatography (TLC) analysis was performed on pre-coated Merck TLC plates (silica gel 60 GF254, 0.25 mm). Visualization of the developed chromatography was performed by checking UV absorbance (254nm) as well as with aqueous ceric ammonium molybdate and potassium permanganate solutions. Organic solutions were concentrated under reduced pressure on a Büchi rotary evaporator.

Materials: Commercial grade reagents and solvents were purchased at the highest commercial quality from Sigma Aldrich or FluoroChem and used as received, unless otherwise stated.

The diverse reaction set up images are available free of charge in literature.[49]

Light-sources emission spectra

The following spectra were recorded using an AvaSpec ULS3648 high-resolution fiber-optic spectrometer which was placed at a fixed distance of 0.5 cm from the light source.

(more info at: https://www.avantes.com/products/spectrometers/starline/item/209-avaspec-uls3648-high-resolution-spectrometer).

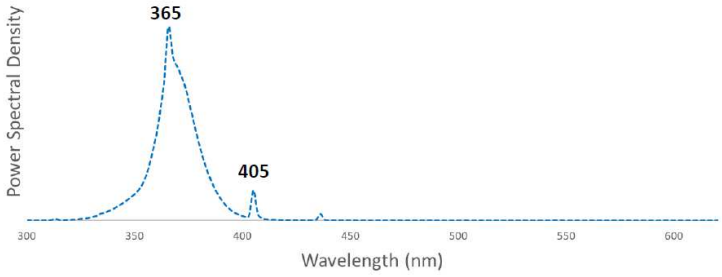

Figure Exp2.10. – Emission spectra of the 9W 365nm bulb light used in this work.

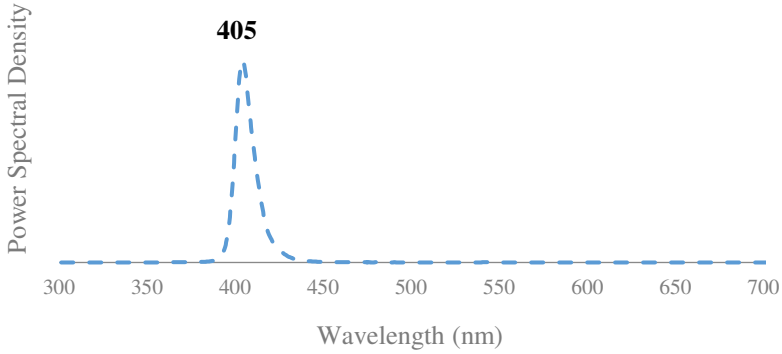

Figure Exp2.11. – Emission spectra of the 20 W 405 nm LED used in this work.

Synthesis and characterization of the used oxindole silyl enol ether derivatives

Preparation of 3-benxyl oxindoles

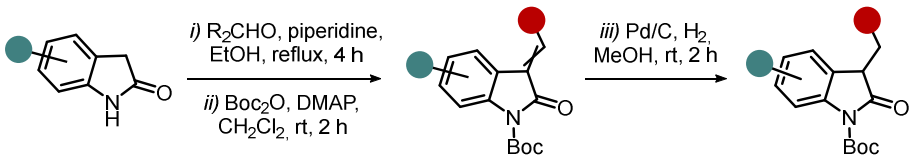

The corresponding aldehyde (4.1 mmol, 1.1 equiv.) and piperidine (0.74 mL, 7.5 mmol, 2.0 equiv.) were added to a suspension of the corresponding oxindole (3.76 mmol, 1.0 equiv.) in ethanol (30 mL, 0,125 M). The resulting mixture was heated to reflux for 4 h. The solution was then allowed to cool to room temperature. The precipitate was filtered, washed with cold ethanol and dried to give 3-benzylideneoxindole as a yellow solid, which was used without further purification.

A 1 mmol fraction of the crude 3-benzylideneoxindole was diluted in CH_2Cl_2 (3.3 mL, 0.3 M) and DMAP was added portionwise (12 mg, 0.1 mmol, 0.1 equiv.). After 5 min, Boc_2O (262 mg, 1.2 mmol, 1.2 equiv.) was added. After

full consumption of the starting material, monitored by TLC (usually after 2 h), the reaction was quenched with 3 mL of cold water. The organic layer was washed with 5 mL of cold water and 5 mL of brine. The combined organic layer was dried with $MgSO_4$ and concentrated under reduced pressure. The crude of the protected benzylideneoxindole was used without further purification.

The crude product was diluted in a two-neck round-bottom flask in MeOH (10 mL, 0.1 M). Pd/C (10 wt%) was added and the flask was filled with H_2. The mixture was stirred at room temperature until full consumption of the starting material, monitored by TLC (usually after 2-4 h). The palladium on carbon was filtered off two filter papers and the solvent was concentrated under reduced pressure. The crude product was purified by column chromatography (9:1, hexane:EtOAc), giving the desired *N*-Boc protected 3-benzyloxindole.

tert-butyl 3-benzyl-2-oxoindoline-1-carboxylate (74a)

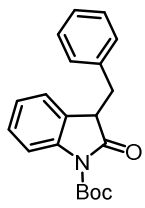

^{1}H-NMR (400 MHz, $CDCl_3$): δ 7.76 (d, *J* = 8.2 Hz, 1H, Ar), 7.23 – 7.31 (m, 4H, Ar), 7.18 (d, *J* = 6.9 Hz, 2H, Ar), 7.03 (t, *J* = 7.5 Hz, 1H, Ar), 6.77 (d, *J* = 7.5 Hz, 1H, Ar), 3.84 (dd, *J* = 9.1, 4.4 Hz, 1H, CH_2a), 3.53 (dd, *J* = 13.9, 4.4 Hz, 1H, CH_2b), 2.98 (dd, *J* = 13.5, 9.1 Hz, 1H, CH), 1.66 (s, 9H, ^{t}Bu-Boc) ppm. **^{13}C-NMR (101 MHz, $CDCl_3$):** δ 175.5, 149.0, 139.9, 137.3, 129.3, 128.3, 128.1, 127.1, 126.7, 124.3, 123.8, 114.7, 84.2, 47.4, 37.5, 28.0 ppm.

tert-butyl 3-(2-fluorobenzyl)-2-oxoindoline-1-carboxylate (74b)

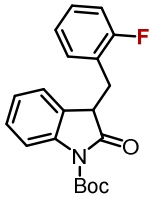

^{1}H-NMR (400 MHz, $CDCl_3$): δ 7.77 (d, *J* = 8.2 Hz, 1H, Ar), 7.31 – 7.13 (m, 3H, Ar), 7.12 – 6.94 (m, 3H, Ar), 6.73 (d, *J* = 7.5 Hz, 1H, Ar), 3.87 (dd, *J* = 9.1, 5.2 Hz, 1H, CH_2a), 3.51 (dd, *J*

= 13.9, 5.2 Hz, 1H, CH_2b), 2.98 (dd, *J* = 13.9, 9.1 Hz, 1H, CH), 1.64 (s, 9H, ^{t}Bu-Boc) ppm. **^{13}C-NMR (101 MHz, $CDCl_3$):** δ 175.4, 161.4 (d, *J* = 246.1 Hz), 149.3, 140.1, 131.8 (d, *J* = 4.5 Hz), 128.9 (d, *J* = 8.2 Hz), 128.4, 127.2, 124.9 (d, *J* = 15.2 Hz), 124.5, 124.2 (d, *J* = 3.7 Hz), 124.1, 115.6 (d, *J* = 22.0 Hz), 114.9, 84.5, 46.2 (d, *J* = 1.7 Hz), 31.1 (d, *J* = 1.9 Hz), 28.2 ppm. **^{19}F NMR (188 MHz, $CDCl_3$)** δ -116.88 (dt, *J* = 12.9, 6.1 Hz, 1F, ArF) ppm.

tert-butyl 3-(3-chlorobenzyl)-2-oxoindoline-1-carboxylate (74c)

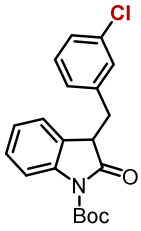

^{1}H-NMR (400 MHz, $CDCl_3$): δ 7.73 (d, *J* = 8.2 Hz, 1H, Ar), 7.25 (q, *J* = 7.8 Hz, 3H, Ar), 7.15 (d, *J* = 7.4 Hz, 2H, Ar), 7.00 (t, *J* = 7.4 Hz, 1H, Ar), 6.74 (d, *J* = 7.4 Hz, 1H, Ar), 3.82 (dd, *J* = 9.2, 4.5 Hz, 1H, CH_2a), 3.50 (dd, *J* = 13.7, 4.5 Hz, 1H CH_2b), 2.95 (dd, *J* = 13.7, 9.2 Hz, 1H, CH), 1.63 (s, 9H, ^{t}Bu-Boc) ppm. **^{13}C-NMR (101 MHz, $CDCl_3$):** δ 175.7, 140.2, 137.5, 130.7, 129.6 (x2), 128.6 (x2), 128.3, 127.4, 127.0, 124.6, 124.1, 115.0, 84.5, 47.7, 37.8, 28.3 (x3). ppm. **HRMS (ESI-MS)** calculated for $C_{20}H_{21}ClNO_3^+$ $[M+H^+]$ 358.1204, found 358.1217.

tert-butyl 3-(3-methoxybenzyl)-2-oxoindoline-1-carboxylate (74d)

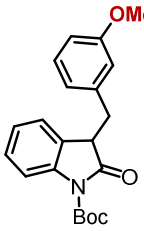

^{1}H-NMR (400 MHz, $CDCl_3$): δ = 7.77 (d, *J* = 8.1 Hz, 1H, Ar), 7.27 (d, *J* = 7.5 Hz, 1H, Ar), 7.20 (t, *J* = 7.8 Hz, 1H, Ar), 7.05 (t, *J* = 7.5 Hz, 1H, Ar), 6.83 – 6.76 (m, 3H, Ar), 6.72 (s, 1H, Ar), 3.85 (dd, *J* = 8.9, 4.2 Hz, 1H, CH_2a), 3,77 (s, 3H, OCH_3), 3.51 (dd, *J* = 13.1, 4.2 Hz, 1H, CH_2b), 2.96 (dd, *J* = 13.1, 8.9

Hz, 1H, CH), 1.66 (s, 9H, ^{t}Bu-Boc) ppm. **^{13}C-NMR (101 MHz, $CDCl_3$):** δ = 175.5, 159.6, 149.2, 140.0, 138.9, 129.4, 128.2, 127.2, 124.5, 123.9, 121.8, 114.9, 114.7, 112.6, 84.1, 55.2, 47.5, 37.7, 28.1 ppm.

tert-butyl 3-(4-methoxybenzyl)-2-oxoindoline-1-carboxylate (74e)

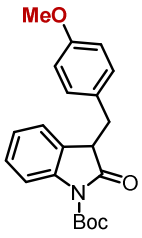

^{1}H-NMR (400 MHz, $CDCl_3$): δ 7.73 (d, *J* = 8.2 Hz, 1H, Ar), 7.27 – 7.20 (m, 1H, Ar), 7.09 – 6.97 (m, 3H, Ar), 6.84 – 6.73 (m, 3H, Ar), 3.78 (s, 4H, OCH_3 and CH_2*a* overlapped), 3.43 (dd, *J* = 13.8, 4.5 Hz, 1H, CH_2*b*), 2.93 (dd, *J* = 13.8, 8.9 Hz, 1H, CH), 1.63 (s, 9H, ^{t}Bu-Boc) ppm. **^{13}C NMR (101 MHz, $CDCl_3$):** δ 175.7, 158.6, 149.3, 140.2, 130.6, 129.4, 128.3, 127.5, 124.6, 124.0, 115.0, 113.9, 84.4, 55.4, 47.9, 36.9, 28.3 ppm.

tert-butyl 3-(4-fluorobenzyl)-2-oxoindoline-1-carboxylate (74f)

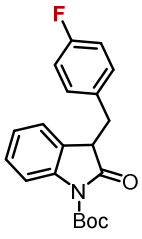

^{1}H-NMR (400 MHz, $CDCl_3$): δ 7.72 (d, *J* = 8.2 Hz, 1H, Ar), 7.25(t, *J* = 7.9 Hz, 1H, Ar) 7.00 – 7.11 (m, 3H, Ar), 6.92 (d, *J* = 8.7 Hz, 2H, Ar), 6.83 (d, *J* = 7.5 Hz, 1H, Ar), 3.79 (dd, *J* = 9.1, 4.4 Hz, 1H, CH_2*a*), 3.42 (dd, *J* = 13.8, 4.4 Hz, 1H, CH_2*b*), 3.02 (dd. *J* = 13.8, 9.1 Hz, 1H, CH), 1.62 (s, 9H, ^{t}Bu-Boc) ppm. **^{13}C-NMR (101 MHz, $CDCl_3$):** δ 175.3, 161.8 (d, *J* = 245.1 Hz), 149.0, 140.1, 132.8 (d, *J* = 3.1 Hz), 130.9 (d, *J* = 8.0 Hz), 128.3, 126.9, 124.1 (d, *J* = 25.0 Hz), 115.3, 115.0 (d, *J* = 16.1 Hz), 84.3, 47.6, 36.7, 28.0 ppm.

***tert*-butyl 3-benzyl-2-oxo-6-(trifluoromethyl)indoline-1-carboxylate (74g)**

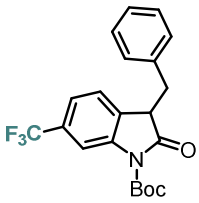

^{1}H-NMR (600 MHz, $CDCl_3$): δ 8.09 – 8.09 (m, 1H), 7.32 – 7.27 (m, 4H, Ar), 7.17 – 7.16 (m, 2H, Ar), 6.82 (d, *J* = 7.8 Hz, 1H, Ar), 3.88 (dd, *J* = 9.1, 4.4 Hz, 1H, CH_2*a*), 3.56 (dd, *J* = 13.8, 4.4 Hz, 1H, CH_2*b*), 2.98 (dd, *J* = 13.8, 9.1 Hz, 1H, CH), 1.66 (s, 9H, ^{t}Bu-Boc) ppm. **^{13}C-NMR (151 MHz, $CDCl_3$):** δ 174.8, 149.0, 140.6, 136.9, 129.5 (x2), 128.8 (x2), 127.3, 124.8, 121.1, 121.0, 112.3, 112.3, 85.2, 47.6, 37.6, 28.2 (x3), 28.1 ppm. **HRMS (ESI-MS)** calculated for $C_{21}H_{21}F_3NO_3^+$ $[M+H^+]$ 392.1468, found 392.1458.

***tert*-butyl 3-benzyl-7-fluoro-2-oxoindoline-1-carboxylate (74h)**

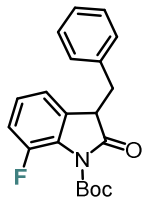

^{1}H-NMR (600 MHz, $CDCl_3$): δ 7.29 – 7.24 (m, 3H, Ar), 7.14 (dd, *J* = 7.9, 1.7 Hz, 2H, Ar), 7.02 – 7.01 (m, 2H, Ar), 6.64 – 6.61 (m, 1H), 3.89 (dd, *J* = 8.6, 4.5 Hz, 1H, CH_2*a*), 3.50 (dd, *J* = 13.8, 4.5 Hz, 1H, CH_2*b*), 3.06 (dd, *J* = 13.8, 8.6 Hz, 1H, CH), 1.59 (s, 9H, ^{t}Bu-Boc).ppm. **^{13}C-NMR (151 MHz, $CDCl_3$):** δ 174.9, 148.7 (d, *J* = 250.6 Hz), 147.5, 136.8, 130.5, 130.5, 129.5 (x2), 128.6 (x2), 127.1, 125.1 (d, *J* = 6.9 Hz), 120.4 (d, *J* = 3.5 Hz), 116.6 (d, *J* = 20.5 Hz), 84.9, 48.0 (d, *J* = 1.4 Hz), 37.6, 27.8 (x3) ppm. **HRMS (ESI-MS)** calculated for $C_{20}H_{21}FNO_3^+$ $[M+H^+]$ 342.1500, found 342.1511.

***tert*-butyl 3-benzyl-5-methoxy-2-oxoindoline-1-carboxylate (74i)**

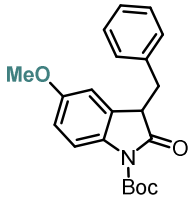

^{1}H-NMR (400 MHz, $CDCl_3$): δ 7.69 (d, *J* = 9.0, 1H, Ar), 7.34 – 7.24 (m, 3H, Ar), 7.21 (d, *J* = 7.9 Hz, 2H, Ar), 6.79 (dd, *J* = 2.8, 8.9 Hz, 1H, Ar), 6.36 (d, *J* = 2.9 Hz, 2H, Ar), 3.81 (dd, *J* = 4.7; 9.4 Hz, 1H, CH_2*a*), 3.67 (s, 3H, OCH_3),

3.55 (dd, *J* = 4.0; 13.5 Hz, 1H, CH_2b), 2.94 (dd, *J* = 9.4; 13.5, 1H, CH), 1.65 (s, 9H, ^{t}Bu-Boc) ppm. **^{13}C-NMR (101 MHz, $CDCl_3$):** δ 175.5, 156.2, 149.2, 137.4, 133.4, 129.5, 128.5, 126.9, 115.9, 113.2, 110.5, 84.1, 55.6, 47.8, 37.7, 28.2 ppm.

tert-butyl 3-(furan-2-ylmethyl)-2-oxoindoline-1-carboxylate (74j)

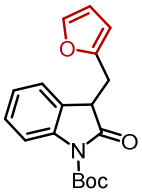

^{1}H-NMR (400 MHz, $CDCl_3$): δ 7.79 (d, *J* = 7.2 Hz, 1H, Ar), 7.31 – 7.37 (m, 1H, Ar), 7.27 (t, *J* = 7.8 Hz, 1H, Ar), 7.05 (t, *J* = 7.5 Hz, 1H, Ar), 6.77 (t, *J* = 7.5 Hz, 1H, Ar), 6.20 – 6.34 (m, 1H, Ar), 6.03 (d, *J* = 3.2 Hz, 1H, Ar), 3.89 (dd, *J* = 9.1, 4.4 Hz, 1H, CH_2a), 3.48 (dd, *J* = 13.9, 4.4 Hz, 1H, CH_2b), 3.00 (dd. *J* = 13.9, 9.1 Hz, 1H, CH), 1.65 (s, 9H, ^{t}Bu-Boc) ppm. **^{13}C-NMR (101 MHz, $CDCl_3$):** δ 175.1, 151.5, 149.2, 141.7, 140.0, 128.3, 127.0, 124.3, 124.2, 114.9, 110.5, 107.7, 84.4, 45.2, 29.9, 28.2 ppm.

Preparation of 3-methyl oxindole

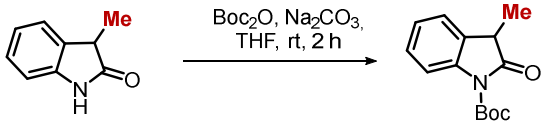

Synthesized following literature procedure starting from 3-methyloxindole (1.47 g, 10 mmol), yielding pure 7**4k** (colorless oil), in >98% yield (2.74 g, 10 mmol).

***tert*-butyl 3-methyl-2-oxoindoline-1-carboxylate (74k)**

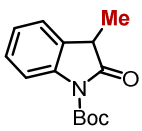

^{1}H-NMR (400 MHz, $CDCl_3$): δ 7.74 (d, *J* = 8.1 Hz, 1H, Ar), 7.13 – 7.33 (m, 2H, Ar), 6.99 – 7.13 (m, 1H, Ar), 3.49 (q, *J* = 7.5 Hz, 1H, CH), 1.57 (s, 9H, ^{t}Bu-Boc), 1.45 (d, *J* = 7.5, 3H, CH_3) ppm. **^{13}C-NMR (101 MHz, $CDCl_3$):** δ 176.9, 149.4, 139.8, 129.4, 128.1, 124.3, 123.4, 115.0, 84.3, 41.0, 28.1, 15.9 ppm.

Preparation of N-Ac protected oxindole

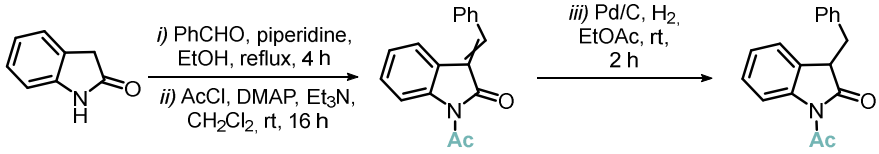

Benzaldehyde (1.7 mL, 17 mmol, 1.13 equiv.) and piperidine (3.0 mL, 30 mmol, 2.0 equiv.) were added to a suspension of 2-oxindole (2.0 g, 15 mmol, 1.0 equiv.) in ethanol (30 mL). The resulting mixture was heated to reflux for 4 h. The solution was then allowed to cool to 0 °C. The precipitate was filtered, washed with small amount of cold ethanol and dried to give 3-benzylideneoxindole as a yellow solid, which was used without further purification.

A 1 mmol fraction of the crude benzylideneoxindole was diluted in CH_2Cl_2 (10 mL, 0.1 M), DMAP was added portionwise (257 mg, 2.1 mmol, 2.1 equiv.) and NEt_3 (293 µL, 2.1 mmol, 2.1 equiv.). After 5 min, AcCl (149 µL, 2.1 mmol, 2.1 equiv.) was added dropwise at 0 °C and stirred at rt. After full consumption of the starting material, monitored by TLC (usually after 16 h), the reaction was quenched with water. The organic layer was washed with 2 x 25 mL of water. The organic layer was dried with $MgSO_4$ and concentrated under

reduced pressure. The crude of the protected benzylideneoxindole was used without further purification.

The crude product was diluted in a two-neck round-bottom flask in EtOAc (10 mL, 0.1 M). Pd/C (10 wt%) was added and the flask was filled with H_2. The mixture was stirred at room temperature until full consumption of the starting material, monitored by TLC (usually after 2-4 h). The palladium on carbon was filtered and the solvent was concentrated under reduced pressure. The crude product was purified by column chromatography (9:1, hexane:EtOAc), giving the desired *N*-Ac protected 3-benzyloxindole in 61% yield after 3 consecutive steps.

1-acetyl-3-benzylindolin-2-one (74l)

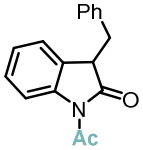

^{1}H-NMR (400 MHz, $CDCl_3$): δ 8.16 (d, *J* = 8.3 Hz, 1H, Ar), 7.31 – 7.22 (m, 4H, Ar), 7.14 – 7.10 (m, 3H, Ar), 6.91(d, *J* = 7.5 Hz, 1H, Ar), 3.92 (dd, *J* = 8.5, 4.7 Hz, 1H, CH_2*a*), 3.48 (dd, *J* = 13.7, 4.7 Hz, 1H, CH_2*b*), 3.09 (dd, *J* = 13.7, 8.5 Hz, 1H, CH), 2.65 (s, 3H, CH_3-Ac) ppm. **^{13}C-NMR (101 MHz, $CDCl_3$):** δ 177.7, 170.8, 140.5, 136.8, 129.4, 128.4, 128.3, 127.4, 127.0, 124.7, 124.1, 116.4, 47.6, 37.6, 26.7 ppm.

Preparation of N-Cbz protected oxindole

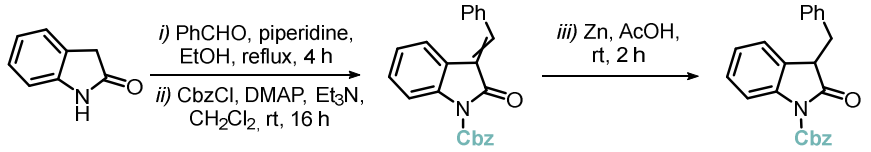

Benzaldehyde (1.7 mL, 17 mmol, 1.13 equiv.) and piperidine (3.0 mL, 30 mmol, 2.0 equiv.) were added to a suspension of 2-oxindole (2.0 g, 15 mmol, 1.0 equiv.) in ethanol (30 mL). The resulting mixture was heated to reflux for

4 h. The solution was then allowed to cool to 0 °C. The precipitate was filtered, washed with small amount of cold ethanol and dried to give 3-benzylideneoxindole as a yellow solid, which was used without further purification.

A 1 mmol fraction of the crude benzylideneoxindole was diluted in CH_2Cl_2 (10 mL, 0.1 M), DMAP was added portionwise (257 mg, 2.1 mmol, 2.1 equiv.) and NEt_3 (293 µL, 2.1 mmol, 2.1 equiv.). After 5 min, CbzCl (300 µL, 2.1 mmol, 2.1 equiv.) was added dropwise at 0 °C and stirred at rt. After full consumption of the starting material, monitored by TLC (usually after 16 h), the reaction was quenched with water. The organic layer was washed with 2 x 25 mL of water. The organic layer was dried with $MgSO_4$ and concentrated under reduced pressure. The crude of the protected benzylideneoxindole was used without further purification.

The crude product was diluted in a round-bottom flask in acetic acid (10 mL, 0.1 M). Zn (1.3 g, 20 mmol, 20.0 equiv.) was added. The mixture was stirred at room temperature until full consumption of the starting material, monitored by TLC (usually after 2 h). The Zn was filtered, and the acid was quenched under vigorous stirring at 0 °C with 60 mL of a saturated $NaHCO_3$ solution. The solution was extracted with 3 x 20 mL of EtOAc, the combined organic layers were dried over $MgSO_4$ and concentrated under reduced pressure. The crude product was purified by column chromatography (9:1, hexane:EtOAc), giving the desired *N*-Cbz protected 3-benzyloxindole in 72% yield after three consecutive steps.

benzyl 3-benzyl-2-oxoindoline-1-carboxylate (74m)

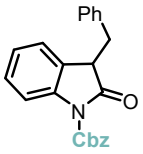

^{1}H-NMR (400 MHz, $CDCl_3$): δ 7.84 (d, *J* = 8.2 Hz, 1H, Ar), 7.54 (d, *J* = 7.8 Hz, 2H, Ar), 7.45 – 7.38 (m, 4H, Ar), 7.29 – 7.25 (m, 3H, Ar), 7.17 – 7.15 (m, 2H, Ar), 7.07 (s, 1H, Ar), 6.83 (d, *J* = 7.5 Hz, 1H, Ar), 5.46 (s, 2H, CH_2), 3.90 (dd, *J* = 8.8, 4.6 Hz, 1H, CH_2*a*), 3.55 – 3.47 (m, 1H, CH_2*b*), 3.04 (dd, *J* = 13.7, 8.8 Hz, 1H, CH) ppm. **^{13}C-NMR (101 MHz, $CDCl_3$):** δ 175.1, 150.7, 139.6, 137.1, 135.1, 129.4, 128.7, 128.5, 128.3, 128.1, 127.8, 127.2, 126.9, 124.4, 124.3, 115.0, 68.5, 47.5, 37.6 ppm.

Preparation of 3-allyl derived oxindole

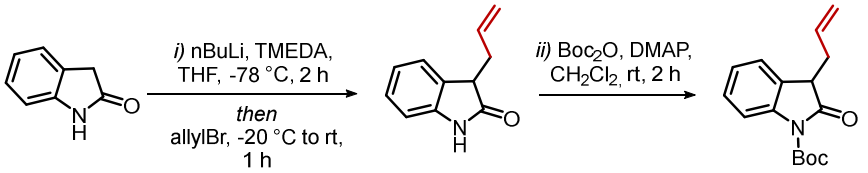

Following literature procedure, 2-oxindole (4.0 g, 30 mmol) gave the 3-substituted unprotected oxindole in 81% yield (4.2 g, 24.3 mmol).

The unprotected oxindole (1.1 g, 6.4 mmol, 1.0 equiv.) was diluted in CH_2Cl_2 (13 mL, 0.5 M) and DMAP was added portionwise (75 mg, 0.6 mmol, 0.1 equiv.). After 5 min, Boc_2O (2.1 g, 9.6 mmol, 1.5 equiv.) was added. After full consumption of the starting material, monitored by TLC (usually after 2 h), the reaction was quenched with a 4 M solution of HCl. The organic layer was washed with 2 x 10 mL of HCl 4 M and 2 x 10 mL $NaHCO_3$. The combined organic layer was dried with $MgSO_4$ and concentrated under reduced pressure. Purification through silica gel chromatography (9:1, hexane:EtOAc) gave **74n** in 94% yield.

***tert*-butyl 3-allyl-2-oxoindoline-1-carboxylate (74n)**

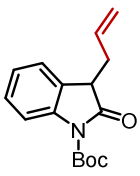

^{1}H-NMR (400 MHz, $CDCl_3$): δ 7.83 (d, *J* = 7.9 Hz, 1H, Ar), 7.34 – 7.28 (m, 2H, Ar), 7.18 – 7.14 (m, 1H, Ar), 5.83 – 5.72 (m, 1H, $C(sp^2)H$), 5.16 – 5.08 (m, 2H, $C(sp^2)H_2$), 3.65 – 3.62 (m, 1H, CH_2a), 2.89 – 2.82 (m, 1H, CH_2b), 2.69 – 2.62 (m, 1H, CH), 1.66 (s, 9H, ^{t}Bu-Boc) ppm. **^{13}C-NMR (101 MHz, $CDCl_3$):** δ 175.5, 149.2, 140.1, 133.5, 128.2, 127.4, 124.2, 124.0, 118.6, 114.9, 84.3, 45.7, 35.4, 28.1 ppm.

Preparation of oxindole-derived SEE

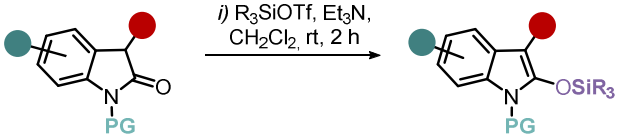

In a round-bottom flask, the *N*-protected oxindole (0.5 mmol, 1.0 equiv.) was dissolved in CH_2Cl_2 (1.7 mL, 0.3 M) under Ar atmosphere. NEt_3 (139 µL, 1.0 mmol, 2.0 equiv.) was added dropwise at 0 °C. After 5 min, R_3SiOTf (0.75 mmol, 1.5 equiv.) was added dropwise at 0 °C and stirred at room temperature. After full consumption of the starting material, monitored by TLC (usually after 2 h), 15 mL of hexane were added. The organic layer was washed with 3 x 10 mL of a saturated solution of $NaHCO_3$, dried over $MgSO_4$ and concentrated under reduced pressure. The crude product was purified by column chromatography (98:2, hexane:EtOAc).

***tert*-butyl 3-benzyl-2-((tert-butyldimethylsilyl)oxy)-1H-indole-1-carboxylate (79a)**

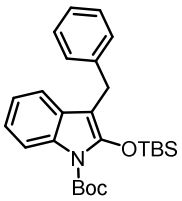

^{1}H-NMR (400 MHz, $CDCl_3$): δ 7.86 (d, *J* = 7.5 Hz, 1H, Ar), 7.29 – 7.26 (m, 4H, Ar), 7.22 – 7.08 (m, 4H, Ar), 4.00 (s, 2H, CH_2), 1.74 (s, 9H, ^{t}Bu-Boc), 1.09 (s, 9H, ^{t}Bu-TBS), 0.26 (s, 6H, 2 x CH_3-TBS) ppm. **^{13}C-NMR (101 MHz, $CDCl_3$):** δ 149.5, 145.2, 140.2, 131.3, 129.0, 128.6 (x2), 128.4 (x2), 126, 122.5, 122.0, 118.4, 114.6, 100.0, 83.6, 29.2, 28.5 (x3), 26.0 (x3), 18.6, -3.9 (x2) ppm. **HRMS (ESI-MS)** calculated for $C_{26}H_{36}NO_3Si^+$ $[M+H^+]$ 438.2459, found 438.2475.

***tert*-butyl 2-((tert-butyldimethylsilyl)oxy)-3-(2-fluorobenzyl)-1H-indole-1-carboxylate (79b)**

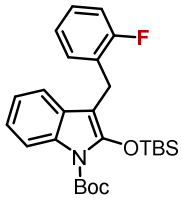

^{1}H-NMR (400 MHz, $CDCl_3$): δ 7.86 – 7.84 (m, 1H, Ar), 7.17 – 6.95 (m, 7H, Ar), 4.00 (s, 2H, CH_2), 1.73 (s, 9H, ^{t}Bu-Boc), 1.07 (s, 9H, ^{t}Bu-TBS), 0.24 (s, 6H, 2 x CH_3-TBS) ppm. **^{13}C-NMR (101 MHz, $CDCl_3$):** δ 161.1 (d, *J* = 244.3 Hz), 149.4, 145.5, 131.2, 130.6 (d, *J* = 4.7 Hz), 128.8, 127.6 (d, *J* = 8.1 Hz), 127.0 (d, *J* = 15.9 Hz), 124.1 (d, *J* = 3.5 Hz), 122.7, 122.2, 118.1, 115.0 (d, *J* = 22.0 Hz), 114.6, 98.5, 83.7, 28.5 (x3), 26.0 (x3), 21.4 (d, *J* = 4.4 Hz), 18.6, -3.9 (x2) ppm. **^{19}F-NMR (376 MHz, $CDCl_3$):** δ - 118.77 (q, J = 8.0 Hz, 1F, ArF) ppm. **HRMS (ESI-MS)** calculated for $C_{26}H_{35}FNO^3Si^+$ $[M+H^+]$ 456.2365, found 456.2336.

***tert*-butyl 2-((tert-butyldimethylsilyl)oxy)-3-(3-chlorobenzyl)-1H-indole-1-carboxylate (79c)**

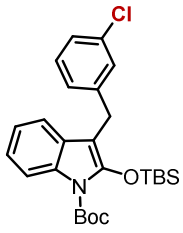

^{1}H-NMR (400 MHz, $CDCl_3$): δ 7.84 (d, *J* = 7.5 Hz, 1H, Ar), 7.30 – 7.24 (m, 3H, Ar), 7.20 – 7.06 (m, 4H, Ar), 3.99 (s, 2H, CH_2), 1.72 (s, 9H, ^{t}Bu-Boc), 1.08 (s, 9H, ^{t}Bu-TBS), 0.25 (s, 6H, 2 x CH_3-TBS) ppm. **^{13}C-NMR (101 MHz, $CDCl_3$):** δ 149.5, 145.2, 140.2, 131.3, 129.0, 128.6 (x2), 128.4 (x2), 126.0, 122.5, 122.0, 118.4, 114.6, 100.0, 83.6, 29.2, 28.5 (x3), 26.0 (x3), 18.5, -4.0 (x2). ppm. **HRMS (ESI-MS)** calculated for $C_{26}H_{35}ClNO_3Si^+$ $[M+H^+]$ 472.2069, found 471.2746.

***tert*-butyl 2-((tert-butyldimethylsilyl)oxy)-3-(3-methoxybenzyl)-1H-indole-1-carboxylate (79d)**

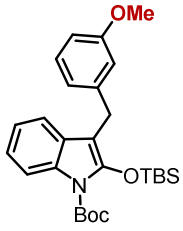

^{1}H-NMR (400 MHz, $CDCl_3$): δ 7.84 (d, *J* = 7.5 Hz, 1H, Ar), 7.20 – 7.09 (m, 4H, Ar), 6.89 – 6.84 (m, 2H, Ar), 6.74 (d, *J* = 7.7 Hz, 1H, Ar), 3.96 (s, 2H, CH_2), 3.76 (s, 3H, OCH_3), 1.73 (s, 9H, ^{t}Bu-Boc), 1.08 (s, 9H, ^{t}Bu-TBS), 0.25 (s, 6H, 2 x CH_3-TBS) ppm. **^{13}C-NMR (101 MHz, $CDCl_3$):** δ 159.8, 149.5, 145.1, 141.9, 131.3, 129.4, 128.9, 122.5, 122.0, 121.1, 118.4, 114.5, 114.4, 111.4, 99.8, 83.6, 55.3, 29.3, 28.5 (x3), 26.0 (x3), 18.5, -3.9 (x2) ppm. **HRMS (ESI-MS)** calculated for $C_{27}H_{38}NO_4Si^+$ $[M+H^+]$ 468.2565, found 468.2583.

***tert*-butyl 2-((tert-butyldimethylsilyl)oxy)-3-(4-methoxybenzyl)-1H-indole-1-carboxylate (79e)**

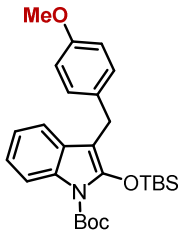

^{1}H-NMR (400 MHz, $CDCl_3$): δ 7.82 (d, *J* = 7.5 Hz, 1H, Ar), 7.18 – 7.05 (m, 5H, Ar), 6.80 (d, *J* = 7.5 Hz, 2H, Ar), 3.91 (s, 2H, CH_2), 3.77 (s, 3H, OCH_3), 1.71 (s, 9H, ^{t}Bu-Boc), 1.06 (s, 9H, ^{t}Bu-TBS), 0.23 (s, 6H, 2 x CH_3-TBS) ppm. **^{13}C-NMR (101 MHz, $CDCl_3$):** δ 158.0, 149.5, 145.0, 132.3, 131.3, 129.5 (x2), 129.0, 122.5, 122.0, 118.4, 114.5, 113.9 (x2), 100.3, 83.6, 55.4, 28.5 (x3), 28.4, 26.0 (x3), 18.6, -4.0 (x2) ppm. **HRMS (ESI-MS)** calculated for $C_{27}H_{38}NO_4Si^+$ $[M+H^+]$ 468.2565, found 468.2583.

***tert*-butyl 2-((tert-butyldimethylsilyl)oxy)-3-(4-fluorobenzyl)-1H-indole-1-carboxylate (79f)**

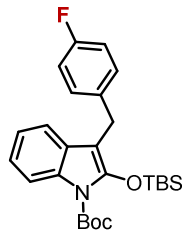

^{1}H-NMR (400 MHz, $CDCl_3$): δ 7.84 (d, *J* = 7.5 Hz, 1H, Ar), 7.18 – 6.94 (m, 7H, Ar), 3.98 (s, 2H, CH_2), 1.71 (s, 9H, ^{t}Bu-Boc), 1.05 (s, 9H, ^{t}Bu-TBS), 0.22 (s, 6H, 2 x CH_3-TBS) ppm. **^{13}C-NMR (101 MHz, $CDCl_3$):** δ 161.1 (d, *J* = 244.6 Hz), 149.4, 145.5, 131.2, 130.6 (d, *J* = 4.4 Hz), 128.8, 127.6 (d, *J* = 8.0 Hz), 127.0 (d, *J* = 15.3 Hz), 124.1 (d, *J* = 3.5 Hz), 122.6, 122.2, 118.1, 115.0 (d, *J* = 22.0 Hz), 114.6, 98.5, 83.7, 28.5 (x3), 26.0 (x3), 21.4, 18.5, -4.0 (x2) ppm. **^{19}F-NMR (376 MHz, $CDCl_3$):** δ -118.7 – -118.8 (m, 1F, ArF) ppm. **HRMS (ESI-MS)** calculated for $C_{26}H_{35}FNO_3Si^+$ $[M+H^+]$ 456.2370, found 456.2336.

***tert*-butyl 2-((tert-butyldimethylsilyl)oxy)-3-(4-methylbenzyl)-1H-indole-1-carboxylate (79g)**

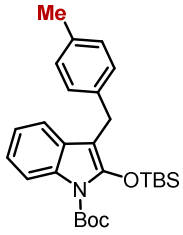

^{1}H-NMR (400 MHz, $CDCl_3$): δ 7.81 (d, *J* = 8.1 Hz, 1H, Ar), 7.14 – 7.04 (m, 6H, Ar), 6.97 (d, *J* = 7.3 Hz, 1H, Ar), 3.91 (s, 2H, CH_2), 2.28 (s, 3H, CH_3), 1.70 (s, 9H, ^{t}Bu-Boc), 1.05 (s, 9H, ^{t}Bu-TBS), 0.22 (s, 6H, 2 x CH_3-TBS) ppm. **^{13}C-NMR (101 MHz, $CDCl_3$):** δ 149.5, 145.1, 140.2, 138.0, 131.3, 129.4, 129.0, 128.3, 126.8, 125.7, 122.5, 122.0, 118.5, 114.5, 100.1, 83.6, 29.2, 28.5 (x3), 26.0 (x3), 21.6, 18.6, -3.9 (x2) ppm. **HRMS (ESI-MS)** calculated for $C_{27}H_{38}NO_3Si^+$ $[M+H^+]$ 452.2615, found 452.2613.

***tert*-butyl 2-((tert-butyldimethylsilyl)oxy)-3-methyl-1H-indole-1-carboxylate (79h)**

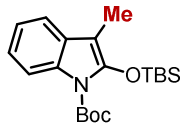

^{1}H-NMR (400 MHz, $CDCl_3$): δ 7.81 (d, *J* = 7.5 Hz, 1H, Ar), 7.32 (d, *J* = 7.5 Hz, 1H, Ar), 7.21 – 7.13 (m, 2H, Ar), 2.08 (s, 3H, CH_3), 1.68 (s, 9H, ^{t}Bu-Boc), 1.06 (s, 9H, ^{t}Bu-TBS), 0.21 (s, 6H, 2 x CH_3-TBS) ppm. **^{13}C-NMR (101 MHz, $CDCl_3$):** δ 149.5, 144.3, 131.2, 129.9, 122.5, 122.0, 117.4, 114.5, 96.9, 83.4, 28.5 (x3), 26.0 (x3), 18.5, 8.0, -4.1 (x2) ppm. **HRMS (ESI-MS)** calculated for $C_{20}H_{32}NO_3Si^+$ $[M+H^+]$ 362.2146, found 362.2145.

***tert*-butyl 3-benzyl-2-((triisopropylsilyl)oxy)-1H-indole-1-carboxylate (79i)**

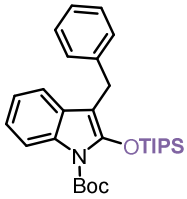

^{1}H-NMR (400 MHz, $CDCl_3$): δ 7.78 (d, *J* = 7.5 Hz, 1H, Ar), 7.26 – 7.02 (m, 8H, Ar), 3.98 (s, 2H, CH_2), 1.69 (s, 9H, ^{t}Bu-Boc), 1.36 (hept, *J* = 7.4 Hz, 3H, 3 x CH-TIPS), 1.11 (d, *J* = 7.8 Hz, 18H, (6 x CH_3-TIPS) ppm. **^{13}C-NMR (101 MHz,**

$CDCl_3$): δ 149.4, 145.8, 140.3, 130.9, 129.1, 128.6 (x2), 128.4 (x2), 126.0, 122.4, 121.8, 118.2, 114.5, 98.9, 83.4, 29.1, 28.5 (x3), 18.1 (x6), 14.0 (x3) ppm. **HRMS (ESI-MS)** calculated for $C_{29}H_{42}NO_3Si^+$ $[M+H^+]$ 480.2928, found 480.2919.

benzyl 3-benzyl-2-((tert-butyldimethylsilyl)oxy)-1H-indole-1-carboxylate (79j)

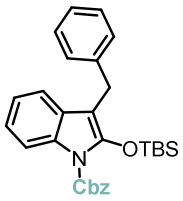

^{1}H-NMR (400 MHz, $CDCl_3$): δ 7.95 (d, *J* = 8.0 Hz, 1H, Ar), 7.53 (d, *J* = 6.4 Hz, 2H, Ar), 7.41 (q, *J* = 8.8, 7.6 Hz, 3H, Ar), 7.27 (d, *J* = 4.4 Hz, 4H, Ar), 7.21 – 7.10 (m, 4H, Ar), 5.48 (s, 2H, CH_2-Cbz), 3.97 (s, 2H, CH_2), 1.03 (s, 9H, ^{t}Bu-TBS), 0.19 (s, 6H, 2 x CH_3-TBS) ppm. **^{13}C-NMR (101 MHz, $CDCl_3$):** δ 151.1, 144.5, 140.0, 135.4, 131.5, 129.1, 128.9 (x2), 128.8 (x2), 128.8, 128.6 (x2), 128.5 (x2), 126.1, 123.0, 122.5, 118.5, 115.0, 100.3, 68.4, 29.3, 25.9 (x3), 18.5, -3.9 (x2). ppm. **HRMS (ESI-MS)** calculated for $C_{29}H_{34}NO_3Si^+$ $[M+H^+]$ 472.2308, found 472.2304.

***tert*-butyl 3-benzyl-2-((tert-butyldimethylsilyl)oxy)-6-trifluoromethyl-1H-indole-1-carboxylate (79k)**

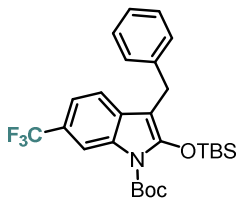

^{1}H-NMR (400 MHz, $CDCl_3$): δ 8.14 (s, 1H, Ar), 7.31 – 7.13 (m, 7H, Ar), 3.98 (s, 2H, CH_2), 1.72 (s, 9H, ^{t}Bu-Boc), 1.06 (s, 9H, ^{t}Bu-TBS), 0.24 (s, 6H, 2 x CH_3-TBS) ppm. **^{13}C-NMR (101 MHz, $CDCl_3$):** δ 148.9, 147.2, 139.7, 131.7, 130.3, 128.6 (x2), 128.5 (x2), 126.3, 126.80 (q, *J* = 273.3 Hz), 123.9 (q, *J* = 32.3 Hz), 119.4 (q, *J* = 3.9, 3.2 Hz), 118.4, 112.15 (q, *J* = 4.1 Hz), 100.1, 84.6, 29.1, 28.4 (x3), 26.0 (x3), 18.6, -3.9 (x2) ppm. **^{19}F-NMR**

(376 MHz, $CDCl_3$): δ -61.32 (s, 3F, $ArCF_3$) ppm. **HRMS (ESI-MS)** calculated for $C_{27}H_{35}F_3NO_3Si^+$ $[M+H^+]$ 506.2333, found 506.2368.

***tert*-butyl 3-benzyl-2-((tert-butyldimethylsilyl)oxy)-7-fluoro-1H-indole-1-carboxylate (79l)**

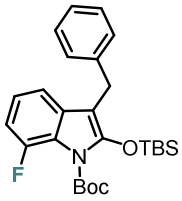

^{1}H-NMR (400 MHz, $CDCl_3$): δ 7.26 – 7.14 (m, 5H, Ar), 6.98 – 6.95 (m, 1H, Ar), 6.94 – 6.79 (m, 2H, Ar), 3.95 (s, 2H, CH_2), 1.62 (s, 9H, ^{t}Bu-Boc), 1.03 (s, 9H, ^{t}Bu-TBS), 0.25 (s, 6H, 2 x CH_3-TBS) ppm. **^{13}C-NMR (101 MHz, $CDCl_3$):** δ 149.33 (d, *J* = 248.9 Hz), 148.7, 145.8, 140.1, 132.5 (d, *J* = 3.7 Hz), 128.5 (x2), 128.5 (x2), 126.1, 122.8 (d, *J* = 7.5 Hz), 118.2 (d, *J* = 8.7 Hz), 114.2 (d, *J* = 3.1 Hz), 109.1 (d, *J* = 21.2 Hz), 98.5, 84.0, 29.3, 27.8 (x3), 26.0 (x3), 18.5, -3.7 (x2) ppm. 19F-NMR (376 MHz, CDCl3): -121.17 (dd, *J* = 12.3, 3.7 Hz, 1F, ArF) ppm. **HRMS (ESI-MS)** calculated for $C_{26}H_{34}FNNaO_3Si^+$ $[M+Na^+]$ 478.2190, found 478.2181.

***tert*-butyl 3-benzyl-2-((tert-butyldimethylsilyl)oxy)-5-methoxy-1H-indole-1-carboxylate (79m)**

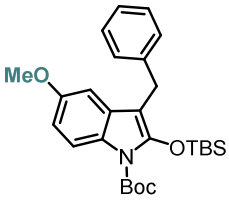

^{1}H-NMR (400 MHz, $CDCl_3$): δ 7.74 (d, *J* = 7.5 Hz, 1H, Ar), 7.29-7.26 (m, 4H, Ar), 7.21-7.18 (m, 1H, Ar), 6.76 (d, *J* = 7.8 Hz, 1H, Ar), 6.61 (s, 1H, Ar), 3.97 (s, 2H, CH_2), 3.73 (s, 3H, OCH_3), 1.72 (s, 9H, ^{t}Bu-Boc), 1.09 (s, 9H, ^{t}Bu-TBS), 0.26 (s, 6H, 2 x CH_3-TBS) ppm. **^{13}C-NMR (101 MHz, $CDCl_3$):** δ 155.8, 149.4, 145.8, 140.1, 129.9, 128.6 (x2), 128.4 (x2), 126.1, 125.8, 115.5, 109.5, 102.2, 100.1, 83.3, 55,7, 29.3, 28.5 (x3), 26.0 (x3), 18.6, -3.9

(x2) ppm. **HRMS (ESI-MS)** calculated for $C_{27}H_{38}NO_4Si^+$ [M+H$^+$] 468.2565, found 468.2566.

***tert*-butyl 3-allyl-2-((tert-butyldimethylsilyl)oxy)-1H-indole-1-carboxylate (79n)**

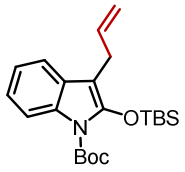

^{1}H-NMR (200 MHz, $CDCl_3$): δ 7.81 (dd, *J* = 6.4, 2.9 Hz, 1H, Ar), 7.39 – 7.35 (m, 1H, Ar), 7.15 (dd, *J* = 5.9, 3.2 Hz, 2H, Ar), 6.03 – 5.84 (m, 1H, CH), 5.17 – 5.04 (m, 2H, C(sp^2)H_2), 3.35 (d, *J* = 6.0 Hz, 2H, C(sp^3)H_2), 1.68 (s, 9H, ^{t}Bu-Boc), 1.06 (s, 9H, ^{t}Bu-TBS), 0.22 (s, 6H, 2 x CH_3-TBS) ppm. **^{13}C-NMR (101 MHz, $CDCl_3$):** δ 149.5, 144.4, 136.2, 131.3, 129.1, 122.4, 122.0, 118.3, 115.8, 114.5, 98.9, 83.6, 28.5 (x3), 27.6, 26.0 (x3), 18.5, -4.0 (x2). ppm. **HRMS (ESI-MS)** calculated for $C_{22}H_{34}NO_3Si^+$ [M+H$^+$] 388.2302, found 388.2298.

***tert*-butyl 2-((tert-butyldimethylsilyl)oxy)-3-(furan-2-ylmethyl)-1H-indole-1-carboxylate (79o)**

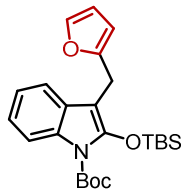

^{1}H-NMR (400 MHz, $CDCl_3$): δ 7.83 (d, *J* = 7.5 Hz, 1H, Ar), 7.31 (s, 1H, Ar), 7.25 (d, *J* = 7.5 Hz, 1H, Ar), 7.18 – 7.12 (m, 2H, Ar), 6.26 (d, *J* = 4.1 Hz, 1H, Ar), 5.96 (d, *J* = 1.8 Hz, 1H, Ar), 3.95 (s, 2H, CH_2), 1.70 (s, 9H, ^{t}Bu-Boc), 1.07 (s, 9H, ^{t}Bu-TBS), 0.22 (s, 6H, 2 x CH_3-TBS) ppm. **^{13}C-NMR (101 MHz, $CDCl_3$):** δ 153.8, 149.4, 145.0, 141.1, 131.2, 128.7, 122.6, 122.1, 118.2, 114.5, 110.4, 106.2, 97.4, 83.7, 28.5 (x3), 26.0 (x3), 22.5, 18.5, -4.1 (x2) ppm. **HRMS (ESI-MS)** calculated for $C_{24}H_{34}NO_4Si^+$ [M+H$^+$] 428.2252, found 428.2264.

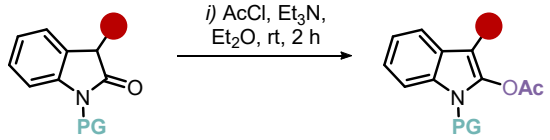

In a round-bottom flask, containing the oxindole 7**4a, 74l** (1.0 mmol, 1.0 equiv) was dissolved in Et_2O (5 mL, 0.5 M) under Ar atmosphere. NEt_3 (1.4 mL, 10.0 mmol, 10.0 equiv.) was added dropwise at 0 °C. After 5 min, AcCl (356 µL, 5.0 mmol, 5.0 equiv.) was added dropwise at 0 °C and stirred at room temperature. After full consumption of the starting material, monitored by TLC (usually after 2 h), the reaction is quenched with water. The organic layer was washed with 3 x 10 mL of a saturated solution of $NaHCO_3$, dried over $MgSO_4$ and concentrated under reduced pressure. The crude product was purified by column chromatography (9:1, hexane:EtOAc).

***tert*-butyl 2-acetoxy-3-benzyl-1H-indole-1-carboxylate (79p)**

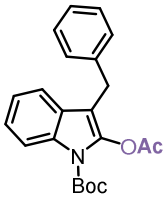

^{1}H-NMR (400 MHz, $CDCl_3$): δ 8.03 (d, *J* = 7.5 Hz, 1H, Ar), 7.32 – 7.14 (m, 8H, Ar), 3.95 (s, 2H, CH_2), 2.30 (s, 3H, CH_3-Ac), 1.67 (s, 9H, ^{t}Bu-Boc) ppm. **^{13}C-NMR (101 MHz, $CDCl_3$):** δ 169.0, 149.1, 139.2, 138.8, 132.6, 128.7 (x2), 128.6 (x2), 127.4, 126.4, 124.2, 123.0, 119.2, 115.6, 107.4, 84.3, 28.9, 28.4 (x3), 20.7 ppm. **HRMS (ESI-MS)** calculated for $C_{22}H_{23}NNaO_4^+$ [M+Na$^+$] 388.1525, found 388.1490.

1-acetyl-3-benzyl-1H-indol-2-yl acetate (79q)

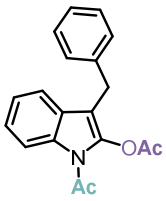

^{1}H-NMR (300 MHz, $CDCl_3$): δ 8.27 (d, *J* = 9.1 Hz, 1H, Ar), 7.33 – 7.18 (m, 8H, Ar), 3.91 (s, 2H, CH_2), 2.59 (s, 3H, CH_3-Ac), 2.26 (s, 3H, CH_3-Ac) ppm. **^{13}C-NMR (101 MHz, $CDCl_3$):** δ 168.3, 168.2, 138.6, 137.9, 132.9, 128.8 (x2), 128.7 (x2), 127.8, 126.6, 125.0, 123.9, 119.2, 116.3, 108.4, 29.3, 26.2, 20.7 ppm. **HRMS (ESI-MS)** calculated for $C_{19}H_{18}NO_3^+$ $[M+H^+]$ 308.1281, found 308.1272.

Synthesis and characterization of the PB products

General MFP Paternò-Buchi reaction

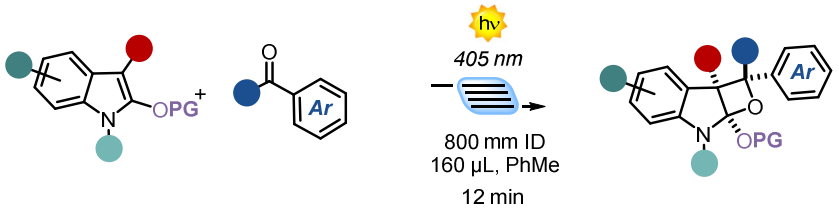

In a 4 mL vial, the enol ether (0.2 mmol, 1.0 equiv.) and the benzophenone derivative (0.6 mmol, 3.0 equiv.) were dissolved in toluene (2 mL, 0.1 M) and the reaction mixture was bubbled with Ar for 30 s. Then, the reaction mixture was reacted using the general microfluidic setup of this section. The crude product was purified by chromatography (6:4, hexane:CH_2Cl_2 or 98:2 hexane:acetone), giving the oxetane products **80-101** in the stated yields and diastereomeric ratio.

***tert*-butyl 2a-benzyl-7a-((*tert*-butyldimethylsilyl)oxy)-2,2-diphenyl-2a,7a-dihydrooxeto[2,3-*b*]indole-7(2*H*)-carboxylate (80)**

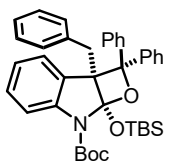

^{1}H-NMR (400 MHz, $CDCl_3$): δ 7.75 (d, *J* = 7.7 Hz, 2H, Ar), 7.42 (t, *J* = 7.6 Hz, 2H, Ar), 7.35 – 7.27 (m, 3H, Ar), 7.14 (d, *J* = 8.0 Hz, 1H, Ar), 7.02 – 6.93 (m, 8H, Ar), 6.87 (t, *J* = 7.3 Hz, 1H, Ar), 6.77 (d, *J* = 8.0 Hz, 1H, Ar), 6.61 (t, *J* = 7.3 Hz, 1H, Ar), 3.43 (d, *J* = 17.0 Hz, 1H, CH_2a), 3.29 (d, *J* = 17.0 Hz, 1H, CH_2b), 1.62 (s, 9H, ^{t}Bu-Boc), 0.77 (s, 9H, ^{t}Bu-TBS), 0.60 (s, 3H, CH_3-TBS), 0.24 (s, 3H, CH_3-TBS) ppm. **^{13}C-NMR (101 MHz, $CDCl_3$):** δ 150.5, 143.7, 142.4, 142.2, 137.5, 130.0 (x2), 128.4, 128.3 (x2), 127.9, 127.7 (x2), 127.4, 127.0 (x2), 126.4 (x2), 126.3, 126.2 (x2), 125.8, 125.6, 121.5, 114.5, 113.8, 87.2, 81.7, 64.9, 35.3, 28.7 (x3), 26.1 (x3), 18.6, -2.0, -2.2 ppm. **HRMS (ESI-MS)** calculated for $C_{39}H_{45}NNaO_4Si^+$ [M-Na^+] 642.3016, found 642.3027.

***tert*-butyl 7a-((*tert*-butyldimethylsilyl)oxy)-2a-(2-fluorobenzyl)-2,2-diphenyl-2a,7a-dihydrooxeto[2,3-*b*]indole-7(2*H*)-carboxylate (81)**

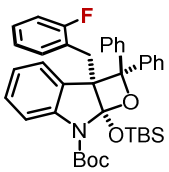

^{1}H-NMR (400 MHz, $CDCl_3$): δ 7.76 (d, *J* = 7.4 Hz, 2H), 7.43 (t, *J* = 7.7 Hz, 2H), 7.36 (d, *J* = 7.2 Hz, 2H), 7.29 (t, *J* = 7.4 Hz, 1H), 7.14 (d, *J* = 8.1 Hz, 1H), 7.01 – 6.94 (m, 4H), 6.90 – 6.85 (m, 4H), 6.68 (dt, *J* = 11.4, 7.6 Hz, 2H), 3.66 (d, *J* = 17.3 Hz, 1H, CH_2a), 3.06 (d, *J* = 17.3 Hz, 1H, CH_2b), 1.63 (s, 9H, ^{t}Bu-Boc), 0.76 (s, 9H, ^{t}Bu-TBS), 0.63 (s, 3H, CH_3-TBS), 0.23 (s, 3H, CH_3-TBS) ppm. **^{13}C-NMR (101 MHz, $CDCl_3$):** δ 161.3 (d, *J* = 243.6 Hz), 150.5, 143.6, 142.4, 142.1, 131.6 (d, *J* = 3.5 Hz), 128.3 (x2), 128.2, 128.1, 127.4, 127.3 (d, *J* = 8.4 Hz), 127.0 (x2), 126.4, 126.2 (x2), 126.0 (x2), 125.0, 124.8 (d, *J* = 13.8 Hz), 123.5 (d, *J* = 3.4 Hz), 121.8, 114.5, 114.4 (d, *J* = 22.8 Hz), 113.7, 87.1, 81.8, 64.4, 28.6 (x3), 26.6 (d, *J* = 5.0 Hz), 26.1 (x3), 18.5, -2.0, -2.3 ppm. **^{19}F**

NMR (376 MHz, $CDCl_3$): δ -117.71 – -117.78 (m, 1F, ArF) ppm. **HRMS (ESI-MS)** calculated for $C_{39}H_{45}FNO_4Si^+$ [M-H$^+$] 638.3096, found 638.3104.

***tert*-butyl 7a-((*tert*-butyldimethylsilyl)oxy)-2a-(3-chlorobenzyl)-2,2-diphenyl-2a,7a-dihydrooxeto[2,3-*b*]indole-7(2*H*)-carboxylate (82)**

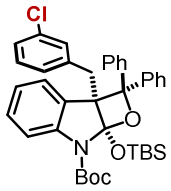

^{1}H-NMR (400 MHz, $CDCl_3$): δ 7.76 (d, *J* = 7.4 Hz, 2H, Ar), 7.43 (t, *J* = 7.8 Hz, 2H, Ar), 7.35 (d, *J* = 7.1 Hz, 2H, Ar), 7.30 (t, *J* = 7.4 Hz, 1H, Ar), 7.15 (d, *J* = 8.1 Hz, 1H, Ar), 7.03 – 6.95 (m, 8H, Ar), 6.88 (t, *J* = 7.8 Hz, 1H, Ar), 6.79 (d, *J* = 7.4 Hz, 1H, Ar), 6.65 (t, *J* = 7.8 Hz, 1H, Ar), 3.45 (d, *J* = 16.9 Hz, 1H, CH_2*a*), 3.30 (d, *J* = 16.9 Hz, 1H, CH_2*b*), 1.63 (s, 9H, ^{t}Bu-Boc), 0.78 (s, 9H, ^{t}Bu-TBS), 0.62 (s, 3H, CH_3-TBS), 0.25 (s, 3H, CH_3-TBS) ppm. . **^{13}C-NMR (101 MHz, $CDCl_3$):** δ 150.5, 143.7, 142.4, 142.2, 137.5, 130.0 (x2), 128.3, 128.3 (x2), 127.9, 127.7 (x2), 127.4, 127.0 (x2), 126.4 (x2), 126.3, 126.2 (x2), 125.8, 125.6, 121.5, 114.5, 113.8, 87.2, 81.7, 64.9, 35.2, 28.6 (x3), 26.1 (x3), 18.5, -2.0, -2.2 ppm. **HRMS (ESI-MS)** calculated for $C_{39}H_{45}ClNO_4Si^+$ [M-H$^+$] 654.2801, found 658.2762.

***tert*-butyl 7a-((*tert*-butyldimethylsilyl)oxy)-2a-(3-methoxybenzyl)-2,2-diphenyl-2a,7a-dihydrooxeto[2,3-*b*]indole-7(2*H*)-carboxylate (83)**

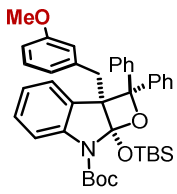

^{1}H-NMR (400 MHz, $CDCl_3$): δ 7.74 (d, *J* = 8.2 Hz, 2H, Ar), 7.41 (t, *J* = 7.7 Hz, 2H, Ar), 7.34 – 7.29 (m, 4H, Ar), 7.18 (d, *J* = 5.3 Hz, 1H, Ar), 7.13 (d, *J* = 8.2 Hz, 1H, Ar), 7.00 – 6.90 (m, 5H, Ar), 6.86 (t, *J* = 7.7 Hz, 1H, Ar), 6.76 (d, *J* = 7.5 Hz, 1H, Ar), 6.64 (t, *J* = 7.5 Hz, 1H, Ar), 6.57 – 6.49 (m, 2H, Ar), 6.43 (s, 1H, Ar), 3.55 (s, 3H, OCH_3), 3.42 (d, *J* = 14.3 Hz, 1H, CH_2*a*), 3.25 (d, *J* = 14.3

Hz, 1H, CH_2b), 1.60 (s, 9H, ^{t}Bu-Boc), 0.74 (s, 9H, ^{t}Bu-TBS), 0.54 (s, 3H, CH_3-TBS), 0.24 (s, 3H, CH_3-TBS) ppm. **^{13}C-NMR (101 MHz, $CDCl_3$):** δ 159.0, 150.6, 143.7, 142.3, 142.2, 139.1, 128.8, 128.6, 128.3 (x2), 128.0, 127.5, 127.4, 127.0 (x2), 126.4 (x2), 126.3 (x2), 125.8, 122.5, 121.6, 115.3, 114.5, 113.7, 111.6, 87.3, 81.7, 64.7, 55.1, 35.2, 28.6 (x3), 26.0 (x3), 18.5, -2.1, -2.3 ppm. **HRMS (ESI-MS)** calculated for $C_{40}H_{48}NO_5Si^+$ [M-H$^+$] 650.3296, found 650.3250.

***tert*-butyl 7a-((*tert*-butyldimethylsilyl)oxy)-2a-(4-methoxybenzyl)-2,2-diphenyl-2a,7a-dihydrooxeto[2,3-*b*]indole-7(2*H*)-carboxylate (84)**

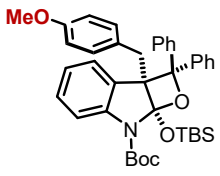

^{1}H-NMR (400 MHz, $CDCl_3$): δ 7.72 (d, *J* = 8.0 Hz, 2H, Ar), 7.40 (t, *J* = 7.7 Hz, 2H, Ar), 7.31 – 7.27 (m, 4H, Ar), 7.18 – 7.17 (m, 2H, Ar), 7.11 (d, *J* = 8.9 Hz, 1H, Ar), 6.98 – 6.91 (m, 4H, Ar), 6.83 (d, *J* = 8.7 Hz, 3H, Ar), 6.74 (d, *J* = 6.6 Hz, 1H, Ar), 6.63 (t, *J* = 7.4 Hz, 1H, Ar), 6.55 (d, *J* = 8.7 Hz, 2H, Ar), 3.66 (s, 3H, OCH_3), 3.35 (d, *J* = 14.2 Hz, 1H, CH_2a), 3.19 (d, *J* = 14.5 Hz, 1H, CH_2b), 1.60 (s, 9H, ^{t}Bu-Boc), 0.77 (s, 9H, ^{t}Bu-TBS), 0.57 (s, 3H, CH_3-TBS), 0.22 (s, 3H, CH_3-TBS) ppm. **^{13}C-NMR (101 MHz, $CDCl_3$):** δ 157.5, 150.6, 144.3, 143.7, 142.4, 142.2, 131.0 (x2), 129.6, 128.8, 128.4, 128.3 (x2), 127.9, 127.5, 127.3, 127.1, 127.0 (x2), 126.4 (x2), 126.3, 126.3 (x2) 125.9, 121.5, 114.5, 113.8, 113.2, 87.2, 81.7, 65.1, 55.2, 34.4, 28.6 (x3), 26.1 (x3), 18.6, -2.0, -2.1 ppm. **HRMS (ESI-MS)** calculated for $C_{40}H_{48}NO_5Si^+$ [M-H$^+$] 650.3302, found 650.3250.

***tert*-butyl -7a-((*tert*-butyldimethylsilyl)oxy)-2a-(4-fluorobenzyl)-2,2-diphenyl-2a,7a-dihydrooxeto[2,3-*b*]indole-7(2*H*)-carboxylate (85)**

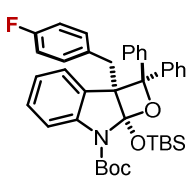

^{1}H-NMR (400 MHz, $CDCl_3$): δ 7.77 (d, *J* = 8.0 Hz, 2H, Ar), 7.44 (t, *J* = 7.7 Hz, 2H, Ar), 7.37 (d, *J* = 7.7 Hz, 2H, Ar), 7.30 (t, *J* = 7.3 Hz, 1H, Ar), 7.15 (d, *J* = 8.0 Hz, 1H, Ar), 6.98 (dt, *J* = 15.3, 7.2 Hz, 4H, Ar), 6.88 (t, *J* = 9.8 Hz, 4H, Ar), 6.72 – 6.66 (m, 2H, Ar), 3.67 (d, *J* = 17.3 Hz, 1H, CH_2*a*), 3.08 (d, *J* = 17.3 Hz, 1H, CH_2*b*), 1.64 (s, 9H, ^{t}Bu-Boc), 0.78 (s, 9H, ^{t}Bu-TBS), 0.64 (s, 3H, CH_3-TBS), 0.24 (s, 3H, CH_3-TBS) ppm. **^{13}C-NMR (101 MHz, $CDCl_3$):** δ 161.4 (d, *J* = 243.6 Hz), 150.5, 143.6, 142.4, 142.1, 131.6 (d, *J* = 3.5 Hz), 128.3 (x2), 128.2, 128.1, 127.4, 127.3 (d, *J* = 8.4 Hz), 127.0 (x2), 126.4, 126.3 (x2), 126.0 (x2), 125.0, 124.8 (d, *J* = 13.7 Hz), 123.5 (d, *J* = 3.5 Hz), 121.8, 114.5, 114.4 (d, *J* = 23.0 Hz), 113.7, 87.2, 81.8, 64.5, 28.6 (x3), 26.57 (d, *J* = 5.1 Hz), 26.1 (x3), 18.5, -2.0, -2.3 ppm.**^{19}F NMR (376 MHz, $CDCl_3$):** δ -117.68 – -117.79 (m, 1F, ArF) ppm. **HRMS (ESI-MS)** calculated for $C_{39}H_{44}FNNaO_4Si^+$ [M-Na^+] 660.2921, found 660.2896.

***tert*-butyl 7a-((*tert*-butyldimethylsilyl)oxy)-2a-(4-methylbenzyl)-2,2-diphenyl-2a,7a-dihydrooxeto[2,3-*b*]indole-7(2*H*)-carboxylate (86)**

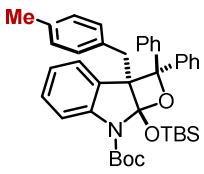

^{1}H-NMR (400 MHz, $CDCl_3$): δ 7.76 (d, *J* = 7.5 Hz, 2H, Ar), 7.43 (t, *J* = 7.7 Hz, 2H, Ar), 7.38 – 7.24 (m, 3H, Ar), 7.15 (d, *J* = 8.1 Hz, 1H, Ar), 7.04 – 6.84 (m, 5H, Ar), 6.84 – 6.74 (m, 3H, Ar), 6.71 (d, *J* = 7.7 Hz, 1H, Ar), 6.65 (t, *J* = 7.5 Hz, 1H, Ar), 3.41 (d, *J* = 16.8 Hz, 1H, CH_2*a*), 3.24 (d, *J* = 16.8 Hz, 1H, CH_2*b*), 2.15 (s, 3H, CH_3), 1.63 (s, 9H, ^{t}Bu-Boc), 0.80 (s, 9H, ^{t}Bu-TBS), 0.60 (s, 3H, CH_3-TBS), 0.25 (s, 3H, CH_3-TBS) ppm. **^{13}C NMR (101 MHz, $CDCl_3$):** δ 150.6, 143.7, 142.4, 142.2, 137.4, 137.0, 130.9, 128.5, 128.3 (x2),

127.9, 127.6, 127.4, 127.1, 127.0 (x2), 126.4 (x2), 126.4, 126.3 (x3), 125.9, 121.5, 114.5, 113.7, 87.2, 81.6, 64.9, 35.2, 28.6(x3), 26.1 (x3), 21.5, 18.5, -2.0, -2.2 ppm. **HRMS (ESI-MS)** calculated for $C_{40}H_{48}NO_4Si^+$ [M-H$^+$] 634.3347, found 634.1819.

***tert*-butyl 7a-((*tert*-butyldimethylsilyl)oxy)-2a-methyl-2,2-diphenyl-2a,7a-dihydrooxeto[2,3-*b*]indole-7(2*H*)-carboxylate (87)**

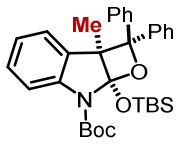

^{1}H-NMR (400 MHz, $CDCl_3$): δ 7.63 (d, *J* = 7.3 Hz, 2H, Ar), 7.36 – 7.28 (m, 4H, Ar), 7.24 – 7.15 (m, 4H, Ar), 7.02 – 6.90 (m, 5H, Ar), 1.60 (s, 9H, ^{t}Bu-Boc), 1.35 (s, 3H, CH_3), 0.91 (s, 9H, ^{t}Bu-TBS), 0.21 (s, 3H, CH_3-TBS), 0.07 (s, 3H, CH_3-TBS) ppm. **^{13}C-NMR (101 MHz, $CDCl_3$):** δ 143.3, 142.7, 142.5, 131.3, 128.8, 128.5, 128.1 (x2), 127.5, 127.1 (x2), 126.4, 126.2 (x2), 125.9 (x2), 124.2, 122.2, 114.9, 113.3, 81.7, 60.9, 53.6, 28.6 (x3), 26.0 (x3), 18.4, 16.5, -2.8, -2.9 ppm. **HRMS (ESI-MS)** calculated for $C_{33}H_{41}NNaO_4Si^+$ [M-Na$^+$] 566.2703, found 566.2988.

***tert*-butyl 2a-benzyl-2,2-diphenyl-7a-((triisopropylsilyl)oxy)-2a,7a-dihydrooxeto[2,3-*b*]indole-7(2*H*)-carboxylate (88)**

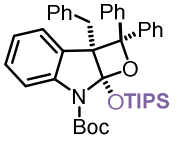

^{1}H-NMR (400 MHz, $CDCl_3$): δ 7.80 (d, *J* = 7.4 Hz, 2H, Ar), 7.41 (t, *J* = 7.4 Hz, 2H, Ar), 7.32 – 7.29 (m, 3H, Ar), 7.12 (d, *J* = 8.2 Hz, 1H, Ar), 7.04 – 6.93 (m, 6H, Ar), 6.90 – 6.86 (m, 3H, Ar), 6.63 (d, *J* = 4.4 Hz, 2H, Ar), 3.47 (d, *J* = 16.7 Hz, 1H, CH_2*a*), 3.34 (d, *J* = 16.7 Hz, 1H, CH_2*b*), 1.60 (s, 9H, ^{t}Bu-Boc), 1.42 (hept, *J* = 7.5 Hz, 3H, 3 x CH-TIPS), 1.14 (d, *J* = 7.5 Hz, 9H, 3 x CH_3-TIPS), 1.08 (d, *J* = 7.5 Hz, 9H, 3 x CH_3-TIPS) ppm. **^{13}C-NMR (101 MHz, $CDCl_3$):** δ 150.8, 143.7, 142.3, 142.1, 137.8, 130.3 (x2), 129.0, 128.2 (x2), 127.8, 127.7 (x2), 127.4,

127.0 (x2), 126.9 (x2), 126.7 (x2), 126.5, 126.3, 125.7, 121.6, 115.1, 112.7, 86.8, 81.7, 65.3, 34.9, 28.6 (x3), 18.7 (x3), 18.6 (x3), 14.0 (x3). **HRMS (ESI-MS)** calculated for $C_{42}H_{52}NO_4Si^+$ [M-Na^+] 684.3485, found 684.3482.

***tert*-butyl 7a-acetoxy-2a-benzyl-2,2-diphenyl-2a,7a-dihydrooxeto[2,3-*b*]indole-7(2*H*)-carboxylate (89)**

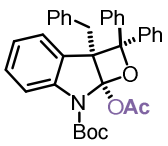

^{1}H-NMR (400 MHz, $CDCl_3$): δ 7.83 (d, *J* = 7.9 Hz, 2H, Ar), 7.47 (t, *J* = 7.7 Hz, 2H, Ar), 7.38 (dt, *J* = 14.4, 7.7 Hz, 2H, Ar), 7.29 – 7.26 (m, 3H, Ar), 7.17 – 6.98 (m, 8H, Ar), 6.89 – 6.81 (m, 4H, Ar), 3.71 (d, *J* = 15.1 Hz, 1H, CH_2*a*), 3.17 (d, *J* = 15.1 Hz, 1H, CH_2*b*), 1.98 (s, 3H, CH_3-Ac), 1.63 (s, 9H, ^{t}Bu-Boc) ppm. **^{13}C-NMR (101 MHz, $CDCl_3$):** δ 166.8, 150.3, 144.1, 141.4, 140.9, 136.2, 130.6 (x2), 128.9, 128.4 (x2), 128.1 (x3), 128.0, 127.3 (x2), 127.1 (x2), 126.7, 126.7, 126.5 (x2), 126.2, 121.8, 114.9, 113.8, 91.1, 82.0, 65.5, 35.3, 28.5 (x3), 21.7 ppm. **HRMS (ESI-MS)** calculated for $C_{35}H_{34}NO_5^+$ [M-H^+] 548.2431, found 548.2415.

7-acetyl-2a-benzyl-2,2-diphenyl-2a,7-dihydrooxeto[2,3-*b*]indol-7a(2*H*)-yl acetate (90)

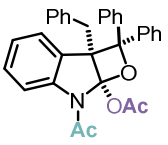

^{1}H NMR (400 MHz, Toluene-d_8): δ 8.29 (d, *J* = 8.2 Hz, 1H, Ar), 7.85 (d, *J* = 7.2 Hz, 1H, Ar), 7.33 – 7.20 (m, 4H, Ar), 6.96 – 6.82 (m, 7H, Ar), 6.75 (m, 5H, Ar), 3.72 (d, *J* = 15.4 Hz, 1H, CH_2*a*), 3.42 (d, *J* = 15.4 Hz, 1H, CH_2*b*), 2.49 (s, 3H, CH_3-OAc), 1.33 (s, 3H, CH_3-NAc) ppm. **^{13}C NMR (101 MHz, Toluene-d_8):** δ 167.0, 165.3, 145.1, 141.4, 140.7, 136.8, 136.1, 135.6, 130.2, 127.1, 127.0, 126.7, 126.4, 126.0, 125.5, 122.4, 116.7, 114.2, 92.0, 65.9, 35.4, 30.0, 23.6. ppm. Overlap with

toluene. **HRMS (ESI-MS)** calculated for $C_{32}H_{28}NO_4^+$ [M-H$^+$] 490.2013, found 490.2023.

benzyl 2a-benzyl-7a-((*tert*-butyldimethylsilyl)oxy)-2,2-diphenyl-2a,7a-dihydrooxeto[2,3-*b*]indole-7(2*H*)-carboxylate (91)

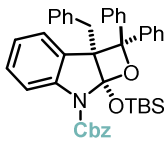

^{1}H NMR (400 MHz, Acetone-d$_6$): δ 7.92 – 7.84 (m, 2H, Ar), 7.65 (d, *J* = 7.5 Hz, 2H, Ar), 7.58 – 7.41 (m, 6H, Ar), 7.37 – 7.20 (m, 4H, Ar), 7.08 – 6.95 (m, 5H, Ar), 6.90 – 6.82 (m, 4H, Ar), 6.71 (td, *J* = 7.5, 1.1 Hz, 1H, Ar), 5.79 – 5.66 (d, *J* = 11.5 Hz, 1H, CH_2*a*-Cbz), 5.29 (d, *J* = 11.5 Hz, 1H, CH_2*a*-Cbz), 3.84 (d, *J* = 16.9 Hz, 1H, CH_2*a*), 3.30 (d, *J* = 16.9 Hz, 1H, CH_2*b*), 0.77 (s, 9H, ^{t}Bu-TBS), 0.69 (s, 3H, CH_3-TBS), 0.15 (s, 3H, CH_3-TBS) ppm. **^{13}C NMR (101 MHz, Acetone-d$_6$):** δ 151.7, 142.6, 142.4, 137.4, 137.0, 131.1, 129.6 (x2), 129.2, 128.7, 128.5 (x2), 128.2, 128.1 (x2), 127.8, 127.5 (x2), 127.2, 126.9 (x2), 126.4, 126.1, 125.8 (x2), 125.7 (x2), 125.4, 121.9, 114.2, 113.9, 87.7, 66.3, 65.0, 54.1, 35.0, 25.4 (x3), 17.9, -2.3, -2.9. ppm. **HRMS (ESI-MS)** calculated for $C_{42}H_{44}NO_4Si^+$ [M-H$^+$] 654.3034, found 654.3024.

***tert*-butyl 2a-benzyl-7a-((*tert*-butyldimethylsilyl)oxy)-2,2-diphenyl-5-(trifluoromethyl)-2a,7a-dihydrooxeto[2,3-*b*]indole-7(2*H*)-carboxylate (92)**

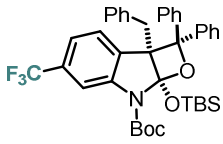

^{1}H-NMR (400 MHz, CDCl$_3$): δ 7.75 – 7.73 (m, 2H, Ar), 7.45 – 7.41 (m, 3H, Ar), 7.33 – 7.26 (m, 3H, Ar), 7.04 – 6.93 (m, 8H, Ar), 6.89 (dd, *J* = 7.7, 0.5 Hz, 1H, Ar), 6.83 (d, *J* = 7.7 Hz, 1H), 3.41 (d, *J* = 16.7 Hz, 1H, CH_2*a*), 3.31 (d, *J* = 16.7 Hz, 1H, CH_2*b*), 1.62 (s, 9H, ^{t}Bu-Boc), 0.79 (s, 9H, ^{t}Bu-TBS), 0.61 (s, 3H, CH_3-TBS),

0.25 (s, 3H, CH_3-TBS) ppm. **^{13}C-NMR (101 MHz, $CDCl_3$):** δ 150.0, 143.9, 141.8, 141.7, 136.9, 132.3 (q, *J* = 1.4 Hz), 130.0 (q, *J* = 32.0 Hz), 129.9 (x2), 128.4 (x2), 128.0 (x2), 127.6, 127.2 (x2), 126.7, 126.2 (x4), 126.0, 125.9, 124.3 (q, *J* = 273.6 Hz), 118.3 (q, *J* = 3.9 Hz), 113.9, 111.5 (q, *J* = 4.2 Hz), 87.1 (q, *J* = 0.8 Hz), 82.5, 65.0, 35.0, 28.5 (x3), 26.1 (x3), 18.6, -2.0, -2.2 ppm. **^{19}F-NMR (376 MHz, $CDCl_3$):** δ -63.05 (s, 3F, $ArCF_3$) ppm. **HRMS (ESI-MS)** calculated for $C_{40}H_{44}F_3NNaO_4Si^+$ [M-Na^+] 710.2889, found 710.2892.

***tert*-butyl 2a-benzyl-7a-((*tert*-butyldimethylsilyl)oxy)-6-fluoro-2,2-diphenyl-2a,7a-dihydrooxeto[2,3-*b*]indole-7(2*H*)-carboxylate (93)**

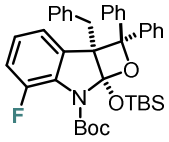

^{1}H-NMR (400 MHz, $CDCl_3$): δ 7.76 (d, *J* = 7.9 Hz, 2H, Ar), 7.40 (t, *J* = 7.6 Hz, 2H, Ar), 7.34 – 7.27 (m, 3H, Ar), 7.07 (t, *J* = 7.6 Hz, 2H, Ar), 7.02 – 7.00 (m, 4H, Ar), 6.81 – 6.80 (m, 2H, Ar), 6.66 – 6.57 (m, 2H, Ar), 6.44 (d, *J* = 7.2 Hz, 1H), 3.29 (d, *J* = 16.5 Hz, 1H, CH_2*a*), 3.21 (d, *J* = 16.5 Hz, 1H, CH_2*b*), 1.50 (s, 9H, ^{t}Bu-Boc), 0.83 (s, 9H, ^{t}Bu-TBS), 0.46 (s, 3H, CH_3-TBS), 0.44 (s, 3H, CH_3-TBS) ppm. **^{13}C NMR (101 MHz, $CDCl_3$):** δ 150.6, 150.5 (d, *J* = 250.7 Hz), 141.8, 141.8, 137.3, 133.2 (d, *J* = 2.7 Hz), 131.6 (d, *J* = 9.6 Hz), 129.9 (x2), 128.3 (x2), 127.8 (x2), 127.7, 127.2 (x2), 127.1 (x2), 126.8 (x2), 126.7, 125.9, 123.1 (d, *J* = 7.2 Hz), 122.4 (d, *J* = 3.4 Hz), 115.9 (d, *J* = 21.5 Hz), 114.4, 86.5, 81.4, 65.6, 35.8, 28.1 x3, 26.1 x3, 18.7, -2.3, -2.9. ppm. **^{19}F NMR (376 MHz, $CDCl_3$):** δ -117.44 – -117.62 (m, 1F, ArF) ppm. **HRMS (ESI-MS)** calculated for $C_{39}H_{45}FNO_4Si^+$ [M-H^+] 638.3096, found 638.3107.

***tert*-butyl 2a-benzyl-7a-((*tert*-butyldimethylsilyl)oxy)-4-methoxy-2,2-di-*p*-tolyl-2a,7a-dihydrooxeto[2,3-*b*]indole-7(2*H*)-carboxylate (94)**

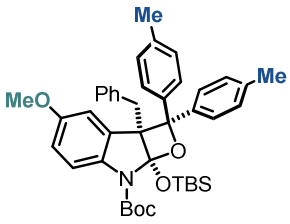

^{1}H NMR (400 MHz, Acetone-d$_6$): δ 7.79 (d, *J* = 8.3 Hz, 2H, Ar), 7.38 (d, *J* = 8.3 Hz, 2H, Ar), 7.27 (d, *J* = 8.0 Hz, 2H, Ar), 7.14 – 6.96 (m, 6H, Ar), 6.85 (d, *J* = 8.1 Hz, 2H, Ar), 6.81 (d, *J* = 2.7 Hz, 1H, Ar), 6.41 (dd, *J* = 8.9, 2.7 Hz, 1H, Ar), 3.70 (d, *J* = 16.6 Hz, 1H, CH_2a), 3.56 (s, 3H, OCH3), 3.31 (d, *J* = 16.6 Hz, 1H, CH_2b), 2.34 (s, 3H, CH_3), 2.11 (s, 3H, CH_3), 1.63 (s, 9H, ^{t}Bu-Boc), 0.79 (s, 9H, ^{t}Bu-TBS), 0.63 (s, 3H, CH_3-TBS), 0.31 (s, 3H, CH_3-TBS) ppm. **^{13}C NMR (101 MHz, Acetone-d$_6$):** δ 154.8, 150.4, 140.3, 139.9, 137.9, 137.2, 136.5, 135.3, 129.8, 129.7 (x2), 128.5 (x2), 127.5 (x2), 127.4 (x2), 126.0 (x2), 125.8 (x2), 125.4, 114.9, 113.9, 113.2, 112.0, 87.1, 80.9, 64.5, 54.9, 35.1, 27.7 (x3), 25.6 (x3), 20.1, 20.0, 18.2, -2.6, -2.7 ppm. **HRMS (ESI-MS)** calculated for $C_{42}H_{52}NO_5Si^{+}$ [M-H^{+}] 678.3609, found 678.3611.

***tert*-butyl 2a-benzyl-7a-((*tert*-butyldimethylsilyl)oxy)-6-fluoro-2,2-di-*p*-tolyl-2a,7a-dihydrooxeto[2,3-*b*]indole-7(2*H*)-carboxylate (95)**

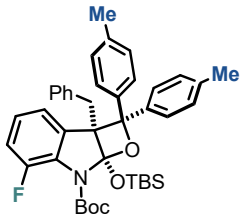

^{1}H NMR (400 MHz, Acetone-d$_6$): δ 7.78 (d, *J* = 8.3 Hz, 1H, Ar), 7.37 (d, *J* = 8.3 Hz, 1H, Ar), 7.27 (d, *J* = 8.1 Hz, 1H, Ar), 7.05 – 6.86 (m, 4H, Ar), 6.77 – 6.61 (m, 1H, Ar), 3.52 (d, *J* = 16.6 Hz, 1H, CH_2a), 3.30 (d, *J* = 16.6 Hz, 1H, , CH_2b), 2.34 (s, 3H, CH_3), 2.15 (s, 3H, CH_3), 1.54 (s, 9H, ^{t}Bu-Boc), 0.82 (s, 9H, ^{t}Bu-TBS), 0.55 (s, 3H, CH_3-TBS), 0.50 (s, 3H, CH_3-TBS) ppm. **^{13}C NMR (101 MHz, Acetone-d$_6$):** δ 150.6, 150.1 (d, *J* = 248.3 Hz), 139.9, 139.4, 137.6, 136.8, 135.6, 133.4 (d, *J* = 2.4 Hz), 131.3 (d, *J* = 9.4 Hz), 129.5 (x2), 128.6 (x2), 127.7 (x2), 127.5 (x2), 126.3 (x2),

126.1 (x2), 125.5, 123.2 (d, J = 7.1 Hz), 122.8, 122.8 (d, J = 3.4 Hz), 115.5, 115.3, 114.7, 86.3, 80.9, 65.0, 35.5, 27.3 (x3), 25.6 (x3), 18.3, -2.8, -3.5 ppm. **^{19}F NMR (188 MHz, Acetone-d$_6$):** δ -119.28 – -119.45 (m, 1F, ArF) ppm. **HRMS (ESI-MS)** calculated for $C_{41}H_{49}FNO_4Si^+$ [M-H$^+$] 666.3409, found 666.3398.

***tert*-butyl 2a-benzyl-7a-((*tert*-butyldimethylsilyl)oxy)-2,2-bis(4-chlorophenyl)-2a,7a-dihydrooxeto[2,3-*b*]indole-7(2*H*)-carboxylate (96)**

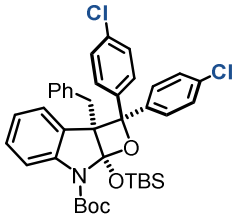

^{1}H NMR (400 MHz, CDCl$_3$): δ 7.61 (d, J = 8.3 Hz, 2H, Ar), 7.39 (d, J = 8.2 Hz, 2H, Ar), 7.21 (d, J = 8.3 Hz, 2H, Ar), 7.15 (d, J = 8.3 Hz, 1H, Ar), 7.02 – 6.98 (m, 3H, Ar), 6.95 (d, J = 8.4 Hz, 2H, Ar), 6.90 – 6.89 (m, 3H, Ar), 6.72 (d, J = 7.4 Hz, 1H, Ar), 6.64 (t, J = 7.4 Hz, 1H, Ar), 3.32 (d, J = 16.9 Hz, 1H, CH$_2$*a*), 3.25 (d, J = 16.9 Hz, 1H, CH$_2$*b*), 1.60 (s, 9H, ^{t}Bu-Boc), 0.74 (s, 9H, ^{t}Bu-TBS), 0.53 (s, 3H, CH$_3$-TBS) 0.23 (s, 1H) ppm. **^{13}C NMR (101 MHz, CDCl$_3$):** δ 150.5, 143.6, 140.8, 140.4, 137.0, 133.6, 132.5, 129.9 (x2), 128.7 (x2), 128.4, 127.9 (x2), 127.7, 127.7 (x2), 127.5 (x2), 127.4 (x2), 125.8, 125.7, 121.8, 114.8, 113.7, 86.5, 82.0, 64.8, 35.2, 28.6 (x3), 26.0 (x3), 18.6, -2.1, -2.1 ppm. **HRMS (ESI-MS)** calculated for $C_{39}H_{43}Cl_2NNaO_4Si^+$ [M-Na$^+$] 710.2236, found 710.2236.

***tert*-butyl 2a-benzyl-7a-((*tert*-butyldimethylsilyl)oxy)-2,2-bis(4-fluorophenyl)-2a,7a-dihydrooxeto[2,3-*b*]indole-7(2*H*)-carboxylate (97)**

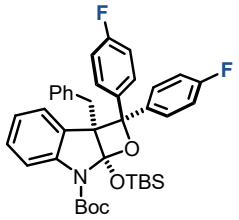

^{1}H-NMR (400 MHz, CDCl$_3$): δ 7.68 (dd, J = 7.1, 5.2 Hz, 2H, Ar), 7. 28 – 7.25 (m, 2H, Ar), 7.14 (q, J = 8.2 Hz, 3H, Ar), 7.05 – 7.00 (m, 3H, Ar), 6.92 – 6.88 (m, 3H, Ar), 6.73 – 6.63 (m, 4H, Ar), 3.34 (d, J = 16.8 Hz, 1H, CH$_2$*a*), 3.27 (d, J = 16.8 Hz, 1H, CH$_2$*b*), 1.62 (s, 9H, ^{t}Bu-

Boc), 0.77 (s, 9H, ^{t}Bu-TBS), 0.56 (s, 3H, CH_3-TBS), 0.26 (s, 3H, CH_3-TBS) ppm. **^{13}C NMR (101 MHz, $CDCl_3$):** δ 162.3 (d, *J* = 246.4 Hz), 160.2 (d, *J* = 245.3 Hz), 150.5, 143.7, 138.1 (d, *J* = 2.9 Hz), 137.9 (d, *J* = 2.9 Hz), 137.2, 129.9 (x2), 128.3, 128.1, 128.0 (x2), 128.0 (d, *J* = 12.3 Hz, x2), 127.8 (x2), 125.7 (d, *J* = 13.6 Hz, x2), 121.7, 115.3 (d, *J* = 21.4 Hz, x2), 114.7, 114.0 (d, *J* = 21.4 Hz, x2), 113.7, 86.7, 81.9, 64.8, 35.2, 28.6 (x3), 26.0 (x3), 18.6, -2.1, -2.2. ppm. **^{19}F NMR (376 MHz, $CDCl_3$):** δ -115.49 – -115.56 (m, 1F, ArF), -116.72 – -116.80 (m, 1F, ArF). **HRMS (ESI-MS)** calculated for $C_{39}H_{43}F_2NNaO_4Si^+$ [M-Na$^+$] 678.2827, found 678.2852.

***tert*-butyl 2a-benzyl-7a-((*tert*-butyldimethylsilyl)oxy)-2,2-diphenyl-2a,7a-dihydrooxeto[2,3-*b*]indole-7(2*H*)-carboxylate (98)**

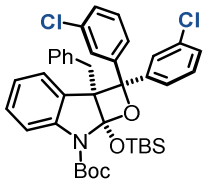

^{1}H-NMR (400 MHz, Acetone-d_6): δ 8.04-7.89 (m, 2H, Ar), 7.74 (m, 1H, Ar), 7.58 – 7.49 (m, 2H, Ar), 7.45 – 7.35 (m, 2H, Ar), 7.29 – 7.11 (m, 4H, Ar), 7.11 – 6.94 (m, 4H, Ar), 6.91 (t, *J* = 7.3 Hz, 1H, Ar), 6.66 (d, *J* = 8.0 Hz, 1H, Ar), 3.79 (d, *J* = 17.0 Hz, 1H, CH_2*a*), 3.33 (d, *J* = 16.6 Hz, 1H, CH_2*b*), 1.67 (s, 9H, ^{t}Bu-Boc), 0.79 (s, 9H, ^{t}Bu-TBS), 0.64 (s, 3H, CH_3-TBS), 0.36 (s, 3H, CH_3-TBS) ppm. **^{13}C-NMR (101 MHz, Acetone-d_6):** δ 150.4, 144.6, 144.0, 143.2, 137.3, 134.0, 132.6, 130.0, 129.7 (x2), 129.2, 128.9, 128.8, 128.2, 127.5 (x2), 126.6, 126.5, 126.0, 125.7, 125.5, 124.8, 124.7, 121.6, 114.3, 113.6, 86.3, 81.9, 64.8, 34.8, 27.7 (x3), 25.5 (x3), 18.2, -2.7, -2.8. ppm. **HRMS (ESI-MS)** calculated for $C_{39}H_{43}Cl_2NNaO_4Si^+$ [M-Na$^+$] 710.2236, found 710.2234.

***tert*-butyl 2a-benzyl-7a-((*tert*-butyldimethylsilyl)oxy)-2,2-bis(3-(trifluoromethyl)phenyl)-2a,7a-dihydrooxeto[2,3-*b*]indole-7(2*H*)-carboxylate (99)**

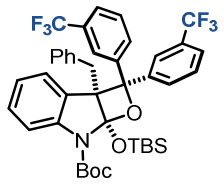

^{1}H-NMR (400 MHz, $CDCl_3$): δ 8.11 (s, 1H, Ar), 7.83 (d, *J* = 7.5 Hz, 1H, Ar), 7.62 – 7.52 (m, 4H, Ar), 7.23 (d, *J* = 7.7 Hz, 1H, Ar), 7.15 (t, *J* = 8.5 Hz, 2H, Ar), 7.01 (t, *J* = 7.4 Hz, 3H, Ar), 6.92 (d, *J* = 7.6 Hz, 2H, Ar), 6.87 (t, *J* = 7.8 Hz, 1H, Ar), 6.76 (d, *J* = 7.4 Hz, 1H, Ar), 6.65 (t, *J* = 7.7 Hz, 1H, Ar), 3.33 (d, *J* = 16.7 Hz, 1H, CH_2*a*), 3.27 (d, *J* = 16.7 Hz, 1H, CH_2*b*), 1.61 (s, 9H, ^{t}Bu-Boc), 0.75 (s, 9H, ^{t}Bu-TBS), 0.58 (s, 3H, CH_3-TBS), 0.26 (s, 3H, CH_3-TBS) ppm. **^{13}C-NMR (101 MHz, $CDCl_3$):** δ 150.4, 143.5, 142.9, 142.6, 136.8, 131.2 (q, *J* = 32.4 Hz), 129.9 (x2) 129.7 (q, *J* = 32.4 Hz), 129.6 (q, *J* = 1.5 Hz), 129.5 (q, *J* = 1.5 Hz), 129.0, 128.5, 127.9 (x2), 127.8, 127.3, 126.0, 125.8, 124.7 (q, *J* = 3.4 Hz), 124.3 (q, *J* = 273.4 Hz), 124.0 (q, *J* = 272.4 Hz), 123.7 (q, *J* = 4.1 Hz), 123.3 (p, *J* = 4.0 Hz, x2), 122.0, 114.6, 113.7, 86.5, 82.3, 65.2, 35.3, 28.5 (x3), 26.0 (x3), 18.6, -2.2, -2.3 ppm. **^{19}F-NMR (376 MHz, $CDCl_3$):** δ -62.98 (s, 3F, $ArCF_3$), -63.07 (s, 3F, $ArCF_3$) ppm. **HRMS (ESI-MS)** calculated for $C_{41}H_{43}F_6NNaO_4Si^+$ [M-Na^+] 778.2763, found 778.2758.

***tert*-butyl 2a-allyl-7a-((*tert*-butyldimethylsilyl)oxy)-2,2-diphenyl-2a,7a-dihydrooxeto[2,3-*b*]indole-7(2*H*)-carboxylate (100)**

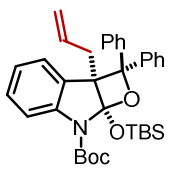

^{1}H-NMR (500 MHz, $CDCl_3$): δ 7.68 (d, *J* = 7.3 Hz, 2H, Ar), 7.40 (t, *J* = 7.8 Hz, 2H, Ar), 7.34 (d, *J* = 7.3 Hz, 2H, Ar), 7.29 – 7.25 (m, 1H, Ar), 7.18 (d, *J* = 8.1 Hz, 1H, Ar), 7.14 (d, *J* = 7.4 Hz, 1H, Ar), 7.03 – 6.92 (m, 4H, Ar), 6.88 (t, *J* = 7.4 Hz, 1H, Ar), 5.62 (dddd, *J* = 17.2, 10.2, 8.5, 4.7 Hz, 1H, C(sp^2)H), 4.99 (dd, *J* =

17.2, 1.2 Hz, 1H, (E) $C(sp^2)H_2$), 4.91 (dd, *J* = 10.2, 1.2 Hz, (Z)$C(sp^2)H_2$), 2.84 (dd, *J* = 15.5, 8.5 Hz, 1H, CH_2a), 2.66 – 2.62 (m, 1H, CH_2b), 1.62 (s, 9H, ^{t}Bu-Boc), 0.93 (s, 9H, ^{t}Bu-TBS), 0.56 (s, 3H, CH_3-TBS), 0.30 (s, 3H, CH_3-TBS) ppm. **^{13}C-NMR (126 MHz, $CDCl_3$):** δ 150.4, 143.8, 142.4, 142.4, 134.7, 128.5, 128.2 (x3), 127.3, 127.1 (x2), 126.4, 126.2 (x2), 125.9 (x2), 125.8, 121.6, 117.7, 114.6, 113.7, 87.1, 81.6, 63.6, 34.6, 28.6 (x3), 26.1 (x3), 18.6. -2.7, -2.9, ppm. **HRMS (ESI-MS)** calculated for $C_{35}H_{44}NO_4Si^+$ [M-H^+] 570.3034, found 570.3033.

***tert*-butyl 7a-((*tert*-butyldimethylsilyl)oxy)-2a-(furan-2-ylmethyl)-2,2-diphenyl-2a,7a-dihydrooxeto[2,3-*b*]indole-7(2*H*)-carboxylate (101)**

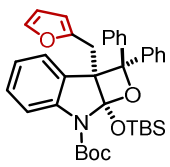

^{1}H-NMR (400 MHz, $CDCl_3$): δ 7.73 (d, *J* = 7.6 Hz, 2H, Ar), 7.41 – 7.36 (m, 4H, Ar), 7.30 – 7.26 (m, 1H, Ar), 7.21 – 7.19 (m, 2H, Ar), 7.05 – 6.96 (m, 5H, Ar), 6.81 (t, *J* = 7.6 Hz, 1H, Ar), 6.06 (dd, *J* = 3.0, 1.9 Hz, 1H, Ar), 5.36 (d, *J* = 3.0 Hz, 1H, Ar), 3.53 (d, *J* = 16.8 Hz, 1H, CH_2a), 3.10 (d, *J* = 16.8 Hz, 1H, CH_2b), 1.63 (s, 9H, ^{t}Bu-Boc), 0.83 (s, 9H, ^{t}Bu-TBS), 0.49 (s, 3H, CH_3-TBS), 0.27 (s, 3H, CH_3-TBS) ppm. **^{13}C-NMR (101 MHz, $CDCl_3$):** δ 151.6, 150.5, 143.7, 142.1, 142.1, 140.1, 128.5, 128.4, 128.2 (x2), 127.4, 127.1 (x2), 126.5, 126.4 (x2), 126.3 (x2), 125.5, 121.8, 114.7, 113.2, 110.5, 107.7, 87.3, 81.7, 63.7, 28.8, 28.6 (x3), 26.0 (x3), 18.5, -2.3, -2.4 ppm. **HRMS (ESI-MS)** calculated for $C_{37}H_{43}NNaO_5Si^+$ [M-Na^+] 632.2808, found 632.2787.

***tert*-butyl 2a-benzyl-7a-((*tert*-butyldimethylsilyl)oxy)-2,2-di-*p*-tolyl-2a,7a-dihydrooxeto[2,3-*b*]indole-7(2*H*)-carboxylate (102)**

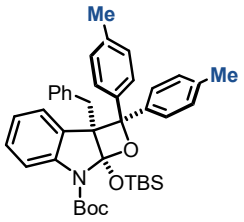

^{1}H-NMR (400 MHz, $CDCl_3$): δ 7.67 (d, *J* = 7.9 Hz, 2H, Ar), 7.32 – 7.22 (m, 5H, Ar), 7.10 – 6.99 (m, 5H, Ar), 6.93 (t, *J* = 7.6 Hz, 1H, Ar), 6.85 – 6.80 (m, 3H, Ar), 6.69 (t, *J* = 7.3 Hz, 1H), 3.47 (d, *J* = 16.9 Hz, 1H, CH_2*a*), 3.35 (d, *J* = 16.9 Hz, 1H, CH_2*a*), 2.41 (s, 3H, CH_3), 2.18 (s, 3H, CH_3), 1.69 (s, 9H, ^{t}Bu-Boc), 0.84 (s, 9H, ^{t}Bu-TBS), 0.66 (s, 3H, CH_3-TBS), 0.31 (s, 3H, CH_3-TBS) ppm. **^{13}C NMR (101 MHz, $CDCl_3$):** δ 150.6, 143.8, 139.7, 139.6, 137.7, 136.8, 135.6, 130.0 (x2), 128.9 (x2), 128.6, 127.8, 127.7 (x4), 126.1 (x4), 125.8, 125.6, 121.5, 114.6, 113.8, 87.3, 81.6, 64.6, 35.4, 28.7 (x3), 26.1(x3), 21.2, 21.1, 18.6, -2.0, -2.2 ppm. **HRMS (ESI-MS)** calculated for $C_{41}H_{50}NO_4Si^+$ [M-H^+] 648.3504, found 648.3505.

X-ray crystallographic analysis of 80

*X-ray structure of **80***

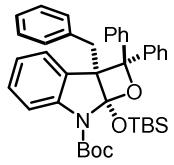

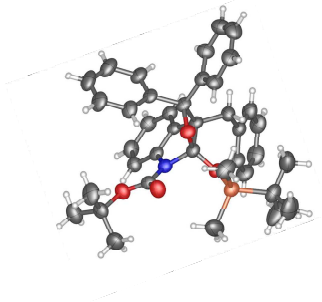

X-Ray structure of **80**.

Colorless crystals of **80** were grown by slow evaporation of a Et_2O solution at ambient temperature.

Crystal data: $C_{39}H_{45}NO_4Si$

Orthorhombic, $P2_12_12_1$, a=10.1848(8)Å, b=16.7586(14)Å, c= 20.4119(18)Å, V= 3484.0(5)Å^3; Z=4; dcalc= 1.182mg/cm^3 , F(000)=1328, mu= 0.906, Tot. refl.= 38933, hkl range= -12<h<12, -16<k<20, -25<l<25; Theta max 73.1°, ref.tot.= 6856, number of parameters = 414, GooF= 1.086, R=0.0611, wR2=0.1761.

CCDC 1943528 contains the supplementary crystallographic data for this compound. These data can be obtained free of charge from The Cambridge Crystallographic Data Centre via www.ccdc.cam.ac.uk/data_request/cif

Spectroscopic data

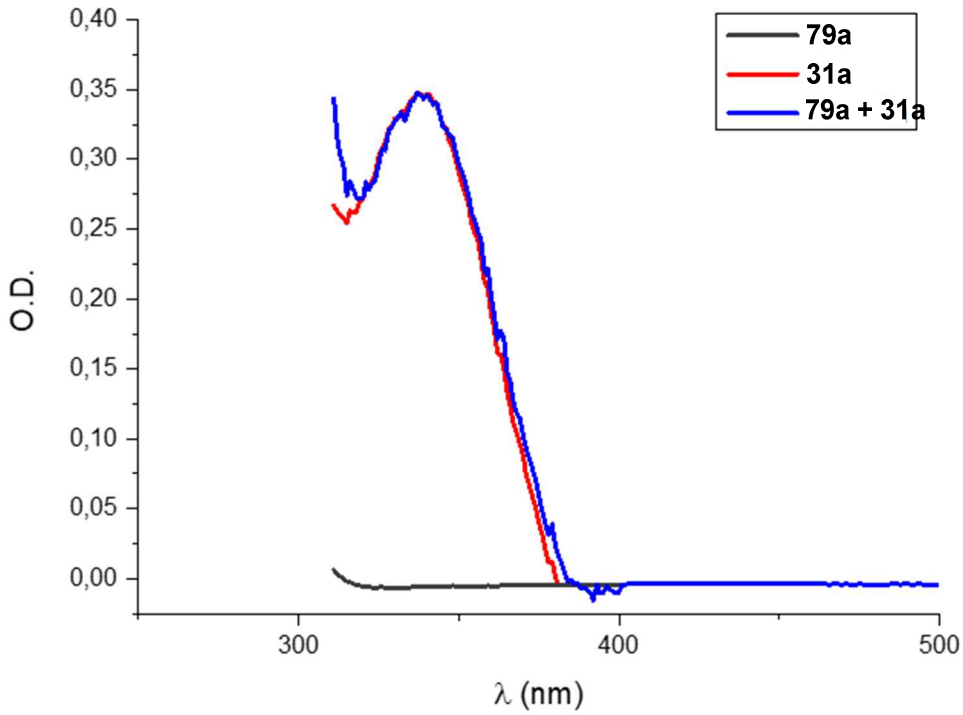

Figure Exp2.12. – UVVis absorbance spectrum of 10^{-3}M solutions in MeCN of **79a**, **31a** and their mixture.

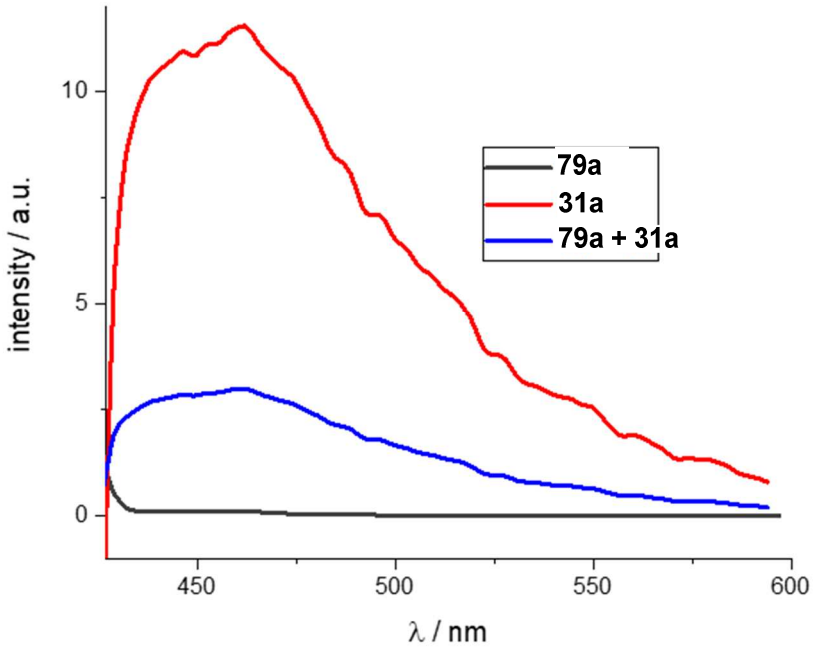

Figure Exp2.13. – UVVis Emission spectrum of 10^{-3}M solutions in MeCN of **79a**, **31a** and their mixture.

ΔG_{PET} Calculations

Using the Gibbs energy of PET equation (Paragraph 2.) the ΔG of the PET process between enol ether **79a** and benzophenone **31a** has been calculated. $E^{ox}(D)$ is the oxidation potential of the donor **79a**, and has been calculated through cyclic voltammetries reported in Figure Exp2.14. $E^{ox}_{peak}(\mathbf{79a})$ = 1.08 mV. $E^{red}(A)$ is the reduction potential of the acceptor **31a** and has been calculated through cyclic voltammetry reported in Figure Exp2.15. $E^{red/2}$ (**31a**) = -2.00 mV. ΔE_{exc} is the excitation energy of the acceptor, reported in literature as 2.20 eV. ΔE_{coul} is a term that takes into account the ability of the solvent to separate the radical-ion pair, its value is reported as 0.05 eV for MeCN.

ΔG_{ET} = 0.93 eV

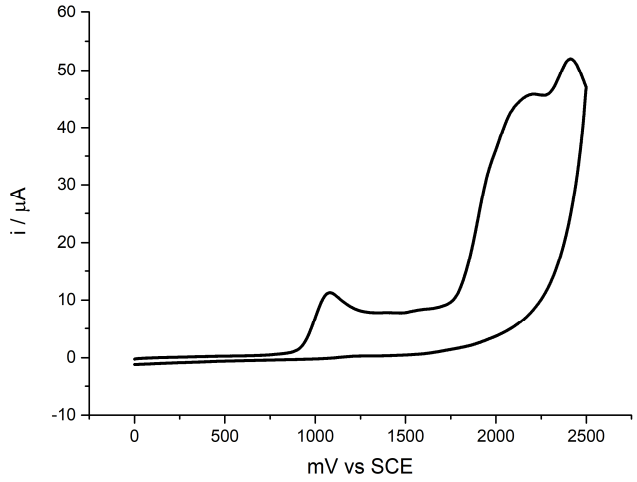

Figure Exp2.14. – Anodic CV of enol ether **79a** in 0.1 M NEt_4PF_6 MeCN solution. GC electrode. Scan rate: 100 mV/s, potential referred to SCE at room temperature using a platinum wire as counter electrode.

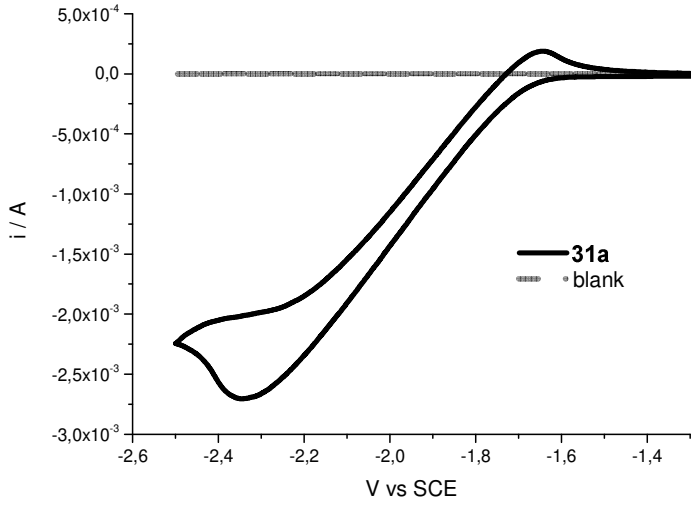

Figure Exp2.15. – Cathodic CV of benzophenone **31a** in 0.1 M NEt_4PF_6 MeCN solution. GC electrode. Scan rate: 100 mV/s, potential referred to SCE at room temperature using a platinum wire as counter electrode.

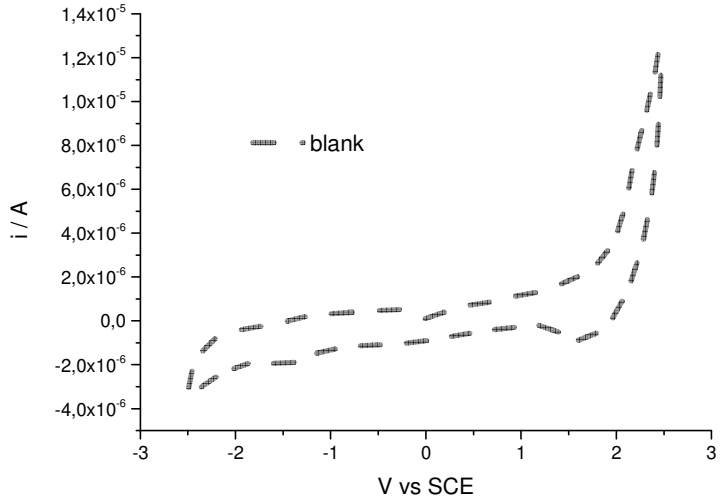

Figure Exp2.16. – CV of blank 0.1 M NEt_4PF_6 MeCN solution. GC electrode. Scan rate: 100 mV/s, potential referred to SCE at room temperature using a platinum wire as counter electrode.

2.3. – References - Chapter II

1. Paternò, E.; Chieffi, G., Sintesi in chimica organica per mezzo della luce. Nota II. Composti degli idrocarburi non saturi con aldeidi e chetoni. *Gazz. Chim. Ital.* **1909,** 39, 341-361.

2. Büchi, G.; Inman, C. G.; Lipinsky, E. S., Light-catalyzed Organic Reactions. I. The Reaction of Carbonyl Compounds with 2-Methyl-2-butene in the Presence of Ultraviolet Light. *J. Am. Chem. Soc.* **1954,** 76, 4327-4331.

3. Hailes, H. C.; Behrendt, J. M., 2.05 - Oxetanes and Oxetenes: Monocyclic. In *Comprehensive Heterocyclic Chemistry III*, Katritzky, A. R.; Ramsden, C. A.; Scriven, E. F. V.; Taylor, R. J. K., Eds. Elsevier: Oxford, 2008; pp 321-364.

4. Bull, J. A.; Croft, R. A.; Davis, O. A.; Doran, R.; Morgan, K. F., Oxetanes: Recent Advances in Synthesis, Reactivity, and Medicinal Chemistry. *Chem. Rev.* **2016,** 116, 12150-12233.

5. (a) D'Auria, M., 5.05 The Paternò–Büchi Reaction. In *Comprehensive Organic Synthesis II*, 2014; pp 159-199. (b) D'Auria, M., The Paternò–Büchi reaction–a comprehensive review. *Photochem. Photobiol. Sci.* **2019,** 18, 2297-2362. (c) D'Auria, M.; Racioppi, R., Oxetane synthesis through the Paterno-Buchi reaction. *Molecules* **2013,** 18, 11384-428. (d) Fréneau, M.; Hoffmann, N., The Paternò-Büchi reaction—Mechanisms and application to organic synthesis. *J. Photochem. Photobiol., C* **2017,** 33, 83-108.

6. Palmer, I. J.; Ragazos, I. N.; Bernardi, F.; Olivucci, M.; Robb, M. A., An MC-SCF Study of the (Photochemical) Paterno-Buchi Reaction. *J. Am. Chem. Soc.* **1994,** 116, 2121-2132.

7. Turro, N. J.; Dalton, J. C.; Dawes, K.; Farrington, G.; Hautala, R.; Morton, D.; Niemczyk, M.; Schore, N., Molecular photochemistry. L. Molecular photochemistry of alkanones in solution. .alpha.-Cleavage, hydrogen abstraction, cycloaddition, and sensitization reactions. *Acc. Chem. Res.* **1972,** 5, 92-101.

8. Dalton, J. C.; Wriede, P. A.; Turro, N. J., Molecular photochemistry. XXIV. Photocycloaddition of acetone to 1,2-dicyanoethylene. *J. Am. Chem. Soc.* **1970,** 92, 1318-1326.

9. Yang, N. C.; Man Him, H.; Shold, D. M.; Turro, N. J.; Hautala, R. R.; Dawes, K.; Dalton, J. C., Chemistry of exciplex. 6. Quenching of the 1n,.pi.* of alkanones by unsaturated compounds. *J. Am. Chem. Soc.* **1977,** 99, 3023-3033.

10. (a) Gersdorf, J.; Mattay, J.; Goerner, H., Radical cations. 3. Photoreactions of biacetyl, benzophenone, and benzil with electron-rich alkenes. *J. Am. Chem. Soc.* **1987,** 109, 1203-1209. (b) Mattay, J.; Gersdorf, J.; Buchkremer, K., Photoreactions of Biacetyl with Electron-rich Olefins.
An Extended Mechanism. *Chem. Ber.* **1987,** 120, 307-318.
11. Zhang, Y.; Xue, J.; Gao, Y.; Fun, H.-K.; Xu, J.-H., Photoinduced [2+2] cycloadditions (the Paterno–Büchi reaction) of 1-acetylisatin with enol ethers—regioselectivity, diastereoselectivity and acid catalysed transformations of the spirooxetane products. *J. Chem. Soc., Perkin Trans.* 1 **2002**, 345-353.
12. Rehm, D.; Weller, A., Kinetik und Mechanismus der Elektronübertragung bei der Fluoreszenzlöschung in Acetonitril. *Ber. Bunsenges. Physik. Chem.* **1969,** 73, 834-839.
13. Eckert, G.; Goez, M., Photoinduced Electron-Transfer Reactions of Aryl Olefins. 1. Investigation of the Paterno-Buechi Reaction between Quinones and Anetholes in Polar Solvents. *J. Am. Chem. Soc.* **1994,** 116, 11999-12009.
14. Mattay, J., Charge Transfer and Radical Ions in Photochemistry. *Angew. Chem. Int. Ed.* **1987,** 26, 825-845.
15. Yang, N.-C.; Loeschen, R. L.; Mitchell, D., Mechanism of the Paterno-Buechi reaction. *J. Am. Chem. Soc.* **1967,** 89, 5465-5466.
16. Mori, T.; Inoue, Y., Charge-transfer excitation: unconventional yet practical means for controlling stereoselectivity in asymmetric photoreactions. *Chem. Soc. Rev.* **2013,** 42, 8122-8133.
17. Sun, D.; Hubig, S. M.; Kochi, J. K., Oxetanes from [2+2] Cycloaddition of Stilbenes to Quinone via Photoinduced Electron Transfer. *J. Org. Chem.* **1999,** 64, 2250-2258.
18. (a) Rykaczewski, K. A.; Schindler, C. S., Visible-Light-Enabled Paterno-Buchi Reaction via Triplet Energy Transfer for the Synthesis of Oxetanes. *Org. Lett.* **2020,** 22, 6516-6519. (b) Zheng, J.; Dong, X.; Yoon, T. P., Divergent Photocatalytic Reactions of alpha-Ketoesters under Triplet Sensitization and Photoredox Conditions. *Org. Lett.* **2020,** 22, 6520-6525. (c) Kumarasamy, E.; Raghunathan, R.; Kandappa, S. K.; Sreenithya, A.; Jockusch, S.; Sunoj, R. B.; Sivaguru, J., Transposed Paternò–Büchi Reaction. *J. Am. Chem. Soc.* **2017,** 139, 655-662.
19. Turro, N. J.; Ramamurthy, V.; Scaiano, J., *Modern Molecular Photochemistry of Organic Molecules*. University Science Books: 2010.

20. Salem, L., Surface crossings and surface touchings in photochemistry. *J. Am. Chem. Soc.* **1974,** 96, 3486-3501.

21. Abe, M.; Ikeda, M.; Shirodai, Y.; Nojima, M., Regio- and stereo-selective formation of 2-siloxy-2-alkoxyoxetanes in the photoreaction of cyclic ketene silyl acetals with 2-naphthaldehyde and their transformation to aldol-type adducts. *Tetrahedron Lett.* **1996,** 37, 5901-5904.

22. Turro, N. J.; Wriede, P. A., Molecular photochemistry. X. Photocycloaddition of acetone to 1-methoxy-1-butene. A comparison of singlet and triplet mechanisms and biradical intermediates. *J. Am. Chem. Soc.* **1968,** 90, 6863-6864.

23. (a) Griesbeck, A. G.; Abe, M.; Bondock, S., Selectivity Control in Electron Spin Inversion Processes: Regio- and Stereochemistry of Paterno`-Bu1chi Photocycloadditions as a Powerful Tool for Mapping Intersystem Crossing Processes. *Acc. Chem. Res.* **2004,** 37, 919-928. (b) Griesbeck, A. G.; Stadtmüller, S., Photocycloaddition of Benzaldehyde to Cyclic Olefins:
Electronic Control of Endo Stereoselectivity. *J. Am. Chem. Soc.* **1990,** 112, 1281-1283.

24. Salem, L.; Rowland, C., The Electronic Properties of Diradicals. *Angew. Chem. Int. Ed.* **1972,** 11, 92-111.

25. Griesbeck, A. G.; Buhr, S.; Fiege, M.; Schmickler, H.; Lex, J., Stereoselectivity of Triplet Photocycloadditions: Diene-Carbonyl Reactions and Solvent Effects. *J. Org. Chem.* **1998,** 63, 3847-3854.

26. (a) Zheng, C.; You, S.-L., Catalytic Asymmetric Dearomatization by Transition-Metal Catalysis: A Method for Transformations of Aromatic Compounds. *Chem* **2016,** 1, 830-857. (b) Wertjes, W. C.; Southgate, E. H.; Sarlah, D., Recent advances in chemical dearomatization of nonactivated arenes. *Chem. Soc. Rev.* **2018,** 47, 7996-8017.

27. Kaushik, N. K.; Kaushik, N.; Attri, P.; Kumar, N.; Kim, C. H.; Verma, A. K.; Choi, E. H., Biomedical Importance of Indoles. *Molecules* **2013,** 18, 6620-6662.

28. Okumura, M.; Sarlah, D., Visible-Light-Induced Dearomatizations. *Eur. J. Org. Chem.* **2020,** 2020, 1259-1273.

29. (a) Zhu, M.; Zheng, C.; Zhang, X.; You, S.-L., Synthesis of Cyclobutane-Fused Angular Tetracyclic Spiroindolines via Visible-Light-Promoted Intramolecular Dearomatization of Indole Derivatives. *J. Am. Chem. Soc.* **2019,** 141, 2636-2644. (b) Oderinde, M. S.; Mao, E.; Ramirez, A.; Pawluczyk, J.; Jorge, C.; Cornelius, L. A. M.; Kempson, J.; Vetrichelvan, M.; Pitchai, M.; Gupta, A.; Gupta, A. K.; Meanwell, N. A.; Mathur,

A.; Dhar, T. G. M., Synthesis of Cyclobutane-Fused Tetracyclic Scaffolds via Visible-Light Photocatalysis for Building Molecular Complexity. *J. Am. Chem. Soc.* **2020,** 142, 3094-3103.

30. Carreira, E. M.; Fessard, T. C., Four-membered ring-containing spirocycles: synthetic strategies and opportunities. *Chem. Rev.* **2014,** 114, 8257-8322.

31. (a) D'Auria, M.; Emanuele, L.; Racioppi, R.; Valente, A., Paternò-Büchi reaction between aromatic carbonyl compounds and 1-(3-furyl) alkanols. *Photochem. Photobiol. Sci.* **2008,** 7, 98-103. (b) Rivas, C.; Bolivar, R. A., Synthesis of oxetanes by photoaddition of carbonyl compounds to 2,5-dirnethylthiophene. *J. Heterocycl. Chem.* **1973,** 10, 967-971. (c) Abe, M.; Torii, E.; Nojima, M., Paternò– Büchi Photocyclization of 2-Siloxyfurans and Carbonyl Compounds. Notable Substituent and Carbonyl (Aldehyde vs Ketone and Singlet- vs Triplet-Excited State) Effects on the Regioselectivity (Double-Bond Selection) in the Formation of Bicyclic e xo-Oxetanes. *J. Org. Chem.* **2000,** 65, 3426-3431. (d) D'Auria, M.; Racioppi, R.; Rofrano, F.; Stoia, S.; Viggiani, L., Investigation of the hydroxyl directing effect on the Paternò–Büchi reaction on 5-(2-triisopropylsilyloxazolyl) methanol derivatives. *Tetrahedron* **2016,** 72, 5142-5148. (e) Schreiber, S. L.; Satake, K., Application of the furan carbonyl photocycloaddition reaction to the synthesis of the bis (tetrahydrofuran) moiety of asteltoxin. *J. Am. Chem. Soc.* **1983,** 105, 6723-6724.

32. (a) Julian, D. R.; Tringham, G. D., Photoaddition of ketones to indoles: synthesis of oxeto[2,3-b]indoles. *J. Chem. Soc., Chem. Commun.* **1973**, 13b-14. (b) Takechi, H.; Machida, M.; Nishizono, N.; Kanaoka, Y., Intramolecular Photoreactions of Phthalimide-Alkene Systems. Macrocyclic Synthesis through the Remote Paterno-Buchi Reaction of Phthalimide with Indole Derivatives. *Chem. Pharm. Bull.* **1994,** 42, 188-196. (c) Takechi, H.; Machida, M.; Kanaoka, Y., Intramolecular photoreactions of phthalimide-alkene systems. Oxetane formation of N-(ω-indol-3-ylalkyl) phthalimides. *Chem. Pharm. Bull.* **1988,** 36, 2853-2863. (d) Takechi, H.; Machida, M.; Kanaoka, Y., Intermolecular photoreactions of phthalimide-alkene systems. Regio-and stereoselective oxetane formation from N-methylphthalimide and N-acetylindole derivatives. *Chem. Pharm. Bull.* **1988,** 36, 3770-3779. (e) Machida, M.; Takechi, H.; Kanaoka, Y., Photochemistry of the Phtalimide System. 32. Photoreaction of N-(Ω-Indol-3-Ylakyl) Phtalimides: Intramolecular Oxetane Formation of the Aromatic Imide System. *Chem. Informationsdienst* **1983,** 14, no-no. (f) Takechi, H.; Machida, M.; Kanaoka, Y., Intermolecular photoaddition of N-methylphthalimide to indole derivatives: regio-and stereoselective formation of oxeto [2, 3-b] indoles. *Heterocycles* (*Sendai*) **1985,** 23, 1373-1376. (g) Usman, A.; Razak, I. A.; Fun, H. K.; Chantrapromma, S.; Zhang, Y.; Xu, J. H.,

Syn- and anticlinal isomers of 2a'-acetoxy-1,7'-diacetyl-7',7a'-dihydro-2-oxospiro[1H-indole-3(2H),2'(2a'H)-oxet o[3,2-b]indole]. *Acta Cryst. C* **2002,** 58, o59-62.

33. Cohen, S. G.; Baumgarten, R. J., Photoreduction of benzophenone by amines, alcohols, and hydrocarbons. Medium effects. Photochemical oxidative deamination. *J. Am. Chem. Soc.* **1967,** 89, 3471-3475.

34. Schultz, D. M.; Yoon, T. P., Solar synthesis: prospects in visible light photocatalysis. *Science* **2014,** 343, 1239176.

35. Dorman, G.; Nakamura, H.; Pulsipher, A.; Prestwich, G. D., The life of Pi star: Exploring the exciting and forbidden worlds of the benzophenone photophore. *Chem. Rev.* **2016,** 116, 15284-15398.

36. Blanksby, S. J.; Ellison, G. B., Bond dissociation energies of organic molecules. *Acc. Chem. Res.* **2003,** 36, 255-263.

37. Spectroscopical analysis ruled out the hypothesis of direct indole excitation leading to reactivity.

38. (a) Peters, K. S.; Lee, J., Picosecond dynamics of the photoreduction of benzophenone by DABCO. *J. Phys. Chem.* **1993,** 97, 3761-3764. (b) Griller, D.; Howard, J. A.; Marriott, P. R.; Scaiano, J. C., Absolute rate constants for the reactions of tert-butoxyl, tert-butylperoxyl, and benzophenone triplet with amines: the importance of a stereoelectronic effect. *J. Am. Chem. Soc.* **1981,** 103, 619-623. (c) Arimitsu, S.; Masuhara, H.; Mataga, N.; Tsubomura, H., Laser photolysis studies on quenching processes of triplet benzophenone by amines in fluid solution. *J. Phys. Chem.* **1975,** 79, 1255-1259. (d) Blanchi, J.-P.; Watkins, A. R., Quenching of triplet benzophenone by electron donors. *J. Chem. Soc., Chem. Commun.* **1974**, 265-266.

39. Mateos, J.; Vega-Penaloza, A.; Franceschi, P.; Rigodanza, F.; Andreetta, P.; Companyo, X.; Pelosi, G.; Bonchio, M.; Dell'Amico, L., A visible-light Paterno-Buchi dearomatisation process towards the construction of oxeto-indolinic polycycles. *Chem. Sci.* **2020,** 11, 6532-6538.

40. (a) Russel, J. S., Oxindoles and Spirocyclic Variations: Strategies for C3 Functionalization. In *Heterocyclic Scaffolds II*: *Reactions and Applications of Indoles*, Gribble, G. W., Ed. Springer Berlin Heidelberg: Berlin, Heidelberg, 2010; pp 397-431. (b) Zhou, F.; Liu, Y.-L.; Zhou, J., Catalytic Asymmetric Synthesis of Oxindoles Bearing a Tetrasubstituted Stereocenter at the C-3 Position. *Adv. Synth. Catal.* **2010,** 352, 1381-1407.

41. (a) Badillo, J. J.; Hanhan, N. V.; Franz, A. K., Enantioselective synthesis of substituted oxindoles and spirooxindoles with applications in drug discovery. *Curr. Opin. Drug Discovery Dev.* **2010,** 13, 758-776. (b) Peddibhotla, S., 3-Substituted-3-hydroxy-2-oxindole, an Emerging New Scaffold for Drug Discovery with Potential Anti-Cancer and other Biological Activities. *Curr. Bioact. Compd.* **2009,** 5, 20-38. (c) Trost, B. M.; Brennan, M. K., Asymmetric syntheses of oxindole and indole spirocyclic alkaloid natural products. *Synthesis* **2009,** 2009, 3003-3025.

42. Tokunaga, T.; Hume, W. E.; Umezome, T.; Okazaki, K.; Ueki, Y.; Kumagai, K.; Hourai, S.; Nagamine, J.; Seki, H.; Taiji, M., Oxindole derivatives as orally active potent growth hormone secretagogues. *J. Med. Chem.* **2001,** 44, 4641-4649.

43. Taylor, A. M.; Altman, R. A.; Buchwald, S. L., Palladium-catalyzed enantioselective α-arylation and α-vinylation of oxindoles facilitated by an axially chiral P-stereogenic ligand. *J. Am. Chem. Soc.* **2009,** 131, 9900-9901.

44. Bariwal, J.; Voskressensky, L. G.; Van der Eycken, E. V., Recent advances in spirocyclization of indole derivatives. *Chem. Soc. Rev.* **2018,** 47, 3831-3848.

45. Shen, K.; Liu, X.; Lin, L.; Feng, X., Recent progress in enantioselective synthesis of C3-functionalized oxindoles: rare earth metals take action. *Chem. Sci.* **2012,** 3, 327-334.

46. Liang, K.; Li, N.; Zhang, Y.; Li, T.; Xia, C., Transition-metal-free α-arylation of oxindoles via visible-light-promoted electron transfer. *Chem. Sci.* **2019,** 10, 3049-3053.

47. Silvi, M.; Melchiorre, P., Enhancing the potential of enantioselective organocatalysis with light. *Nature* **2018,** 554, 41-49.

48. Cambie, D.; Bottecchia, C.; Straathof, N. J.; Hessel, V.; Noel, T., Applications of continuous-flow photochemistry in organic synthesis, material science, and water treatment. *Chem. Rev.* **2016,** 116, 10276-10341.

49. Franceschi, P.; Mateos, J.; Vega-Peñaloza, A.; Dell'Amico, L., Microfluidic Visible-Light Paternò–Büchi Reaction of Oxindole Enol Ethers. *Eur. J. Org. Chem.* **2020,** 2020, 6718-6722.

Chapter III

New strategies in CO_2 fixation: electro- and photocarboxylation

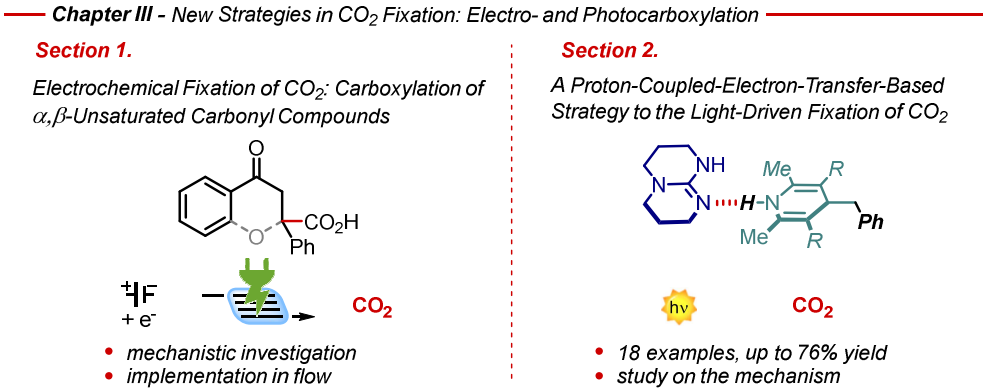

This Chapter describes the exploitation of CO_2 in organic synthesis as a single carbon atom building block. After a description of the molecular properties of CO_2, a brief overview of the carboxylation strategies using CO_2 is given. Section 1 and 2 further analyse the electro- and photochemical carboxylation processes.

Pubblications:

- Franceschi, P.; Nicoletti, C.; Bonetto, R.; Bonchio, M.; Natali, M.; Dell'Amico, L.; Sartorel, A. *Basicity as a Thermodynamic Descriptor of Carbanions Reactivity with Carbon Dioxide*: *Application to the Carboxylation of α,β-Unsaturated Ketones. Front. Chem.* **2021**, 9, 783993.
- Franceschi, P.; Rossin, E.; Scopano, A.; Vega-Peñaloza, A.; Goti, G.; Singh, D.; Sartorel, A.; Dell'Amico, L. *A Proton-Coupled-Electron-Transfer-Based Strategy to the Light-Driven Fixation of CO_2*. Manuscript under preparation.

3. – CO_2 as a C source in organic synthesis

Carbon dioxide (CO_2) is an optimal carbon-atom source: it is neither explosive nor flammable, it is non-toxic, and it is widely available.[1] Indeed, it can be considered as a renewable resource, as it is continuously produced by nature, with animal and plant respiration,[1] and by men, mainly through combustion of fossil fuels.[2] To give an example, the actual CO_2 consumption for chemical synthesis at industrial level is around 116 million of tons per year,[3] while yearly energy-related global emissions are 33.4 billion of tons.[4]

Since long, chemist have tried to employ CO_2 as a reagent, focusing on its reduction or on its incorporation into organic substrates. Reduction of CO_2 yields carbon monoxide, formic acid, methanol or different aldehydes and alcohols, depending on the conditions used, and is usually accomplished via hydrogenation or electrochemical reduction. Along incorporation into organic substrates, the carbon atom in CO_2 generally retains its oxidation state, as for carbonate and carbamate synthesis, or is slightly reduced, as it occurs in carboxylation reactions, where carboxylic acids or their derivatives are obtained (Figure 3.1).[5]

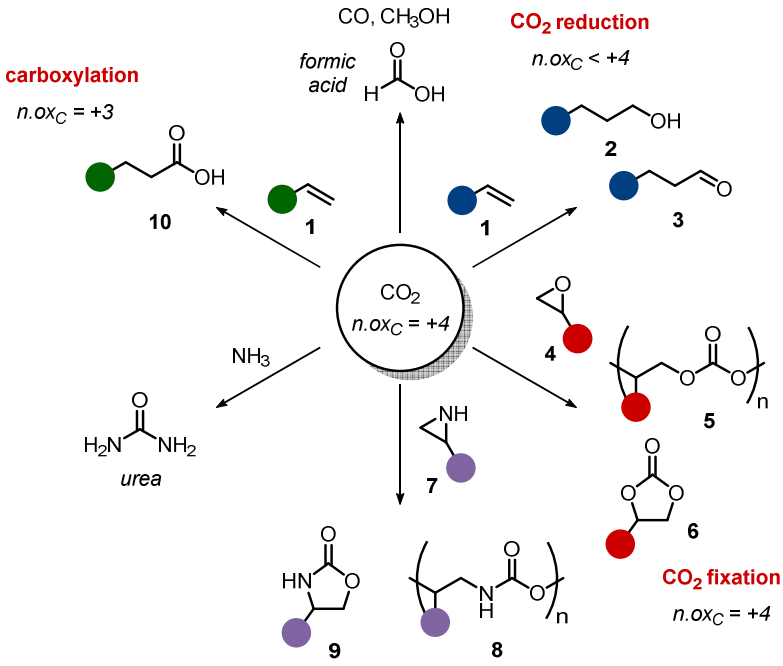

Figure 3.1. – Applications of CO_2 as a C atom source.

However, stability and inertness of CO_2 hamper these processes. To overcome these barriers, classically, high temperatures and high pressures, excess of additives, or use of high-energy reagents have been employed. This greatly increases the economic cost and environmental impact of the process. More recently, efficient catalytic systems have been exploited to solve the issues of classical methods, by activation of CO_2 or of the substrates.[6] In the next paragraphs, a brief overview of the physicochemical characteristics of CO_2, needed to understand its reactivity, and of the strategies employed in carboxylation processes, theme of this chapter, are given.

Molecular properties of CO_2

CO_2 is a linear molecule, with two symmetrical C=O double bonds. Although the molecule has no permanent dipole moment, the two C=O bonds are

polarised. The carbon atom carries a partial positive charge (+0.528),[7] thus it is electrophilic, while the two oxygen atoms carry a partial negative charge (-0.264), thus they are weakly nucleophilic.[1] The molecular orbital diagram for CO_2 is shown in Figure 3.2: in its ground state there are two degenerate HOMOs of non-bonding character localised on the p_x and p_y atomic orbitals (AOs) of the oxygen atoms, which indeed are slightly nucleophilic. Two degenerate LUMOs of anti-bonding character are mainly localised on the p_x and p_y AOs of carbon, explaining its electrophilicity.[8]

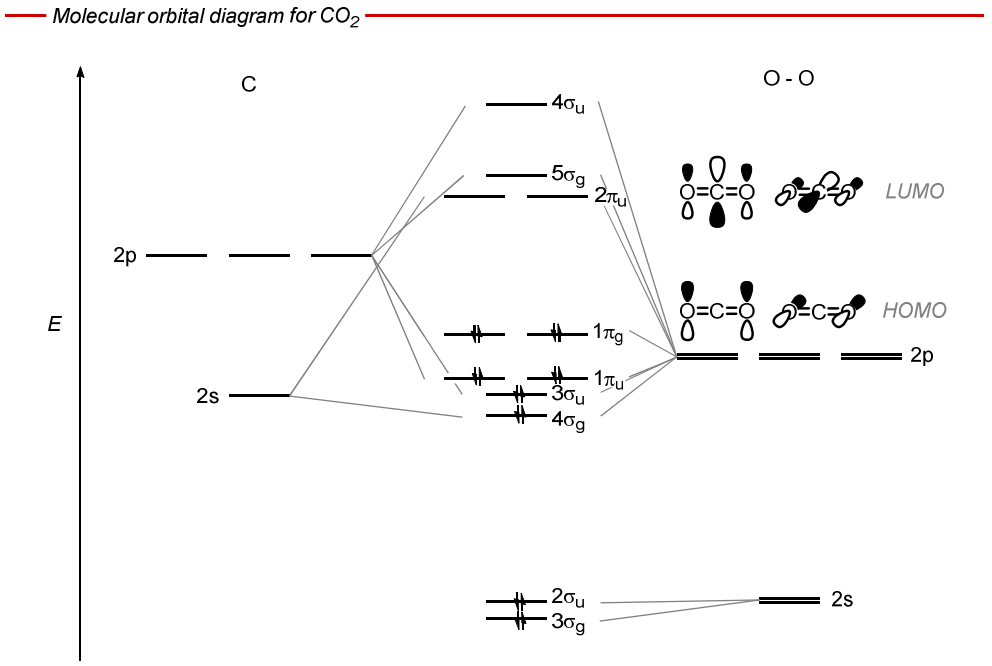

Figure 3.2. – Molecular orbital diagram for CO_2 and graphical representation of HOMOs and LUMOs.[8]

CO_2 is a highly stable and inert molecule, indeed it has a standard Gibbs free energy of formation $\Delta G_f^\circ = -394$ kJ mol^{-1} (as a comparison, for liquid benzene $\Delta G_f^\circ = +119$ kJ mol^{-1}, while for benzoic acid $\Delta G_f^\circ = -255$ kJ mol^{-1}).[1]

Moreover, reactions involving capture of CO_2 usually have a negative entropy variation (ΔS_r), because a gas (CO_2) is transformed into a solid or a liquid, and because one product is formed from two reagents. According to the definition of Gibbs free energy variation (ΔG_r, Equation 3.1),[9] for a negative ΔS_r term there will be a temperature over which the unfavourable entropy term prevails, and CO_2 capture is thermodynamically uphill $(\Delta G_r > 0)$. Furthermore, even when thermodynamically allowed, these processes are usually characterised by a high activation barrier, due to the inertness of CO_2.

$$\Delta G_r = \Delta H_r - T\Delta S_r \qquad \text{Equation 3.1.}$$

Where ΔG_r is the reaction Gibbs free energy variation, ΔH_r is the reaction enthalpy variation, T the absolute temperature and ΔS_r is the reaction entropy variation.

Overview of carboxylation strategies using CO_2

Carbon dioxide can be used as a C1 source[10] for the synthesis of carboxylic acids taking advantage of the electrophilicity of its carbon atom. Classically this has involved the use of strong nucleophiles such as metal enolates, Grignard and alkyl-lithium reagents or other organometallic species, in combination with high temperature and pressure. However, the use of stoichiometric amounts of metals, as well as sensitive and dangerous reagents reduces the attractiveness of these strategies.[5] One notable example is the Kolbe-Schmitt reaction[11] (Scheme 3.1a), which, besides being the first reported application of CO_2 in organic synthesis, is also one of the most important industrial applications of carbon dioxide. Salicylic acid **14a** and 4-methoxybenzoic acid **14b**, precursors of aspirin and parabens respectively, are synthesized using this process, where high temperature and pressure of CO_2 allow the carboxylation of phenolate **12**.[12]

The implementation of appropriate catalytic systems has helped overcoming the drawbacks of the first carboxylation procedures and has expanded the scope of the possible applications. In particular, exploiting the peculiar properties of transition metals (TMs), carboxylation of simple and stable reagents, like olefins and organic halides, has been reported. The substrate is activated by coordination or oxidative addition, at the same time CO_2 is activated through different binding modes (Scheme 3.1b).[6e] One limitation of TM catalysis is that, oftentimes, stoichiometric amounts of a reducing metal agent, typically Mn or Zn, are required to close the catalytic cycle. Nevertheless, electrochemistry, and more recently photoredox catalysis, have been proposed and investigated as valid substitutes to these metallic single-electron reductants.[13]

Electro- and photochemistry are also competent alternatives for the carboxylation of simple and available substrates. Harnessing the energy of light or by the direct input of electrons, high-energy intermediates are generated directly in situ, under mild conditions.[14] These strategies generally rely on the formation of anionic nucleophilic species through reduction processes (Scheme 3.1c), and will be explained in more detail in the following chapters.

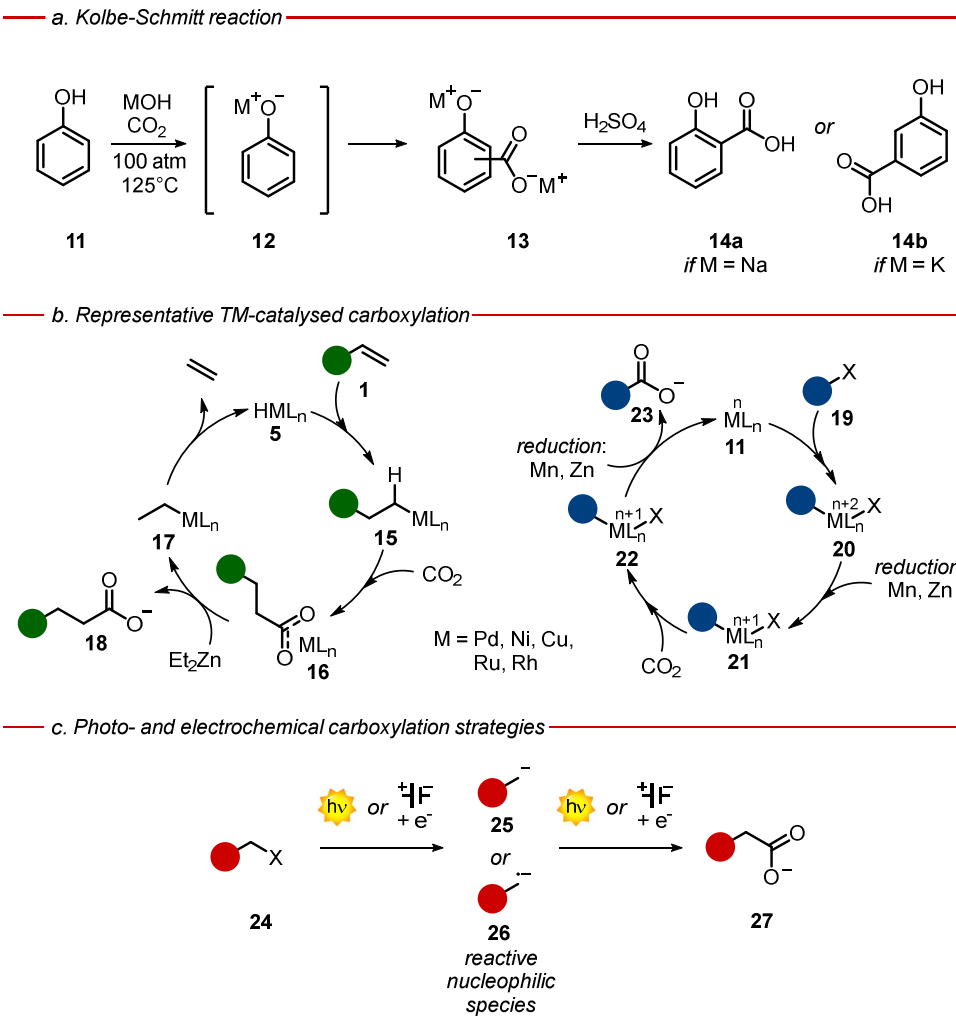

Scheme 3.1. – a. Kolbe-Schmitt reaction. b. TM-catalysed carboxylation of olefins and organic halides. c. General photo- and electrochemical carboxylation strategies

Chapter III – Section 1

Electrochemical Fixation of CO_2: Carboxylation of α,β-Unsaturated Carbonyl Compounds

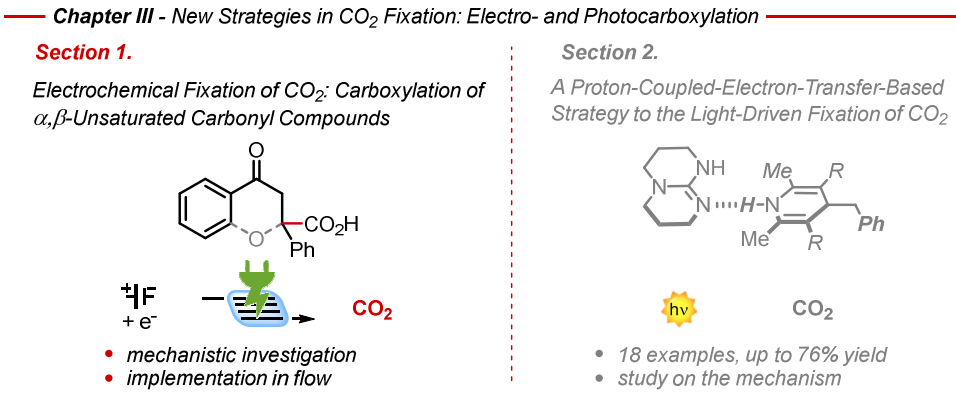

This Section describes the electrochemical carboxylation of α,β-unsaturated carbonyl compounds, developed into two projects. In the first, the mechanism of the transformation was investigated through CPE experiments. In the second, the implementation in a flow electrochemical cell was studied in collaboration with the group of Prof. Nöel at University of Amsterdam, under the supervision of Dr Lars Wesenberg.

This work has been published: Franceschi, P.; Nicoletti, C.; Bonetto, R.; Bonchio, M.; Natali, M.; Dell'Amico, L.; Sartorel, A. *Basicity as a Thermodynamic Descriptor of Carbanions Reactivity with Carbon Dioxide*: *Application to the Carboxylation of α,β-Unsaturated Ketones. Front. Chem.* **2021**, 9, 783993.

3.1.1. – Electrochemical carboxylation of flavone and chalcone: a mechanistic investigation

Electrochemical CO_2 fixation: reaction pathways

Electrochemistry is a powerful tool to drive carbon dioxide fixation. With this approach, mild reaction conditions can be used, and the simplest reducing agent is used: electrons. In this way atom economy is increased, and the use of toxic or harmful reducing agents is avoided.

Electrochemical studies on CO_2 have a long history, starting already in the mid-1900s,[15] and have evolved into the still very active field of electrocatalytic CO_2 reduction.[16] In parallel, first examples on electrosynthetic carboxylation were reported by Wawzonek *et al.*[17] and later by Tyssee *et al.*,[18] followed by intense mechanistic studies.[19] Interest in the field never ceased,[20] but it was only in recent years that a more synthetic-focused approach has been utilized.[21] Typical strategies for electrochemical carboxylation of organic substrates are: *i*) reduction of unsaturated compounds such as olefins,[18c, 22] alkynes,[23] carbonyls[17, 24] and imines;[25] *ii*) reductive cleavage of organic halides[26] and pseudo-halides;[27] *iii*) combination of electrochemistry and transition metal catalysis.[21g] In the first case, different mechanisms can be hypothesized, depending on the reduction potential of the substrates (Scheme 4.1a).[19] When the unsaturated species **28** is reduced more easily than CO_2 (E^0 = -2.41 V vs Fc^+/Fc in DMF, all potential in this chapter are referred to Fc^+/Fc[28] unless otherwise stated),[29] the radical anion **29** can act as a nucleophile on CO_2 (path a), to give species **30**, which is then further reduced to the dianion **31.** Finally, reaction with proton sources like H_2O gives **32**, or alternatively, interception of another CO_2 molecule gives the dicarboxylated product **33**. If **28** is less prone to reduction (E^0 < -3.0 V, path b), the radical anion **29** homogeneously transfers an electron to CO_2 (path b), then coupling of CO_2 radical anion with another unit of **29** yields the dianion **31** which reacts as above. Direct reduction of CO_2 to its radical anion at the

electrode can also take place, even though this is rare because of the slow kinetics and high overpotentials often associated. In this case $CO_2^{\bullet-}$ can attack the olefin forming the carboxylated product or dimerise to oxalate dianion.

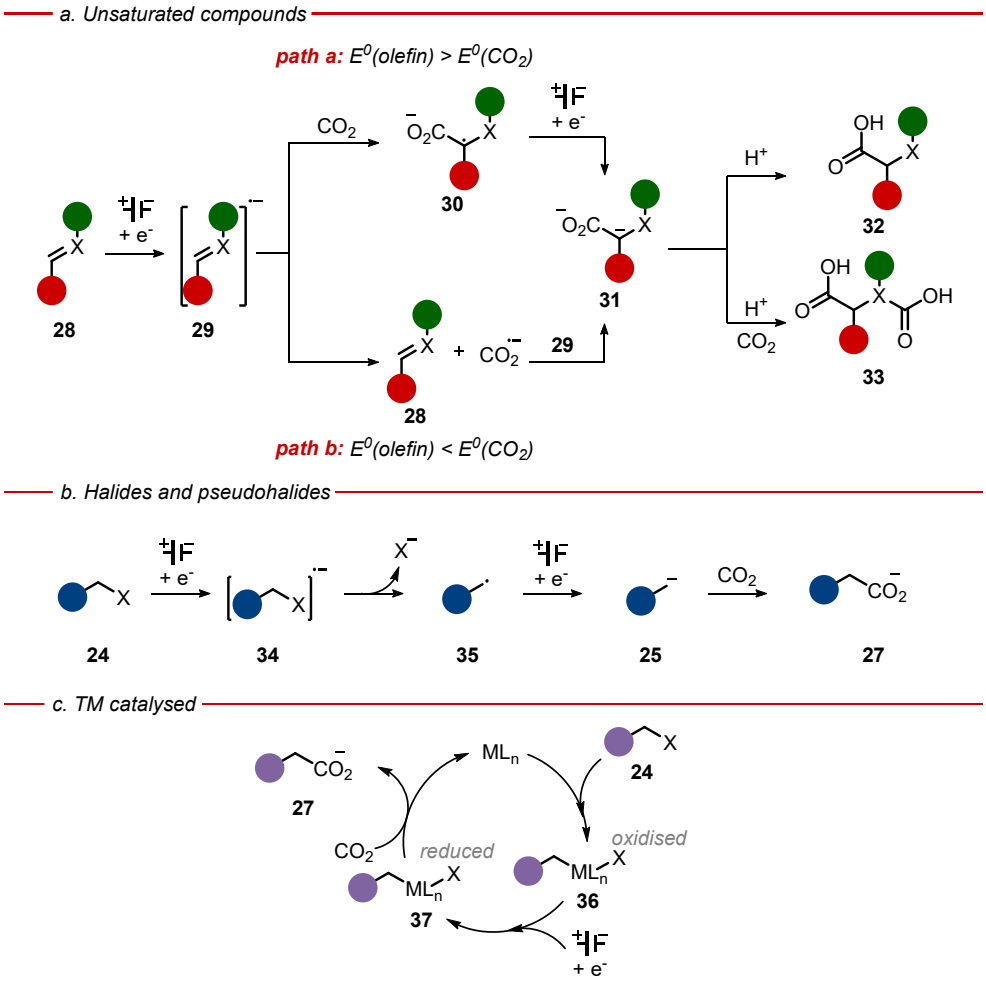

Scheme 3.4. – Strategies for electrochemical carboxylation using CO_2: a. reduction of unsaturated compounds, b. reduction of halides and pseudo-halides and c. combination of TM catalysis and electrochemistry.

In the case of organic halides **24**, reduction to the radical anion **34** is followed by heterolytic cleavage of the C-X bond to give X^- and radical **35**. Further

electrochemical reduction to the anion **25** is followed by nucleophilic attack on CO_2, with formation of product **27** (Scheme 3.4b).[14a] In the last case, the reaction mechanism is usually similar to that of TM catalysed reaction (Scheme 3.4c). Oxidative addition of organic halides and pseudo-halides to a metal complex ML_n generates organometallic species **36**, followed by cathodic reduction to **37** and carboxylation to product **27**,[21g] while restoring the catalyst in its initial state.

Electrocarboxylation of α,β-unsaturated carbonyl compounds

α,β-unsaturated carbonyl compounds are important substances, both as intermediates in many industrial processes and as biologically relevant compounds.[30] In particular, coumarins,[31] chalcones,[32] flavones[33] and their derivatives are intensively studied for their pharmacological properties. Flavonoids are a class of natural compounds present in many plants, fruits, and vegetables where they have a significant impact on various aspect of plant biology.[34] Numerous molecules of this family have shown diverse medicinal benefits, including anticancer, antioxidant and anti-inflammatory properties.[33] For example, LW-215, a newly synthesized derivative of wogonin, showed anti-angiogenic properties, both *in vitro* and *in vivo*,[35] while several other flavonoids have been studied for their PKC inhibitor activity[36] (Figure 3.3).

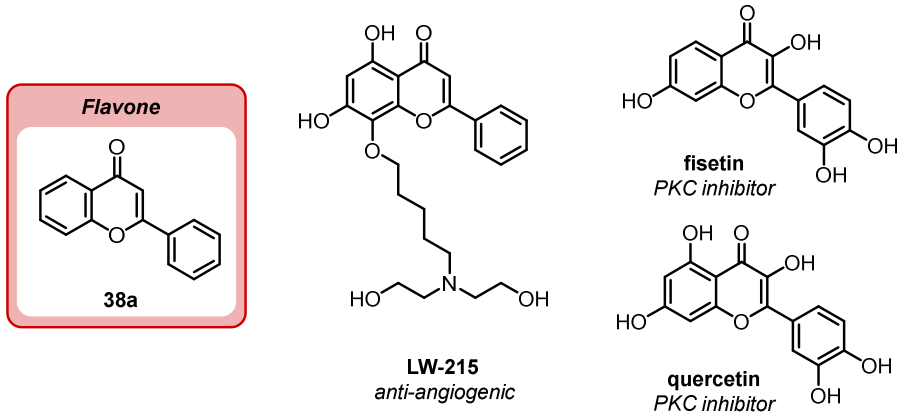

Figure 3.3. – Examples of biologically active flavonoids.

Furthermore, β-carboxyl ketones, which can be obtained from carboxylation of α,β-unsaturated carbonyls, are also important as precursors in the synthesis of bioactive drugs and natural products. [37]

Due to their relevance, several examples have been reported on carboxylation of these scaffolds, especially employing electrochemical methods. A lot of work in particular has been done on α,β-unsaturated esters and amides,[18c, 38] though some examples have also been reported on carboxylation of chalcone, flavone and other α,β-unsaturated ketones (Scheme 3.5). In a seminal report,[39] Wawzonek *et al.* obtained carboxylation of chalcone **38b** using a polarographic divided cell setup with a Hg pool cathode at a constant line voltage of 85 V. Using KI as supporting electrolyte carboxylation was observed at the first reduction wave of chalcone,[40] where chalcone radical anion **39b** is formed at the cathode. Using NBu_4I, reduction at the second wave was observed,[41] where chalcone dianion **40b** is produced. In both cases monocarboxylic acid **41b** is obtained after acidification of the catholyte, but higher yield and selectivity were observed in the second experiment. A dicarboxylate product **45b**, which would

liberate CO_2 when treated with acid, was postulated, and in the first case observed as a potassium salt. Twenty years later, Kunai *et al.*[42] reported the carboxylation of chalcone and similar substrates in a divided cell setup with a Hg pool cathode under potentiostatic control. Electrolysis at the potential of the first wave gave the carboxylated product **41b** with less selectivity and less efficiently than at the second reduction wave (35% vs 77% yield respectively), with formation of dimer **46b** and other polymeric species. Compounds with aliphatic substituents on the alkene, which do not show generation of the dianion in absence of CO_2, also gave low selectivity toward carboxylation (43%) with high amounts of dimeric product **46** (50%). The yield could be increased (67%) using low current density in a galvanostatic setup, where the radical anion (identified as the species responsible for competitive dimerisation) was obtained in reduced concentration at the electrode surface.

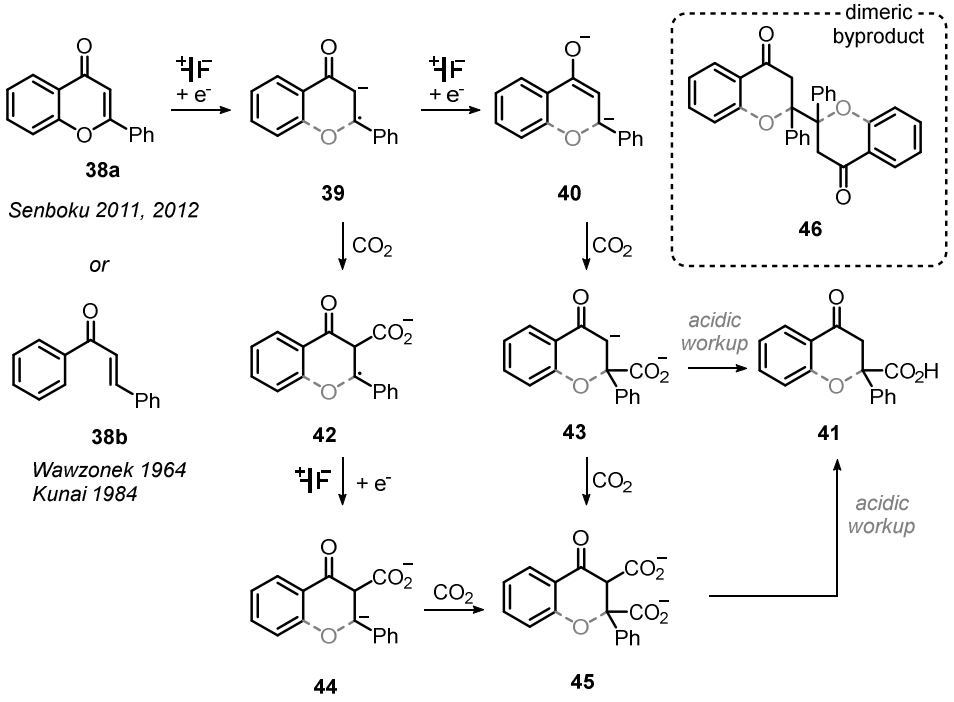

Scheme 3.5. – Possible mechanism for carboxylation of chalcone and flavone.

Carboxylation of flavone **38a** to yield monocarboxylated product **41a** was reported in 2011 by Senboku,[43] using an undivided cell with a Pt cathode and a sacrificial Mg anode under galvanostatic control. Subsequent experiments[44] where the electrolyzed solution was directly treated with benzyl bromide, showed only the formation of the ester derived from monocarboxylate **43a**, suggesting no formation of a dicarboxylated species such as **45a**. This was considered as a proof against a radical anion mechanism: if carboxylation of radical anion **39a** is supposed to happen, a dicarboxylate product should form before acid treatment of the electrolysed mixture.

3.1.2. – Aim of the project

Prompted by the interest in these compounds and by open questions on the reaction mechanism, the aim of this project was to investigate further the activity of the proposed intermediates towards carboxylation, while developing a general tool to predict reactivity towards CO_2. As a matter of facts, most of the previous reports were performed in galvanostatic conditions, where the potential at which the transformation occurs, and consequently the intermediates produced, are not controlled.[38a, 38c, 42-45] Bearing this in mind, we decided to analyse the electrochemical carboxylation process with a potentiostatic set up, in order to control the generated reduced form of the substrate and to understand which one is needed to achieve the carboxylation. Additionally, a divided-cell setup was employed, in order to avoid any interference by the species generated at the counter electrode. For this purpose, flavone **38a** was selected as the substrate, because of its higher synthetic and biological interest, and because of a higher amount of data on its transformations.[46]

3.1.3. – Results and discussions

Initial electrochemical analyses

First electrochemical analyses on flavone **38a** were done by cyclic voltammetry (CV), under N_2 atmosphere, under cathodic scan, where two waves were observed (Figure 3.4, black trace). The first, quasi reversible wave at $E_{1/2}$ = -2.09 V can be attributed to the one electron reduction to the flavone radical anion **39a**. The second, irreversible wave at E_p = -2.71 V; can be attributed to the further reduction to flavone dianion **40a**. This wave is correlated to more than one electron transfer processes due to the further reduction of flavone dianion, as pointed out by previous polarographic studies.[46]

CVs were recorded also under CO_2 atmosphere. Eventual changes in the electrochemical profile are possibly ascribable to a reactivity between the reduced intermediates and CO_2 (Figure 3.4, red trace). In this case, both reduction peak potentials are slightly shifted toward more positive values (anodic shift) with respect to those observed under N_2 atmosphere: the first is peaking at −2.10 V and the second at −2.50 V. Both waves indicate an irreversible reduction of the substrates, and the second is characterised by a decrease in current. This latter can be explained on the basis of a reactivity of **40a** with CO_2, preventing its further reduction. The major changes associated to the second reduction wave suggest that **40a** could be the key-intermediate which reacts with CO_2.

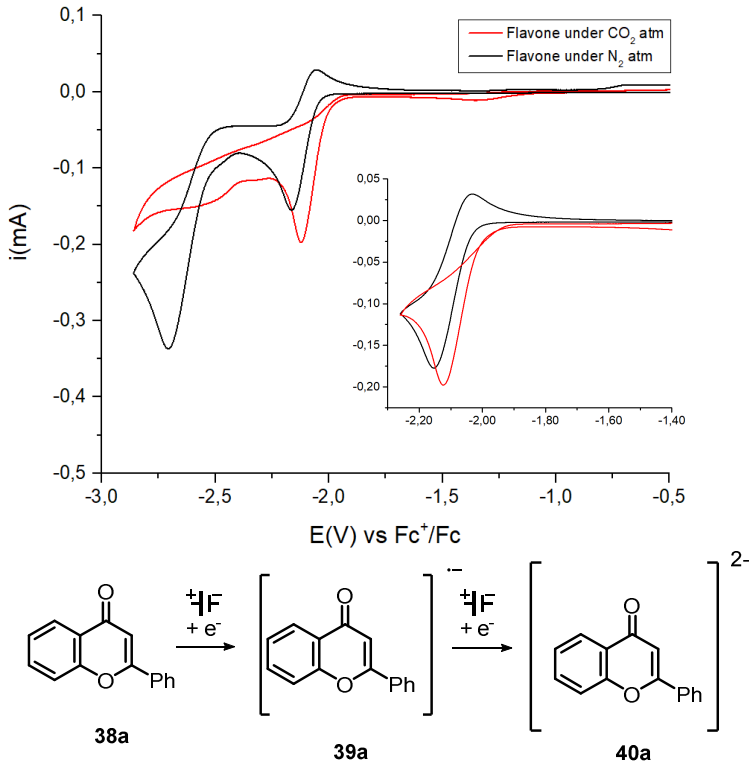

Figure 3.4. – Cyclic voltammetry of flavone **4** in MeCN under N_2 (black traces) and CO_2 (red traces) atmosphere. The inset shows the scan conducted in a narrow potential range, isolating the first reduction process. The reduced species **39a** and **40a** formed at the electrode are also indicated.

Controlled-potential electrolysis experiments

In a second step, CPE experiments in the presence of CO_2 were carried out at the potential associated with formation of the two reactive anionic species **39a** and **40a**. The electrolysis mixture was then treated with $MeOH/H_2SO_4$ to obtain the corresponding ester **47**, which can be easily isolated via silica chromatography. When the electrolysis was conducted at -2.21 V[47] (the potential associated with formation of radical anion **39a**), while passing a total

charge equivalent to two electrons per flavone substrate, 65% conversion of flavone **38a** was observed, but only 3% of the carboxylated product **47a** was generated. Instead, the main products observed were the different isomers of 2,2-biflavanone **46a**, obtained by dimerization of the radical anion (Scheme 3.5).

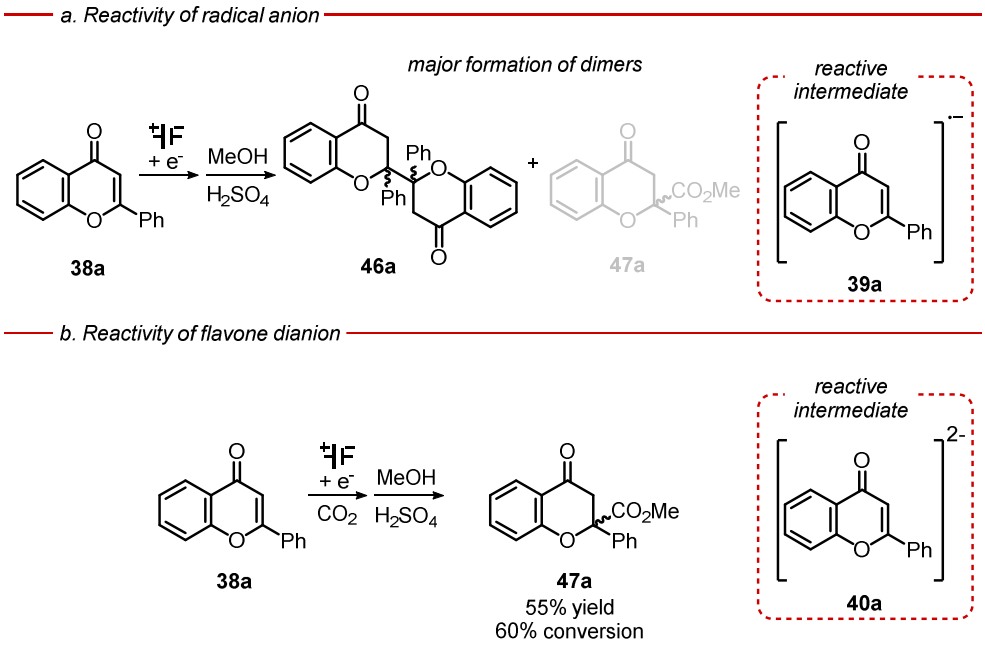

Scheme **3.5.** – CPE of flavone **38a** at a. -2.21 V and b. -2.56 V. Complete conditions are indicated in the experimental section (Paragraph 3.1.9).

On the other hand, electrolysis experiments performed at the second reduction wave of flavone (E = -2.56 V), still passing a total charge equivalent to two electrons per flavone substrate, lead to the almost exclusive formation of carboxylated product **47a**, isolated in 55% yield with 60% conversion of **38a** (92% selectivity toward carboxylation,[48] Scheme 3.5b). These results gave a clear picture of the intermediates active in the carboxylation reaction pathway:

the dianion **40a** is a better nucleophile toward the CO_2 molecule, while the radical anion **39a** is a weaker nucleophile and is more prone to dimerization than to attack CO_2 in these conditions.

Analogously to flavone, also chalcone **38b** could be carboxylated with the same procedure. Also in this case, a CV analysis was carried out (Figure 3.5), that showed a similar electrochemical behaviour to flavone. Under N_2 atmosphere, two reduction waves were observed and associated to the generation of chalcone radical anion **39b** and chalcone dianion **40b**: the first wave peaks at -1.90 V, while the second one is observed between -2.30 V and -2.45 V. This latter is split into two contributions with ca. halved intensity with respect to the first one; this effect could be ascribed to the rotation of the C-C bond in the radical anion, leading to two cis/trans isomeric forms that are further reduced to the dianion at slightly different potentials. Changing to CO_2 atmosphere, the first wave was slightly affected, while the second showed a marked change in shape, imputable to chemical reactivity of the dianion **40b** with CO_2.

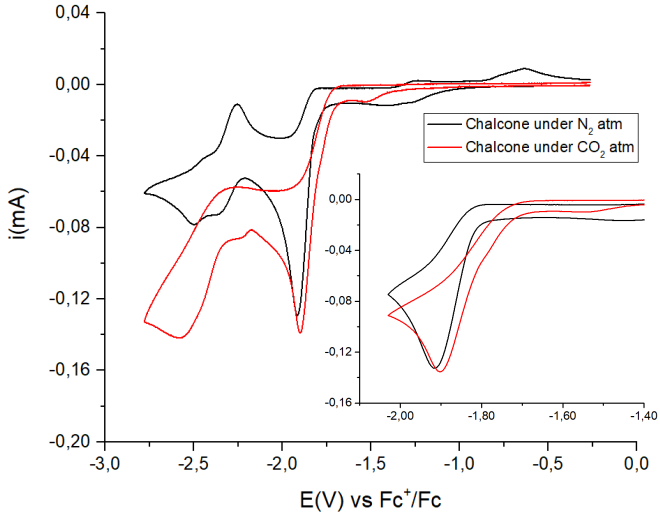

Figure 3.5. – Cyclic voltammetry of chalcone **38b** in MeCN under N_2 (black traces) and CO_2 (red traces) atmosphere. The inset shows the scan conducted in a narrow potential range, isolating the first reduction process.

Thus, CPE of chalcone was conducted at -2.70 V in presence of CO_2: 80% conversion of **38b** was observed, and the carboxylated product **47b** was isolated in 43% yield (54% selectivity for carboxylation), after esterification of the electrolysis mixture (Scheme 3.6).

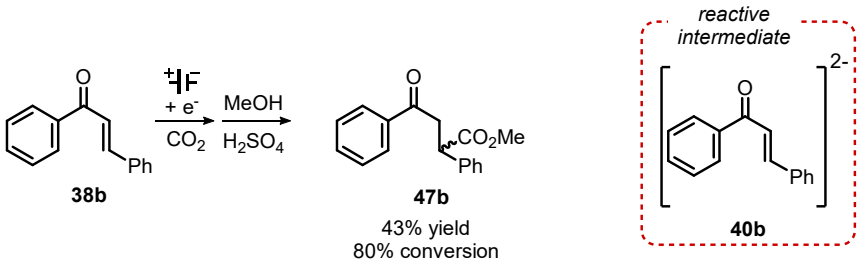

Scheme 3.6. –CPE of chalcone **38b** at -2.70 V. Complete conditions are indicated in the experimental section (Paragraph 3.1.9).

Further proofs

Additional proofs for the different capability to attack CO_2 by radical anions and dianions of α,β-unsaturated carbonyls, were given by generation of these species under different conditions. Light irradiation of a solution of chalcone **38b** and *N*,*N*-dicyclohexylmethylamine (DCMA) gave rise to a photoinduced electron transfer (PET) between the two, generating radical anion **39b** along with the radical cation of DCMA.[49] Both in presence of N_2 and CO_2 atmosphere, no carboxylation of chalcone occurred, while dimeric species **46b** was obtained (Scheme 3.7a). Using Mg^0 as a reductant, generation of dianion **40b** can be accomplished;[50] in this case, under CO_2 atmosphere carboxylated product **41b** was observed in 56% yield by NMR analysis (Scheme 3.7b). The results observed highlight the same difference in reactivity between radical anions and dianions observed in the electrochemical setup, though the generation of these species was done in different conditions from the CPEs described above, thus they should be carefully considered.

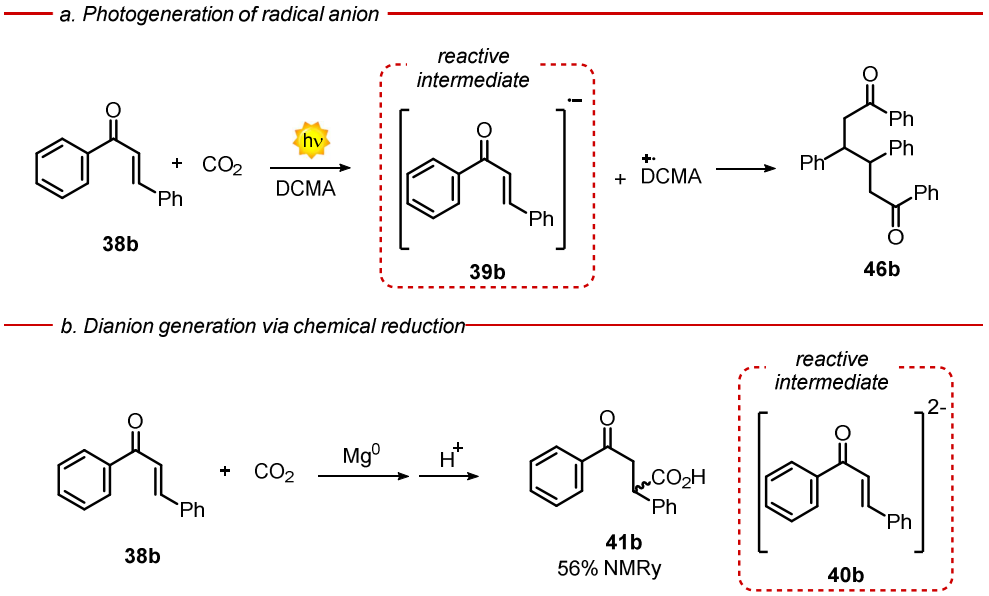

Scheme 3.7. – a. Photogeneration of radical anion **39b** and reaction in the presence of CO_2. b. Carboxylation of **38b** through chemical reduction to dianion **40b**.

The study was further supported by computational studies carried out by colleagues of the group, which I briefly report here for clarity and completeness purposes. A thermodynamic analysis of the carboxylation reaction of a general carbanion C^- allowed to linearly correlate the standard free energy of the process (ΔG^0_{carbox}) with the basicity of C^-, expressed as the $pKa_{CH/C-}$ of the conjugated acid CH (Figure 3.6). A threshold $pKa_{CH/C-}$ was identified, when $pKa_{CH/C-}$ > ~36 (in MeCN) ΔG^0_{carbox} is negative, indicating a thermodynamically favourable process. Nowadays, pKa can be estimated using density functional theory (DFT) calculations,[51] thus the model could be applied to the electrochemical carboxylation of flavone and chalcone, confirming the experimental results. For both dianions **40a** and **40b** the calculated pKa of the conjugate acid resulted > 50, and the ΔG^0_{carbox} was predicted to be -12.8 and

−20.0 kcal·mol^{-1} respectively. Radical anions **39a** and **39b**, instead, showed ΔG^0_{carbox} > +20 kcal·mol^{-1} in both cases, consistent with calculated pKa of the conjugate acid < 18.5.

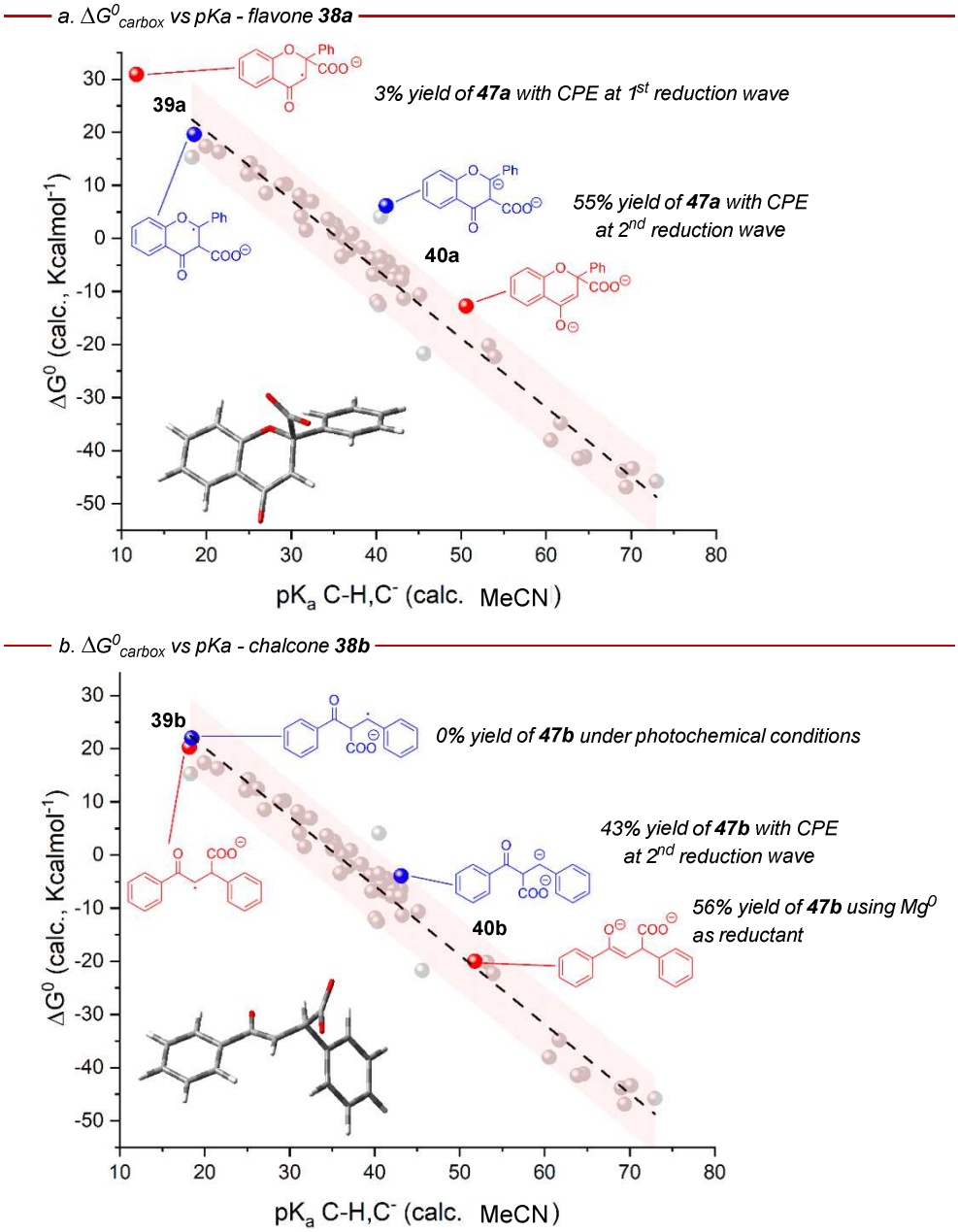

Figure 3.6. – Plot of calculated ΔG^0_{carbox} vs. calculated $pKa_{CH/C-}$. for radical anion **39** and dianion **40** for a. flavone **38a** and b. chalcone **38b**. The blue dots refer to the possible carboxylation in α to the carbonyl, the grey dots refer to a series of 50 small organic compounds used in the DFT calculations.

3.1.4. – Concluding remarks

In summary, we have disclosed the active intermediates in the carboxylation of α,β-unsaturated carbonyl compounds. Initial electrochemical characterisations were done with CV, to understand the conditions needed for electrogeneration of the two reactive anionic species. Subsequently, CPEs were carried out in the presence of CO_2, and analysis of the products led to the conclusion, suggested also by the CV profiles, that the dianion species is able to attack CO_2 while the radical anion is not. This interpretation was further supported by generation of these species *via* alternative photochemical and chemical systems, as well as by DFT calculations and theoretical models developed by the group.

3.1.5. – Electrochemical carboxylation in flow of α,β-unsaturated carbonyl compounds

Flow chemistry has recently emerged as an enabling technology, in particular for photo- and electrochemical processes. An increasing number of examples of flow electrochemistry are being reported, due to the advantages of this technique, in particular improved mass transfer, that ensure increased productivity, reproducibility and selectivity of the reaction.[52] Recently, this technology has been applied also in the context of electrochemical carboxylation reactions, though only few examples have been reported. In 2015, a seminal work by Abe *et al.* showed the carboxylation of benzyl halides **48** using a glassy carbon (GC) cathode and a Pt anode (Scheme 3.8a).[53] Few years later, the same group employed an analogous setup in the carboxylation of imines **50**, allowing the one-step synthesis of α-aminoacids **51** (Scheme 3.8b).[54]

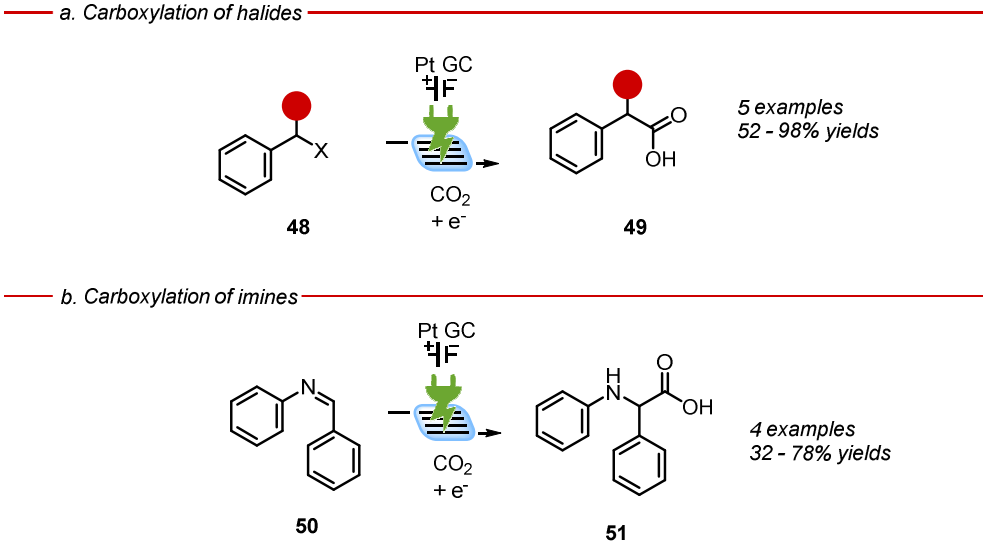

Scheme 3.8. – Flow electrochemical carboxylation of a. benzyl halides and b. aromatic imines reported by Atobe *et al.*

The process was later coupled with synthesis of imines in flow, thus enabling the synthesis of α-aminoacids directly from commercially available aldehydes and amines.[55] Despite these first advancement in the field of flow electrocarboxylation, the range of applicable substrates is narrow, and some limitations are present. For example, in the setup used by Atobe *et al*. the Pt electrode employed is expensive, in particular when working on bigger scales.

3.1.6. – Aim of the project

Having developed a method for carboxylation of α,β-unsaturated carbonyl compounds, we realised that this process is underexplored in terms of generality of the scope, as few substrate are usually tested. Moreover, despite the benefits related to flow electrochemistry, we saw that reports on carboxylation of activated olefins are still missing. In collaboration with Prof. Nöel's research group, experts in the field of flow chemistry, we sought to adapt our procedure to a flow reactor, and perform a first example of flow electrocarboxylation of α,β-unsaturated carbonyl compounds.

3.1.7. – Results and discussions

Initial tests on flavone

Our study started with an optimisation of the conditions with the aim of establishing a reliable undivided-cell galvanostatic process. This in fact is necessary in order to avoid complex flow setups, which would require a more sophisticated engineering, thus making the procedure less appealing. A first CPE was run in an undivided-cell setup, keeping the same conditions used in the mechanistic investigation, upon addition of the amine DCMA as a sacrificial reagent for the anodic reaction (Table 3.1, entry 1).[21b] In this case only 4% formation of carboxylated **47a** was observed, possibly due to coupling of flavone

radical anion **39a** with the amine radical cation. Subsequently, an Al anode was tested, to avoid both the use of the expensive Pt electrode and of the sacrificial amine. A first experiment resulted in Al anode passivation, that was avoided by using NBu_4Cl as supporting electrolyte, enabling the formation of soluble $AlCl_n^{n-3}$ species. However, NBu_4Cl is highly hygroscopic and led to lower yields of **47a** (15% after 80% conversion, see Table 3.1, entry 2) and formation of the hydrogenated product **52**, supposedly generating from protonation of dianion **40a**. After these preliminary experiments, we switched to a two-electrode undivided cell, also employing galvanostatic conditions, where faster reactions allowed a rapid optimisation. However, after screening of different sacrificial reductants, such as amines and alcohols, supporting electrolytes, and electrodes no satisfactory results were obtained (Table 3.1).

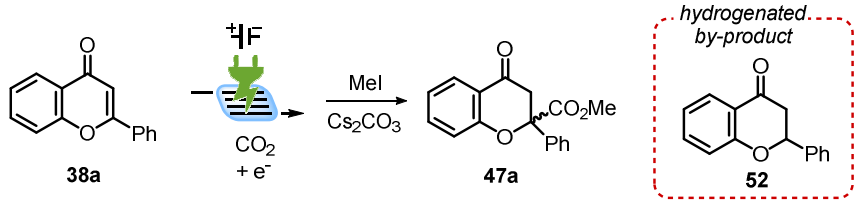

entry	J	Q	supporting electrolyte	additive	solvent	cathode	anode	yield
1[a]	-	2.1	NBu_4PF_6	DCMA	MeCN	GC	Pt	4%
2[a]	-	2.1	NBu_4Cl	-	MeCN	GC	Al	15%
3	5.0	2.1	NBu_4PF_6	NEt_3	DMF	C	Mg	3%
4	15.0	3.0	NBu4Br	TMEDA	THF/MeCN 1/3	C	Mg	n.d.
5	8.0	3.5	NBu_4PF_6	MeOH	MeCN	GC	C	n.d.
6	8.0	3.5	NBu_4PF_6	EtOH	MeCN	GC	C	n.d.
7	20.0	5.0	NEt_4I	TEOA	MeCN	GC	C	n.d.
8	20.0	5.0	NEt_4I	TEOA	MeCN	SS	C	n.d.
9	20.0	5.0	NEt_4I	TEOA	MeCN	Ni	C	n.d.
10[b]	-	10.0	NEt_4I	TEOA	DMF	C	C	n.d.

Table 3.1. – Screening of different conditions for flavone electrochemical carboxylation. a. Three-electrode setup potentiostatic electrolysis run at -2.7 V. b. A constant voltage of 10 V was kept between the two electrodes. TMEDA: *N,N,N',N'*-tetramethylethylenediamine. TEOA: triethanolamine.

In these experiments, complex mixtures were always obtained, where the product of interest could not be identified. Moreover, passivation of the anodes and formation of solids, deleterious in view of an upgrade to flow setup, were also observed. Thus, flavone was discarded, and α,β-unsaturated esters, which had been reported to undergo carboxylation in batch in good yields,[21e] were selected as new model substrates.

Optimisation on methyl crotonate

Starting from the conditions reported by Buckley on methyl crotonate **53a**[21e] (Table 3.2), some initial tests in batch were done, to check if galvanostatic conditions were applicable. 62% yield of **54** was obtained with constant *i* = 100 mA, furthermore the same yield was obtained using a more practical stainless steel (SS) cathode. Hence, we started optimising the parameters of the flow reactor using a SS cathode and a graphite (C) anode under galvanostatic conditions. Screening different flow rates, current intensities and electron equivalents (Table 3.2), a 53-fold increase of the productivity of the process was observed, compared to the reported batch result (from 0.19 mmol/h to 10.1 mmol/h). The selected conditions are shown in entry 7 of Table 3.2.

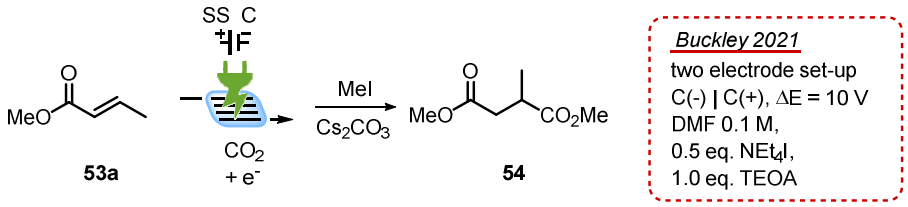

entry	*i*	*E*	*Q*	*tr*	*yield*	*entry*	*i*	*E*	*Q*	*tr*	*yield*
1	60	3.0	3.0	12	55%	**7**	**260**	**3.9**	**5.0**	**4.5**	**84%**
2	60	2.9	4.0	15.5	40%	8	260	4.2	6.0	5.4	71%
3	60	3.0	5.0	20	58%	9	500	4.1	3.0	1.4	71%
4	60	3.1	6.0	23	62%	10	500	4.2	4.0	1.9	73%
5	260	3.5	3.0	2.7	78%	11	500	4.4	5.0	2.3	81%
6	260	3.7	4.0	3.6	80%	12	500	4.5	6.0	2.8	65%

Table 3.2. – Screening of different conditions for methyl crotonate **53a** flow electrochemical carboxylation.

Investigation of the scope

With optimised condition in hand, we started investigating the scope of the reaction. Initial experiments were conducted on different type of α,β-

unsaturated esters already tested in batch, shown in Table 3.3. The yields obtained, although decent, were not satisfactory, since much better yields were reported for the procedure in batch (>75%);[21e] still the productivity is higher, but only three-fold. Also styrene **53d**, which undergoes carboxylation in batch in good yields,[21b] was tested, but similar unsatisfactory results were obtained. To probe if the problem was related to the working-electrode potential being not negative enough for reduction of the substrates, we tested ethyl maleate **54e**, which is easier to be reduced. In this case no product was observed, though this could also be ascribed to reduced nucleophilicity of the reduced species generated from the electron-poor **54e**. Furthermore, we ran electrolysis experiments keeping a constant cell potential using methyl acrylate **53c** as substrate; applying three increasing voltages the yield was improved up to 42%, but still resulted too low.

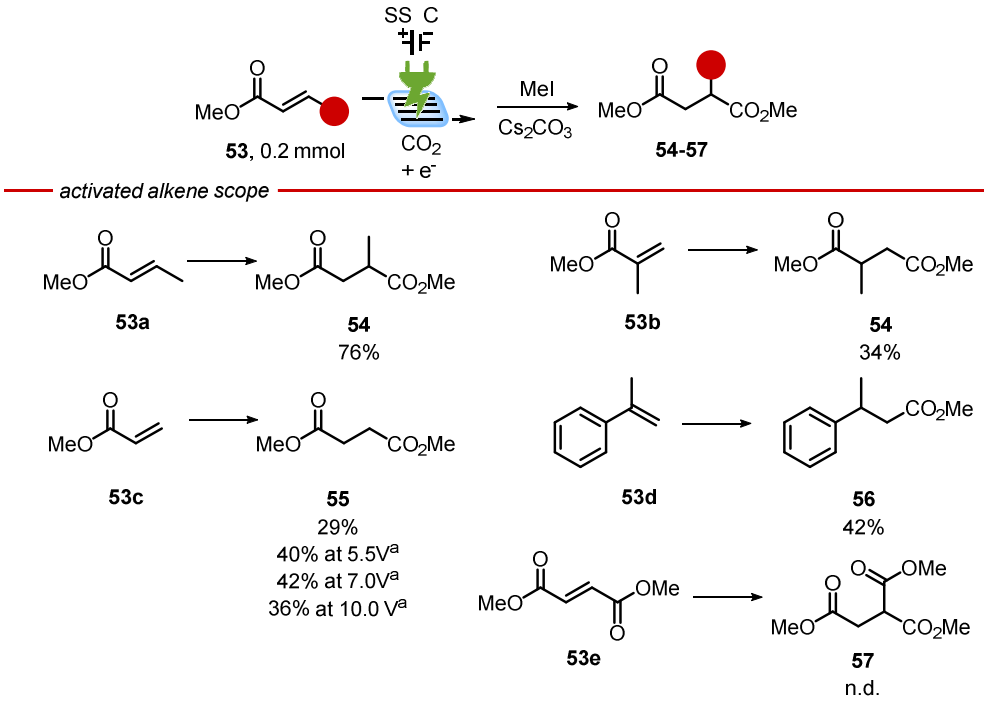

Table 3.3. – Substrate screening of activated alkenes. Yields were calculated using Q-NMR with trichloroethylene as internal standard, average of 2 results. a. Experiments performed at constant cell potential.

In all these experiments, besides poor reactivity we were also facing reproducibility issues. H_2 bubbles production, caused by reduction of protons was identified as causing this variability.[56] Possible proton sources could be TEOA and traces of water in the hygroscopic NEt_4I used as supporting electrolyte. Trying to solve both reactivity and variability issues, we performed a small re-optimisation of the conditions with the microfluidic setup, trying aprotic amines such as NEt_3 and TMEDA. Lower bubble formation and increased reproducibility were observed, but the yields dropped dramatically (Table 3.4, entries 1 and 2). The crucial role both of TEOA and NEt_4I was evident also from tests in batch in which a different supporting electrolyte (NEt_4BF_4) or sacrificial amine (NEt_3) gave deluding results (33% and 11%

carboxylation yield, respectively). Further experiments in flow were conducted using sacrificial anodes such as SS, Zn and Mg. These are disadvantageous in a continuous flow setup as they are consumed during the reaction, but generate cations that can stabilize intermediates and products, favouring the process, and avoiding the use of sacrificial TEOA. Using SS as sacrificial anode only small amounts of product were obtained in both constant current and constant cell potential electrolyses (Table 3.4 entries 3 to 6). With a Zn anode, development of Zn^{2+} gave deposition on the cathode and solid formation, which can cause clogging and so needs to be avoided with flow setups. Use of Mg would avoid deposition problems ($E^0_{Mg2+/Mg}$ = - 2.36 V vs SHE[17]), but unfortunately the Mg plate at our disposition was not fitting the reactor and caused leakage.

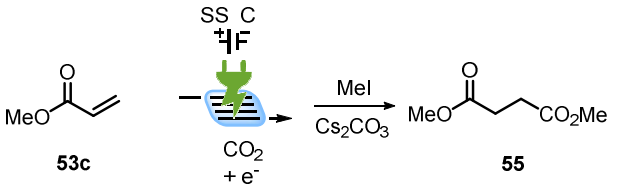

entry	sacrificial amine/ anode	i	E	yield	entry	sacrificial amine/ anode	i	E	yield
1	TMEDA	260	-	28%	5	SS	-	3.5	<5%
2	NEt_3	260	-	19%	6	SS	-	4.0	<5%
3	SS	260	-	n.d.	7	Zn	260	-	-
4	SS	-	3.0	<5%	8	Mg	260	-	-

Table 3.4. – Re-optimisation experiments. Yields were calculated using Q-NMR with trichloroethylene as internal standard, average of 2 results. a. Methyl crotonate used as substrate. b. Experiments performed at constant cell potential.

Investigation of other types of activated alkenes

Final attempts were made using other types of activated alkenes that had not been previously reported. Chalcone **38b** did not yield any carboxylation product resulting in dimerization and saturation. Acetophenone **58** was tested under

both constant current and cell potential conditions, with the expected carboxylation product **59** that could be observed with gas chromatography only in traces, but it could not be isolated, both as acid and as methyl ester. Also vinyl phosphonate **60** and electron poor vinyl enamine **62** were tested under constant current and constant cell potential control, **61** was synthesized but only in poor yields, while **63** could not be obtained (Table 3.5).

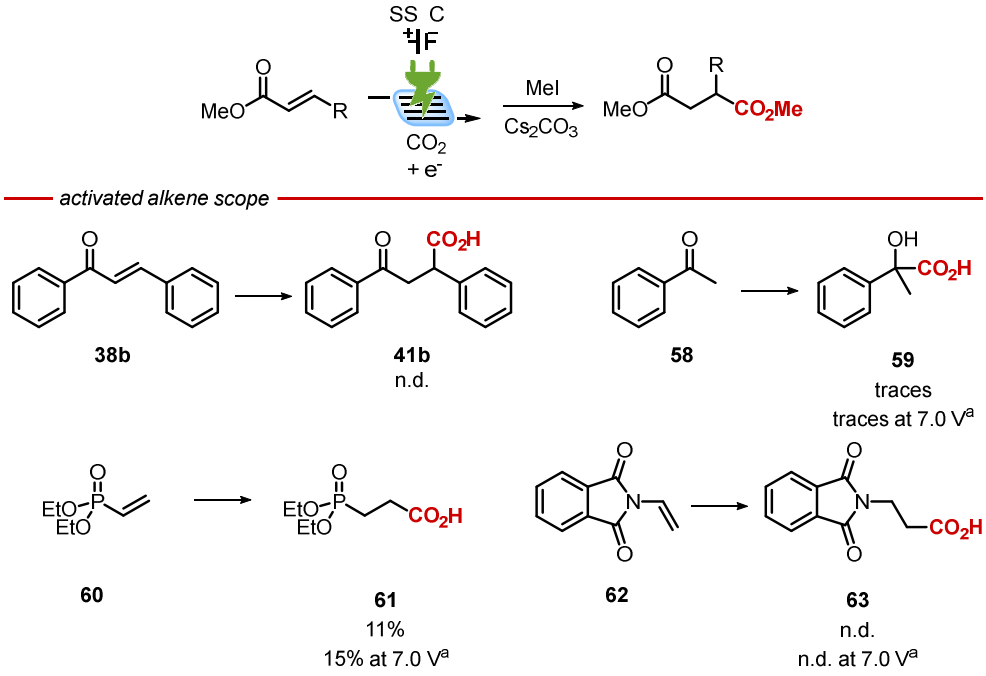

Table 3.5. – Screening of other activated alkenes. Yields were calculated using Q-NMR with trichloroethylene as internal standard, average of 2 results. a. Experiments performed at constant cell potential.

3.1.8. – Concluding remarks

Reproducibility and poor reactivity, as well as poor predictability have been hurdles to the development of the project. The role of the sacrificial amine and

of the supporting electrolyte are still to understand, and no investigation has been carried out in the reports from literature. Nonetheless, their presence is indispensable for a good reactivity, though deleterious in flow, so further studies need to be done to elucidate their role.

3.1.9. – Experimental section

NMR spectra were recorded on Bruker 300 Advance spectrometer equipped with BBO probe head 5 mm. The chemical shifts (δ) for ^{1}H and ^{13}C are given in ppm relative to residual signals of the solvents ($CHCl_3$ @ 7.26 ppm ^{1}H NMR, 77.16 ppm ^{13}C NMR). Coupling constants are given in Hz. The following abbreviations are used to indicate the multiplicity: s, singlet; d, doublet; t, triplet; q, quartet; m, multiplet; bs, broad signal. NMR spectra were processed using MestReNova software.

EI-MS spectra were registered using an Agilent 6850 Network gas chromatography system equipped with a 5975 Series MSD detector. The analyses were performed using an HP-5MS column (30 m length, 0.25 mm, Ø 0.25 mm, 0.25 micron film thickness).

ESI-MS spectra were acquired with an Agilent Technology LC/MSD Trap SL, interfaced to an Agilent 1100 binary pump. All mass spectra were registered upon flow injection of samples diluted in acetonitrile, to reach a concentration of 10^{-5} M. The eluent composition was chosen as pure HPLC-grade acetonitrile with 0.1% formic acid.

The ESI-MS spectra are available free of charge in literature.

Gas chromatographic analyses were performed on a Shimadzu GC-2010 Pro gas chromatograph equipped with a flame ionization detector (FID). The analyses were performed using an equity-5 column (15 m, Ø 0.1mm, 0.1 micron film thickness) and helium as a carrier gas. Every measurement was performed by automatic injection of 1 μL of the sample solution. Column oven temperature program: 70°C (hold for 2 min), then 25°C/s until 270 °C (hold for 9 min), total program time: 19 min.

The electrochemical characterizations were carried out on a BASi EC Epsilon potentiostat-galvanostat in a typical three-electrode cell.

Electrosynthesis experiments were performed with a Metrohm Autolab PGSTAT 2014 potentiostat-galvanostat in combination with the Nova 2.1.4 software (https://www.metrohm-autolab.com/Products/Echem/Software/Nova.html).

The microwave reactor used in esterification procedure was a CEM Discover (300 W maximum power).

Chromatographic purification was accomplished using flash chromatography on silica gel (SiO_2, 0.04-0.063 mm) purchased from Machery-Nagel, with the indicated solvent system according to the standard techniques. Thin-layer chromatography (TLC) analysis was performed on pre-coated Merck TLC plates (silica gel 60 GF254, 0.25 mm). Visualization of the developed chromatography was performed by checking UV absorbance (254 nm and 365 nm) as well as with phosphomolybdic acid and potassium permanganate aqueous solutions. Organic solutions were concentrated under reduced pressure on a Büchi rotary evaporator.

Materials: Commercial grade reagents and solvents were purchased at the highest commercial quality from Sigma Aldrich and used as received, unless otherwise stated.

The diverse reaction set up images, and all the procedures and data for DFT calculations are available free of charge in literature.

Cyclic voltammetry procedures

A typical three-electrode cell was employed, combining a GC working electrode (BioLogic, 3 mm nominal diameter, 7 mm^2 geometric area), a Pt electrode (BASi) as counter electrode and a Ag/AgCl electrode (Ag/AgCl/3M NaCl) as reference electrode. Oxygen was removed by saturating the solution with high-purity N_2 or CO_2. The glass electrochemical cell was kept closed during the measurements, the headspace of the cell being also degassed to prevent dioxygen contamination.

Unless otherwise stated, experiments were conducted in MeCN, with 0.1 M NBu_4PF_6 at room temperature, and with a scan rate of 0.1 $V{\cdot}s^{-1}$. All potentials were then converted to Fc^+/Fc, using an internal reference system, upon addition, at the end of each experiment session, of ferrocene to the analyte solutions, and running a cyclic voltammogram from which the $E_{1/2}$ of the couple was measured.

The glassy carbon WE was polished before any measurement with a 1 μm diamond paste on a microfiber cloth (Struers), carefully rinsed with de-ionized water, then methanol and rinsed by applying ultrasonic for 5 minutes. After each series of CV experiments, the electrochemical cell was carefully rinsed with ethanol, acetone, and de-ionised water; afterwards, the cell and the magnetic stirrer were sonicated for 5 min with acetone.

Gas chromatographic analysis

Quantitative gas chromatography analyses were carried out for evaluation of starting material conversion and ester product yield.

500 μL aliquot of the reaction mixture, was transferred into a 1.5 mL screw thread 1.5 mL vial, containing 500 μL of a mesitylene solution (10 mM in MeCN) as an internal standard.

The response factor of the initial substrate was used also to quantify the ester product, since the presence of one -CO_2CH_3 additional group with respect to the initial substrate is expected to have a minor effect in the FID response.
The quantification was done by evaluating the ratio between the areas of the analyte and that of the standard and using this ratio value in the equation $(S1)$. From the know value of the internal standard (mesitylene), the concentration of the analyte can be derived.

$$\frac{A_{analyte}}{A_{STD}} = f \frac{mol_{analyte}}{mol_{STD}} \qquad (S1)$$

Flavone 38a calibration curve

Calibration curve of **38a** by gas chromatography-FID was obtained analysing three solutions in MeCN with constant concentration of mesitylene (10 mM) and three different concentrations of **38a**, obtained by subsequent dilution of a 20 mM **38a** stock solution; these were prepared by adding in a 1.5 mL vial: 500 μL of mesitylene (5 μmol); 500, 250 or 100 μL of the **38a** stock solution, (corresponding to 10, 5 and 2 μmol of flavone, respectively); the corresponding volume of MeCN (0, 250 and 400 μL, respectively) to reach a 1 mL total volume. The samples were analysed at the gas chromatograph, collecting the area of the peaks of **38a** and of the standard. The resulting calibration curve is depicted below.

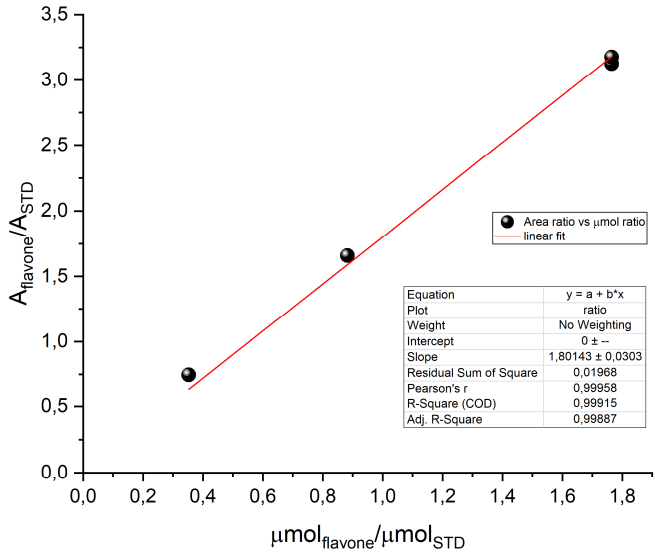

Figure Exp3.1. – Calibration curve used to evaluate the flavone **38a** conversion after the electrosynthesis experiments and to evaluate the methyl ester yield.

Linear fitting of the experimental data provided the following equation $(S2)$:

$$\frac{A_F}{A_{STD}} = 1.80\ \frac{\mu mol_F}{\mu mol_{STD}} \qquad (S2)$$

Which can be converted into equation $(S3)$ used to quantify the analyte:

$$\frac{A_F}{A_{STD}}\ \frac{\mu mol_{STD}}{1.80} = \mu mol_F \qquad (S3)$$

Chalcone 38b calibration curve

Calibration of chalcone was carried out by gas chromatography-FID chromatography, using the same analytical procedure described in the previous section for flavone.

The resulting calibration curve is depicted below.

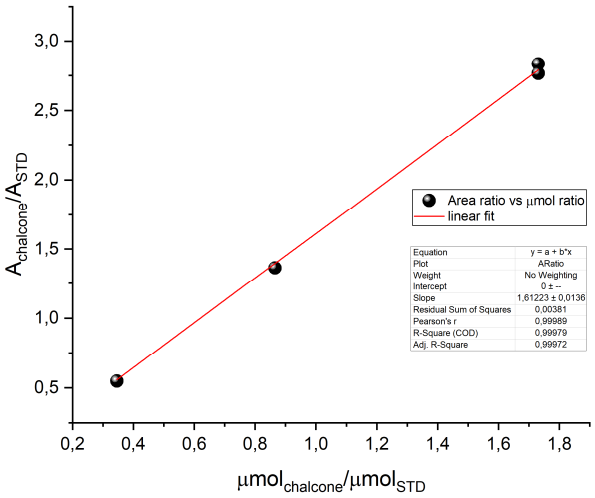

Figure Exp3.2. – Calibration curve used to evaluate the chalcone **38b** conversion after the electrosynthesis experiments and to evaluate the methyl ester yield.

Linear fitting of the experimental data provided the following equation $(S3)$, in which the intercept was fixed at 0 value:

$$\frac{A_C}{A_{STD}} = 1.61 \frac{\mu mol_C}{\mu mol_{STD}} \qquad (S4)$$

Which can be converted into equation $(S5)$ used to quantify the analyte:

$$\frac{A_C}{A_{STD}} \frac{\mu mol_{STD}}{1.61} = \mu mol_C \qquad (S5)$$

Esterification procedure

10 mL of electrolysis solution (initially containing 0.2 mmol of substrate) were evaporated under vacuum and then dissolved in 1.5 mL of anhydrous MeOH. 66 µL of concentrated H_2SO_4 were added and the mixture was placed in a microwave reactor setting the bulk temperature at 80 °C for 1 h, with constant stirring. Reaction progress was controlled by TLC (hexane:EtOAc, 4:6 + 2% acetic acid).

After the MW induced heating, the reaction mixture was treated with 10 mL of water and then extracted adding 3 x 10 mL of EtOAc. The reunited organic

phases were finally washed with water and then dried with anhydrous $MgSO_4$ before evaporating the solvent. For the quantification of the product by gas chromatography analysis, the solid was dissolved in MeCN, using the same amount as the initial volume of electrolysis solution esterified (10 mL or 5 mL), in order to reach the same initial concentration as in the crude electrolysis solution.

General procedures for electrolysis in 2-compartment cell

CPE experiments were performed in a custom-made 6-necked 2-compartment glass cell, the two compartments being separated by a porous glass frit under stirring conditions of the solution with a magnetic stirring bar.

Cathodic compartment: 25 mL of a MeCN solution containing 20 mM of substrate and 0.1 M of NBu_4PF_6 as supporting electrolyte (except otherwise specified); glassy carbon rod working electrode (SIGRADUR, HTW, ca 1.5 cm^2 geometric area); Ag/AgCl (NaCl 3 M) as reference electrode. The reference electrode was separated from the bulk solution by means of a salt bridge (equipped with a Coralpor frit) filled with electrolyte solution. The reference electrode was fit inside the upper part of the bridge. This latter was constituted by a screw joint allowing the content of the bridge to be sealed by means of a PTFE O-ring.

Anodic compartment: 10 mL of MeCN solution containing 0.1 M of NBu_4PF_6 solution and 0.2 M of NEt_3 (10 equiv.) as sacrificial electron donor; Platinum coiled wire as counter electrode.

After saturating the electrolyte solution in both compartments with CO_2 bubbling it for ca. 20 min a CO_2 atmosphere was kept above the solutions during the electrolysis experiments.

WE potential: -2.56 V vs Fc^+/Fc

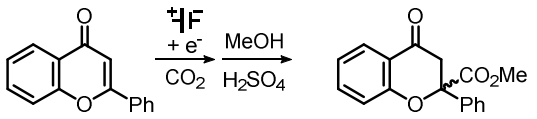

The experiment started with an initial current of – 12 mA. The experiment was stopped at *Q*= −99.5 C with a final current of – 3 mA. Conversion of **38a** was 60%. Ester **47a** was isolated by a flash chromatography on silica gel (hexane:EtOAc, 9:1 → 8:2), yielding pure **47a** (yellow oil) in 55% yield (34.05 mg, 0.120 mmol).

methyl 4-oxo-2-phenylchromane-2-carboxylate (47a)

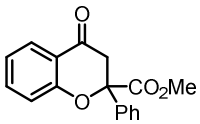

^{1}H NMR (300 MHz, $CDCl_3$): δ 7.83 (ddd, *J* = 7.8, 1.8, 0.5 Hz, 1H), 7.62 – 7.56 (m, 2H), 7.52 (ddd, *J* = 8.4, 7.2, 1.8 Hz, 1H), 7.42 – 7.30 (m, 3H), 7.21 (ddd, *J* = 8.4, 1.1, 0.5 Hz, 1H), 7.03 (ddd, *J* = 7.8, 7.2, 1.1 Hz, 1H), 3.63 (s, 3H), 3.59 (d, *J* = 16.8 Hz, 1H), 3.27 (d, *J* = 16.8 Hz, 1H).

WE potential: -2.21 V vs Fc^+/Fc

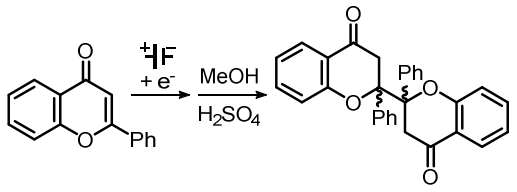

The experiment started with an initial current of – 9.5 mA. The experiment was stopped at *Q*= −71 C with a final current of – 1.7 mA. Conversion of **38a** was 65%. gas chromatographic yield for **47a** 3%. By-product **46a** and **46a'**were obtained.

(2R,2'S)-2,2'-diphenyl-[2,2'-bichromane]-4,4'-dione (46a)

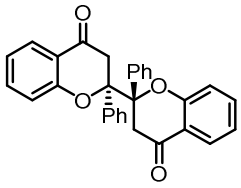

^{1}H NMR (300 MHz, $CDCl_3$): δ 7.72 – 6.76 (m, 18H), 3.62 (d, *J* = 16.1 Hz, 1H), 3.10 (d, *J* = 16.2 Hz, 1H).

2,2'-diphenyl-[2,2'-bichromane]-4,4'-dione (46a')

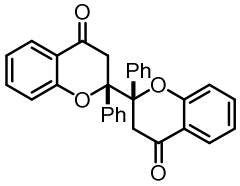

Racemic mixture

^{1}H NMR (300 MHz, $CDCl_3$): δ 7.72 – 6.76 (m, 18H), 3.93 (d, J = 16.3 Hz, 1H), 3.33 (d, J = 16.3 Hz, 1H).

WE potential: -2.7 V vs Fc+/Fc

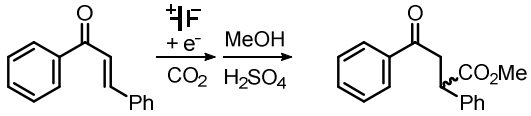

The experiment started with an initial current of – 26 mA. The experiment was stopped at *Q*= –100 C with a final current of – 9 mA. Conversion of **38b** was 79.5%. Ester **47b** was isolated by a flash chromatographic column on silica gel (hexane:EtOAc, 9:1 → 8:2), yielding pure **47b** (yellow oil) in 43% isolated yield (10 mg, 0.037 mmol).

methyl 4-oxo-2,4-diphenylbutanoate (47b)

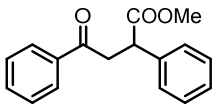

^{1}H NMR (300 MHz, $CDCl_3$): δ 8.09 – 7.81 (m, 2H), 7.64 – 7.17 (m, 8H), 4.29 (dd, J = 10.3, 4.1 Hz, 1H), 3.93 (dd, J = 18.0, 10.3 Hz, 1H), 3.68 (s, 3H), 3.26 (dd, J = 18.0, 4.1 Hz, 1H). **EI-MS:** 51, 77, 105, 130.9, 208, 236, 268 ($M^{\bullet+}$) m/z.

Procedure for photochemical experiment with chalcone 38b

Photochemical experiment

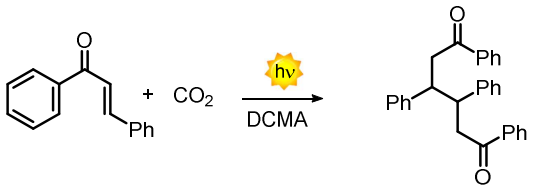

In a 4 mL vial 0.1 mmol of **38b** was dissolved in 1 mL of anhydrous MeCN under CO_2 atmosphere. 2 equiv. of DCMA were added, then the reaction was left stirring under 405nm LED lamp irradiation for 1.5 h. **46b** is obtained as a white solid, isolated by centrifugation. The remaining solution was moved in a separating funnel using 10 mL of hexane and 10 mL of NaOH 1 M were added. The two phases were separated, then the aqueous phase was washed 2 more times with hexane. The reunited aqueous phase was acidified adding HCl 2 M dropwise until pH 2 is reached. The acidified aqueous phase was extracted with EtOAc (5 x 15 mL). After concentration under vacuum the crude was analysed by ^{1}H-NMR but no traces of acid **41b** were detected.

Procedure for reductive carboxylation of chalcone 38b with Mg

Reductive carboxylation with Mg

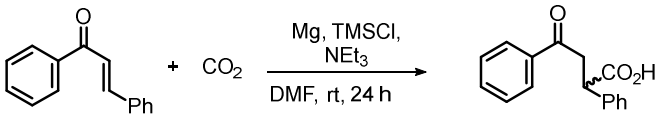

In a 4 mL vial, to 0.1 mmol of **38b** and 5 equiv of Mg turnings 1 mL of DMF was added under CO_2 atmosphere. After adding 3 equiv of TMSCl and 3 equiv. of NEt_3, the mixture was left stirring 24 h at rt. After this, the solution was moved in a separating funnel using 10 mL of hexane and 10 mL of NaOH 1 M were added. The two phases were separated, then the aqueous phase was washed

2 more times with hexane. The reunited aqueous phase was acidified adding HCl 2 M dropwise until pH 2 is reached. The acidified aqueous phase was extracted with EtOAc (5 x 15 mL). After concentration under vacuum the crude was analysed by ^{1}H-NMR showing 56% yield of **41b**.

General procedures for electrolysis in "home-made" single compartment cell

Set-up of the electrolysis in single compartment cell:

- Al counter electrode: 25 mL of a 0.1 M solution in MeCN of NBu_4Cl or NEt_4BF_4 as supporting electrolyte and 20 mM substrate solution in MeCN were placed in the cell with the GC rod as working electrode (ca 1.5 cm^2 geometric area), the Ag/AgCl (3 M NaCl) *via* a salt bridge as reference electrode and aluminium (Al) wire as counter electrode.
- Pt counter electrode + sacrificial donor: 25 mL of a 0.1 M solution in MeCN of NEt_4PF_6 as supporting electrolyte, 20mM substrate solution in MeCN and 2 equivalents (40 mM) of DCMA were placed in the cell with the GC rod as working electrode (ca 1.5 cm^2 geometric area), the Ag/AgCl (3 M NaCl) *via* salt bridge as reference electrode and Pt wire as counter electrode.

The cell has a Schlenk-type side arm fitted with a ground glass stopcock, which allows the vessel to be filled with CO_2. The saturation was done by the insertion in the side arm of a Teflon tube connected by a line to a tailed flask full of dry ice. After saturating the electrolyte solution by with CO_2 for ca 20 min, the Teflon tube was removed from the solution and the stopcock closed.

All working electrode potentials of experiments were then reported vs Fc^+/Fc in order to be consistent with CV traces.

WE potential: -2.6 V vs Fc^+/Fc, single compartment cell (Al, NBu_4Cl)

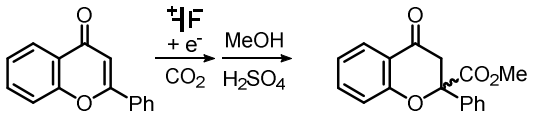

The experiment started with an initial current of – 18 mA. The experiment was stopped at *Q*= –101 C with a final current of – 4 mA. Conversion of **38a** (by gas chromatography): 80.2%. A solid was produced on the solution and deposited on the CE Al wire electrode, during the electrosynthesis. The solid was acidified with HCl 2 M and the aqueous part was extracted with EtOAc, washed and anhydrified, and the solvent removed at the rotavapor. The characterization of the solid was not effective. The crude electrolysis solution (10 mL) was subject to esterification. The gas chromatography yield of the esterification sample give a 14.7% yield of **47a**.

WE potential: -2.6 V vs Fc^+/Fc, single compartment cell (Al, NEt_4BF_4)

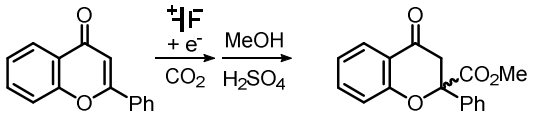

The experiment was stopped after few minutes as the potential was not stable with this setup.

WE potential: -2.6 V vs Fc^+/Fc, single compartment cell (Pt, NBu_4PF_6)

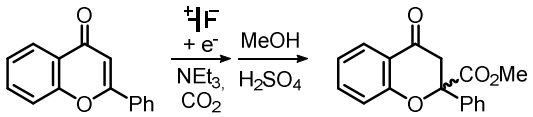

The experiment started with an initial current of – 14 mA. The experiment was stopped at *Q*= –64 C with a final current of – 0.2 mA. Conversion of **38a** (by

gas chromatography): 83%. The crude electrolysis solution (5 mL) was esterified. gas chromatography yield for **47a**: 4.2%.

General procedure for flow electrochemical cell setup

For all electrochemical continuous-flow reactions, a homemade flow cell was used, together with a Rhode-Schwarz R&S®HMP4040 power supply. The cell consists of a working electrode and a counter electrode, with a PTFE (Polytetrafluoroethylene) gasket containing micro-channels in between. The active reactor volume is 700µL. This results in an undivided electrochemical cell. In the cell, direct contact between the electrode surface and the reaction mixture is established. The reaction mixture is pumped through the system via syringe pump, and is collected in a glass vial. All the technical data of the electrochemical microreactor are reported elsewhere.[57]

In a 50 mL volumetric flask the selected substrate, supporting electrolyte and sacrificial reductant were dissolved in the selected solvent until 50 mL volume is reached. The solution was bubbled for 30 min with CO_2, then it was transferred in a syringe and pumped through the microreactor. The collected solution (usually 2 mL) was then acidified with HCl 1 M and extracted with Et_2O (3 x 5 mL). The collected organic phases were washed with brine, anhydrified using $MgSO_4$, filtered and concentrated under vacuum. The resulting crude was dissolved in $CDCl_3$ and analysed using ^{1}H-NMR. CH_2Br_2 was used as internal standard to infer the yield.

Chapter III – Section 2

A Proton-Coupled-Electron-Transfer-Based Strategy to the Light-Driven Fixation of CO_2

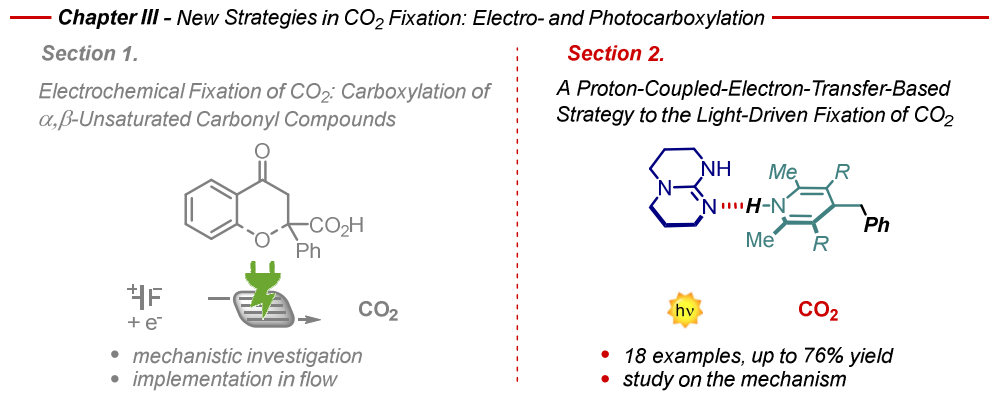

In this Section a redox-neutral photocatalytic carboxylation strategy is described. The process has been designed such as no sacrificial redox agents are required, moreover, room temperature and pressure can be employed. The method was tested on 18 different substrates, giving the carboxylic acid product in good yield. The mechanism was studied in deep, showing an unprecedented example of proton-coupled electron transfer based carbon dioxide fixation.

A Manuscript on this work is under preparation and will be soon submitted to peer-review: Franceschi, P.; Rossin, E.; Scopano, A.; Vega-Peñaloza, A.; Goti, G.; Singh, D.; Sartorel, A.; Dell'Amico, L. *A Proton-Coupled-Electron-Transfer-Based Strategy to the Light-Driven Fixation of CO_2.*

3.2.1. - Introduction

With the renaissance of synthetic photochemistry in the first years of 2000,[58] new methods have been disclosed, and many applications in CO_2 fixation have been reported.[21d, 59] Pioneering reports by Tazuke *et al.*[60] in 1975 were based on photo-induced electron transfer for generation of the reactive radical anion of anthracene. With the advent of photocatalysis, new and more efficient strategies were conceived.[59c] The approaches used are: *i*) reduction of CO_2 to its radical anion; *ii*) combination of transition-metal (TM) catalysis and photocatalysis; *iii*) activation of the organic substrate by its transformation into nucleophilic anionic species.

The first approach usually requires the use of UV light and has been scarcely applied, but interesting transformation with unusual selectivity can be obtained.[61] Using a highly reducing photocatalyst (PC), CO_2 can be reduced to its radical anion, that can attack olefins **64** forming radical anion **65**. After protonation and photocatalytic reduction, **65** can yield product **67** (Scheme 3.9a).[62] $CO_2^{\bullet-}$ can also intercept other radical species and react through radical recombination.[63] When photocatalysis is supported by a transition-metal catalyst ML_n, the special features of the latter, like the ability to give oxidative addition of halides and pseudo-halides **24** to give the organometallic species **36**, that can be further reduced to by the photocatalyst to **37**, and the ability of **37** to undergo M-C bond insertion of CO_2 are central to the mechanism. (Scheme 3.9b).[64]

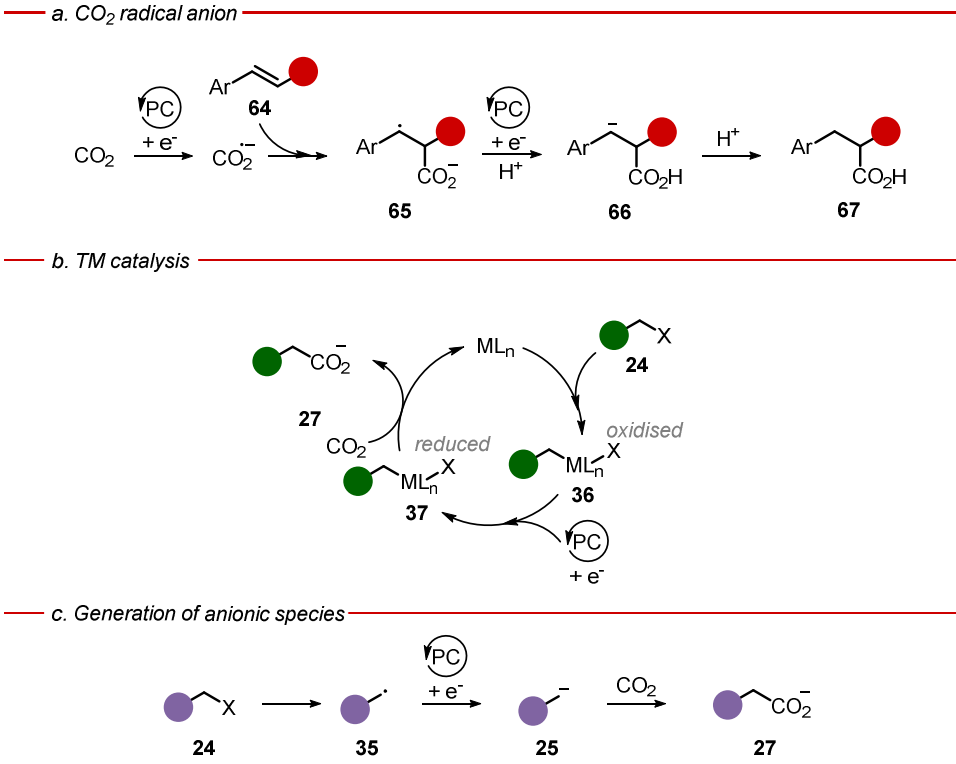

Scheme 3.9. –General approaches to photocatalytic carboxylation using CO_2: a. Direct CO_2 reduction. b. Combination of TM- and photoredox catalysis. c. Photocatalytic generation of anionic species.

Nonetheless, use of transition-metals, which can be rare, costly or toxic, can be avoided with strategy *iii*), which is also the most employed approach.[59b] This strategy envisages the generation of a radical **35** from a suitable precursor **24**, followed by reduction of radical **35** to the corresponding anion **25** through a single electron transfer (SET) from the photocatalyst. This step is followed by nucleophilic attack of **25** to CO_2 to generate the carboxylate product **27** (Scheme 3.9c). Possibilities of generation of radical species follow two main strategies: SET and hydrogen atom transfer (HAT).[65] With SET, substrate **68** is oxidised or reduced to its radical ion **69**, which, if properly designed, can lose a charged leaving group to generate the reactive radical species **70** (Scheme

3.10a). In HAT, a catalytic or stoichiometric hydrogen atom abstractor **72**, usually activated by light-irradiation or by photocatalysis, cleaves a C-H bond of the substrate to generate a C-centred radical **70** (Scheme 3.10b). More recently, multi-site proton-coupled electron transfer (MS-PCET) has been explored as a new photochemical strategy for the generation of radicals.[66] As in all PCET processes, a proton and an electron are taken (or given) together, but in this case the proton and the electron are transferred to (or from) two different reagents: a Bronsted base (or acid) and a photoredox catalyst (Scheme 3.10c).

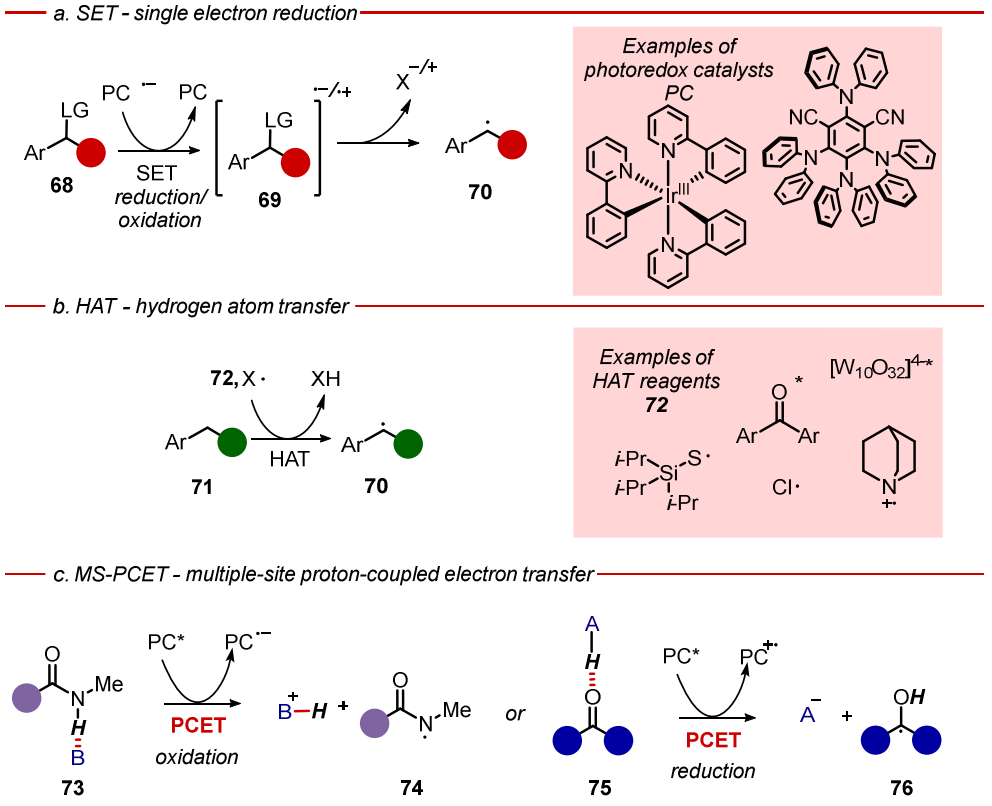

Scheme 3.10. – General scheme of radical generation in photocatalysis using a. HAT, b. SET and c. MS-PCET strategies.

From a synthetic point of view, a MS-PCET is equivalent to a HAT, as it concerns the formal transfer of a hydrogen radical (a proton and an electron) from the substrate, although it has a different selectivity and a wider thermodynamic range of action. Furthermore, a proton transfer can increase the driving force of a subsequent SET: adding a proton to the substrate gives an easier-to-reduce cation, or vice versa the deprotonation of a species makes it easier to be oxidized. Besides, in MS-PCET processes the transfer of the proton and of the electron can be simultaneous (concerted proton electron transfer, CPET), thus avoiding the formation of high-energy charged intermediates, while lowering the activation barrier of the reaction. A requirement for a CPET to occur is the preassociation of the substrate with the proton acceptor (base) or donor (acid) in a hydrogen-bonding network.

Application of the radical generation strategies in carboxylation reactions has proven successfully with both HAT and SET approaches. Key recent examples in this area are shown in Scheme 3.11. Konig *et al.* reported the generation of benzylic radicals **70** using an organo-silanethiol HAT reagent **79**. Subsequent reductive SET, using 4CzIPN as photoredox catalyst, afforded anion 77^- which, by nucleophilic attack on CO_2 yields carboxylated product **78** (Scheme 3.11a).[67] More recently, Yu *et al.* achieved the carboxylation of in-situ-generated benzyl acetates **68a** via two consecutive reductive SET steps, which required an excess of *N,N*-diisopropylethylamine (DIPEA) as a sacrificial reductant (Scheme 3.11b).[68]

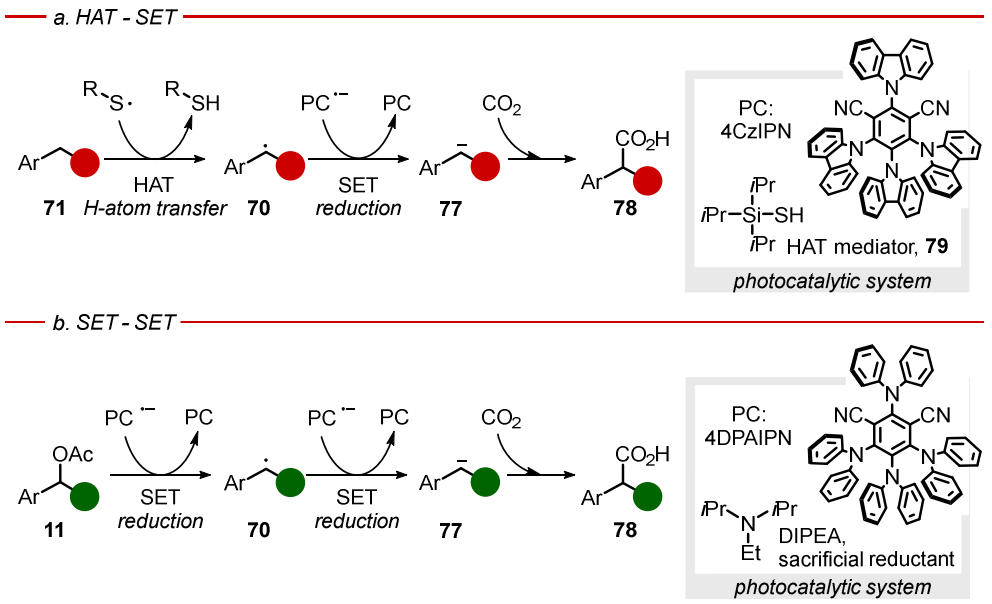

Scheme 3.11. – Examples of photocatalytic CO_2 fixation using anionic species generated through an a. HAT-SET or b. SET-SET approach.

3.2.2. – Aim of the project

Despite the novel possibility of exploiting a PCET to generate a radical species, and the high generality that a PCET manifold can offer, to the best of our knowledge, a PCET-SET strategy has never been applied to carboxylation processes. Prompted by this gap, and by the attractiveness of carbon dioxide as a resource, we devised a photocatalytic strategy for CO_2 fixation started by a MS-PCET process. In particular, we aimed at establishing a redox-neutral transformation, where the absence of external oxidant or reductant helps improving the sustainability of the process. We envisioned that, using suitable precursors, we could generate a radical through an oxidation step, then, in a following reduction step, we could transform the radical into a carbanion able to attack CO_2. Hence, the photocatalytic cycle is closed only by productive steps, and additional waste is avoided.

3.2.3. – Results and discussion

Substrate selection

Using a rational approach, we selected as substrate a suitable radical precursor based on its molecular structure and redox properties. With the idea of a redox-neutral process in mind (Figure 3.7), the radical must be produced through an oxidation step. The potential for the oxidation of the radical precursor should also be as low as possible, to enlarge the choice of adequate photocatalysts. Moreover, aiming at a PCET process, an acidic proton is needed. Therefore, diethyl 4-benzyl-2,6-dimethyl-1,4-dihydropyridine-3,5-dicarboxylate (4-BnDHP) **80a** was chosen as substrate (Figure 3.7). 4-substituted DHPs are easy to synthesize and require common reagents; they are known as radical precursor, and the potential for their oxidation is in the range of typically employed photocatalysts (E ~ 0.6 V).[69] Benzyl substituent was selected due to the relatively long lifetime of benzyl radicals, as well as less negative reduction potential respect to the corresponding alkyl radicals.[70]

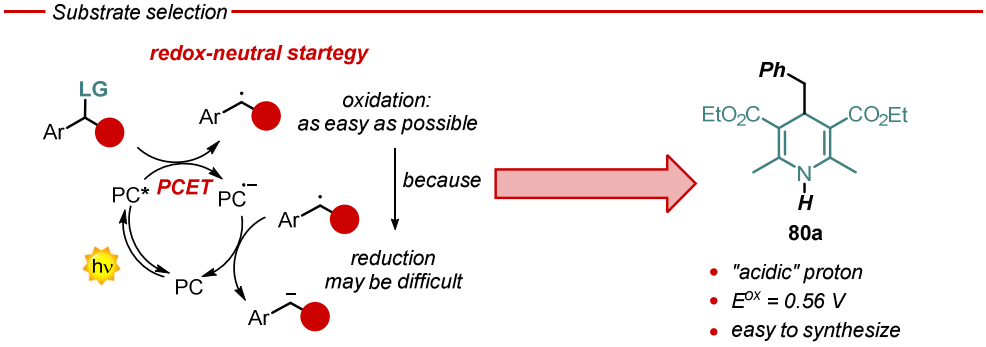

Figure 3.7. – Features of the optimal substrate **80a**.

Reaction optimisation

Our investigation started using 4-BnDHP **80a** as the substrate, Cs_2CO_3 as the base and 4CzIPN as the photocatalyst. After 6 h of irradiation with simple blue

LEDs (λ_{max} = 435 nm) product **81** was obtained in 54% yield. We tested different photocatalysts and bases and a combination of 4CzIPN and 1,5,7-Triazabicyclo[4.4.0]dec-5-ene (TBD) revealed to be the best, leading to the formation of **81** in 71% yield. In particular, besides the reaction yield, TBD provided a 3-fold higher reaction rate with respect to other bases tested (see experimental section in Paragraph 3.3.5).[71] After testing also different PC loadings, solvents, concentrations, light sources and reaction times (Table 3.6, see also experimental section in Paragraph 3.3.5), product **81** could be obtained in 76% yield (63% isolated yield) with the conditions showed in entry 10. Control experiments were conducted in absence of PC, base, CO_2 or light and gave negligible yields or no product at all, thus confirming the key role of all the components for the success of the reaction (Table 3.6 entries 11-14).

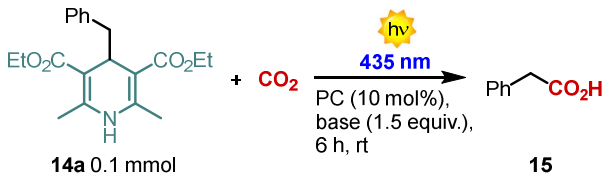

entry	*PC*	*base*	*solvent*	*yield*[a]
1	4CzIPN	Cs_2CO_3	DMF 0.1M	54%
2[b]	phenoxazine	Cs_2CO_3	DMF 0.1M	16%
3[b]	3-hydroxynaphthochromenone	Cs_2CO_3	DMF 0.1M	2%
4	4CzIPN	TBD	DMF 0.1M	71%
5	4CzIPN	NEt_3	DMF 0.1M	49%
6	4CzIPN	Me-TBD	DMF 0.1M	58%
7	4CzIPN	TMG	DMF 0.1M	51%
8	4CzIPN	TBD	MeCN 0.1M	68%
9	4CzIPN	TBD	MeCN 0.05M	73%
10	4CzIPN 2 mol%	TBD	MeCN 0.05M	76%
11[c]	-	TBD	MeCN 0.05M	1%
12[c]	4CzIPN 2 mol%	-	MeCN 0.05M	traces
13[c,d]	4CzIPN 2 mol%	TBD	MeCN 0.05M	0%
14[c,e]	4CzIPN 2 mol%	TBD	MeCN 0.05M	0%

Table 3.6. – Optimization of reaction parameters on **80a**. TMG: 1,1,3,3-tetramethylguanidine. a. Yields inferred by ^{1}H-NMR analysis using CH_2Br_2 as internal standard. b. 405 nm LED lamp was used. c. 16 h reaction time. d. No CO_2, Ar atmosphere. e. No light irradiation.

Generality of the reaction

With optimised conditions in hand, we explored the scope of the process by testing different DHPs **80** (Table). Substitution on the aryl ring with both EWGs and EDGs was well tolerated, as products **82-85** were obtained in 40-65% yield. Secondary benzylic substrates were also reactive and produced the related products **86-88** in 35-58% yield. Different naphthyl derivatives could also be employed, as products **89-91** were obtained in 48-60% yield.

Interestingly, using DHP **80b**, product **92**, derived from opening of the propyl ring, was isolated in 37% yield.

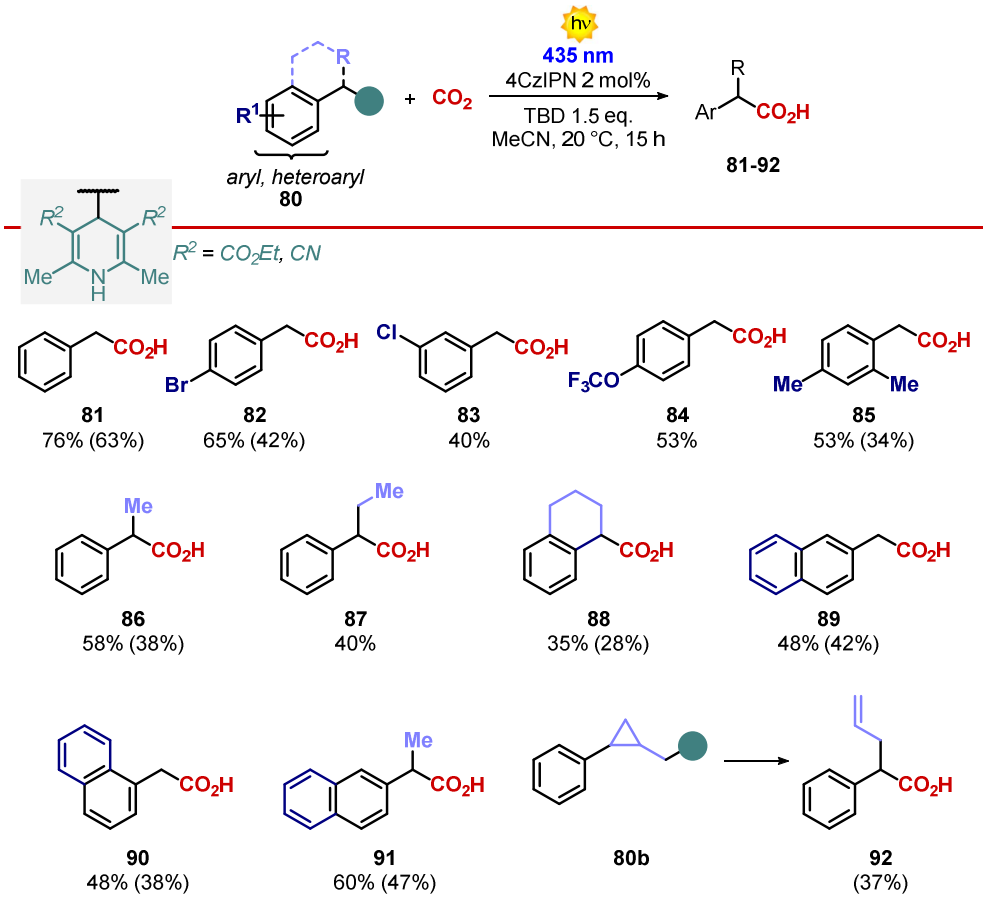

Table 3.7. – Scope of the reaction with DHPs **80**. The indicated yields were inferred by ^{1}H-NMR analysis in the presence of CH_2Br_2 as internal standard. Yields in parenthesis refer to isolated yields.

For particularly electron-rich substrates the transformation was not efficient. However, when 2,4,6-Tris(diphenylamino)-3,5-difluorobenzonitrile (3DPA2FBN) was used as photocatalyst, the products **93-95** were isolated in 37-43% yield.

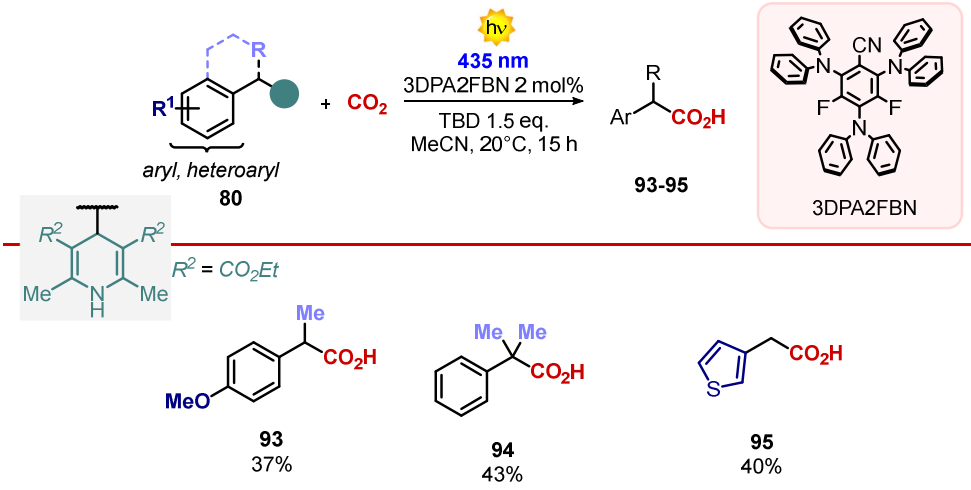

Table 3.8. – Scope of the reaction with DHPs **80** using 3DPA2FBN as PC. The indicated yields refer to isolated yields.

Beside DHPs, other radical sources were also tested. Benzylic BF_3K and BF_3NBu_4 salts **96** afforded the respective products **81**, **97** and **98** in 23-71% yields.

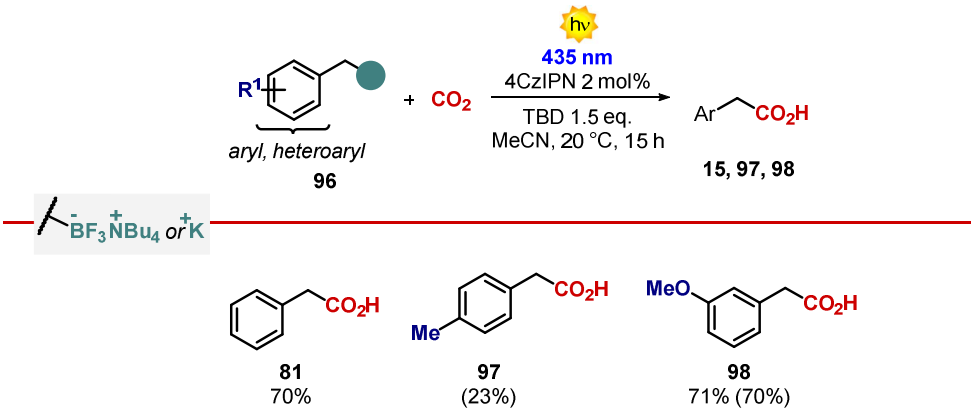

Table 3.9. – Scope of the reaction with BF_3K and BF_3NBu_4 salts **96**. The indicated yields were inferred by ^{1}H-NMR analysis in presence of CH_2Br_2 as internal standard. Yields in parenthesis refer to isolated yields.

Products manipulation

Carboxylic acids can be useful synthetic intermediates. As a demonstration we tested some of the products obtained in the carboxylation process in different transformations, as shown in Scheme 3.12. Starting from **80**, carbamate **99** was obtained in 78% yield by in-situ azide formation followed by Curtius rearrangement. Alternatively, simple esterification with L-menthol gave product **100** in 79% yield. Furthermore, acid **86** was converted into the corresponding Weinreb amide **101**, and subsequently combined with phenyl magnesium bromide to yield 66% of ketone **102** over two steps.

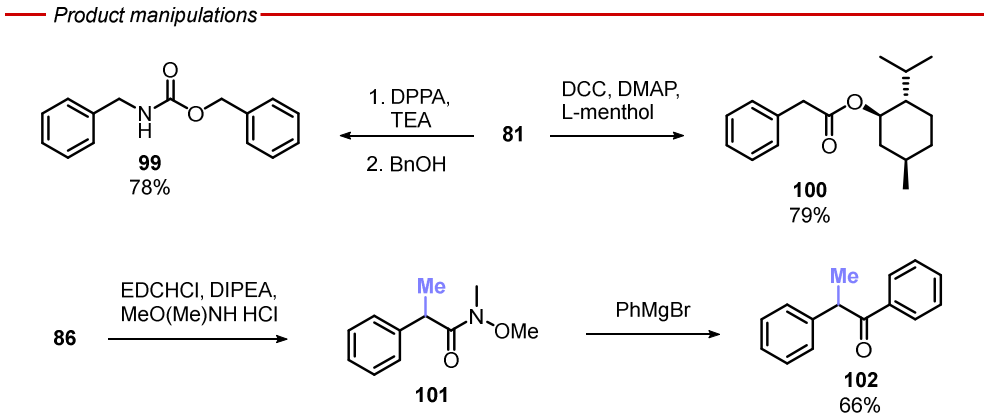

Scheme 3.12. – Product manipulations.

Mechanistic considerations

After having demonstrated the synthetic applicability and utility of the process, we investigated the mechanism of the reaction. In particular, prompted by the great enhancement in reactivity observed with TBD, its role was investigated. First, UV-Vis analysis were carried out, in order to verify a possible interaction of TBD with the reactant (Figure 3.8). Indeed, the absorption spectra of **80a** in the presence of TBD shows a ca 10 nm red-shift with respect to the parent spectrum and a tail of absorption extending up to 480 nm, thus suggesting a

chemical interaction between the two reagents. This shift was not observed in presence of Cs_2CO_3 or NEt_3, which also gave lower carboxylation yields when investigated in the optimisation step.

UV-Vis analysis

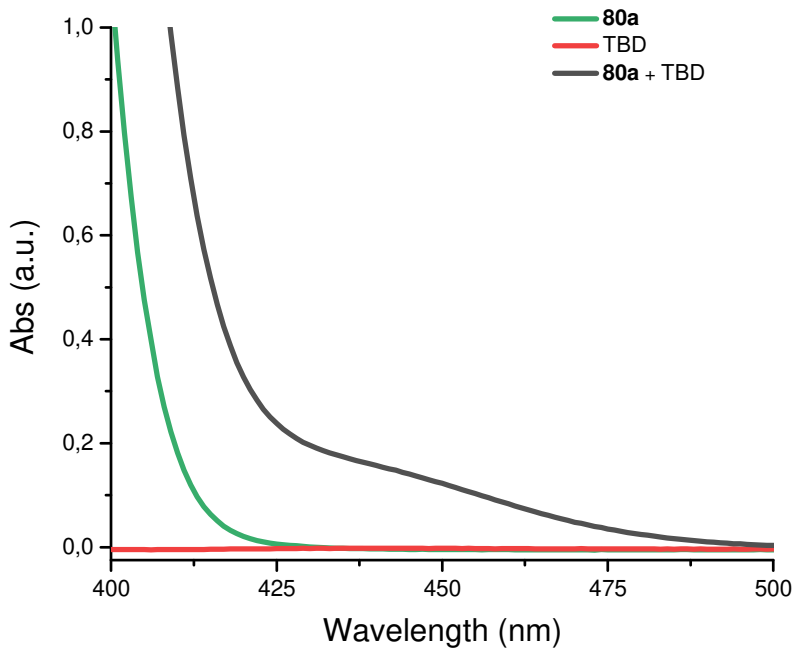

Figure 3.8. – UV-Vis Absorption profiles in MeCN of **80a** (0.05 M, green line), TBD (0.075 M, red line) and a mixture of **80a** and TBD (0.05 M and 0.075 M, respectively, black line).

Furthermore, the ^{1}H-NMR spectrum of 4-BnDHP **80a** shows an upfield shift of the N-H signal after addition of TBD (from 6.68 to 5.01 ppm), accompanied by a broadening of the signal (Figure 3.9, red and green lines). Conversely, the other signals of **80a** undergo minor chemical shift changes, in the order of 0.01 ppm. When adding Schreiner's thiourea **103**, which is a competitive H-bond

donor, the pristine N-H signal of **80a** is restored (Figure 3.9, blue line). These changes suggest the formation of a hydrogen bond between the N-H hydrogen of **80a** and the sp^2 lone pair of the N in TBD, with this bond being then disrupted in the presence of **103**. Deprotonation of **80a** by TBD within an acid base reactivity can be ruled out on the basis of the low acidity of the N-H group of **80a** ($pKa_{\mathbf{80a/80a^-}}$ ~ 31 in MeCN),[72] with respect to the one of the TBDH+/TBD couple ($pKa_{TBDH+/TBD}$ = 26 in MeCN).[73]

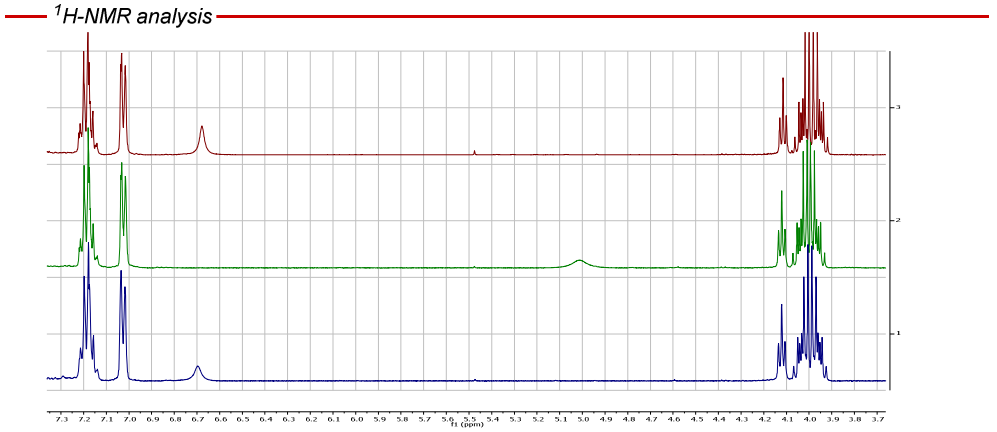

Figure 3.9. – ^{1}H-NMR spectra of **80a** (red), equimolar amounts of **80a** and TBD (green) and equimolar amounts of **80a**, TBD and **103** (blue) in MeCN-d_3.

The formation of a **80a**-TBD hydrogen bond would impact the redox properties of **80a**, thus we used cyclic voltammetry (CV) as a tool for observing these changes. Under anodic scan in CO_2 atmosphere, **80a** (Figure 3.10, green trace) shows an irreversible wave with an anodic peak potential E_{pa} = +0.56 V, ascribable to a one electron oxidation of **80a** and subsequent homolytic C-C bond cleavage.[69, 74] In the presence of TBD (Figure 3.10, black trace), the wave is decreased in intensity, while a new process appears at less positive potentials and peaking at E_{pa} = + 0.31 V, ascribable to a more favourable one electron

oxidation of **80a** in the H-bonded adduct. In the same potential range, the TBD alone gives an anodic process peaking at E_{pa}=+0.85 V (Figure 3.10, red trace).

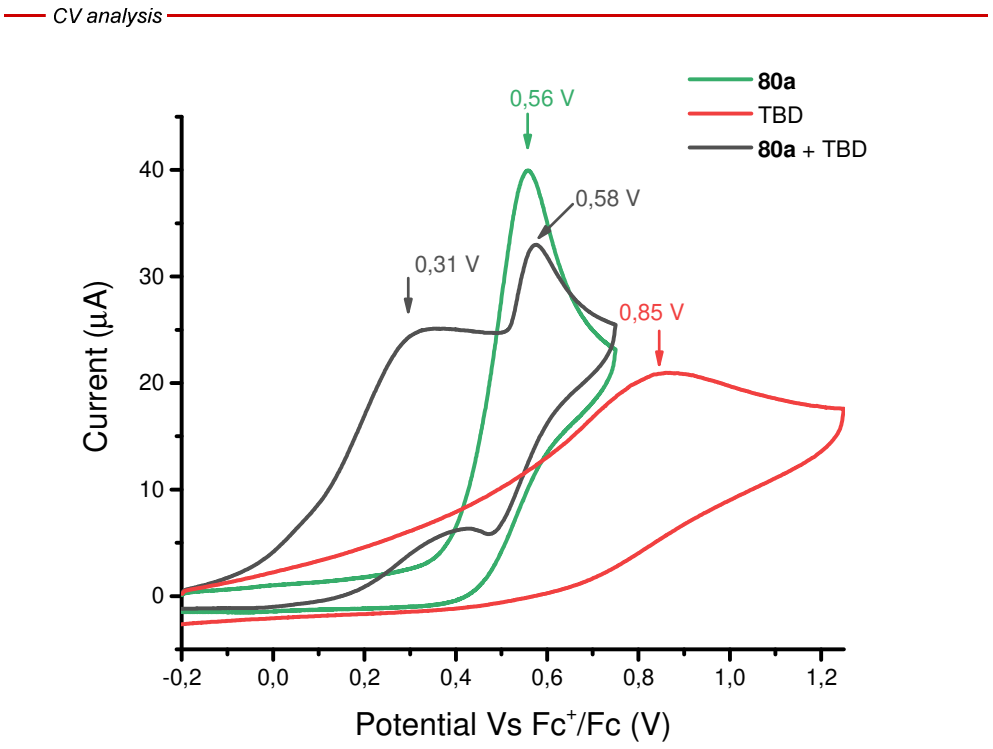

Figure 3.10. – CV analysis of **80a** (green), TBD (red) and a 1:1.5 molar ratio mixture of **80a** and TBD (black) in MeCN.

The presence of a hydrogen bond between **80a** and TBD was further supported by computational studies, carried out by colleagues of the group. The optimised geometry of the **80a**-TBD adduct (optimised as a neutral, singlet species), revealed a N-H···N hydrogen bond with N-H and H···N distances of 1.04 and 1.87 Å, respectively, and a NĤN angle of 178.8° (Figure 3.11a).[75,76] Interestingly, when optimizing the oxidized **80a**-TBD adduct (cationic species with doublet multiplicity), the proton from the N-H group of **80a** moves to the

nitrogen of TBD, while the spin density is entirely localized on the DHP scaffold of the resulting **104** (Figure Xb).

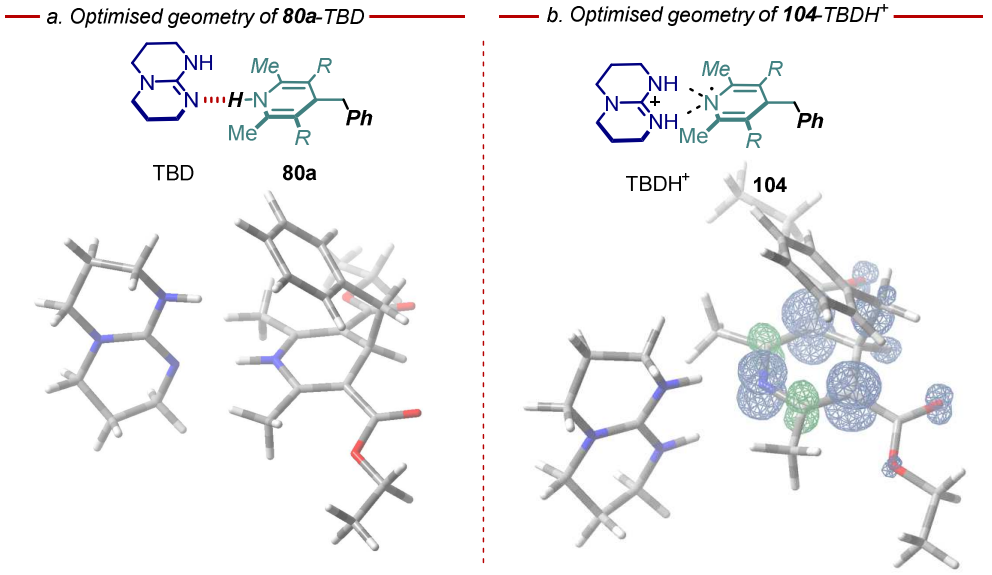

Figure 3.11. – Optimized geometries of a. **80a**-TBD complex and b. oxidized **104**-TBDH$^+$ complex with representation of spin density. Geometries optimized at the B3LYP/6–311+g(d,p) level of theory, including a polarizable continuum model of acetonitrile solvent.

Within the photocatalytic system, the one electron oxidation of adduct **80a**-TBD to **104**-TBDH$^+$ is accomplished by the excited state of the active photocatalyst, 4CzBnBN*, which is obtained in situ in oxidative quenching cycles of 4CzIPN, as reported by König (light red box in Scheme 3.12).[77] Involvement of 4CzBnBN* was proven by a >75% abatement of emission of 4CzBnBN* in the presence of an equimolar mixture of **80a** and TBD.

Overall, the reaction mechanism can be represented as in Scheme 3.12. Formation of a H-bonded complex between **80a** and TBD (step I) leads to an

easier oxidation process by the excited photocatalyst (PC*), with formation of radical **105** and as by-products **106** and $TBDH^+$ (step II). This oxidation process is feasible, as the redox potential of PC* ($E_{PC^*/PC^{\bullet-}}$ = 0.81 V)[77] is higher than the one of the **80a**-TBD adduct $Ep_{\mathbf{104}\text{-}TBDH^+/\mathbf{80a}\text{-}TBD}$ = 0.36 V). Radical **105** is then reduced by $PC^{\bullet-}$, yielding anion **107** (step III), as suggested by the more negative reduction potential of $PC^{\bullet-}$ ($E_{PC/PC^{\bullet-}}$ = -2.12 V)[77] respect to that of **105** ($E_{\mathbf{105}/\mathbf{107}^{\bullet-}}$ = -1.86 V).[70b, 78] Finally, anion **107** attacks CO_2 (step IV) to generate, after acidification, product **81**.

Proposed mechanism

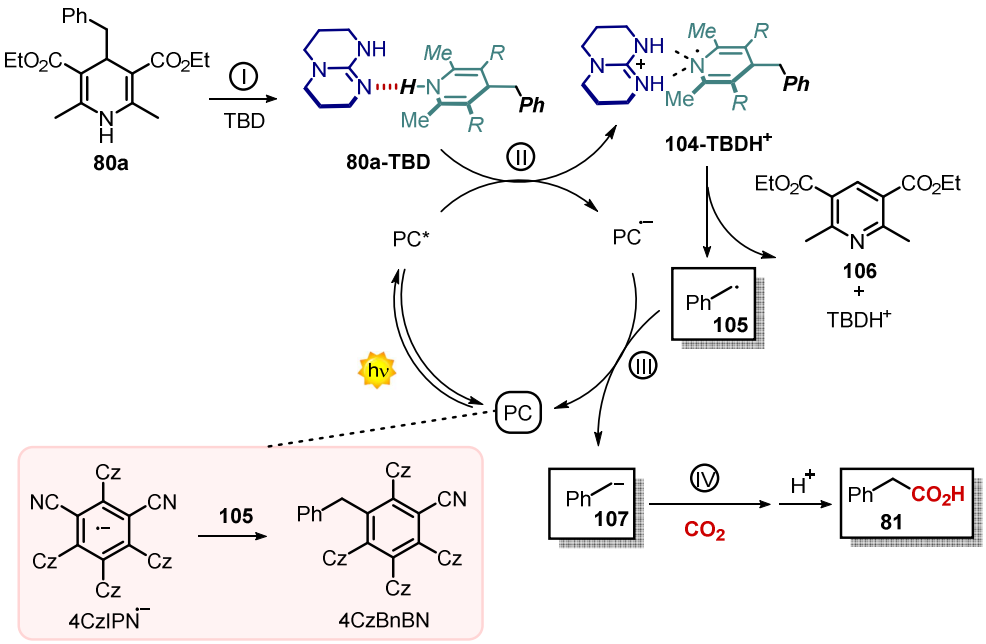

Scheme 3.12. – Proposed reaction mechanism. Formation of the active photocatalyst is showed in the light red box.

3.2.4. – Concluding Remarks

In conclusion, photocarboxylation using CO_2 was accomplished through a redox-neutral PCET-SET strategy. Additionally, nor high pressure of CO_2, nor lower temperatures (usually employed to help solubilisation of CO_2) are required, diminishing further the requirements of the method. Different substrates were tested, and some of the carboxylic acid obtained were employed as intermediates in other transformations, demonstrating their synthetic utility. Mechanistic analyses showed the crucial role of TBD in allowing the formation of a hydrogen-bonded complex necessary for the PCET oxidation, and let us depict a possible mechanism of the reaction.

Nonetheless, the process showed some limitations. Though ambient pressure and temperature can be used, the yields obtained are not excellent, as often less than 50% of product formation was observed. Moreover, the presence of an aryl ring is always needed in order to stabilise the radical intermediate **105**. Indeed, when attempting the reaction with non-benzylic substrates no product was observed.

3.2.5. – Experimental section

435 nm LEDs were purchased on Amazon (https://www.amazon.it/Striscia-Tesfish-Larghezza-Strisce-Decorazione/dp/B09439PFYH/ref=sr_1_3?__mk_it_IT=%C3%85M%C3%85%C5%BD%C3%95%C3%91&crid=1FX05NAFDZC41&keywords=blue%2Bled%2B12%2BV&qid=1667899334&sprefix=blue%2Bled%2B12%2Caps%2C478&sr=8-3&th=1), as well as the waterproof silicone tubing used for submerging the LEDs under water (https://www.amazon.it/Silicone-Guaine-Flessibile-BobinaStriscia/dp/B00TOM6NWO/ref=sr_1_4?__mk_it_IT=%C3%85M%C3%85%C5%BD%C3%95%C3%91&dchild=1&keywords=tubo+silicone+led&qid=1622812658&s=lighting&sr=1-4).

Chromatographic purification of products was accomplished using flash chromatography on silica gel (SiO_2, 0.04-0.063 mm) purchased from Machery-Nagel, with the indicated solvent system according to the standard techniques. Thin-layer chromatography (TLC) analysis was performed on pre-coated Merck TLC plates (silica gel 60 GF254, 0.25 mm). Visualization of the developed chromatography was performed by checking UV absorbance (254 nm and 365 nm) as well as with phosphomolybdic acid and potassium permanganate solutions. Organic solutions were concentrated under reduced pressure on a Büchi rotary evaporator.

NMR spectra were recorded on Bruker 400 Avance III HD equipped with a BBI-z grad probehead 5mm, Bruker 500 Avance III equipped with a BBI-ATM-z grad probehead 5mm, and Bruker Neo 600 equipped with a Prodigy probehead. The chemical shifts (δ) for ^{1}H and ^{13}C are given in ppm relative to residual signals of the solvents ($CHCl_3$ @ 7.26 ppm ^{1}H NMR, 77.2 ppm ^{13}C NMR). Coupling constants are given in Hz. The following abbreviations are used to indicate the multiplicity: s, singlet; d, doublet; t, triplet; q, quartet; m,

multiplet; bs, broad signal. NMR yields were calculated by using dibromomethane (4.85 ppm, s, 2H) as internal standard.

High-Resolution Mass Spectra (HRMS) were obtained using Waters GCT gas chromatograph coupled with a time-of-flight mass spectrometer with electron ionization (EI).

Steady-state absorption spectroscopy studies have been performed at room temperature on a Varian Cary 50 UV-Vis double beam spectrophotometer; 10 mm path length Hellma Analytics 100 QS quartz cuvettes have been used.

Nanosecond transient absorption measurements were performed with an Applied Photophysics laser flash photolysis apparatus, using a frequency-doubled (532 nm, 330 mJ) or tripled (355 nm, 160 mJ) Surelite Continuum II Nd/YAG laser (half-width 6-8 ns) as excitation source. Transient detection was obtained using a photomultiplier-oscilloscope combination (Hamamatsu R928, LeCroy 9360).

The electrochemical characterizations were carried out in acetonitrile (acetonitrile)/0.1 M tetrabutylammonium hexafluorophosphate (NEt_4PF_6) at room temperature, on a BASi EC Epsilon potentiostat-galvanostat. A typical three-electrode cell was employed, which was composed of glassy carbon (GC) working electrode (3 mm diameter), a platinum wire as counter electrode and a silver/silver chloride electrode (Ag/AgCl (NaCl 3 M)) as reference electrode. The reference electrode is a silver wire that is coated with a thin layer of silver chloride; the electrode body contains sodium chloride (NaCl 3 M). Oxygen was removed by purging the acetonitrile solution with high-purity N_2. The potential of ferrocenium/ferrocene (Fc/Fc^+) couple was measured and found to be 0.45 V vs SCE, in agreement with the value reported in literature (in acetonitrile).[1] The GC electrode was polished before any measurement with diamond paste and ultrasonically rinsed with deionized water for 15 minutes. The electrode was

electrochemically activated in the background solution by means of several voltammetric cycles at 100 mV/s between the anodic and cathodic solvent/electrolyte discharges.

Materials: Commercial grade reagents and solvents were purchased at the highest commercial quality from Sigma Aldrich or FluoroChem and used as received, unless otherwise stated. Carbon dioxide 99.5% cylinder was purchased from ForHome (https://www.forhome.it/Bombola-Co2-da-4Kg-Acciaio-Ricarcabile-Nuova-Con-Valvola-Residuale-Certificata-per-sistemi-di-gasatura-acqua) and 99.99% cylinder from SAPIO (https://www.sapio.it/).

Light Sources Emission Spectra

The following spectra were recorded by an AvaSpec ULS3648 high-resolution fiber-optic spectrometer which was placed at a fixed distance of 0.5 cm from the light source. (more info at: https://www.avantes.com/products/spectrometers/starline/item/209-avaspec-uls3648-high-resolution-spectrometer).

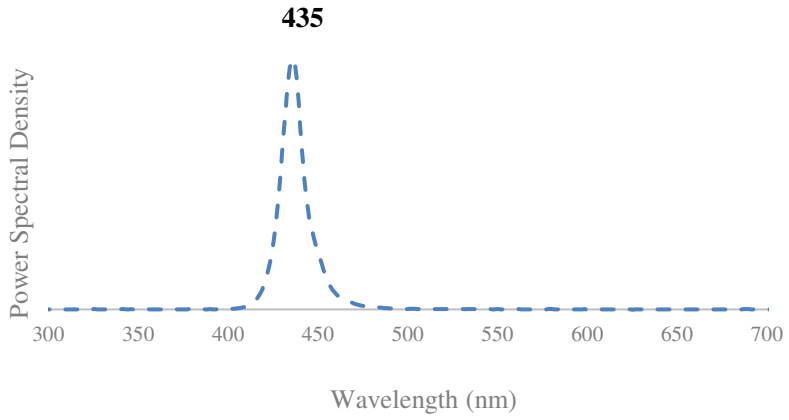

Figure Exp3.3. – Emission spectra of the 435nm LED strip used in this work.

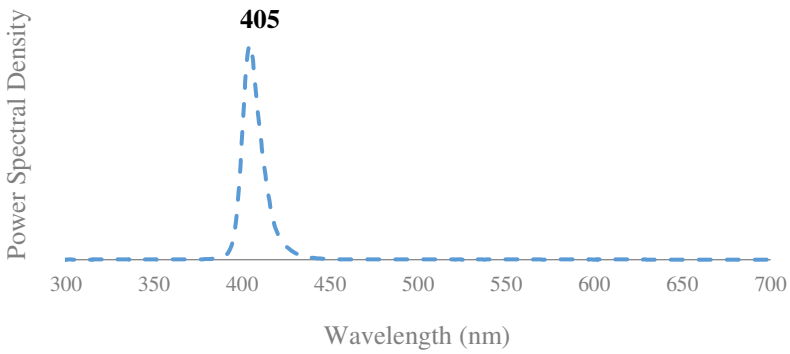

Figure Exp3.4. – Emission spectra of the 20 W 405 nm LED lamp used in this work.

The following spectrum is reported in the Kessil website (http://www.kessil.com/science/PR160L.php).

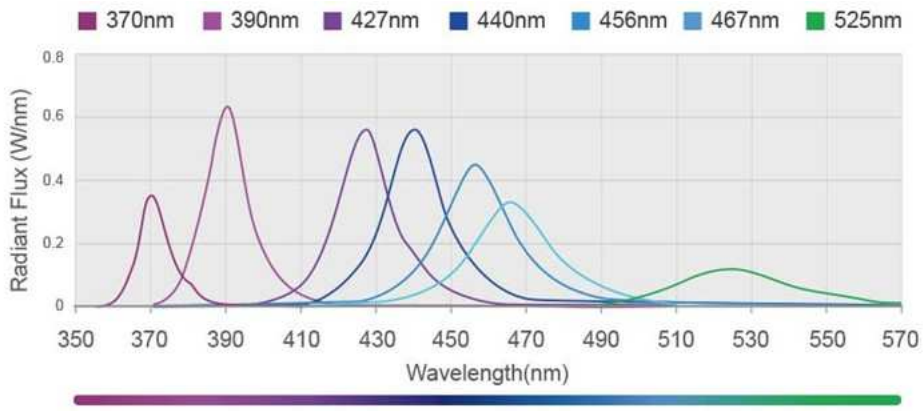

Figure Exp3.5. – Emission spectra of the 427nm, and other, Kessil lamp used in this work.

Reaction Optimisation

Table Exp3.1. – PC optimisation. General reaction conditions: 0.1 mmol of substrate, DMF 1 mL, Cs_2CO_3 1.1 equiv., PC 10 mol%, CO_2 1 atm, irradiation with 435nm LEDs at 20 °C for 6 h. Yields were calculated by NMR analysis using dibromomethane as internal standard. a. 405 nm LED lamp was used.

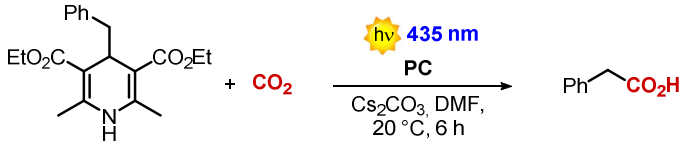

entry	*PC*	*yield*
1	4CzIPN	50%
2	4CzBnBN	52%
3[a]	3-hydroxynaphthochromenone	2% (20% conv.)
4[a]	phenoxazine	16%
5	3DPAFIPN	49%
6[b]	3DPA2FBN	46%

Table Exp3.2. – Base optimisation. General reaction conditions: 0.1 mmol of substrate, DMF 1 mL, base 1.5 equiv., 4CzIPN 10 mol%, CO_2 1 atm, irradiation with 435nm LEDs at 20 °C for 6 h. Yields were calculated by NMR analysis using dibromomethane as internal standard. a. 1.1 equiv. of base was used. b. 73% conversion. c. PC 2 mol%, MeCN 0.05 M.

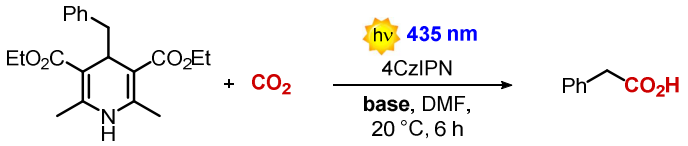

entry	*base*	*yield*
1[a]	Cs_2CO_3	50%
2	Cs_2CO_3	54%
3	K_2CO_3	50%
4[b]	NEt_3	49%
5	DBU	68%
6	TMG	51%
7	TBD	71%
8	Me-TBD	58%
9	DBN	54%
10[c]	DMAP	33%

Table Exp3.3. – Solvent optimisation. General reaction conditions: 0.1 mmol of substrate, TBD 1.5 equiv., 4CzIPN 10 mol%, CO_2 1 atm, irradiation with 435nm LEDs at 20 °C for 6 h. Yields were calculated by NMR analysis using dibromomethane as internal standard.

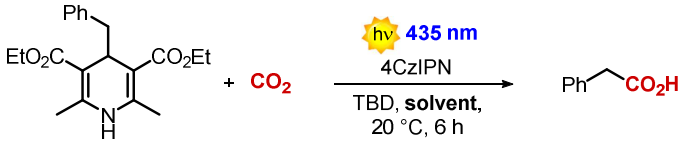

entry	*solvent*	*concentration (80a)*	*yield*
1	DMF	0.1 M	71%
2	MeCN	0.1 M	68%
3	DMSO	0.1 M	54%
4	DMAc	0.1 M	72%
5	DMAc	0.05 M	76%
6	MeCN	0.05 M	73%

MeCN was selected over DMAc because it was easier to evaporate and remove.

Table Exp3.4. – PC loading optimisation. General reaction conditions: 0.1 mmol of substrate, MeCN 2 mL, TBD 1.5 equiv., 4CzIPN, CO_2 1 atm, irradiation with 435nm LEDs at 20 °C for 6 h. Yields were calculated by NMR analysis using dibromomethane as internal standard. a. 76% conversion.

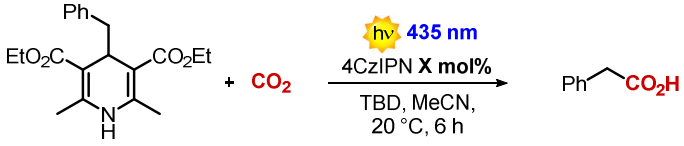

entry	*PC loading*	*yield*
1	10 mol%	73%
2	5 mol%	76%
3	2 mol%	76%
4[a]	1 mol%	48%

Table Exp3.5. – Light source optimisation. General reaction conditions: 0.1 mmol of substrate, MeCN 2 mL, TBD 1.5 equiv., 4CzIPN 2 mol%, CO_2 1 atm, irradiation with 435nm LEDs or Kessil lamps at 25% power at 20 °C for 3 h. Yields were calculated by NMR analysis using dibromomethane as internal standard. a. 49% conversion.

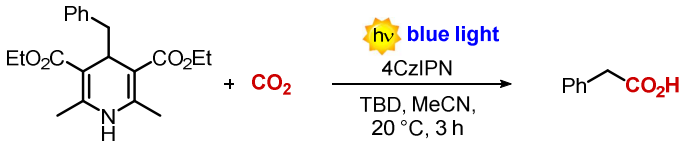

entry	*light source*	*yield*
1[a]	Kessil 456 nm	33%
2	Kessil 427 nm	76%
3	LED 435 nm	76%

LED strips were selected as cheap and available light source.

Table Exp3.6. – Reaction time optimisation. General reaction conditions: 0.1 mmol of substrate, MeCN 2 mL, TBD 1.5 equiv., 4CzIPN 2 mol%, CO_2 1 atm, irradiation with 435nm LEDs at 20 °C. Yields were calculated by NMR analysis using dibromomethane as internal standard. a. 60% conversion.

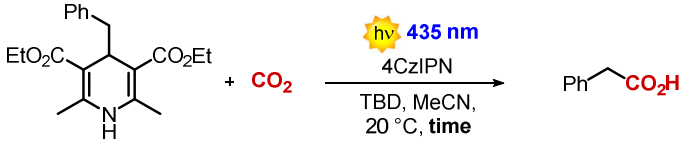

entry	*reaction time*	*yield*
1[a]	30 min	43%
2	1 h	73%
3	3 h	76%
4	6 h	76%
5	15 h	76%

Longer reaction time of 15 h was selected in order to observe full conversion of the starting material with all the other substrates, as no photodegradation of the product is observed (the yield remains the same).

Table Exp3.7. – Temperature optimisation. General reaction conditions: 0.1 mmol of substrate, MeCN 2 mL, TBD 1.5 equiv., 4CzIPN 2 mol%, CO_2 1 atm, irradiation with 435nm LEDs for 3 h. Yields were calculated by NMR analysis using dibromomethane as internal standard.

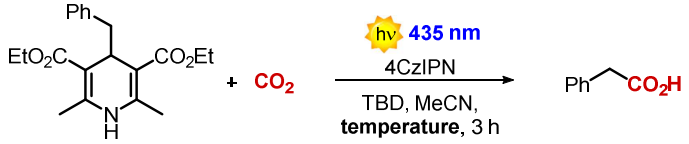

entry	*temperature*	*yield*
1	20 °C	76%
2	50 °C	55%

Table Exp3.8. – Blank experiments. General reaction conditions: 0.1 mmol of substrate, MeCN 2 mL, TBD 1.5 equiv., 4CzIPN 2 mol%, CO_2 1 atm, irradiation with 435nm LEDs at 20 °C for 24 h. Yields were calculated by NMR analysis using dibromomethane as internal standard. a. Reaction time was 6 h.

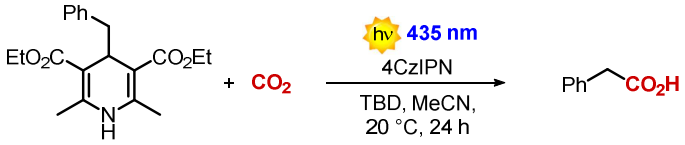

entry	*change*	*yield*	*conversion*
1	no CO_2	0%	100%
2	no light	0%	6%
3	no PC	1%	51%
4	no TBD	traces	100%
5[a]	0.3 equiv. TBD	43%	100%
6[a]	1 equiv. TBD	70%	100%

Synthesis and characterisation of DHPs and BF_3 salts

*Synthesis oh DHPs **80***

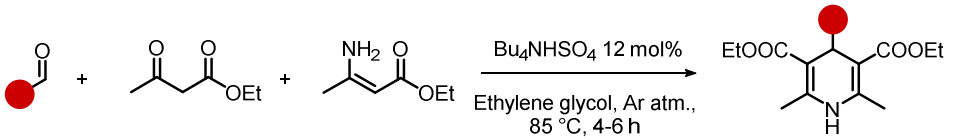

80

4-substituted-2,6-dimethyl-1,4-dihydropyridine-3,5-dicarboxylates **48a-g, 48l-o, 48r** were prepared according to literature.[79] Ethylene glycol (2.5 M in aldehyde) was added under Argon atmosphere in a 100 mL flame-dried round-bottom flask. To this it was added, in order, the corresponding aldehyde (1 equiv.), ethyl 3-oxobutanoate (1 equiv.) and ethyl 3-aminobut-2-enoate (1 equiv.) under Argon atmosphere. Finally, Bu_4NHSO_4 (12 mol%) was added and the mixture was stirred and heated at 85 °C. Consumption of starting materials, monitored by TLC, took 4-6 h. After that, the reaction mixture was allowed to reach room temperature and was quenched adding 5 mL of water. EtOAc and water were added to the reaction mixture, the aqueous phase was extracted with EtOAc (3 x 50 mL). The combined organic phases were washed with water (2 x 30 mL) and once with brine, dried over $MgSO_4$, filtered, and concentrated under reduced pressure. Finally, the products were purified by column chromatography on silica gel using hexane: EtOAc as eluent mixture.

Diethyl 4-benzyl-2,6-dimethyl-1,4-dihydropyridine-3,5-dicarboxylate (80a)

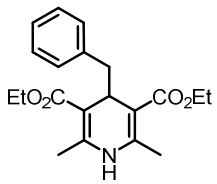

^{1}H-NMR (400 MHz, $CDCl_3$): δ 7.21 – 7.09 (m, 3H), 7.07 – 6.96 (m, 2H), 5.36 (s, 1H), 4.19 (t, *J* = 5.5 Hz, 1H), 4.12 – 3.97 (m, 4H), 2.58 (d, *J* = 5.5 Hz, 2H), 2.17 (s, 6H), 1.23 (t, *J* = 7.1 Hz, 6H) ppm. **^{13}C NMR (101 MHz,**

$CDCl_3$): δ 167.9, 145.4, 139.4, 130.2, 127.4, 125.7, 102.0, 59.7, 42.4, 35.6, 19.3, 14.5 ppm.

Diethyl 4-(4-bromobenzyl)-2,6-dimethyl-1,4-dihydropyridine-3,5-dicarboxylate (80c)

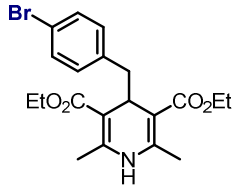

^{1}H-NMR (400 MHz, $CDCl_3$): δ 7.29 (d, *J* = 8.1 Hz, 2H), 6.89 (d, *J* = 8.1 Hz, 2H), 5.59 (s, 1H), 4.17 (t, *J* = 5.2 Hz, 1H), 4.15 – 4.00 (m, 4H), 2.53 (d, *J* = 5.2 Hz, 2H), 2.17 (s, 6H), 1.25 (t, *J* = 7.1 Hz, 6H) ppm. **^{13}C NMR (101 MHz, $CDCl_3$):** δ 167.8, 145.8, 138.4, 131.9, 130.3, 119.7, 101.5, 59.8, 41.7, 35.4, 19.3, 14.5 ppm.

Diethyl 4-(3-chlorobenzyl)-2,6-dimethyl-1,4-dihydropyridine-3,5-dicarboxylate (80d)

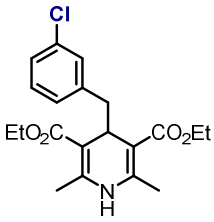

^{1}H NMR (400 MHz, $CDCl_3$): δ 7.15 – 7.01 (m, 3H), 6.87 (dt, *J* = 7.0, 1.6 Hz, 1H), 5.41 (s, 1H), 4.19 (t, *J* = 5.4 Hz, 1H), 4.15 – 4.00 (m, 4H), 2.55 (d, *J* = 5.4 Hz, 2H), 2.18 (s, 6H), 1.25 (t, *J* = 7.1 Hz, 6H) ppm. **^{13}C NMR (101 MHz, $CDCl_3$):** δ 167.8, 145.8, 141.6, 133.2, 130.3, 128.6, 128.5, 125.9, 101.7, 59.9, 42.1, 35.6, 19.4, 14.5 ppm. **HRMS (ESI-MS)** calculated for $C_{20}H_{23}ClNO_4^-$ $[M-H]^-$ 376,1321, found 372.1322.

Diethyl 2,6 – dimethyl – 4 - (4 -(trifluoromethoxy)benzyl)- 1,4 – dihydropyridine - 3,5 - dicarboxylate (80e)

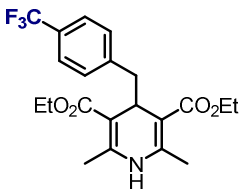

^{1}H-NMR (600 MHz, $CDCl_3$): δ 7.03 (s, 4H), 5.29 (s, 1H), 4.18 (t, *J* = 5.6 Hz, 1H), 4.14 – 3.95 (m, 4H), 2.58 (d, *J* = 5.6 Hz, 2H), 2.18 (s, 5H), 1.23 (t, *J* = 7.1 Hz, 6H) ppm. **^{13}C NMR (151 MHz, $CDCl_3$):** δ 167.6, 147.6 (q, *J* = 1.6 Hz), 145.4, 138.3, 131.2, 120.5 (q, *J* = 254.9 Hz), 119.9, 101.8, 59.7, 41.6, 35.5, 19.3, 14.3 ppm. **^{19}F NMR (188 MHz, $CDCl_3$):** δ -58.38 (s, 3F) ppm. **HRMS (ESI-MS)** calculated for $C_{21}H_{23}F_3NO_5^-$ $[M-H]^-$ 426.1534, found 426.1563.

Diethyl 4-(2,4-dimethylbenzyl) - 2,6- dimethyl- 1,4- dihydropyridine-3,5- dicarboxylate (80f)

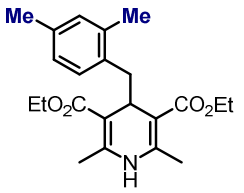

^{1}H NMR (400 MHz, $CDCl_3$): δ 6.89 (s, 1H), 6.84 – 6.74 (m, 3H), 5.80 (s, 1H), 4.20 (t, *J* = 7.0 Hz, 1H), 4.03 – 3.79 (m, 4H), 2.54 (d, *J* = 7.0 Hz, 2H), 2.34 (s, 3H), 2.29 (s, 6H), 2.24 (s, 3H), 1.17 (t, *J* = 7.1 Hz, 3H) ppm. **^{13}C NMR (101 MHz, $CDCl_3$):** δ 168.0, 145.2, 137.1, 135.3, 134.1, 131.2, 130.6, 125.8, 103.0, 59.7, 39.3, 33.7, 21.0, 19.5, 19.4, 14.3 ppm. **HRMS (ESI-MS)** calculated for $C_{22}H_{28}NO_4^-$ $[M-H]^-$ 370.2024, found 370.2011.

Diethyl 2,6-dimethyl-4-(1-phenylethyl)-1,4-dihydropyridine-3,5-dicarboxylate (80g)

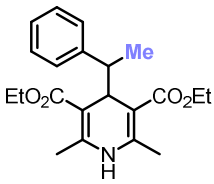

^{1}H-NMR (400 MHz, $CDCl_3$): δ δ 7.19 – 6.95 (m, 5H), 5.28 (s, 1H), 4.18 (d, *J* = 5.1 Hz, 1H), 4.03 – 3.88 (m, 3H), 3.79 (m, 1H), 2.66 (qd, *J* = 7.2, 4.9 Hz, 1H), 2.10 (s, 6H), 1.18 (t, *J* = 7.1 Hz, 4H), 1.13 – 1.02 (m, 6H) ppm. **^{13}C NMR (101 MHz, $CDCl_3$):** δ 168.7, 168.7, 145.5, 145.2, 144.5, 128.8, 127.5, 126.1, 101.4, 101.3, 59.9, 59.9, 46.3, 19.6, 19.5, 15.8, 14.7, 14.6 ppm.

Diethyl 4-(1-(4-methoxyphenyl)ethyl)-2,6-dimethyl-1,4-dihydropyridine-3,5-dicarboxylate (80h)

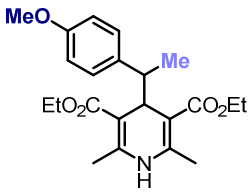

^{1}H-NMR (400 MHz, $CDCl_3$): δ 6.99 (d, *J* = 8.6 Hz, 4H), 6.73 (d, *J* = 8.6 Hz, 2H), 5.48 (s, 1H), 4.22 (d, *J* = 5.0 Hz, 1H), 4.11 – 3.88 (m, 4H), 3.75 (s, 3H), 2.69 (qd, *J* = 7.2, 4.8 Hz, 1H), 2.19 – 2.16 (m, 6H), 1.27 (t, *J* = 7.1 Hz, 3H), 1.20 (t, J = 7.1 Hz, 3H), 1.13 (d, *J* = 7.3 Hz, 3H) ppm. **^{13}C NMR (101 MHz, $CDCl_3$):** δ 168.6, 168.5, 158.0, 145.3, 145.0, 136.4, 129.5, 112.7, 101.2, 101.0, 59.7, 59.7, 55.4, 45.3, 40.3, 19.4, 19.2, 15.9, 14.5, 14.4 ppm. **HRMS (ESI-MS)** calculated for $C_{22}H_{28}NO_5^-$ $[M-H]^-$ 386.1973, found 386.2026.

Diethyl 2,6-dimethyl-4-(1-phenylpropyl)-1,4-dihydropyridine-3,5-dicarboxylate (80i)

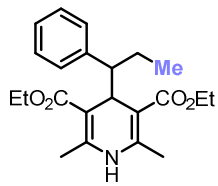

^{1}H-NMR (400 MHz, $CDCl_3$): δ 7.19 – 7.08 (m, 3H), 7.03 – 6.96 (m, 2H), 5.13 (s, 1H), 4.33 (d, *J* = 4.6 Hz, 1H), 4.18 – 4.00 (m, 4H), 2.42 (dt, *J* = 10.1, 5.2 Hz, 1H), 2.13 (s, 3H), 2.10 (s, 3H), 1.75 – 1.53 (m, 2H), 1.27 (td, *J* =

7.1, 4.8 Hz, 6H), 0.76 (t, *J* = 7.3 Hz, 3H) ppm**^{13}C NMR (101 MHz, $CDCl_3$):** δ 169.0, 168.5, 145.6, 145.5, 142.5, 129.6, 127.2, 126.1, 101.6, 100.9, 59.9, 59.9, 55.0, 39.0, 23.3, 19.5, 14.7, 14.7, 12.9 ppm.

Diethyl 2,6 – dimethyl – 4 – (naphthalen – 1 – ylmethyl) – 1,4 – dihydropyridine – 3,5 – dicarboxylate (80j)

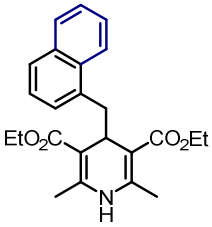

^{1}H-NMR (400 MHz, $CDCl_3$): δ 8.38 (d, 1H, *J* = 8.4 Hz), 7.80 (d, 1H, *J* = 7.6 Hz), 7.65 (d, 1H, *J* = 7.6 Hz), 7.51 – 7.44 (m, 2H), 7.30 – 7.26 (m, 2H), 7.04 (d, 1H, *J* = 6.8 Hz), 5.80 (s, 1H), 4.43 (t, 1H, *J* = 6.7 Hz), 3.93 – 3.85 (m, 2H), 3.65-3.57 (m, 2H), 3.02 (d, 2H, *J* = 6.7 Hz), 2.24 (s, 6H), 0.93 (t, 3H, *J* = 7.2 Hz) ppm. **^{13}C NMR (101 MHz, $CDCl_3$):** δ 167.9, 145.4, 135.2, 133.7, 133.2, 128.3, 128.1, 126.6, 125.4, 125.3, 125.1, 124.9, 102.8, 59.6, 39.8, 34.2, 19.4, 13.8 ppm.

Diethyl 2,6 – dimethyl – 4 – (naphthalen – 2 – ylmethyl) –1,4 – dihydropyridine – 3,5 – dicarboxylate (80k)

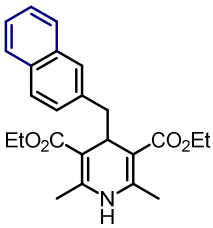

^{1}H-NMR (400 MHz, $CDCl_3$): δ 7.80 – 7.70 (m, 2H), 7.65 (d, *J* = 8.4 Hz, 1H), 7.47 – 7.34 (m, 3H), 7.20 (dd, *J* = 8.4, 1.7 Hz, 1H), 5.19 (s, 1H), 4.28 (t, *J* = 5.3 Hz, 1H), 4.12 – 3.91 (m, 4H), 2.75 (d, *J* = 5.3 Hz, 2H), 2.12 (s, 6H), 1.19 (t, *J* = 7.1 Hz, 6H) ppm. **^{13}C NMR (101 MHz, $CDCl_3$):** δ 168.0, 145.6, 137.1, 133.4, 132.1, 129.3, 128.4, 127.6, 127.6, 126.5, 125.7, 125.1, 101.9, 59.7, 42.6, 35.8, 19.3, 14.5 ppm. **HRMS (ESI-MS)** calculated for $C_{24}H_{26}NO_4^-$ $[M-H]^-$ 392.1867, found 392.1870.

Diethyl 2,6-dimethyl-4-(1-(naphthalen-2-yl)ethyl)-1,4-dihydropyridine-3,5-dicarboxylate (80l)

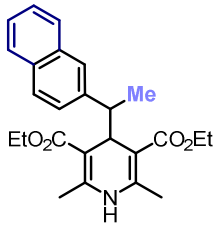

^{1}H-NMR (400 MHz, $CDCl_3$): δ 7.75 (m, 2H), 7.67 (d, *J* = 8.5 Hz, 1H), 7.48 (as, 1H), 7.43 – 7.35 (m, 2H), 7.31 (dd, *J* = 8.5, 1.8 Hz, 1H), 5.24 (s, 1H), 4.37 (d, *J* = 4.7 Hz, 1H), 4.03 (q, *J* = 7.1 Hz, 2H), 3.92 (dq, *J* = 10.8, 7.1 Hz, 1H), 3.72 (dq, *J* = 10.8, 7.1 Hz, 1H), 2.94 (m, 1H), 2.16 (s, 3H), 2.14 (s, 3H), 1.29 – 1.20 (m, 6H), 1.08 (t, *J* = 7.1 Hz, 3H) ppm. **^{13}C NMR (101 MHz, $CDCl_3$):** δ 168.7, 168.6, 145.7, 145.3, 142.0, 133.4, 132.5, 128.0, 127.9, 127.7, 126.9, 126.6, 125.8, 125.3, 101.3, 101.1, 59.9, 59.9, 46.5, 40.5, 19.6, 19.4, 15.8, 14.6, 14.4 ppm.

Diethyl 2,6 – dimethyl – 4 – (thiophen – 3 – ylmethyl) – 1,4 – dihydropyridine – 3,5 - dicarboxylate (80m)

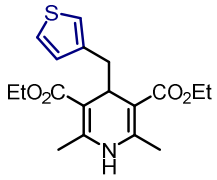

^{1}H NMR (600 MHz, $CDCl_3$): δ 7.10 (dd, *J* = 4.9, 3.0 Hz, 1H), 6.81 (dd, *J* = 4.9, 1.2 Hz, 1H), 6.76 (d, *J* = 2.8 Hz, 1H), 5.34 (s, 1H), 4.16 (t, *J* = 5.4 Hz, 1H), 4.14 – 4.05 (m, 4H), 2.61 (d, *J* = 5.4 Hz, 2H), 2.18 (s, 6H), 1.26 (t, *J* = 7.1 Hz, 6H) ppm. **^{13}C NMR (151 MHz, $CDCl_3$):** δ 168.0, 145.4, 139.7, 130.1, 123.7, 122.0, 102.1, 59.8, 36.6, 35.2, 19.5, 14.6 ppm. **HRMS (ESI-MS)** calculated for $C_{18}H_{22}NO_4S^-$ $[M-H]^-$ 348.1275, found 348.1310.

Diethyl 2,6-dimethyl-4-((2-phenylcyclopropyl)methyl)-1,4-dihydropyridine-3,5-dicarboxylate (80b)

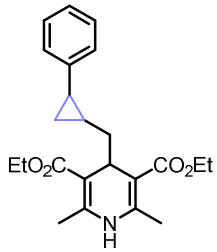

^{1}H NMR (400 MHz, $CDCl_3$): δ 7.20 (t, *J* = 7.7 Hz, 2H), 7.08 (t, *J* = 7.3 Hz, 1H), 6.93 (d, *J* = 6.8 Hz, 2H), 5.33 (s, 1H), 4.16 – 4.01 (m, 5H), 2.23 (s, 3H), 2.09 (s, 3H), 1.59 (dt, *J* = 13.9, 5.4 Hz, 1H), 1.49 (dt, *J* = 8.9, 4.7 Hz, 1H), 1.31 (dd, *J* = 8.3, 5.5 Hz, 1H), 1.28 – 1.21 (m, 6H), 1.10 – 0.97 (m, 1H), 0.78 – 0.64 (m, 2H) ppm. **^{13}C NMR (101 MHz, $CDCl_3$):** δ 168.1, 168.0, 145.2, 145.0, 144.6, 128.2, 125.4, 125.1, 103.2, 102.8, 59.7, 40.9, 33.6, 23.9, 20.7, 19.6, 19.6, 16.5, 14.6 ppm. **HRMS (ESI-MS)** calculated for $C_{23}H_{28}NO_4^-$ $[M-H]^-$ 382.2024, found 382.2046.

*Synthesis of DHPs **80n, o***

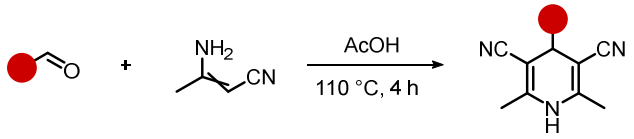

80n, o were synthetized according to literature.[80] 1.0 equiv. of the corresponding aldehyde were dissolved in acetic acid (1 M in the aldehyde) in a round-bottom flask. 2.0 equiv. of 3-aminocrotononitrile were added and the reaction was heated at 110 °C with stirring for 4 hours. The crude reaction mixture was allowed to cool to room temperature, then was diluted with water and extracted with EtOAc (3 x 15 ml). The combined organic layers were neutralised with a saturated $NaHCO_3$ solution until the removal of acetic acid was achieved, washed once with brine, dried over $MgSO_4$, filtered, and concentrated under reduced pressure. The residue was purified by flash chromatography on silica gel using hexane: EtOAc as eluent mixture to afford the pure product.

2,6-dimethyl-4-(1,2,3,4-tetrahydronaphthalen-1-yl)-1,4-dihydropyridine-3,5-dicarbonitrile (80n)

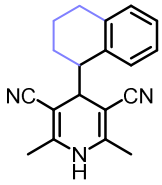

^{1}H NMR (400 MHz, $CDCl_3$): δ 7.25 – 7.20 (m, 1H), 7.20 – 7.12 (m, 2H), 7.12 – 7.06 (m, 1H), 5.91 (s, 1H), 3.86 (d, J = 3.7 Hz, 1H), 3.17 (q, J = 7.1, 6.5 Hz, 1H), 2.82 – 2.68 (m, 2H), 2.11 (s, 3H), 2.05 (s, 3H), 1.99 – 1.89 (m, 2H), 1.82 – 1.64 (m, 1H) ppm. **^{13}C NMR (101 MHz, $CDCl_3$):** δ 147.5, 146.9, 139.0, 135.1, 129.3, 128.8, 126.5, 125.9, 118.7, 117.8, 84.4, 82.7, 43.5, 42.1, 30.2, 24.9, 21.4, 18.7, 18.7 ppm. **HRMS (ESI-MS)** calculated for $C_{19}H_{18}N_3^-$ $[M-H]^-$ 288.1506, found 288.1543.

2,6-dimethyl-4-(2-phenylpropan-2-yl)-1,4-dihydropyridine-3,5-dicarbonitrile (80o)

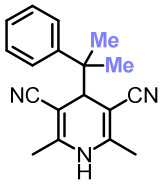

^{1}H-NMR (400 MHz, $CDCl_3$): δ 7.26 – 7.17 (m, 5H), 6.23 (s, 1H), 3.22 (s, 1H), 1.95 (s, 6H), 1.35 (s, 6H) ppm. **^{13}C NMR (101 MHz, $CDCl_3$):** δ 148.6, 144.2, 127.8, 127.0, 126.7, 119.7, 81.0, 47.6, 46.6, 24.6, 18.3 ppm.

Synthesis of Boron salts ***96***

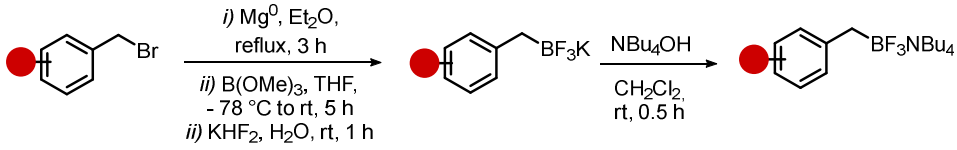

Following a reported procedure,[81] an oven-dried 2-necked round-bottom flask fitted with a reflux condenser was charged with 80 mg of Mg turnings (3.3 mmol, 1.1 equiv.), which was then activated by stirring it under N_2 overnight.

Et_2O (6.5 mL), the corresponding benzyl bromide (3.0 mmol, 1 equiv.) and a small crystal of iodine were added to the magnesium. The suspension was refluxed for 3 h, then cooled to room temperature. To a separate flame-dried flask 502 μL of trimethyl borate (4.50 mmol, 1.5 equiv.) and THF (6.0 mL) were added under N_2. The flask was cooled to -78 °C, then the Grignard reagent previously prepared in the other flask was added dropwise at -78 °C. The reaction was stirred for 1 h at -78 °C, then slowly warmed to room temperature over 1 h and stirring continued for 3 more hours at room temperature. After this time the reaction mixture was cooled at 0 °C and MeOH (4.0 mL) was added over 5 min. Then, 1.41 g of KHF_2 (18.0 mmol, 6 equiv.) and water (4.0 mL) were added successively, and the mixture was stirred for an additional 1 hour at room temperature. The solvent was removed, and then the remaining water was removed by azeotrope with toluene under reduced pressure. The residue was dried under high vacuum overnight. Acetone (60 mL) was added, and the solution was filtrated over Celite. The filtrate was partially concentrated under reduce pressure and Et_2O (30 mL) was added. The solution was cooled at 0 °C and the potassium benzyltrifluoroborate precipitated as a white solid and was recovered by filtration.

Tetra-*n*-butylammonium benzyltrifluoroborate **96a** and **96b** were prepared from the corresponding potassium salts by ion-exchange according to the literature procedures:[82] to a suspension of the potassium trifluoroborate salt (1 equiv.) in dichloromethane (0.15 M), a 1.54 M solution of NBu_4OH (1 equiv.) was added, and the solution was stirred for 30 minutes. The organic phase was separated and washed with water (2 x 15 mL), dried over $MgSO_4$, filtered, and concentrated under reduced pressure The yield of this step was quantitative.

Tetrabuthyl ammonium benzyltrifluoroborate (96a)

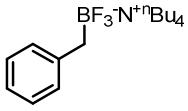

^{1}H-NMR (400 MHz, Acetone-d_6): δ 7.12 – 7.10 (m, 2H), 7.06 – 7.02 (m, 2H), 6.88 (1H, br t, *J* = 7.3 Hz), 1.65 (s, 2H) ppm. **^{13}C-NMR (101 MHz, Acetone-d_6):** δ 148.0, 129.7, 127.8, 122.9, 30.4, 30.0 ppm.

Tetrabuthyl ammonium 4-methylbenzyltrifluoroborate (96b)

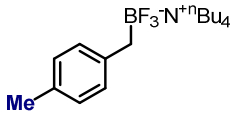

^{1}H-NMR (400 MHz, Acetone-d_6): δ 6.98 (d, *J* = 7.6 Hz, 2H), 6.85 (d, *J* = 7.5 Hz, 2H), 2.19 (s, 3H), 1.58 (bs, 2H) ppm. **^{13}C-NMR (101 MHz, Acetone-d_6):** δ 144.7, 131.5, 129.7, 128.6, 21.0 ppm.

Potassium 2-methoxybenzyltrifluoroborate (96c)

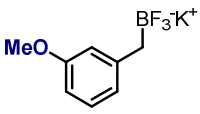

^{1}H-NMR (400 MHz, Acetone-d_6): δ 6.93 (t, *J* = 7.8 Hz, 1H), 6.70 – 6.60 (m, 2H), 6.45 (dd, *J* = 8.0, 2.6 Hz, 1H), 3.69 (s, 3H), 1.61 (s, 2H) ppm. **^{13}C-NMR (101 MHz, Acetone-d_6):** δ 160.0, 149.7, 128.5, 122.4, 115.4, 108.5, 55.0 ppm.

Synthesis and characterisation of the carboxylation product

Carboxylation procedure

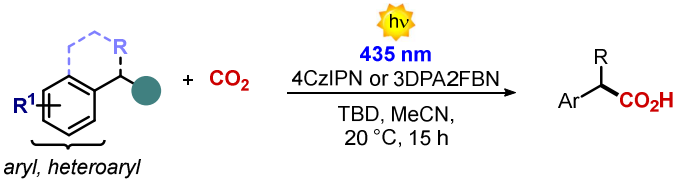

In a 4 mL vial, DHPs **80** or trifluoroborate salts **96** (0.1 mmol, 1.0 equiv.), photocatalyst (0.002 mmol, 2 mol%) and TBD (1.5 mmol, 2 equiv.) were

added, then the vial was closed with PTFE/silicone septum caps and degassed with CO_2. The reagents were dissolved in CO_2-degassed MeCN (2 mL, 0.05 M) and the reaction mixture was bubbled with CO_2 for 30 s. Then, the solution was irradiated for 15 h. NMR yield was measured using 14 µL of CH_2Br_2 and 25 µL of acetic acid. After this, the solvent was removed, and the crude mixture was transferred in a separating funnel using 10 mL of hexane:CH_2Cl_2 9:1. 10 mL of NaOH 1 M were added, then the two phases were separated, and the aqueous phase was washed 2 more times with hexane:CH_2Cl_2 9:1. The reunited aqueous phases were acidified adding HCl 2 M dropwise until pH 2 is reached. The acidified aqueous phase was extracted with EtOAc (5 x 15 mL). The organic phases were collected, dried over $MgSO_4$, filtered, and concentrated under reduced pressure giving the pure products in the stated yields.

2-phenylacetic acid (81)

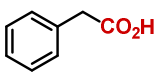

^{1}H-NMR (400 MHz, $CDCl_3$): δ 7.35 – 7.30 (m, 5H), 3.66 (s, 2H) ppm. **^{13}C NMR (101 MHz, $CDCl_3$):** δ 178.1, 133.2, 129.3, 128.6, 127.3, 41.1 ppm.

2-(4-bromophenyl)acetic acid (82)

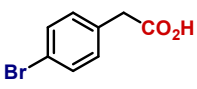

^{1}H-NMR (400 MHz, $CDCl_3$): δ 7.46 (d, *J* = 8.4 Hz, 2H), 7.16 (d, *J* = 8.4 Hz, 2H), 3.61 (s, 2H) ppm. **^{13}C NMR (101 MHz, $CDCl_3$):** δ 176.9, 132.1, 131.8, 131.1, 121.5, 40.3 ppm.

2-(2,4-dimethylphenyl)acetic acid (85)

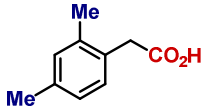

^{1}H-NMR (600 MHz, $CDCl_3$): δ 7.08 (d, *J* = 7.7 Hz, 1H), 7.01 (s, 1H), 6.98 (d, *J* = 7.6 Hz, 1H), 3.63 (s, 2H), 2.30 (s, 3H), 2.28 (s, 3H) ppm. **^{13}C-NMR (151 MHz, $CDCl_3$):** δ

177.5, 137.5, 136.9, 131.5, 130.4, 129.2, 127.1, 38.6, 21.2, 19.7 ppm. **HRMS (ESI-MS)** calculated for $C_{10}H_{11}O_2^-$ $[M-H]^-$ 163.0765, found 163.0748.

2-phenylpropanoic acid (86)

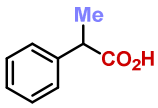

^{1}H-NMR (400 MHz, $CDCl_3$): δ 7.31 – 7.16 (m, 5H), 3.68 (q, *J* = 7.2 Hz, 1H), 1.45 (d, *J* = 7.2 Hz, 3H) ppm. **^{13}C NMR (101 MHz, $CDCl_3$):** δ 181.0, 139.9, 128.8, 127.7, 127.5, 45.5, 18.2 ppm.

2-(4-methoxyphenyl)propanoic acid (93)

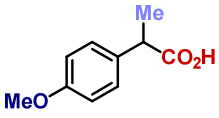

^{1}H-NMR (400 MHz, $CDCl_3$): δ 7.29 – 7.19 (m, 2H), 6.91 – 6.82 (m, 2H), 3.79 (s, 3H), 3.69 (q, *J* = 7.2 Hz, 1H), 1.49 (d, *J* = 7.1 Hz, 3H) ppm. **^{13}C NMR (101 MHz, $CDCl_3$):** δ 180.8, 159.0, 132.0, 128.8, 114.2, 55.4, 44.6, 18.3 ppm.

1,2,3,4-tetrahydronaphthalene-1-carboxylic acid (88)

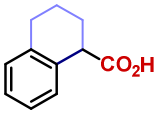

^{1}H-NMR (400 MHz, $CDCl_3$): δ 7.22 – 7.10 (m, 4H), 3.84 (br s, 1H), 2.86 – 2.72 (m, 2H), 2.18 – 2.17 (m, 1H), 2.02-1.96 (m, 2H), 1.79 – 1.76 (m, 1H) ppm. **^{13}C NMR (101 MHz, $CDCl_3$):** δ 181.3, 137.3, 132.6, 129.6, 129.5, 127.1, 125.8, 44.5, 29.1, 26.5, 20.4 ppm.

2-methyl-2-phenylpropanoic acid (94)

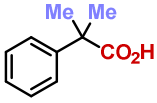

^{1}H-NMR (400 MHz, $CDCl_3$): δ 7.32 – 7.29 (m, 2H), 7.25 – 7.21 (m, 2H), 7.18 – 7.13 (m, 1H), 3.22 (s, 1H), 1.52 (s, 6H) ppm. **^{13}C NMR (101 MHz, $CDCl_3$):** δ 142.9, 127.4, 125.9, 12.8, 45.3, 26.2 ppm.

2-(naphthalen-1-yl)acetic acid (90)

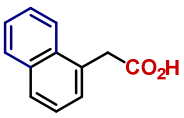

^{1}H-NMR (400 MHz, $CDCl_3$): δ 8.00 (d, *J* = 8.3 Hz, 1H), 7.90 (dd, *J* = 7.5, 2.1 Hz, 1H), 7.84 (d, *J* = 7.7 Hz, 1H), 7.58 – 7.51 (m, 2H), 7.49 – 7.41 (m, 2H), 4.10 (s, 2H) ppm. **^{13}C NMR (101 MHz, $CDCl_3$):** δ 178.2, 133.9, 132.1, 129.9, 128.9, 128.5, 128.3, 126.6, 126.0, 125.6, 123.8, 38.9 ppm.

2-(naphthalen-2-yl)acetic acid (89)

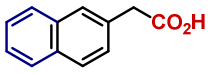

^{1}H-NMR (400 MHz, $CDCl_3$): δ 7.81 (t, 3H, *J* = 9.1 Hz), 7.74 (s, 1H), 7.47 – 7.44 (m, 2H), 7.41 (dd, 1H, *J* = 8.4, 1.8 Hz), 3.82 (s, 2H) ppm. **^{13}C NMR (101 MHz, $CDCl_3$):** δ 177.4, 133.4, 132.6, 130.7, 128.3, 128.2, 127.7, 127.7, 127.3, 126.2, 125.9, 41.1 ppm.

2-(naphthalen-2-yl)propanoic acid (91)

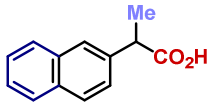

^{1}H-NMR (400 MHz, $CDCl_3$): δ 7.85 – 7.78 (m, 3H), 7.76 (s, 1H), 7.51 – 7.42 (m, 3H), 3.92 (q, *J* = 7.1 Hz, 1H), 1.61 (d, *J* = 7.2 Hz, 3H) ppm. **^{13}C NMR (101 MHz, $CDCl_3$):** δ 180.5, 137.4, 133.6, 132.9, 128.6, 128.0, 127.8, 126.6, 126.4, 126.1, 125.9, 45.6, 18.3 ppm.

2-(thiophen-3-yl)acetic acid (95)

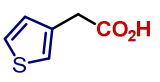

^{1}H-NMR (400 MHz, $CDCl_3$): δ 7.31 (dd, *J* = 5.0, 3.0 Hz, 1H), 7.18 (d, *J* = 1.6 Hz, 1H), 7.05 (dd, *J* = 4.9, 1.3 Hz, 1H), 3.71 (s, 2H) ppm. **^{13}C-NMR (101 MHz, $CDCl_3$):** δ 176.9, 132.9, 128.6, 126.1, 123.5, 35.6 ppm. **HRMS (ESI-MS)** calculated for $C_6H_5O_2S^-$ $[M-H]^-$ 141.0016, found 141.0048.

2-phenylpent-4-enoic acid (92)

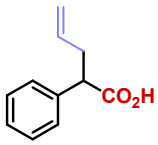

^{1}H-NMR (400 MHz, $CDCl_3$): δ 7.38 – 7.26 (m, 5H), 5.79 – 5.69 (m, 1H), 5.16 – 4.95 (m, 2H), 3.66 (dd, *J* = 8.2, 7.2 Hz, 1H), 2.90 – 2.77 (m, 1H), 2.58 – 2.51 (m, 1H) ppm. **^{13}C NMR (101 MHz, $CDCl_3$):** δ 179.7, 137.9, 134.9, 128.7, 128.2, 127.6, 117.3, 51.4, 37.1 ppm.

2-(p-tolyl)acetic acid (97)

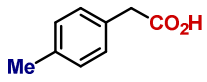

^{1}H-NMR (400 MHz, $CDCl_3$): δ 7.23 – 7.15 (m, 4H), 3.64 (s, 2H), 2.37 (s, 3H) ppm. **^{13}C NMR (101 MHz, $CDCl_3$):** δ 178.5, 137.1, 130.3, 129.5, 129.4, 40.8, 21.2 ppm.

2-(3-methoxyphenyl)acetic acid (98)

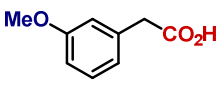

^{1}H-NMR (400 MHz, $CDCl_3$): δ 7.31 – 7.21 (m, 1H), 6.94 – 6.79 (m, 3H), 3.83 (s, 3H), 3.65 (s, 2H) ppm. **^{13}C NMR (101 MHz, $CDCl_3$):** δ 177.7, 159.7, 134.7, 129.6, 121.7, 115.1, 112.9, 55.2, 41.1 ppm.

Procedures For Product Manipulations

Curtius rearrangement

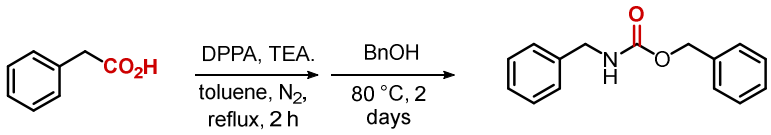

The procedure was adapted from a report in literature.[83] 68.1 mg of **81** (0.5 mmol, 1 equiv.) were dissolved in 2 mL of toluene, 119 µL of diphenylphosphoryazide (0.55 mmol, 1.1 equiv.) and 77 µL triethylamine (0.55 mmol, 1.1 equiv.) were added. The mixture was refluxed for 2 h under N_2. Gas release was observed. The reaction mixture was cooled to 60 °C, and 62 µL of

benzyl alcohol (0.6 mmol, 1.2 equiv.) were added in one portion. The mixture was heated to 80 °C for 2 days. After cooling to room temperature, 40 mL of water were added, and the mixture was extracted with EtOAc (3 x 30 mL). The combined organic phases were washed with water (2 x 30 mL) and once with brine, dried over $MgSO_4$, filtered, and concentrated under reduced pressure. The residual oil was purified by column chromatography on silica gel using toluene:EtOAc 98:2 to 95:5 as eluent mixture, giving **99** in 78% yield (93.5 mg, 0.39 mmol) as a white solid.

benzyl benzylcarbamate (99)

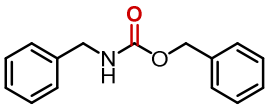

^{1}H-NMR (400 MHz, $CDCl_3$): δ 7.42 – 7.26 (m, 10H), 5.14 (s, 2H), 5.07 (s, 1H), 4.39 (d, *J* = 5.9 Hz, 2H) ppm. **^{13}C NMR (101 MHz, $CDCl_3$):** δ 156.6, 138.5, 136.6, 128.8, 128.7, 128.3, 127.7, 67.0, 45.3 ppm.

Menthol esterification

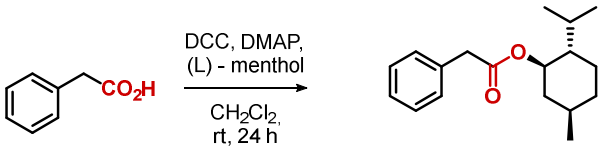

Following a reported procedure,[84] 5.5 mg of 4-dimethylaminopyridine (0.045 mmol, 0.8 equiv.), 11.2 mg of **81** (0.056 mmol, 1.0 equiv.) then 26.6 mg of (−)-menthol (0.17 mmol, 3.0 equiv.) were added to a stirred solution of 12.8 mg of N,N'-dicicloesilcarbodiimmide (0.062 mmol, 1.1 equiv.) in 0.31 mL of dichloromethane at 0 °C. The resulting mixture was stirred at rt for 24 h. The mixture was concentrated in vacuo, diluted with 2 mL of Et_2O and filtered through Celite. The filtrate was washed with 2 mL of 1 M NaOH (aq), 2 mL of 1 M HCl (aq) and 2 mL of brine. Finally, it was dried over $MgSO_4$, filtered, and

concentrated under reduced pressure. Purification by column chromatography using flash chromatography on silica gel (hexane: EtOAc 8:2 to 7:3) afforded the racemic product **100** in 79% yield (14.9 mg, 0.044 mmol) as a pale-yellow oil.

2-isopropyl-5-methylcyclohexyl 2-(naphthalen-2-yl)propanoate (100)

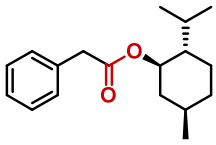

^{1}H-NMR (400 MHz, $CDCl_3$): δ 7.37 – 7.26 (m, 5H), 4.71 (td, *J* = 11.2, 4.0 Hz, 1H), 3.63 (s, 2H), 2.03 – 1.94 (m, 1H), 1.80 – 1.74 (m, 1H), 1.73 – 1.65 (m, 2H), 1.54 – 1.33 (m, 2H), 1.11 – 1.01 (m, 1H), 1.00 – 0.89 (m, 2H), 0.94 – 0.86 (m, *J* = 6.8 Hz, (6H), 0.72 (d, *J* = 6.8 Hz, 3H). ppm. **^{13}C NMR (101 MHz, $CDCl_3$):** δ 171.2, 134.4, 129.2, 128.5, 126.9, 74.7, 47.1, 41.9, 40.8, 34.3, 31.4, 26.1, 23.4, 22.0, 20.7, 16.3 ppm.

Weinreb ketone synthesis

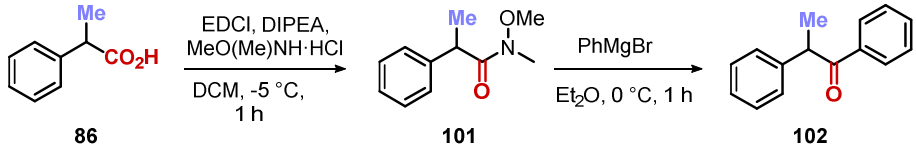

86 **101** **102**

Following a procedure from a literature report,[85] 26.7 mg of **86** (0.18 mmol, 1.0 equiv.) were dissolved in 1.25 mL of CH_2Cl_2 and cooled to −5 °C. To this, 17.3 mg of *N,O*-dimethylhydroxylamine hydrochloride (0.18 mmol, 1.0 equiv.), 31 µL of diisopropylethylamine (0.18 mmol, 1.0 equiv.) were added. Then, a solution of 33.9 mg of EDCl (0.18 mmol, 1 equiv.) in 0.25 mL of CH_2Cl_2 was added dropwise. The mixture was left stirring for 1 h at −5 °C, then the mixture was washed with HCl (aq) 1 M (2 × 2 mL). The combined organic phases were dried over $MgSO_4$, filtered, and concentrated under reduced pressure to afford the Weinreb amide **101** in 72% yield (24.7 mg, 0.13 mmol) as a yellow oil.

***N*-methoxy-*N*-methyl-2-phenylpropanamide (101)**

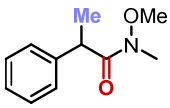

^{1}H-NMR (400 MHz, $CDCl_3$): δ 7.35 – 7.24 (m, 5H), 4.12 (q, *J* = 7.0 Hz, 1H), 3.39 (s, 3H), 3.14 (s, 3H), 1.43 (d, *J* = 7.0 Hz, 3H) ppm. **^{13}C NMR (101 MHz, $CDCl_3$):** δ 175.5, 142.3, 129.3, 128.2, 127.4, 61.2, 42.0, 32.4, 19.7 ppm.

24.7 mg of **101** (0.13 mmol. 1.0 equiv.) were dissolved in 1.3 mL of diethylether and cooled to 0 °C, then 128 µL of methylmagnesium bromide (3 M solution in Et_2O (0.39 mmol, 3 equiv.) were added dropwise. A white precipitate quickly appeared. After 1 h, the reaction was quenched by the addition of saturated NH_4Cl (aq) (10 mL) and extracted with EtOAc (3 × 10 mL). The combined organic phases were dried over $MgSO_4$, filtered, and concentrated under reduced pressure. Pure **102** was obtained using flash chromatography on silica gel (hexane: EtOAc 95:5) as a colourless oil in 91% yield (24.5 mg, 0.12 mmol, 66% over 2 steps).

1,2-diphenylpropan-1-one (102)

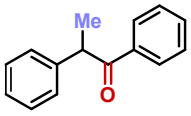

^{1}H-NMR (400 MHz, $CDCl_3$): δ 7.25 (t, *J* = 7.4 Hz, 2H), 7.19 – 7.13 (m, 3H), 3.68 (q, *J* = 7.0 Hz, 1H), 1.95 (s, 3H), 1.32 (d, *J* = 7.1 Hz, 3H) ppm. **^{13}C NMR (101 MHz, $CDCl_3$):** δ 208.3, 140.7, 128.9, 127.8, 127.1, 53.6, 28.2, 17.2 ppm.

Spectroscopic data

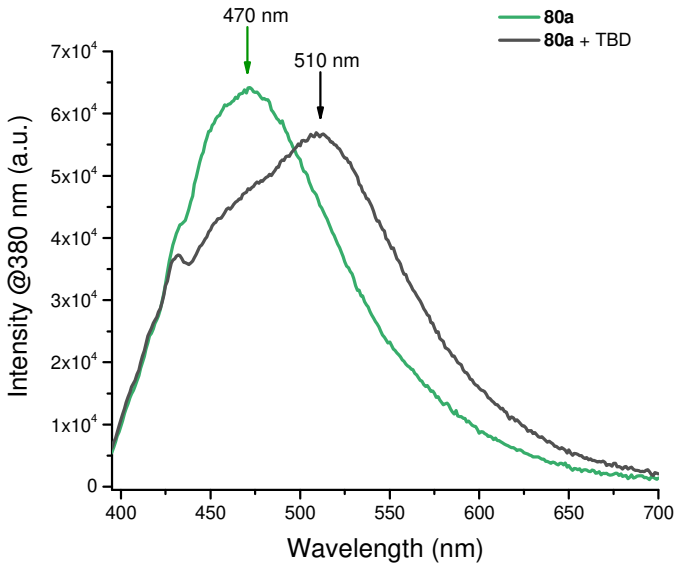

Figure Exp3.6. – UVVis emission spectrum of 10^{-4}M solutions in MeCN of **80a**, and a mixture of **80a** and TBD.

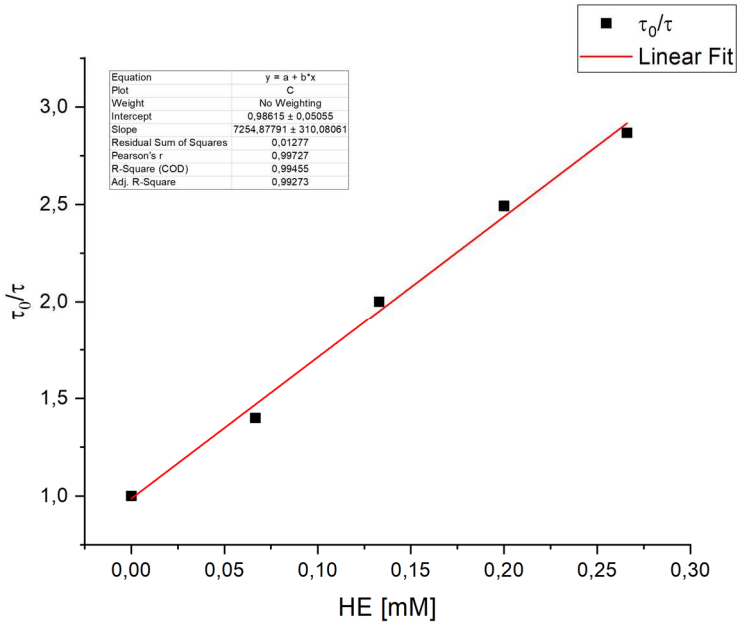

Figure Exp3.7. – Stern-Volmer quenching experiments of 4CzBnBN with a mixture of **80a** and TBD

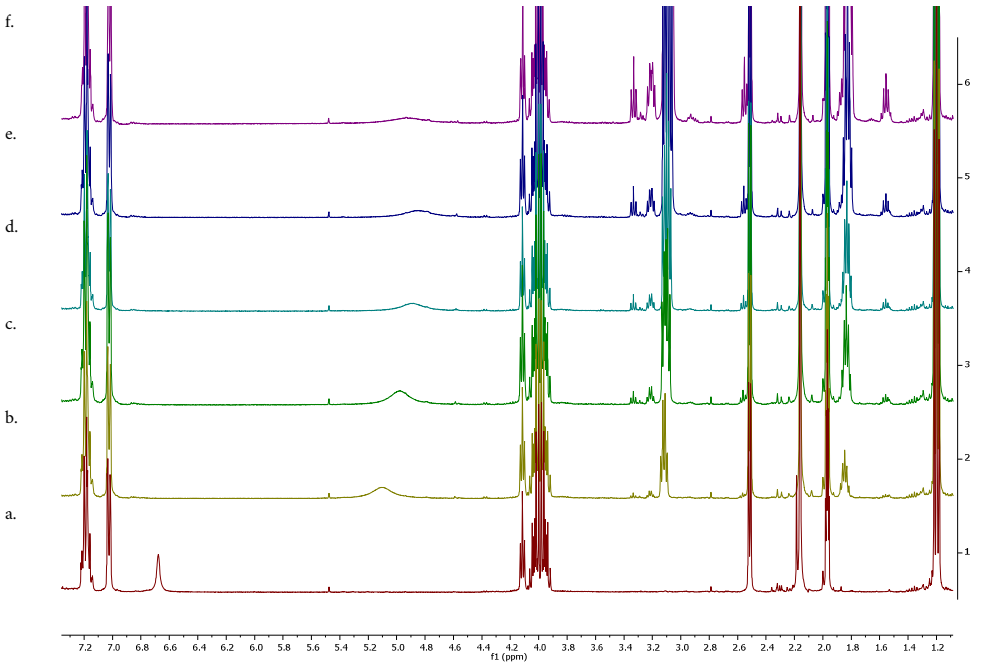

Figure Exp3.8. – ^{1}H-NMR analysis of **80a** in MeCN-d_3 in the presence of a. 0 equiv., b. 0.1 equiv., c. 0.2 equiv., d. 0.3 equiv., e. 0.5 equiv., f. 1.0 equiv. of TBD.

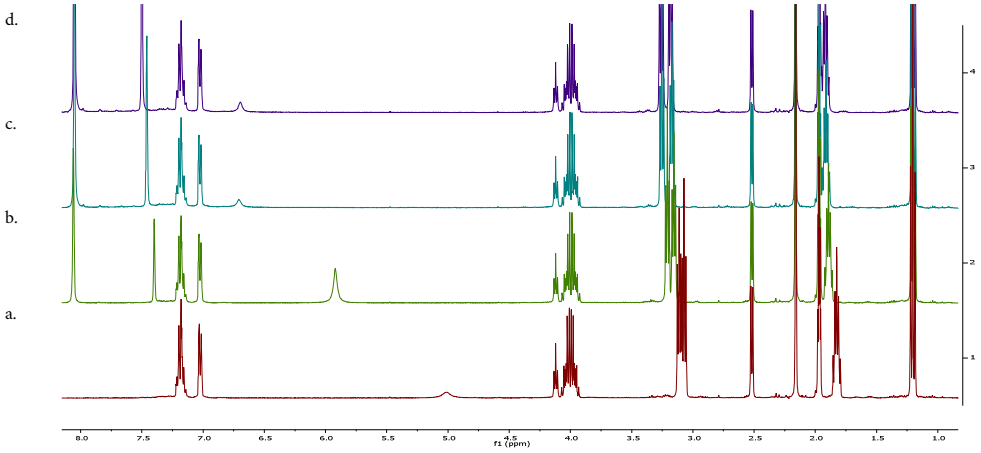

Figure Exp3.9. – ^{1}H-NMR analysis of **80a** in MeCN-d_3 in the presence of 1.5 equiv. of TBD and a. 0 equiv., b. 0.4 equiv., c. 0.8 equiv., d. 1.0 equiv. of Schreiner's thiourea.

3.3. – References - Chapter III

1. North, M., What is CO2? Thermodynamics, Basic Reactions and Physical Chemistry. In *Carbon Dioxide Utilisation*, 2015; pp 3-17.

2. Aresta, M.; Angelini, A., The Carbon Dioxide Molecule and the Effects of Its Interaction with Electrophiles and Nucleophiles. In *Carbon Dioxide and Organometallics*, Lu, X.-B., Ed. Springer International Publishing: Cham, 2016; pp 1-38.

3. Otto, A.; Grube, T.; Schiebahn, S.; Stolten, D., Closing the loop: captured CO2 as a feedstock in the chemical industry. *Energy Environ. Sci.* **2015,** 8 (11), 3283-3297.

4. https://www.iea.org/reports/global-energy-review-2021/co2-emissions

5. Sakakura, T.; Choi, J.-C.; Yasuda, H., Transformation of Carbon Dioxide. *Chem. Rev.* **2007,** 107 (6), 2365-2387.

6. a. *CO2 as a Building Block in Organic Synthesis*. WILEY-VCH GmbH: Weinheim, Germany, 2020; b. Zhou, H.; Lu, X., Lewis base-CO2 adducts as organocatalysts for CO2 transformation. *Sci. China*: *Chem.* **2017,** 60 (7), 904-911; c. Ashley, A. E.; O'Hare, D., FLP-Mediated Activations and Reductions of CO2 and CO. In *Frustrated Lewis Pairs II*: *Expanding the Scope*, Erker, G.; Stephan, D. W., Eds. Springer Berlin Heidelberg: Berlin, Heidelberg, 2013; pp 191-217; d. Chen, P.; Xiong, T.; Pan, Y.; Liang, Y., Recent Progress on N-heterocyclic Carbene Catalysts in Chemical Fixation of CO2. *Asian J. Org. Chem.* **2022,** 11 (3), e202100738; e. Tortajada, A.; Julia-Hernandez, F.; Borjesson, M.; Moragas, T.; Martin, R., Transition-Metal-Catalyzed Carboxylation Reactions with Carbon Dioxide. *Angew. Chem. Int. Ed.* **2018,** 57 (49), 15948-15982.

7. from a Mulliken analysis on a DFT optimised geometry of CO2)

8. Aresta, M.; Dibenedetto, A.; Quaranta, E., The Carbon Dioxide Molecule. In *Reaction Mechanisms in Carbon Dioxide Conversion*, Aresta, M.; Dibenedetto, A.; Quaranta, E., Eds. Springer Berlin Heidelberg: Berlin, Heidelberg, 2016; pp 1-34.

9. Calvert, J. G., Glossary of atmospheric chemistry terms (Recommendations 1990). *Pure Appl. Chem.* **1990,** 62 (11), 2167-2219.

10. a. Yuan, G.; Qi, C.; Wu, W.; Jiang, H., Recent advances in organic synthesis with CO2 as C1 synthon. *Curr. Opin. Green Sustainable Chem.* **2017,** 3, 22-27; b. Fujihara, T.; Tsuji, Y., Carboxylation Reactions Using Carbon Dioxide as the C1 Source via Catalytically Generated Allyl Metal Intermediates. *Front. Chem.* **2019,** 7.

11. a. Kolbe, H., Ueber Synthese der Salicylsäure. *Justus Liebigs Ann. Chem.* **1860,** 113 (1), 125-127; b. Schmitt, R., Beitrag zur Kenntniss der Kolbe'schen Salicylsäure Synthese. *J. Prakt. Chem.* **1885,** 31 (1), 397-411.

12. Zevaco, T.; Dinjus, E., Main Group Element- and Transition Metal-Promoted Carboxylation of Organic Substrates (Alkanes, Alkenes, Alkynes, Aromatics, and Others). In *Carbon Dioxide as Chemical Feedstock*, 2010; pp 89-120.

13. Nandi, S.; Jana, R., Toward Sustainable Photo-/Electrocatalytic Carboxylation of Organic Substrates with CO2. *Asian J. Org. Chem.* **2022**.

14. a. Cherubini-Celli, A.; Mateos, J.; Bonchio, M.; Dell'Amico, L.; Companyo, X., Transition Metal-Free CO2 Fixation into New Carbon-Carbon Bonds. *ChemSusChem* **2018,** 11 (18), 3056-3070; b. Cao, Y.; He, X.; Wang, N.; Li, H.-R.; He, L.-N., Photochemical and Electrochemical Carbon Dioxide Utilization with Organic Compounds. *Chin. J. Chem.* **2018,** 36 (7), 644-659.

15. a. Rysselberghe, P. V.; Alkire, G. J., Polarographic Reduction of Carbon Dioxide. *J. Am. Chem. Soc.* **1944,** 66 (10), 1801-1801; b. Teeter, T. E.; Rysselberghe, P. V., Reduction of Carbon Dioxide on Mercury Cathodes. *J. Chem. Phys.* **1954,** 22 (4), 759-760.

16. a. Qiao, J.; Liu, Y.; Hong, F.; Zhang, J., A review of catalysts for the electroreduction of carbon dioxide to produce low-carbon fuels. *Chem. Soc. Rev.* **2014,** 43 (2), 631-675; b. Wang, G.; Chen, J.; Ding, Y.; Cai, P.; Yi, L.; Li, Y.; Tu, C.; Hou, Y.; Wen, Z.; Dai, L., Electrocatalysis for CO2 conversion: from fundamentals to value-added products. *Chem. Soc. Rev.* **2021,** 50 (8), 4993-5061.

17. Wawzonek, S.; Gundersen, A., Polarographic Studies in Acetonitrile and Dimethylformamide: V . Behavior of Aromatic Ketones and Aldehydes. *J. Electrochem. Soc.* **1960,** 107.

18. a. Tyssee, D. A.; Wagenknecht, J. H.; Baizer, M. M.; Chruma, J. L., Some Cathodic Organic Syntheses Involving Carbon Dioxide. *Tetrahedron Lett.* **1972,** 47, 4809-4812; b. Tyssee, D. A.; Baizer, M. M., Electrocarboxylation. I. Mono- and Dicarboxylation of Activated Olefins. *J. Org. Chem.* **1974,** 39 (19); c. Tyssee, D. A.; Baizer, M. M., Electrocarboxylation. II.1 Electrocarboxylative Dimerization and Cyclization. *J. Org. Chem.* **1974,** 39 (19), 2823-2828.

19. a. Lamy, E.; Nadjo, L., Sur la carboxylation électrochimique des olefins activées. *Nouv. J. Chim.* **1979,** 3, 21-29; b. Filiardo, G.; Gambini, S.; Silvestro, G.; Gennaro, A.;

Vianello, E., Electrocarboxylation of Styrene Through Homogeneous Redox Catalysis. *J, Electroanal. Chem.* **1984,** 177, 303-309.

20. a. Matthessen, R.; Fransaer, J.; Binnemans, K.; De Vos, D. E., Electrocarboxylation: towards sustainable and efficient synthesis of valuable carboxylic acids. *Beilstein J. Org. Chem.* **2014,** 10, 2484-500; b. Senboku, H., Electrochemical Fixation of Carbon Dioxide. In *Transformation and Utilization of Carbon Dioxide*, 2014; pp 245-262; c. Senboku, H.; Katayama, A., Electrochemical carboxylation with carbon dioxide. *Curr. Opin. Green Sustainable Chem.* **2017,** 3, 50-54.

21. a. Yang, D.-T.; Zhu, M.; Schiffer, Z. J.; Williams, K.; Song, X.; Liu, X.; Manthiram, K., Direct Electrochemical Carboxylation of Benzylic C–N Bonds with Carbon Dioxide. *ACS Catal.* **2019,** 9 (5), 4699-4705; b. Alkayal, A.; Tabas, V.; Montanaro, S.; Wright, I. A.; Malkov, A. V.; Buckley, B. R., Harnessing Applied Potential: Selective beta-Hydrocarboxylation of Substituted Olefins. *J. Am. Chem. Soc.* **2020,** 142 (4), 1780-1785; c. Ang, N. W. J.; Oliveira, J. C. A.; Ackermann, L., Electroreductive Cobalt-Catalyzed Carboxylation: Cross-Electrophile Electrocoupling with Atmospheric CO2. *Angew. Chem. Int. Ed.* **2020,** 59 (31), 12842-12847; d. Zhang, Z.; Ye, J.-H.; Ju, T.; Liao, L.-L.; Huang, H.; Gui, Y.-Y.; Zhou, W.-J.; Yu, D.-G., Visible-Light-Driven Catalytic Reductive Carboxylation with CO2. *ACS Catal.* **2020,** 10 (19), 10871-10885; e. Sheta, A. M.; Alkayal, A.; Mashaly, M. A.; Said, S. B.; Elmorsy, S. S.; Malkov, A. V.; Buckley, B. R., Selective Electrosynthetic Hydrocarboxylation of alpha,beta-Unsaturated Esters with Carbon Dioxide*. *Angew. Chem. Int. Ed.* **2021,** 60 (40), 21832-21837; f. Liao, L. L.; Wang, Z. H.; Cao, K. G.; Sun, G. Q.; Zhang, W.; Ran, C. K.; Li, Y.; Chen, L.; Cao, G. M.; Yu, D. G., Electrochemical Ring-Opening Dicarboxylation of Strained Carbon-Carbon Single Bonds with CO2: Facile Synthesis of Diacids and Derivatization into Polyesters. *J. Am. Chem. Soc.* **2022,** 144 (5), 2062-2068; g. Liu, X.-F.; Zhang, K.; Tao, L.; Lu, X.-B.; Zhang, W.-Z., Recent advances in electrochemical carboxylation reactions using carbon dioxide. *GreenChE* **2022,** 3 (2), 125-137; h. You, Y.; Kanna, W.; Takano, H.; Hayashi, H.; Maeda, S.; Mita, T., Electrochemical Dearomative Dicarboxylation of Heterocycles with Highly Negative Reduction Potentials. *J. Am. Chem. Soc.* **2022,** 144 (8), 3685-3695; i. Zhang, K.; Ren, B. H.; Liu, X. F.; Wang, L. L.; Zhang, M.; Ren, W. M.; Lu, X. B.; Zhang, W. Z., Direct and Selective Electrocarboxylation of Styrene Oxides with CO2 for Accessing beta-Hydroxy Acids. *Angew. Chem. Int. Ed.* **2022**, e202207660.

22. a. Wang, H.; Lin, M.-Y.; Fang, H.-J.; Chen, T.-T. C.; Lu, J.-X., Electrochemical Dicarboxylation of Styrene: Synthesis of 2-Phenylsuccinic Acid. *Chin. J. Chem.* **2007,** 25, 913-916; b. Song, L.; Fu, D. M.; Chen, L.; Jiang, Y. X.; Ye, J. H.; Zhu, L.; Lan, Y.; Fu, Q.; Yu, D. G., Visible-Light Photoredox- Catalyzed Remote Difunctionalizing Carboxylation of Unactivated Alkenes with CO2. *Angew. Chem. Int. Ed.* **2020,** 59 (47), 21121-21128.

23. a. Köster, F.; Dinjus, E.; Dunäch, E., Electrochemical Selective Incorporation of CO2 into Terminal Alkynes and Diynes. *Eur. J. Org. Chem.* **2001**, 2507-2511; b. Li, C.; Yuan, G.; Jiang, H., Electrocarboxylation of Alkynes with Carbon Dioxide in the Presence of Metal Salt Catalysts. *Chin. J. Chem.* **2010,** 28, 1685-1689.

24. Khaja Lateef, S.; Ramesh Raju, R.; Krishna Mohan, S.; Jayarama Reddy, S., Electrochemical Synthesis of α-Hydroxycarboxylic Acids From Acetophenones. *Synth. Commun.* **2006,** 36 (1), 31-36.

25. Li, C.-H.; Song, X.-Z.; Tao, L.-M.; Li, Q.-G.; Xie, J.-Q.; Peng, M.-N.; Pan, L.; Jiang, C.; Peng, Z.-Y.; Xu, M.-F., Electrogenerated-bases promoted electrochemical synthesis of N-bromoamino acids from imines and carbon dioxide. *Tetrahedron* **2014,** 70 (10), 1855-1860.

26. Isse, A. A.; Gennaro, A., Electrocatalytic carboxylation of benzyl chlorides at silver cathodes in acetonitrile. *Chem. Commun.* **2002,** (23), 2798-9.

27. Senboku, H.; Minemura, Y.; Suzuki, Y.; Matsuno, H.; Takakuwa, M., Synthesis of N-Boc-alpha-amino Acids from Carbon Dioxide by Electrochemical Carboxylation of N-Boc-alpha-aminosulfones. *J. Org. Chem.* **2021,** 86 (22), 16077-16083.

28. For the sake of comparison, also the potential reported vs SCE are converted to the Fc+/Fc couple, using the conversion E(Fc+/Fc) = E(SCE) - 0.4 V.

29. Lamy, E.; Nadjo, L.; Saveant, J. M., Standard potential and kinetic parameters of the electrochemical reduction of carbon dioxide in dimethylformamide. *J. Electroanal. Chem. Interfacial Electrochem.* **1977,** 78 (2), 403-407.

30. Zhang, S.; Neumann, H.; Beller, M., Synthesis of alpha,beta-unsaturated carbonyl compounds by carbonylation reactions. *Chem. Soc. Rev.* **2020,** 49 (10), 3187-3210.

31. Bouhaoui, A.; Eddahmi, M.; Dib, M.; Khouili, M.; Aires, A.; Catto, M.; Bouissane, L., Synthesis and Biological Properties of Coumarin Derivatives. A Review. *ChemistrySelect* **2021,** 6 (24), 5848-5870.

32. Salehi, B.; Quispe, C.; Chamkhi, I.; El Omari, N.; Balahbib, A.; Sharifi-Rad, J.; Bouyahya, A.; Akram, M.; Iqbal, M.; Docea, A. O.; Caruntu, C.; Leyva-Gomez, G.; Dey,

A.; Martorell, M.; Calina, D.; Lopez, V.; Les, F., Pharmacological Properties of Chalcones: A Review of Preclinical Including Molecular Mechanisms and Clinical Evidence. *Front. Pharmacol.* **2020,** 11, 592654.

33. Ullah, A.; Munir, S.; Badshah, S. L.; Khan, N.; Ghani, L.; Poulson, B. G.; Emwas, A. H.; Jaremko, M., Important Flavonoids and Their Role as a Therapeutic Agent. *Molecules* **2020,** 25 (22).

34. Panche, A. N.; Diwan, A. D.; Chandra, S. R., Flavonoids: an overview. *J. Nutr. Sci.* **2016,** 5, e47.

35. Zhao, K.; Yuan, Y.; Lin, B.; Miao, Z.; Li, Z.; Guo, Q.; Lu, N., LW-215, a newly synthesized flavonoid, exhibits potent anti-angiogenic activity in vitro and in vivo. *Gene* **2018,** 642, 533-541.

36. Zhao, L.; Yuan, X.; Wang, J.; Feng, Y.; Ji, F.; Li, Z.; Bian, J., A review on flavones targeting serine/threonine protein kinases for potential anticancer drugs. *Bioorg. Med. Chem.* **2019,** 27 (5), 677-685.

37. a. Ismail, M. A.; Abouzid, K. A.; Mohamed, N. S.; Dokla, E. M., Ligand design, synthesis and biological anti-HCV evaluations for genotypes 1b and 4a of certain 4-(3- & 4-[3-(3,5-dibromo-4-hydroxyphenyl)-propylamino]phenyl) butyric acids and 3-(3,5-dibromo-4-hydroxyphenyl)-propylamino-acetamidobenzoic acid esters. *J. Enzyme Inhib. Med. Chem.* **2013,** 28 (6), 1274-90; b. Singh, J.; Saini, V.; Kumar, A.; Bansal, R., Synthesis, molecular docking and biological evaluation of some newer 2-substituted-4-(benzo[d][1,3]dioxol-5-yl)-6-phenylpyridazin-3(2H)-ones as potential anti-inflammatory and analgesic agents. *Bioorg. Chem.* **2017,** 71, 201-210.

38. a. Orsini, M.; Feroci, M.; Sotgiu, G.; Inesi, A., Stereoselective electrochemical carboxylation: 2-phenylsuccinates from chiral cinnamic acid derivatives. *Org. Biomol. Chem.* **2005,** 3 (7), 1202-8; b. Wang, H.; Zhang, G.; Liu, Y.; Luo, Y.; Lu, J., Electrocarboxylation of activated olefins in ionic liquid BMIMBF4. *Electrochem. Commun.* **2007,** 9 (9), 2235-2239; c. Wang, H.; Zhang, K.; Liu, Y.-Z.; Lin, M.-Y.; Lu, J.-X., Electrochemical carboxylation of cinnamate esters in MeCN. *Tetrahedron* **2008,** 64 (2), 314-318.

39. Wawzonek, S.; Gundersen, A., Polarographic Studies in Acetonitrile and Dimethylformamide IX. Behavior of α,β-Unsaturated Carbonyl Compounds. *J. Electrochem. Soc.* **1964,** 111 (3).

40. based on formation of a trimer in absence of CO2 and of a carboxylated ciclyc dimer in presence of CO2

41. based on formation of a polymer in absence of CO2 and of 1,3,4,6-Tetraphenyl-1,5-hexanedione in presence of CO2

42. Harada, J.; Sakakibara, Y.; Kunai, A.; Sasaki, K., Electrochemical Carboxylation of α,β-unsaturated Ketones with Carbon Dioxide. *Bull, Chem. Soc. Jpn.* **1984,** 57, 611-612.

43. Senboku, H.; Yamauchi, Y.; Kobayashi, N.; Fukui, A.; Hara, S., Electrochemical Carboxylation of Flavones: Facile Synthesis of Flavanone-2-carboxylic Acids. *Electrochemistry* **2011,** 11, 862-864.

44. Senboku, H.; Yamauchi, Y.; Kobayashi, N.; Fukui, A.; Hara, S., Some mechanistic studies on electrochemical carboxylation of flavones to yield flavanone-2-carboxylic acids. *Electrochim. Acta* **2012,** 82, 450-456.

45. Yuan, G.-Q.; Jiang, H.-F.; Lin, C.; Liao, S.-J., Efficient electrochemical synthesis of 2-arylsuccinic acids from CO2 and aryl-substituted alkenes with nickel as the cathode. *Electrochim. Acta* **2008,** 53 (5), 2170-2176.

46. Vakulskaya, T. I.; Larina, L. I.; Vashchenko, A. V., Radical anions of flavonoids. *Magn. Reson. Chem.* **2011,** 49 (8), 508-13.

47. The working electrode potential was set to a value 0.1 V more negative than thr reduction peak measured by cyclic voltammetry, to achieve adequate generation of the desired species.

48. Selectivity is calculated as the ratio of yield to conversion.

49. Jian-Hua, X.; Chuan-Feng, C.; Xue, O.; Jing-Hua, W.; You-Cheng, L., Photoinduced reductions of chalcone derivatives in the presence of amines. *J. Photochem. Photobiol., A* **1996,** 97 (1), 33-43.

50. Maekawa, H.; Murakami, T.; Miyazaki, T.; Nishiguchi, I., Practical Synthesis of Diethyl Phenylsuccinate by Mg-promoted Carboxylation of Ethyl Cinnamate. *Chem. Lett.* **2011,** 40 (4), 368-369.

51. Roszak, R.; Beker, W.; Molga, K.; Grzybowski, B. A., Rapid and Accurate Prediction of pKa Values of C–H Acids Using Graph Convolutional Neural Networks. *J. Am. Chem. Soc.* **2019,** 141 (43), 17142-17149.

52. Noel, T.; Cao, Y.; Laudadio, G., The Fundamentals Behind the Use of Flow Reactors in Electrochemistry. *Acc. Chem. Res.* **2019,** 52 (10), 2858-2869.

53. Tateno, H.; Matsumura, Y.; Nakabayashi, K.; Senboku, H.; Atobe, M., Development of a novel electrochemical carboxylation system using a microreactor. *RSC Adv.* **2015,** 5 (119), 98721-98723.

54. Qu, Y.; Tsuneishi, C.; Tateno, H.; Matsumura, Y.; Atobe, M., Green synthesis of α-amino acids by electrochemical carboxylation of imines in a flow microreactor. *React. Chem. Eng.* **2017,** 2 (6), 871-875.

55. Naito, Y.; Nakamura, Y.; Shida, N.; Senboku, H.; Tanaka, K.; Atobe, M., Integrated Flow Synthesis of alpha-Amino Acids by In Situ Generation of Aldimines and Subsequent Electrochemical Carboxylation. *J. Org. Chem.* **2021,** 86 (22), 15953-15960.

56. Cao, Y.; Soares, C.; Padoin, N.; Noël, T., Gas bubbles have controversial effects on Taylor flow electrochemistry. *Chem. Eng. J.* **2021,** 406, 126811.

57. Laudadio, G.; De Smet, W.; Struik, L.; Cao, Y.; Noël, T., Design and application of a modular and scalable electrochemical flow microreactor. *J. Flow Chem.* **2018,** 8 (3), 157-165.

58. Lefebvre, C.; Hoffmann, N., Chapter Eight - Photochemical rearrangements in organic synthesis and the concept of the photon as a traceless reagent. In *Nontraditional Activation Methods in Green and Sustainable Applications*, Török, B.; Schäfer, C., Eds. Elsevier: 2021; pp 283-328.

59. a. Tan, F.; Yin, G., Homogeneous Light-Driven Catalytic Direct Carboxylation with CO2. *Chin. J. Chem.* **2018,** 36 (6), 545-554; b. Huang, W.; Lin, J.; Deng, F.; Zhong, H., Photocatalytic Carboxylation with CO2: A Review of Recent Studies. *Asian J. Org. Chem.* **2022,** 11 (7), e202200220; c. Yeung, C. S., Photoredox Catalysis as a Strategy for CO2 Incorporation: Direct Access to Carboxylic Acids from a Renewable Feedstock. *Angew. Chem. Int. Ed.* **2019,** 58 (17), 5492-5502; d. Fan, Z.; Zhang, Z.; Xi, C., Light-Mediated Carboxylation Using Carbon Dioxide. *ChemSusChem* **2020,** 13 (23), 6201-6218; e. He, X.; Qiu, L.-Q.; Wang, W.-J.; Chen, K.-H.; He, L.-N., Photocarboxylation with CO2: an appealing and sustainable strategy for CO2 fixation. *Green Chem.* **2020,** 22 (21), 7301-7320; f. Pradhan, S.; Roy, S.; Sahoo, B.; Chatterjee, I., Utilization of CO2 Feedstock for Organic Synthesis by Visible-Light Photoredox Catalysis. *Chemistry* **2021,** 27 (7), 2254-2269.

60. Tazuke, S.; Ozawa, H., Photofixation of Carbon Dioxide : Formation of 9,10-Dihydrophenanthrene -9-carboxylic Acid from Phenanthrene-Amine-Carbon Dioxide Systems. *J. Chem. Soc., Chem. Comm.* **1975,** 7.

61. Seo, H.; Liu, A.; Jamison, T. F., Direct beta-Selective Hydrocarboxylation of Styrenes with CO2 Enabled by Continuous Flow Photoredox Catalysis. *J. Am. Chem. Soc.* **2017,** 139 (40), 13969-13972.

62. Song, L.; Wang, W.; Yue, J.-P.; Jiang, Y.-X.; Wei, M.-K.; Zhang, H.-P.; Yan, S.-S.; Liao, L.-L.; Yu, D.-G., Visible-light photocatalytic di- and hydro-carboxylation of unactivated alkenes with CO2. *Nat. Catal.* **2022**.

63. Seo, H.; Katcher, M. H.; Jamison, T. F., Photoredox activation of carbon dioxide for amino acid synthesis in continuous flow. *Nat. Chem.* **2017,** 9 (5), 453-456.

64. Shimomaki, K.; Murata, K.; Martin, R.; Iwasawa, N., Visible-Light-Driven Carboxylation of Aryl Halides by the Combined Use of Palladium and Photoredox Catalysts. *J. Am. Chem. Soc.* **2017,** 139 (28), 9467-9470.

65. Crespi, S.; Fagnoni, M., Generation of Alkyl Radicals: From the Tyranny of Tin to the Photon Democracy. *Chem. Rev.* **2020,** 120 (17), 9790-9833.

66. Murray, P. R. D.; Cox, J. H.; Chiappini, N. D.; Roos, C. B.; McLoughlin, E. A.; Hejna, B. G.; Nguyen, S. T.; Ripberger, H. H.; Ganley, J. M.; Tsui, E.; Shin, N. Y.; Koronkiewicz, B.; Qiu, G.; Knowles, R. R., Photochemical and Electrochemical Applications of Proton-Coupled Electron Transfer in Organic Synthesis. *Chem. Rev.* **2022,** 122 (2), 2017-2291.

67. Meng, Q. Y.; Schirmer, T. E.; Berger, A. L.; Donabauer, K.; Konig, B., Photocarboxylation of Benzylic C-H Bonds. *J. Am. Chem. Soc.* **2019,** 141 (29), 11393-11397.

68. Ran, C.-K.; Niu, Y.-N.; Song, L.; Wei, M.-K.; Cao, Y.-F.; Luo, S.-P.; Yu, Y.-M.; Liao, L.-L.; Yu, D.-G., Visible-Light Photoredox-Catalyzed Carboxylation of Activated C(sp3)—O Bonds with CO2. *ACS Catal.* **2021,** 12 (1), 18-24.

69. Wang, P.-Z.; Chen, J.-R.; Xiao, W.-J., Hantzsch esters: an emerging versatile class of reagents in photoredox catalyzed organic synthesis. *Org. Biomol. Chem.* **2019,** 17 (29), 6936-6951.

70. a. Occhialini, D.; Kristensen, J. S.; Daasbjerg, K.; Lund, H.; Khan, A., Estimation of reduction and standard potentials of some allyl and substituted alkyl radicals. *Acta Chem. Scand.* **1992,** 46 (5), 474; b. Fu, Y.; Liu, L.; Yu, H.-Z.; Wang, Y.-M.; Guo, Q.-X., Quantum-Chemical Predictions of Absolute Standard Redox Potentials of Diverse Organic Molecules and Free Radicals in Acetonitrile. *J. Am. Chem. Soc.* **2005,** 127 (19), 7227-7234.

71. Scopano, A. A novel benzylic photocarboxylation method using carbon dioxide. University of Padova, 2020.

72. a. Kütt, A.; Tshepelevitsh, S.; Saame, J.; Lõkov, M.; Kaljurand, I.; Selberg, S.; Leito, I., Strengths of Acids in Acetonitrile. *Eur. J. Org. Chem.* **2021,** 2021 (9), 1407-1419;

b. Gallage, P. C.; Pitre, S. P., Direct photolysis of 4-tert-alkyl-1,4-dihydropyridines under blue-light irradiation for the generation of tertiary alkyl radicals. *Green Chem.* **2022,** 24 (18), 6845-6848.

73. Taylor, J. E.; Bull, S. D.; Williams, J. M. J., Amidines, isothioureas, and guanidines as nucleophilic catalysts. *Chem. Soc. Rev.* **2012,** 41 (6), 2109-2121.

74. Nakajima, K.; Nojima, S.; Sakata, K.; Nishibayashi, Y., Visible-Light-Mediated Aromatic Substitution Reactions of Cyanoarenes with 4-Alkyl-1,4-dihydropyridines through Double Carbon–Carbon Bond Cleavage. *ChemCatChem* **2016,** 8 (6), 1028-1032.

75. Several relative orientations of 14 and TBD can be considered, showing similar distances and angles.

76. a. Dunitz, J. D.; Bürgi, H.-B., *Structure Correlation*. John Wiley & Sons: 1994; b. Chapter 1 Hydrogen Bond – Definitions, Criteria of Existence and Various Types. In *Understanding Hydrogen Bonds*: *Theoretical and Experimental Views*, The Royal Society of Chemistry: 2021; pp 1-40.

77. Donabauer, K.; Maity, M.; Berger, A. L.; Huff, G. S.; Crespi, S.; König, B., Photocatalytic carbanion generation – benzylation of aliphatic aldehydes to secondary alcohols. *Chem. Sci.* **2019,** 10 (19), 5162-5166.

78. Potential vs Fc+/Fc was calculated following E(Fc+/Fc) = E(NHE) - 0.65 V

79. Gandolfo, E.; Tang, X.; Raha Roy, S.; Melchiorre, P., Photochemical Asymmetric Nickel-Catalyzed Acyl Cross-Coupling. *Angew. Chem. Int. Ed.* **2019,** 131 (47), 17010-17014.

80. Chen, W.; Liu, Z.; Tian, J.; Li, J.; Ma, J.; Cheng, X.; Li, G., Building congested ketone: substituted hantzsch ester and nitrile as alkylation reagents in photoredox catalysis. *J. Am. Chem. Soc.* **2016,** 138 (38), 12312-12315.

81. Han, Q.-Q.; Li, G.-H.; Sun, Y.-Y.; Chen, D.-M.; Wang, Z.-L.; Yu, X.-Y.; Xu, X.-M., Silver-catalyzed cascade radical cyclization of sodium sulfinates and o-(allyloxy) arylaldehydes towards functionalized chroman-4-ones. *Tetrahedron Lett.* **2020,** 61 (14), 151704.

82. Batey, R. A.; Quach, T. D., Synthesis and cross-coupling reactions of tetraalkylammonium organotrifluoroborate salts. *Tetrahedron Lett.* **2001,** 42 (52), 9099-9103.

83. Liang, J.; Cochran, J. E.; Dorsch, W. A.; Davies, I.; Clark, M. P., Development of a scalable synthesis of an azaindolyl-pyrimidine inhibitor of influenza virus replication. *Org. Process Res. Dev.* **2016,** 20 (5), 965-969.

84. Green, S. P.; Wheelhouse, K. M.; Payne, A. D.; Hallett, J. P.; Miller, P. W.; Bull, J. A., Thermal stability and explosive hazard assessment of diazo compounds and diazo transfer reagents. *Org. Process Res. Dev.* **2019,** 24 (1), 67-84.

85. Deng, T.; Mazumdar, W.; Ford, R. L.; Jana, N.; Izar, R.; Wink, D. J.; Driver, T. G., Oxidation of nonactivated anilines to generate N-aryl nitrenoids. *J. Am. Chem. Soc.* **2020,** 142 (9), 4456-4463.

General Conclusions

In this doctoral thesis new synthetic possibilities have been disclosed. Prompted by the increasing interest in the environmental impact of chemistry, we directed our interest toward the application of photo-, electro- and flow chemistry to organic synthesis.

In Chapter II it is shown how the use of visible light allows for a better diastereocontrol of photochemical reactions. Aryl ketones have been employed in a Paternò-Büchi reaction aimed at the dearomatisation of indoles with excellent results, both in terms of yield (up to > 98%) and selectivity (dr > 20:1). Moreover, the process was employed in the functionalisation of oxindole-derived silyl enol ethers. Implementation of the process in a microfluidic setup greatly improved the productivity (13-fold increase with respect to batch conditions) while maintaining the high levels of yield (up to > 98%) and selectivity (dr > 20:1).

***Chapter II** - Visible-light Paternò-Büchi Reaction for the Construction of Indolinic Structures*

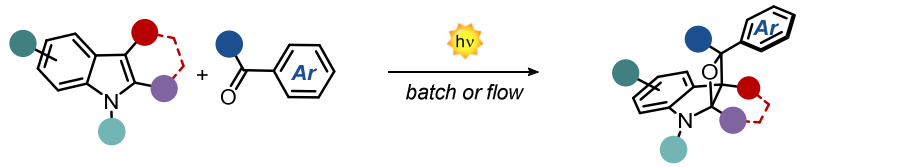

- *available substrates*
- *mild, catalyst-free conditions*

- *34 examples in batch, 22 in flow - up to >98% yield*
- *high regio- & diastereocontrol*

In Chapter III different methods for CO_2 utilisation are described. First, we investigated the mechanism of electrochemical carboxylation of flavone and chalcone, as representative of α,β-unsaturated carbonyls. Using circular voltammetry and controlled-potential electrolysis we identified the active

dianion intermediate in the carboxylation step, which lead to 55% yield of carboxylated product on a 60% conversion of starting material. Next, the electrochemical carboxylation of other α,β-unsaturated carbonyl compounds was studied in flow. High productivity was achieved for methyl crotonate (more than 50-fold increase respect to batch), though problems of reactivity and reproducibility prevented the realisation of a general procedure.

Finally, carbon dioxide fixation was achieved also through a photocatalytic approach. We designed a redox-neutral process that avoided the use of sacrificial redox agents, and we exploited a proton-coupled electron transfer for the activation of dihydropyridines. Carboxylated products were obtained with a broad scope in good yields (18 examples, up to 76% yield).

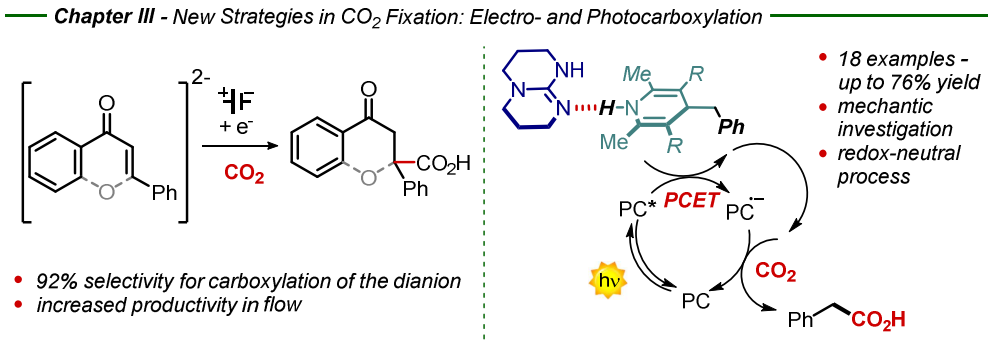

In summary, during my PhD studies, I explored the application of innovative methods towards a more sustainable and efficient organic synthesis, an important target that the entire chemical community should aim for. Increasingly efforts are required to further develop these processes, also making them congenial tools for the industrial application of such valuable sources and methods. Furthermore, new approaches, such as photoelectrochemistry, need to be explored for the development of even more effective strategies for organic synthesis.